# Toxicological Profiling of Copper Oxide and Silver Nanoparticles and Polyoxometalate Ionic Liquids with Medically Relevant Bacteria and Mammalian Cells *in vitro*

ANNA-LIISA  KUBO

**TAL
TECH** PRESS

TALLINN UNIVERSITY OF TECHNOLOGY
School of Science
Department of Chemistry and Biotechnology
NATIONAL INSTITUTE OF CHEMICAL PHYSICS AND BIOPHYSICS
Laboratory of Environmental Toxicology
This dissertation was accepted for the defence of the degree on April 3$^{rd}$, 2019.

**Supervisors**:        Dr. Olesja Bondarenko, Senior Research Scientist
Laboratory of Environmental Toxicology
National Institute of Chemical Physics and Biophysics, Estonia

Academician Dr. Anne Kahru
Head of the Laboratory of Environmental Toxicology
National Institute of Chemical Physics and Biophysics, Estonia

**Advisor:**        Prof. emer. Lilian Järvekülg
School of Science, Department of Chemistry and Biotechnology
Tallinn University of Technology, Estonia

**Opponents**:        Prof. Richard Handy
School of Biological and Marine Sciences
Faculty of Science and Engineering
University of Plymouth, United Kingdom

Prof. Karin Kogermann
Institute of Pharmacy, Faculty of Medicine
University of Tartu, Estonia

**Defence of the thesis**: May 24$^{th}$, 2019, Tallinn

**Declaration:**
Hereby I declare that this doctoral thesis, my original investigation and achievement, submitted for the doctoral degree at Tallinn University of Technology has not been submitted for doctoral or equivalent academic degree.
Anna-Liisa Kubo

_____
signature

# Vaskoksiidi ja hõbeda nanoosakeste ning polüoksometalaat-ioonvedelike toksilisuse uuringud meditsiiniliselt oluliste bakterite ja imetajarakkudega *in vitro*

ANNA-LIISA KUBO

# Contents

# List of publications

I    Käkinen, A., Kahru, A., Nurmsoo, H., **Kubo, A. L.**, Bondarenko, O. M. (2016). Solubility-driven toxicity of CuO nanoparticles to Caco2 cells and *Escherichia coli*: Effect of sonication energy and test environment. Toxicology in Vitro, 36, 172–179.

II    **Kubo, A. L.**, Capjak, I., Vrček, I. V., Bondarenko, O. M., Kurvet, I., Vija, H., Kahru, A. (2018). Antimicrobial potency of differently coated 10 and 50 nm silver nanoparticles against clinically relevant bacteria *Escherichia coli* and *Staphylococcus aureus*. Colloids and Surfaces B: Biointerfaces, 170(February), 401–410.

III    **Kubo, A. L.**, Kremer, L., Herrmann, S., Mitchell, S. G., Bondarenko, O. M., Kahru, A., Streb, C. (2017). Antimicrobial activity of polyoxometalate ionic liquids against clinically relevant pathogens. ChemPlusChem, 82(6), 867–871.

Manuscript  **Kubo, A. L.**, Vassiljev, G., Vija, H., Kristall, J., Tõugu, V., Kahru, A., Bondarenko, O. M. Towards (immuno)safety of antibacterial nanomaterials: surface functionalization of CuO with carboxyl- or polyethylene decreases their cytotoxicity to human cells *in vitro* (manuscript in preparation).

# Author's contribution to the publications

I    The author participated in the development of the viability assay and study design for safety evaluation of CuO nanoparticles on Caco-2 cell model. She prepared the nanoparticle suspensions and conducted the viability assessment experiments on Caco-2 cells *in vitro*.

II    The author participated in the study design and performed most of the experiments: assays on antibacterial activity of nanoparticles and their coatings, flow cytometry experiment, solubility analysis and results analysis of the bioavailability experiment. She did partly the statistical analysis and the artwork, interpreted the data and took part in the preparation of the manuscript.

III    The author participated in the study design and antibacterial efficiency evaluation of polyoxometalate ionic liquids. She prepared the working solutions of the chemicals and conducted all antibacterial assays. She also interpreted the data and participated in preparation of the manuscript.

Manuscript  The author participated in the study design and performed most of the experiments. She prepared the suspensions of the nanoparticles, did the safety evaluation of nanoparticles on THP-1 cells and HaCaT keratinocytes *in vitro*, antibacterial efficiency evaluation, ROS determination and was responsible for the data analysis. She participated in preparation of the manuscript.

## Other publications

Talja, I., **Kubo, A. L.**, Veijola, R., Knip, M., Simell, O., Ilonen, J., Vähä-Mäkilä, M., Sepp, E., Mikelsaar, M., Utt, M., Uibo, R. (2014). Antibodies to lactobacilli and bifidobacteria in young children with different propensity to develop islet autoimmunity. Journal of Immunology Research. 2014:325938.

Rekker, K., Saare, M., Roost, AM., **Kubo, A. L.**, Zarovni, N., Chiesi, A., Salumets, A., Peters, M. (2014). Comparison of serum exosome isolation methods for microRNA profiling. Clinical Biochemistry, 47, 135–138.

**Prangli, A. L.**, Utt, M., Talja, I., Sepp, E., Mikelsaar, M., Rajasalu, T., Uibo, O., Tillmann, V., Uibo, R. (2009). Antigenic proteins of *Lactobacillus acidophilus* that are recognised by serum IgG antibodies in children with type 1 diabetes and coeliac disease. Pediatric Allergy and Immunology, 21 (4), E772–E779.

# Introduction

The high prevalence of infectious diseases necessitates finding new means to combat the spread of bacteria. Currently, the design and testing of new antimicrobial agents for prevention and cure of the bacterial infections is a major healthcare concern. The probability to acquire an infection from the hospital settings is up to 10% [1]. Moreover, the high concentrations of antibiotics used in the hospitals in combination with extensive invasive procedures raise additional concerns over increasing tolerance of bacteria to antibiotics. Among several alternatives to traditional antibacterial agents, metal-based nanoparticles (NPs) and polyoxometalate ionic liquids (POM-ILs) are strong candidates.

Selected metals and metal-based NPs (particles with at least one dimension between 1–100 nm) have proven to be good alternatives to the traditional antibiotics due to their catalyst properties and high affinity for various biomolecules. From all the currently studied metal-based NPs, silver and copper oxide nanoparticles are the most efficient to combat bacterial infections. Antimicrobial properties of CuO and Ag NPs are gaining remarkable attention also due to their applications in biomedical industry. The small size gives the NPs large surface area, leading to unique physico-chemical and antibacterial properties. The NPs comprising of CuO and Ag can be deployed as bactericidal agents in e.g. textiles or in wound dressings or in topical coatings for touch surfaces. There is, however, relatively little known about the impact of physico-chemical properties of the NPs on respective toxic effects, especially of CuO NPs that are less exploited than Ag NPs. The studies of these effects are also complicated as the preparation protocols for suspensions of CuO and Ag NPs are not standardized yet.

The hypothesis of the current thesis was that the physico-chemical properties can influence the toxicological profiles of CuO NPs, Ag NPs and POM-ILs. The objectives of the work were: 1) to determine the influence of applied sonication energy on the toxicity of CuO NPs on bacterial and on mammalian cells *in vitro*; 2) to assess the toxicity of NPs and POM-ILs on Gram-negative *E. coli* and on Gram-positive *S. aureus* bacteria; 3) to evaluate the size and the surface modification-dependent toxic effects of NPs and POM-ILs with different carbon alkyl chain lengths.

Altogether, 20 NPs and POM-ILs were studied, including 10 nm and 50 nm Ag NPs with 6 surface coatings, CuO NPs with several surface functionalizations and from various commercial sources, and POM-ILs with different alkyl chain lengths ($Q^x$-ILs). The main results of the thesis were the following: 1) the optimization of the sonication protocol for CuO NPs revealed that applying higher sonication energy resulted in better dispersed NPs` suspensions that had an influence on the toxicity evaluation of NPs with bacterial and mammalian cells *in vitro*; 2) antibacterial efficiency estimation of NPs and POM-ILs using various bacteria with the focus on Gram-negative *Escherichia coli* and Gram-positive *Staphylococcus aureus* showed that the Ag NPs were more toxic to *E. coli* and the POM-ILs were more toxic to *S. aureus* whereas the highest toxicity of all the tested compounds was seen for the Ag NPs (0.1-6.5 mg Ag/L); 3) toxicity evaluation of a panel of NPs with different sizes and surface functionalizations and the POM-ILs with different alkyl chain lengths (carbon=C= 6, 7 ,8) showed that the smaller and positively charged NPs proved to be the most toxic to all tested bacteria as well as to mammalian cells *in vitro* and the best antibacterial results were achieved with the ILs with carbon chain length consisting of seven carbon atoms ($Q^7$); 4) the physico-chemical properties` dependent mechanisms of toxicity/safety of CuO NPs evaluation revealed that the

least toxic compounds to mammalian cells were the CuO NPs functionalized with polyethylene glycol and carboxyl.

To summarise, the toxicity of CuO and Ag NPs depended on their size, surface modification and dispersion protocols used. Thus, the antibacterial properties of Ag and CuO NPs can be significantly tuned with size and surface modification, whereas for ILs the carbon chain length can be adjusted to achieve the same goal.

# Abbreviations

| | |
|---|---|
| AAS | atomic absorption spectroscopy |
| AOT | bis(2-ethylhexyl) sulfosuccinate |
| ATCC | American Type Culture Collection |
| CA-MHB | cation adjusted Mueller-Hinton broth (bacterial growth medium) |
| CCM | cell culture medium |
| CIT | citrate |
| -COOH | carboxyl functionalization |
| CTAB | cetyltrimethylammonium bromide |
| $D_h$ | hydrodynamic diameter |
| DI water | distilled sterilised water |
| DLS | dynamic light scattering |
| DMEM | Dulbecco's modification of Eagle medium |
| DMSO | dimethyl sulfoxide |
| EC50 | 50% effective dose |
| ECHA | the European Chemicals Agency |
| Espec | delivered acoustic energy |
| FBS | fetal bovine serum |
| $H_2DCFDA$ | 2',7'-dichlorodihydrofluorescein diacetate |
| HAI | hospital associated infection |
| ISO | the International Standardization Organisation |
| LB | Luria Bertani medium (bacterial growth medium) |
| MBC | minimum bactericidal concentration |
| MEM | modified Eagles medium (cell growth medium) |
| -NH$_2$ | amine functionalization |
| NPs | nanoparticles |
| PCA | principal component analysis |
| PDI | polydispersity index |
| PEG | polyethylene glycol |
| PLL | poly-l-lysine |
| PMA | phorbol 12-myristate 13-acetate |
| POM-IL | polyoxometalate ionic liquid |
| PVP | polyvinylpyrrolidone |
| REACH | Registration, Evaluation, Authorisation and Restriction of Chemicals |
| RLU | relative light unit |
| ROS | reactive oxygen species |
| RPMI | Roswell Park Memorial Institute medium (cell growth medium) |
| Tween 80 | polysorbate 80 |
| UV-vis | ultraviolet-visible |

# 1 Literature review

## 1.1 The need for alternative antibacterial agents

The spread of microbial infections is a worldwide problem and the increasing resistance of bacteria to conventional antibiotics is a major concern in healthcare settings (http://www.who.int) [2]. Since the discovery of the first antibiotic penicillin by Alexander Fleming in 1928, antibiotics have given relief and saved lives for decades. However, the first cases of antibiotic resistance to bacteria occurred in the 1960s and since then bacterial mechanisms of resistance to nearly all known antibiotics have emerged [3]. Thus, finding alternatives to traditional antibiotics is a major healthcare challenge.

The development of new antibiotics is no longer economically profitable [4]. Thus, the new approaches for the antibiotic stewardship – the reduction of use and the prevention of transmission of bacterial infections – are gaining attention. Another concern regarding antibacterial resistance is the prevalence of hospital associated infections (HAIs). HAIs occur in hospitals where vulnerable patients are accommodated and involved in several invasive procedures. The most common bacteria causing HAIs are *Escherichia coli* and *Staphylococcus aureus* (15.9% and 12.3% of HAIs respectively), followed by *Enterococcus spp.* (9.6%) and *Pseudomonas aeruginosa* (8.9%) [5].

## 1.2 Metal-based nanoparticles (NPs) as alternatives to traditional antibacterial agents

Metals have donor atom selectivity (for example, dissolved metal ions bind to O, N and S atoms of functional molecules [6–8]) and reduction potential that give them many advantages as antimicrobial agents [9]. Notably, there are only a few cases of antibacterial resistance reported towards metals [10]. Certain metals such as silver and copper are efficient antimicrobials and strong alternatives to traditional antibiotics [6]. The antimicrobial properties of metals can be potentially improved by employing them as NPs. Compared to their bulk counterparts, the metal-based NPs have additional useful (e.g., antibacterial) physico-chemical properties that are driven by their size accompanied by large surface area and catalytic features. Due to the small size, the NPs have large active surface that drive many of their toxic effects [11–14] (Figure 1).

Metal-based NPs can be used to impair the emergence of HAIs and drug-resistant bacteria, by using them in coatings for the touch surfaces in hospitals [11,15] or potentially engaging them in decontaminating water filters [16].
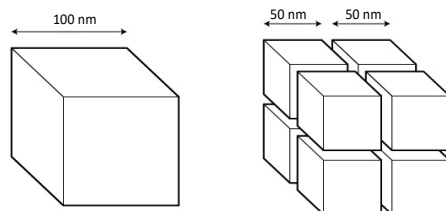


*Figure 1. Nanoparticles` specific surface area: a schematic representation. The increased number of smaller parts raises the specific surface area (in the current example, the volume of the cube remained the same while the surface area increased twice).*

### 1.2.1 Definition of NPs

There are different approaches in defining nanomaterials [17]. The EU adopted definition for engineered or naturally occurring nanomaterials in 2011 states the following: *„Nanomaterial means a natural, incidental or manufactured material containing particles, in an unbound state or as an aggregate or as an agglomerate and where, for 50% or more of the particles in the number size distribution, one or more external dimensions is in the* **size range 1 nm - 100 nm***"* (EC 2011/696/EU).

Thus, relying on the above definition, nanomaterial is a substance that has at least one dimension between 1-100 nm. In 2014 the definition was amended by European Joint Research Centre as follows: *"[…] Where technically feasible and requested in specific legislation, compliance with the definition […] may be determined on the basis* **of the specific surface area by volume.** *A material should be considered as falling under the definition […] where the specific surface area by volume of the material is greater than 60 $m^2/cm^3$. However, a material which, based on its number size distribution, is a nanomaterial should be considered as complying with the definition […] even if the material has a specific surface area lower than 60 $m^2/cm^3$."*

The final revised version of the EC definition (as of July 2018) entails specifications for the determination of specific surface area to volume ratio (a report on scientific-technical considerations of the definition: EUR 27240 EN). Essentially, the above definition is also in the EU biocidal products regulation [18] and thus relevant for defining the NPs as the antibacterial constituents of products for the customers.

### 1.2.2 Ag NPs as antibacterial agents

It is known already from ancient times that silver is a very efficient antibacterial metal. To this day, either in ionic, colloidal or nanoparticulate form, silver has been extensively used for its bactericidal properties and NPs of silver have been deployed in a plethora of consumer products such as textiles, cosmetics, filters, cleaning supplements etc. (http://nanotechproject.org/). Several studies have shown that Ag has antibacterial activity against a wide range of Gram-positive and Gram-negative bacteria (e.g. *E. coli, P. aeruginosa, S. aureus, Streptococcus pneumoniae, Shigella flexneri, Listeria monocytogenes* and *Salmonella typhimurium*) [19–21]. Silver is also an especially interesting antibacterial agent in the combat of antimicrobial resistance by acting against biofilm forming bacteria *E. coli*, *P. aeruginosa*, *S. flexneri* and *S. aureus* [20,22–25]. Silver can sensitise bacteria to antibiotics. For example, Ag in combination with antibiotics such as vancomycin, ampicillin, chloramphenicol, erythromycin, gentamicin and tetracycline showed improved therapeutic effects [19,20].

### 1.2.3 CuO NPs as antibacterial agents

Historically, copper has been used for bactericidal purposes in household and industry [12]. CuO NPs have been applied in several consumer products [12] (http://statnano.com/) and can be found in textiles, in hospital equipment, in wood preservation and in antifouling paints [26]. Also, CuO NPs have antibacterial properties against a wide array of Gram-positive and Gram-negative bacteria such as *E. coli*, *Bacillus subtilis*, *S. aureus, Streptococcus mutans, Lactobacillus acidophilus, P. aeruginosa* [27–32] and the toxic effects are driven by their physico-chemical properties such as size, dissolution, agglomeration and aggregation [14,32]. For example, the CuO NPs with the size 30 nm were ca 48 fold and CuSO4 ca 2300 fold more toxic than their bulk counterpart to Gram-negative *V. fischeri* bacterium [14]. The biological activity of CuO

NPs can be modulated by their surface functionalizations in *in vitro* conditions [31] and in *in vivo* conditions [33].

## 1.3. Antibacterial effects and toxicity mechanisms of metal-based NPs

Antibacterial metal-based NPs applied in biomedicine contain silver (Ag), zinc (Zn), copper (Cu), titanium (Ti), magnesium (Mg) [34–36]. Additionally, several metal oxide NPs such as $Co_3O_4$, $CoO$, $Cr_2O_3$, $CuO$, $Mn_2O_3$, $Ni_2O_3$, $ZnO$, and $Fe_3O_4$ have antibacterial properties [37,38].

It has been postulated that metal-based NPs exert bactericidal activity mainly by acting on the bacterial membranes [6,19,20]. The dissolution of the NPs results in the adsorption of metal ions on the cell membranes and depends on their properties such as the membrane lipid composition and mobility, [39] the donnan potential [40], and the ligands [9,13]. Also, reactive oxygen species (ROS) in the close vicinity of bacterial membranes can impair functions of the membranes, including the electron transport chain [9,41,42]. Some fraction of the dissolved metal can enter bacterial cells via the metal ion transporters [6,7,43,44] and cause toxicity.

Thus, the main toxicity mechanisms of metal-based NPs could be the release of metal ions (dissolution), formation of ROS and due to that destabilization of bacterial membranes (Figure 2). The toxic effects can be modulated depending on the content and surface modification of NPs. The details of each mechanism are described below.

### 1.2.4 The role of physico-chemical properties in the toxicity of metal-based NPs

The physico-chemical properties such as type of the metal, size and surface charge mostly drive the toxic effects of metal-based NPs. The NPs of Ag, CuO, ZnO, $TiO_2$ have the best potential as antibacterial agents for biomedical applications [6,27,34]. For the metal-based NPs, the size of the nanoparticles can be important driver of the toxic effects. Also, surface charge can have an effect on toxicity [45–47]. The properties of NPs can be altered by their preparation, e.g., dispersion in solvents. Due to the steric hindrance and electrostatic repulsion, the NPs` suspension can be modified by applying sonication energy [48,49]. Several studies have addressed the effect of ultrasonication to particle dispersion that subsequently, have an effect on their hydrodynamic size ($D_h$), dispersibility (expressed as polydispersity index PDI) and dissolution [48–55].
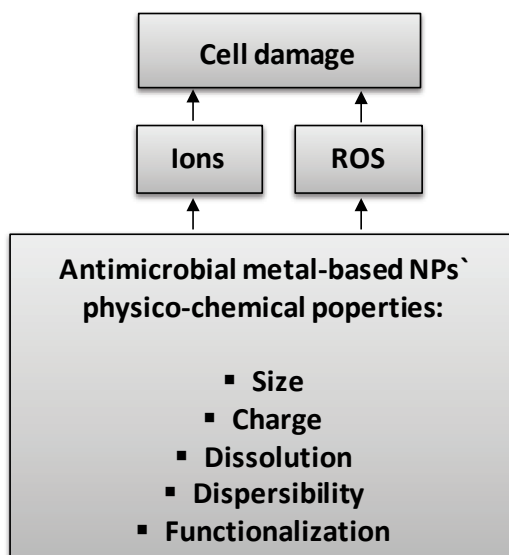
*Figure 2. A summary of the antimicrobial behaviour of metal-based NPs (compiled on the basis of Palza et al 2015* [9]*).*

### 1.2.5 The role of surface coatings in the toxicity of CuO and Ag NPs

Silver in the form of NPs is often coated with organic chemicals for stabilizing or giving charge [56]. Many chemicals such as polymers, anionic, cationic or non-ionic surfactants, ionic liquids and reducing agents can be used for coating the surface of Ag NPs or for providing protective, stabilizing or functional properties [45]. Aqueous dispersions of Ag NPs can be stabilised by steric repulsion, e.g., by using non-ionic surfactants (polysorbate 80 ((Tween 80)), Triton X-100) or polymers polyvinylpyrrolidone (PVP); or by electrostatic repulsion by using anionic sodium dodecyl sulfate or cationic surfactants cetyltrimethyl-ammonium bromide (CTAB) [57,58]. Sodium bis(2-ethylhexyl) sulfosuccinate (AOT) for example is used for the synthesis of stable Ag NPs [59].

Applying the coatings on NPs can influence the interactions of NPs with cells. For example, the surface of NPs can be camouflaged by the biological molecules in body fluids (formation of protein corona takes place) which can be regulated to some extent with the use of coating material. For example, glycan coating was used to prevent the covering of NPs with blood proteins [60,61]. Additionally, the surface charge is a property of NPs that can alter the NPs` interactions with cells. Positively charged Ag NPs coated with branched polyethylenimine (bPEI) have been shown to cause higher toxicity to bacteria as compared to Ag NPs coated with PVP rendering negative charge [62].

The coatings on Ag NPs are often used to give them better dispersibility and to tune their physico-chemical properties for different applications. Biomedically relevant Ag NPs can be used as drug supplements, as surface coating agents and as constituents in bactericidal materials, e.g., in wound bandages [63,64] (http://statnano.com/). For achieving excellent disinfectants, applying the coating agents on Ag NPs that themselves have antibacterial properties is a possibility (e.g. quaternary ammonium compounds, citrate or surfactants, chitosan) [23,65].

The search in Thomson Reuters Web of Science revealed altogether 4298 publications that investigated the use of Ag NPs for antibacterial purposes in biomedical applications (Figure 3). The search revealed that the citrate and PVP were coatings on Ag NPs in 4.5% and 4.2% respectively of the overall results. The studies that entailed Tween 80, AOT, CTAB and PLL as coating materials comprised 0.2% to 0.6% of publications each. Approximately 90% of the studies included other coatings (e.g., polyethylene glycol ((PEG)), proteins and peptides, mannitol, branched polyethylenimine, ammonium, etc.) [66].
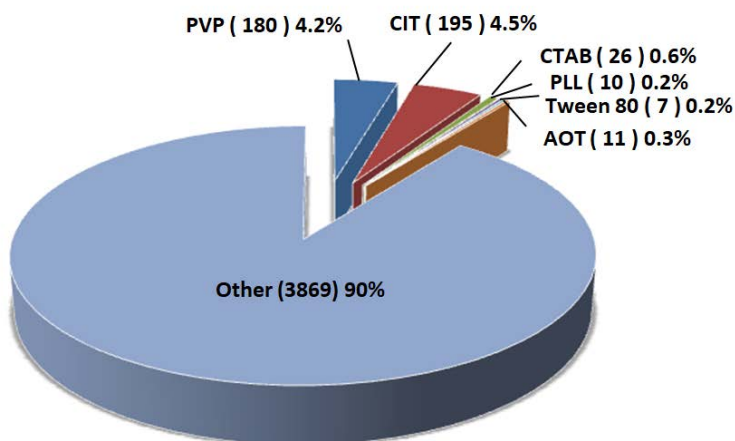


*Figure 3. Share of publications describing the use of coating materials on Ag NPs. Search was limited to the coating agents used in the current study and was performed in 15.09.2017 (publication II).*

Such coatings, however, can be used to tune antibacterial effects of Ag NPs, to protect them from direct interactions with the environment, oxidation, dissolution, or aggregation [15,21,67] and are also important for controlled release of toxic Ag ions [45]. For example, surfactants such as Tween 80, CTAB, AOT are used in the production process of Ag NPs for giving shape and for stabilizing them [59,68]. Essentially, antibacterial interactions of Ag NPs with microbial cells can be facilitated by applying coating agents [69]. The coatings on NPs can modify surface charge which in turn can alter toxicity.

The CuO NPs with different coatings, however, have been less studied as compared to Ag NPs (The search in Thomson Reuters Web of Science with the keywords: „CuO nanoparticl*" AND „coat* OR capp* OR functional*" resulted in 155 outcomes, and search „CuO nanoparticl*" AND „coat* OR capp* OR functional*" AND capping or coating agent resulted in only a few outcomes. The search was done on July 16, 2018.)

Coatings are also important for driving the toxic effects of CuO NPs. For example, Javed *et al* demonstrated that PEG and PVP coated CuO NPs had superior antibacterial effects over uncoated CuO NPs [31]. The carboxyl coated CuO NPs exhibited different toxicity profile as compared to uncoated CuO NPs in a rat [33]. Similarly to the Ag NPs, the dissolution could have substantial influence on the toxic effects of CuO NPs. CuO NPs can be highly dissolved in organic-rich media [70,71] and the dissolution can be modified with the coating materials [71].

### 1.2.6 The role of dissolution in the toxicity of CuO and Ag NPs

The toxicity of metal-based nanoparticles is sometimes a result of released metal ions [72,73]. For example, the dissolution is an important driver of toxic effects of Ag NPs [74,75] but also of ZnO NPs and of CuO NPs [76]. It has been shown that in ultrapure water and in the organic rich media smaller Ag NPs are more toxic and also more soluble as compared to larger counterparts [77,78]. The dissolution of the Ag NPs (and other metal NPs) can depend on the test media: The Ag NPs dissolved better in media containing organics than in plain water [77]. In addition, the dissolution of Ag NPs is facilitated by oxidation [79] and by the more acidic pH (higher dissolution of Ag NPs was seen at pH 1.12 as compared to pH 7.52) [80]. Additionally, the Ag ions are prone to form complexes with sulphur, organic matter, chlorine and proteins [21,57,75,81].

Similarly to Ag NPs, higher dissolution rate of CuO NPs in some organic-rich media was observed as compared to DI water [82]. However, the released Cu ions are less bioavailable in organic-containing media, a phenomenon that could be explained by the property of Cu ions to form complexes with ligands [83]. Also, the size of CuO NPs can be important for dissolution. For example, Semisch *et al.* showed that the CuO particles with the primary size range from 20 to 200 nm released 11 fold more ions in DMEM cell culture medium supplemented with 10% FCS as compared to their microsize counterparts (size up to 10 µM) [84].

The uptake of metals by bacterial cells is essential for antibacterial properties [6] and relevant target for combating resistance (e.g. for Cu and Ag) [44]. Soluble Cu and Ag can exert toxic effects by influencing the metal transporters of the cells. The fraction of bioavailable metals can depend on the testing media and on the target organism. Cu is transported into the cells via metal transporters and can be toxic in higher concentrations. Cu is a di-valent metal that has two oxidation states: $Cu^+$ and $Cu^{2+}$. In mammalian and bacterial cells, Cu is a microelement and the soluble Cu can be transported to the cells via passive and active metal uptake. The unspecific transportation of divalent cation metals is with the Nramp (natural resistance- associated macrophage protein) type transporters that are present in mammalian and bacterial cells or the proton-coupled metal ion divalent cation transporter 1 (DCT1) that is relevant for the absorption of metals (e.g. iron) from the gastrointestinal tract [85]. The induced metal transporters have higher affinity for the substrate and they use energy for metal translocation (such as P-type ATPase transporter family proteins) [6,86]. Also, dissolved $Cu^{2+}$ is moved with Na channels [87] and $Cu^+$ with the high affinity Cu copper transporter ion channel Ctr1 [88].

Ag is a non-essential metal in humans, Ag has higher affinity for sulphur as compared to Cu (the solubility product of $Ag_2S$ was $6.62 \times 10^{-50}$ and of CuS was $1.28 \times 10^{-36}$ and was related to the higher toxicity of Ag [44]). Ions from Ag can be introduced to the cells in similar ways to Cu and can possess higher affinity for proteins. For example, in the constituent of proteins, silver competes with the Cu binding sites of the P-ATPases for Cu transport [43]. In bacteria, the Cu effluxing ATPases CopB has been shown to transport both, Cu and Ag [44,89].

### 1.2.7 The role of ROS in the toxicity mechanisms of CuO and Ag NPs

Reactive oxygen species (ROS) are chemical species containing oxygen, such as peroxides, superoxide and hydroxyl radicals. ROS are normal by-products of oxidative metabolism and occur in bacteria and in mammalian cells for which cells have adapted methods to compensate. For example, human cells produce catalases, glutathione

peroxidases, glutathione S-transferases, superoxide dismutases, to cope with the excess of ROS [90].

The formation of ROS is a part of toxicity for many metals and NPs. ROS and metal dissolution can be the major mechanisms of toxicity for metal-containing NPs and can be also considered as predictors of toxicity [38]. For example, the metals that actively induce ROS are Mn, Fe, Ni, Cu. Ivask *et al* demonstrated that out of 11 metal oxide NPs, CuO NPs were among the three most active ROS inducers [70].

There is controversial information, however, about the relevance of ROS in the toxic effects of Ag NPs on bacteria. For example, Morones-Ramirez demonstrated that hydroxyl radicals from $AgNO_3$ sensitises *E. coli* bacteria to vancomycin antibiotic that is traditionally used to treat infections caused by Gram-positive bacteria [22]. Gurunathan *et al* showed that nanosilver sensitised *P. aeruginosa*, *Shigella flexneri*, *S. aureus* and *Streptococcus pneumonia* bacteria to ampicillin, gentamicin, chloramphenicol, erythromycin, tetracyclin and vancomycin antibiotics and the toxicity was enhanced in the presence of higher levels of induced ROS[20]. But the fraction of dissolved ions from Ag NPs can be more influential in their toxic effects. It has been shown that ROS induced by Ag NPs were more abundantly present than ROS induced by $AgNO_3$ salt [91]. In another study, it was shown that Ag NPs were inducers of ROS in *in vitro* conditions, but the ROS were not causing toxicity to *S. cerevisiae* [92]. Instead, in bacteria, the bioavailable Ag from 10-80 nm Ag NPs (rather than ROS) explained the toxicity of Ag NPs [78].

There is more clear indication, on the other hand, about ROS-dependent toxic effects of CuO NPs on cells [93,94]. CuO NPs are inducers of ROS via the Haber-Weiss reaction that results in production of hydroxyl radicals [9,95]. It has been shown that CuO NPs rather than Cu ions exhibit higher ROS levels in human A549 lung epithelial cells and HepG2 hepatocytes, with the resulting cytotoxic effects [93,96–98]. The CuO particles both in micro- and nanosize induced oxidative DNA damage to the lung alveolar epithelial cells A549 at concentration 40 μg/cm$^2$ after 4-h exposure in *in vitro* conditions [99]. The ability to induce reactive oxygen species depends on the cell type and on the conditions such as abiotic (acellular) and biotic (cellular) testing environments. For example, Rodhe *et al* demonstrated that CuO NPs induced small amounts of ROS in abiotic conditions (ROS was seen for 175 mg/L NPs after 350 min) and that was most probably related to their decreased toxicity to the leukemic cell line HL60 [100].

**1.2.8 CuO and Ag NPs potential to damage bacterial membranes**

Based on their membrane structure and composition, bacteria are divided into Gram-negative and Gram-positive. The Gram-negative bacteria have the outer membrane, a thin peptidoglycan layer and an inner membrane (plasma membrane). The Gram-positive bacteria, on the other hand, have a peptidoglycan cell wall surrounding only a single plasma membrane. Some solutes ($O_2$, $CO_2$, $NH_2$, $H_2S$) and ROS species can passively permeate the bacterial membranes [86] damaging the DNA and proteins inside the cells. Larger molecules up to 600 Da can internalise the bacteria through the porins (the diameter 3-5 nm) [79]. Although, the bacteria do not internalize the NPs *a priori*, to a small extent, the NPs can be also taken inside the bacteria through the porins and cause intracellular toxic effects (Figure 4).

Silver NPs bind to lipopolysaccharides on the outer membrane of Gram-negative bacteria and affect the bacterial inner membrane [101]. For example, Ag dissolved from

Ag NPs destabilizes the inner membrane, disrupts the bacterial electron transport chain by increasing proton leakage that in turn disturbs ATP synthesis [6,77,101,102].

Specific surface area and coating can influence the antibacterial activity of Ag NPs [103,104]. For example, the coatings of Ag NPs rendering positive surface charge can modify the interactions between positively charged NPs and negatively charged cell membranes towards more toxic effects [105]. Also, the higher intracellular concentration of silver ions explains the toxicity of Ag NPs [78,106] emphasizing the importance of membrane damage among toxicity mechanisms of these NPs. The membrane damage could be facilitated by applying coating agents on Ag NPs. Thus, it could be relevant to test the toxicity of coating materials themselves that are used on the Ag NPs [74].

As described in chapter 1.3, Cu is an essential nutritional element for the microbes and the metabolism of Cu by the bacterial cells have been thoroughly investigated; considerably less is known about the effects of CuO NPs to the bacterial membranes. Copper causes ROS-dependent damage resulting in alterations in the structure and destabilization of the membranes or interacts with amine and hydroxyl groups on the bacterial membranes [9,34]. The interactions of CuO NPs with the bacterial membranes can be also size-dependent [107].
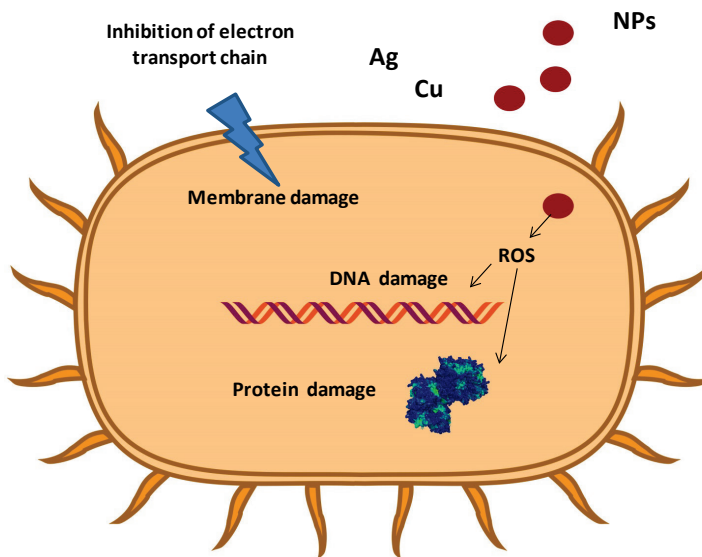


Figure 4. Examples of the CuO- and Ag-based NPs` toxic effects on bacteria (modified from Wang et al [42]).

## 1.3 Polyoxometalate ionic liquids

### 1.3.1 POM-ILs as antibacterial agents

Ionic liquids with polyoxometalates (POM-ILs) are chemicals with unique physico-chemical properties such as water immiscibility and hydrophobicity [108,109]. They have several applications in biology, medicine and material sciences. Due to their catalyst properties they can be used for sensors and for energy storing and conversion applications such as fuel cells for ultralight-weight electronics, for electrochemical analysis of pharmaceuticals and for temperature sensors [110]. POMs are metal oxide

clusters with adjustable structure and reactivity. The most commonly used POM is the Keggin heteropolyanion [111]. The Keggin heteropolyanion formula is $[XM_{12}O_{40}]^{n-}$, where M is a transition metal such as tungsten ($W^{6+}$) and X the heteroatom (silica or phosphorus). The Keggin anion entails twelve $MO_6$ octahedrons sharing their corners or edges with a central $XO_4$ tetrahedron. The lacunary Keggin type POMs have different number of oxide fragments (Figure 5A). The size of the Keggin type POM atomic cluster is between 1 to 6 nm [111]. When the metal polyanion is in conjunction with a cationic polymer, a POM-IL is formed with two active components (Figure 5B). The cationic polymer can be an organic compound, for example a known bactericidal agent quaternary ammonium [111] or chitosan [112]. Thus, the POM-ILs are zwitterionic surfactants possessing both, anionic and cationic properties and have thus broader chemical diversity, a useful feature for exploitation of these chemicals for antibacterial applications. The POM-ILs can be applied for coating of the interior surfaces or for water purification systems [113].



**A**

$[\alpha\text{-}SiW_{11}O_{39}]^{8-}$

$[\alpha\text{-}SiW_{12}O_{40}]^{4-}$

**B**

# POM-IL

Quaternary
ammonium cation

Polyoxometalate
anion
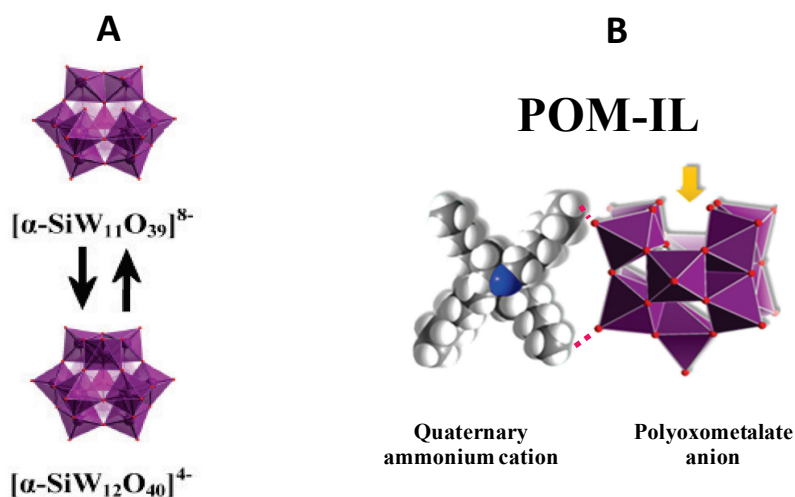
*Figure 5. Structure of a lacunary Keggin type polyoxometalates (POM) employed in this thesis. Example of the formation of lacunary Keggin structure with different number of metal oxide fragments (A). The removal of atoms from the Keggin structure results in elimination of a sufficient number of octahedra. The POM ionic liquids (POM-IL) structure (B). The colours are as follows: Red-oxygen, blue-ammonium, white-carbon, purple-tungsten. The orange arrow indicates the additional binding site of metals. The pink dots represent the hydrogen bonds. The illustration is adapted from Herrmann et al [114].*

### 1.3.2 Toxicity of POM-ILs to bacteria

There are different transient metals used in POM-ILs, mostly tungsten (W), molybdenum (Mo) and vanadium (V). From these POM-ILs, W-based POM-ILs are the most deployed and studied for antibacterial effects [113]. For example, Feng *et al* showed that films with chitosan and W containing POM had no antibacterial effects to *E. coli* [112]. In another study, W containing POMs were more efficient sensitizers of β-lactam antibiotic oxacillin to MRSA *S. aureus* as compared to Mo containing POMs (the growth inhibitory effect from disc diffusion method was seen between 200-12800 mg/L and 800-25600 mg/L respectively) [115]. Also, the POMs with Mo and with W showed a

synergistic antibacterial effect with oxacillin to methicillin resistant *S. aureus*. The susceptibility was seen at the POM 50 µM concentration [116]. Also, 60 µm peptide nanofibers in combination with 26.7 µm POMs containing W showed superior antibacterial effects to *E. coli* compared to either component alone [109].

## 1.4　Safety of metal-based antibacterial compounds

The increasing production of metal-based NPs raises concerns over their toxicity to the environment [66] and the risks to humans [12]. The use of antimicrobial NPs is regulated by the European Commission Biocidal Products Regulation [18]. A separate dossier that meets all data requirements must usually be prepared for nanomaterials as active substances. Currently, a special risk assessment is necessary [117] for nanomaterials used as the active or non-active substances in biocidal products and the label of the biocidal product must contain the name of each nanomaterial containing word "nano".

There are already several implications about the toxic effects of NPs on humans. Depending on the route of exposure, they have toxic effects on lungs, gastro-intestinal tract and on skin [118–120]. For example, aerosols can be deposited in the alveolar and tracheal regions of the lung whereas the deposition localization is dependent on the size and on the agglomeration state of the nanoparticles [119]. The translocation of the inhaled NPs to the system can be via the surface macrophages of the lung alveoli [119]. From the inhalation studies it was shown that up to 10% of 20 nm iridium nanoparticles were translocated to extra-pulmonary organs (including liver, spleen, kidneys) [121]. The testing with the animal models have shown that most of the nanoparticles from the gastrointestinal tract are excreted with faeces [118]. The absorbed NPs, however, are distributed mainly to liver [122]. The adsorption depends on the size, hydrophobicity and the charge of the NPs [123]. Interestingly, there is no data demonstrating a clear nanoparticle transdermal absorption through the intact human skin [118]. When administered intravenously, metal-based NPs can potentially cause systemic damage. Affected organs can be kidneys, liver, heart, muscles, nervous system, hematopoietic organs, lymphatics, lungs [120,124]. For example, $TiO_2$ NPs with the size below 100 nm were administered to rats at 5 mg/kg body weight concentration and showed distribution mostly to liver followed by spleen, lung and kidney [124].

### 1.4.1 *In vitro* mammalian cell models for safety assessment of NPs

The introduction of the 3Rs principle (Replace Reduce Refine) by Russell and Burch in 1959 [125] has taken much attention towards replacing experiments made on laboratory animals with *in vitro* mammalian cell models [125]. In 2010 the European Commission banned the exploitation of animals for safety assessment of cosmetic products [126]. As described by the US National Research Council in the vision of toxicity testing in the 21st century the rising concern for human exposure to environmental chemicals can potentially be managed by assessing the changes in metabolic pathways (so called adverse outcome pathways) in *in vitro* mammalian cell models [127]. With regard to the most optimistic prospective, the use of human cell models instead of animals could enable risk assessment for the toxicity evaluation of the chemicals done in the 21st century largely *in vitro* [128].

The limitations for using *in vitro* models, however, are the possibility of misestimating the exposed dose, the absence of physical barriers and the deviations in the inflammation responses [129,130]. Thus, for more elaborate analysis for biokinetics

and biodistribution, sometimes the entire organ response is necessary. The toxicity evaluation in *in vitro* conditions is relevant for obtaining the first indication of toxicity of multiple compounds. For *in vitro* toxicity testing of chemicals, several mammalian cells are used, either primary cultivated cells from patients or immortalized cells from culture collections (e.g. ATCC) [131]. However, the toxicity assessment of metal-based NPs on human cell models gained attention only recently [132,133]. Metal-based NPs can possess many mechanisms of toxicity. It is known that the NPs` physico-chemical properties such as size, dispersibility and surface charge drive toxic effects on cells, [12,13,134–136]. Additionally, external metal ions or their complexes can replace original metals present in biomolecules and lead to impairment of cellular functions [9]. Such disturbances result in oxidative stress, mitochondrial impairment, modulation of immune responses, changes in receptor and channel functions [137].

In the current thesis, the *in vitro* models for toxicity testing were chosen because (i) epithelium of the skin (represented by HaCaT cell model) and the intestine (Caco-2 cells) are important biological barriers upon organism exposure to NPs; (ii) human THP-1 monocytes are important models for testing the toxicity of immune cells capable of phagocytosis.

**1.4.2 Caco-2 cell line for *in vitro* toxicity testing**

Caco-2 cells are the immortalized colon adenocarcinoma cells that have been widely used in toxicity testing of chemicals. Caco-2 cells are suitable replacement for animals to study intestinal absorption of pharmaceuticals across the small intestine [133]. Caco-2 cells are enterocyte like cells that originate from the epithelial cells of colon. They participate in the formation of intestinal epithelial barrier which also has a function of defence against pathogens. In coculture with lymphocytes, Caco-2 cells can be differentiated into M like cells that are similar to transporting M cells in Peyer`s Patches in the gut [138].

Caco-2 cells form a confluent monolayer and produce mucus when they are stimulated mechanically and cultivated in semi-wet conditions [139]. They can also be used to form human organoids [140]. In toxicity testing, the Caco-2 is a model for toxicity evaluation where it represents the colon epithelial barrier for chemicals. Of concern is the use of Caco-2 cells as models because of the variability of toxicity estimates due to the difference in the conditions for cell culture [141]. The Caco-2 cells have been employed in a nanotoxicology study where the effects of 5 and 30 nm Au NPs on cellular metabolic activity and protein expression were studied [142]. It was shown that the exposition of nanoparticles with different sizes resulted in various profiles of protein expression to the cells (the proteins associated with the morphology and energy were the most affected by smaller NPs) while the expression of metabolites of the exposed cells was not changed.

**1.4.3 HaCaT cell line for *in vitro* toxicity testing**

HaCaT cells are spontaneously transformed human keratinocytes that represent the basal epidermal keratinocytes. In the human skin, keratinocytes are located in the epidermal layer with Merkel cells, Langerhans cells and melanocytes. HaCaT cells have been used to study epidermal homeostasis and pathophysiology of the skin [143]. They can be used as a model to study the pathogenesis of psoriasis, which is a disease characterized by the hyperproliferation of keratinocytes. They can also be used as an *in vitro* model to study the wound healing where they represent the highly proliferative

epidermis [144] or as an *in vitro* model to study the toxic effects of antimicrobial agents on human skin [145]. The spontaneously immortalized HaCaT cell line has been deployed as a keratinocyte model to assess the skin irritation potential of chemicals [146]. The HaCaT cells have been used previously for nanosafety studies to evaluate the toxicity potential of 16 metal oxide nanoparticles to HaCaT cells and to *E. coli* to obtain theoretical descriptors for predicting the toxicity of the compounds depending on their electronic, physical and chemical properties (e.g. quantum-mechanical properties, visual descriptors and periodic table descriptors). Notably, there was a correlation between the toxic effects of *E. coli* bacteria and HaCaT cells [147].

### 1.4.4 THP-1 cell line for *in vitro* toxicity testing

THP-1 monocytes originate from a cell line of acute monocytic leukaemia derived from a small boy. They exhibit monocyte properties and can be induced to macrophage-like cells. THP-1 cells are extensively used in the immunotoxicity evaluation of chemicals [133]. Monocytes in humans are distributed in the body and differentiated to macrophages in target tissues. Macrophages are specialized phagocytosing cells that participate in the native immune responses of an organism. The macrophages phagocytose/digest invaders such as bacteria and viruses. They metabolize the proteins and expose the antigens to immune system on the surface of the cells via HLA-2 receptor [148].

In *in vitro* conditions, the monocyte differentiation to macrophages is initiated with bacterial components or several chemical agents such as polymyristyl-phorbol ester (PMA) [149,150]. In general, macrophages can be classified into M1 type (inflammation promoters), M2 type (adaptive immune response activators with anti-inflammatory potential) or tumour associated macrophages (possessing more immunosuppressive functions) [151]. It has been shown that the higher concentration of PMA (100 ng/mL) causes THP-1 differentiation to more M1 inflammatory type macrophages [150]. THP-1 cells have been used in nanotoxicology studies to evaluate the capability of phagocytosis of the silica and superparamagnetic iron oxide NPs and the modulation of immune responses as a result of the NPs` ingestion [152]. Also, the uptake of NPs by phagocytes and non-phagocytes is important for determining the NPs` toxicity. Firstly, phagocytes can digest the NPs to a larger extent than the non-phagocytic cells [153] and secondly, the toxic effects of the cells can be different for the phagocytosed NPs as compared to the non-phagocytosed NPs. For example, activated phagocytes were involved in the increased cytotoxicity of doxorubicin loaded poly(alkylcyanoacrylate) NPs as determined with the co-cultures of M5076 murine ovarian sarcoma cells and J774.A1 macrophages [154].

### 1.4.5 Safety *versus* toxicity of antibacterial CuO and Ag NPs

The toxicity mechanisms of CuO and Ag NPs relevant for bacteria (chapter 1.3) are also relevant for mammalian cells *in vitro*. In addition, mammalian cells have the capacity for the uptake of NPs that bacterial cells do not pose. The lipid bilayer membrane of mammalian cells is dynamic and has several NP uptake possibilities (Figure 6). The main routes of uptake depend on the origins and differentiation states of the cells and on the physico-chemical properties of NPs. Some possibilities entail phagocytosis (Figure 6A) or endocytosis such as pinocytosis (Figure 6B), through the clathrin-mediated pits (Figure 6C) or through the caveolin rich area (Figure 6D). The clathrin-mediated internalization is the main internalization pathway for smaller NPs (below 100 nm) that

can end up in intracellular vesicles [155]. Essentially, the surface coating could play a role in the choice of the uptake pathways [156]. For example, the attachment of PEG, poloxamer and poloxamine polymers on NPs could prevent phagocytosis by reducing the binding of the proteins on NPs [157]. The surface charge can modulate the uptake of NPs. The negatively charged NPs have been shown to be taken up by the cells more via the clathrin independent pathways and positively charged NPs via the caveolin and clathrin-mediated endocytosis [158]. Also, size of NPs might influence their uptake pathway. It has been postulated that NPs with smaller size (~120 nm) are endocytosed while larger (> 500 nm) are phagocytosed by phagocytic cells (e.g. macrophages) [159,160].
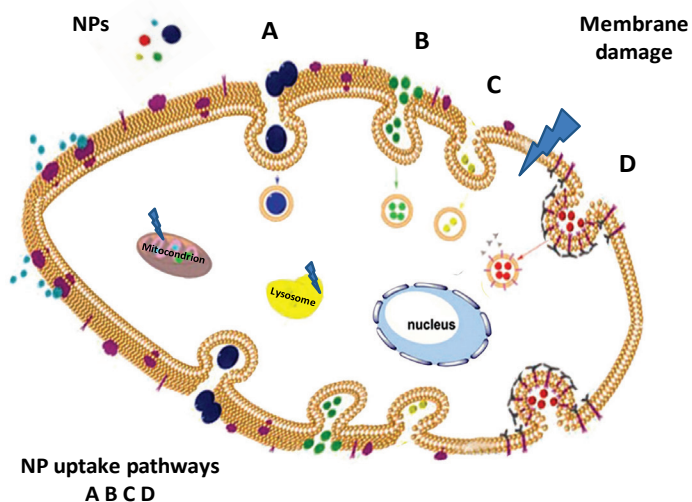


*Figure 6. Possible uptake pathways of NPs in mammalian cells and toxicity. (Modified from Zhao et al [161]). The uptake routes: phagocytosis (A), pinocytosis (B), clathrin-dependent endocytosis (C), caveolae-dependent endocytosis (D).*

In case of mammalian cells that (in contrast to bacteria) have the mechanisms for NPs` uptake, it is suggested that toxicity of CuO and Ag NPs is mainly exerted inside the cells. The release of the metal ions may take place after internalization of the NPs e.g. by a Trojan horse mechanism [130]. For example, the higher dissolution rate of smaller Ag NPs in the lysosomes were involved in the higher toxicity and inflammatory responses of macrophages as compared to their larger counterparts [162]. It has been shown that the total dissolution of internalized CuO takes place inside lysosomal compartments (pH 4.5) [84]. Once dissolved, the Cu can cause proton sponge effect that is characterized by the swelling and rupture of the lysosomes [13]. Additionally, CuO NPs exert ROS-mediated cytotoxicity and DNA damage [94,97,163,164].

# Aims of the study

The main aim of this thesis was to investigate the toxicity of metal-based NPs to find the most effective antibacterial agents among differently sized and coated CuO and Ag NPs and polyoxometalate ionic liquids; to assess the biological safety of CuO NPs on mammalian cell *in vitro* models and to link antibacterial effects and safety of NPs to their physico-chemical properties.

Specific aims were the following:

1) To optimize sonication protocols of CuO NPs for antibacterial efficiency evaluation with *Escherichia coli* and for safety evaluation with Caco-2 cells.

2) To evaluate the effect of size and coating of silver nanoparticles on their antibacterial properties to *Escherichia coli* and *Staphylococcus aureus*.

3) To reveal the effect of variation of the tetraalkylammonium cation chain length on the antibacterial potency of polyoxometalate ionic liquids using three biomedically relevant bacteria: *Escherichia coli*, *Pseudomonas aeruginosa* and *Staphylococcus aureus*.

4) To compare the toxicity of CuO NPs without coating and CuO NPs with different surface functionalizations on *Escherichia coli* bacteria, on differentiated THP-1 macrophages and on HaCaT keratinocytes *in vitro*.

# 2 Materials and methods

The work was done at the National Institute of Chemical Physics and Biophysics at the Laboratory of Environmental Toxicology in collaboration with the Institute of Materials Science of Aragón (ICMA) and the Croatian Institute of Transfusion Medicine (CITM). Prior to the biological testing of the NPs, the physico-chemical characterization was done by measuring the NPs` hydrodynamic size ($D_h$) in DI water, surface charge (zeta-potential) in DI water and in organic-rich test media, polydispersity index (PDI) and metal content. Additionally, dissolution and bioavailable fraction of CuO NPs and Ag NPs were quantified using elemental analysis or bacterial biosensors, respectively (Figure 7).

The antibacterial potency of Ag NPs was evaluated with Gram-positive bacteria *S. aureus* and Gram-negative bacteria *E. coli* and *P. aeruginosa*. The antibacterial properties and the safety of CuO NPs with different functionalizations were investigated with toxicologically relevant *in vitro* test models representing the gastrointestinal barriers (Caco-2 epithelial cells), the skin barriers (HaCaT keratinocytes) and the immune responses (differentiated THP-1 macrophages). Additionally, mechanistic studies were applied (e.g. the ROS measurements in abiotic conditions and the immune responses of dTHP-1 cells).
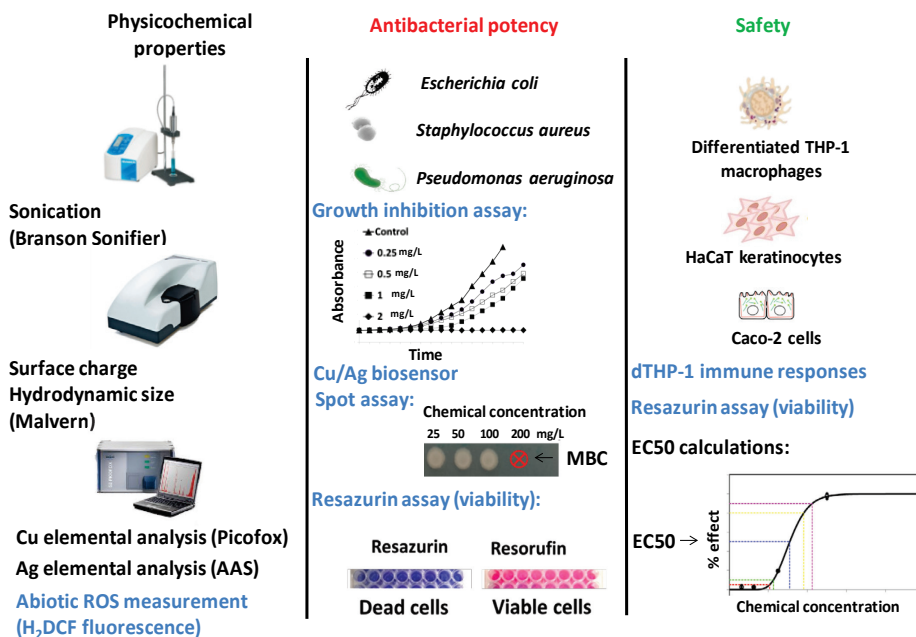


*Figure 7. A scheme of materials and methods in the study.*

## 2.1 Physico-chemical characteristics of metal-based NPs and POM-ILs

### 2.1.1 CuO NPs

The Cu compounds used in the study are summarized in Table 1. The CuO NPs were from Sigma Aldrich (CuO S, CAS Number 1317-38-0) and from Intrinsiq Materials (CuO I). The NPs were provided within the EU FP7 flagship project NANOVALID (particle code: NNV-011). The CuO P, CuO-NH$_2$, CuO-COOH and CuO-PEG were a gift from project partners (Prof. Bengt Fadeel, Karolinska Institutet, Sweden) in the FP7 funded project Nanosolutions. All the CuO NPs and CuSO$_4$ provided were powders.

Table 1. CuO NPs and CuSO$_4$ metal salt employed in the study. The number before the metal component in the "primary size" column indicates the primary size of the nano (n) compound.

| Designation of the compound | Primary size, nm | Organic coating | Origin | Bacterial strain for antibacterial efficiency evaluation | Biological safety testing on cell lines | Publication |
|---|---|---|---|---|---|---|
| **CuO S** | 30nCuO$^{\pm}$ | - | Sigma-Aldrich | *E. coli* MC1061 (pSLCueR/pDNcopAlux) | Caco-2 | I |
| **CuO I** | 25nCuO$^{\dagger}$ | - | Intrinsiq Materials | *E. coli* MC1061 (pSLCueR/pDNcopAlux) | Caco-2 | I |
| **CuO P** | 18nCuO$^{¥}$ | - | Nano Solutions | *E. coli* MG1655 | THP-1, HaCaT | manuscrip$^{\ddagger}$ |
| **CuO-NH$_2$** | 9nCuO$^{¥}$ | amine | Nano Solutions | *E. coli* MG1655 | THP-1, HaCaT | manuscript |
| **CuO-COOH** | 8nCuO$^{¥}$ | carboxyl | Nano Solutions | *E. coli* MG1655 | THP-1, HaCaT | manuscript |
| **CuO-PEG** | 7nCuO$^{¥}$ | polyethylene glycol | Nano Solutions | *E. coli* MG1655 | THP-1, HaCaT | manuscript |
| **CuSO$_4$** | CuSO$_4$ | - | Alfa Aesar | *E. coli* MG1655 | THP-1, HaCaT, Caco-2 | manuscript |

The primary sizes were determined by: ± - Ivask *et al* [91], † - Bondarenko *et al* [165], ¥ - Zhang *et al* [163] ‡- manuscript in preparation.

For preparing the dispersions of NPs, one approach is to sonicate the NPs in water and to make the subsequent dilutions in test media. The other approach is to sonicate and dilute the solutions directly in the test media [48,53]. Different studies use different protocols that may produce inconsistencies in toxicity data. The CuO I and CuO S NPs stock suspensions in the current thesis were done at 1000 mg Cu/L in DI water (the weight of the NPs was adjusted with regard to the Cu content), LB or MEM applying different approaches as follows: (i) no sonication, (ii) bath sonication and (iii) probe sonication (with the delivered acoustic energy Espec = 5.3 * 10$^4$ kJ/m$^3$ and Espec =6 * 10$^5$ kJ/m$^3$). Uncoated CuO P or CuO-NH$_2$, CuO-COOH and CuO-PEG NP suspensions were prepared at concentrations 1000-2000 mg/L weight volume in DI water using probe sonication (Espec = 3.9 * 10$^5$ kJ/m$^3$).

Measurements of D$_h$ and PDI with the DLS method and zeta-potential with the electrophoretic light scattering method were carried out with Zetasizer Nano ZS (Malvern, UK) immediately after preparation of the working solutions (more

information in publications I, II and manuscript). Cu content was measured with total X-ray fluorescence (Picofox) whereas the Cu content of dissolved NPs was measured between 0- and 24-hours (publication I and manuscript).

**2.1.2 Ag NPs**

A panel of Ag NPs with two sizes and with six coatings rendering NPs with different charges were studied. The Ag NPs of 10 nm and 50 nm were synthesized at the Croatian Institute of Transfusion Medicine (CITM) and are summarized in Table 2 (more detailed information about the synthesis is in publication II Supplementary Material). Briefly, the synthesis of differently coated Ag NPs was done using the following coating agents: trisodium citrate dihydrate (CIT), sodium bis(2-ethylhexyl) sulfosuccinate (AOT), cetyltrimethyl-ammonium bromide (CTAB), poly(vinylpyrrolidone) (PVP), polysorbate 80 (Tween 80). Poly-l-lysine (PLL) was used as a coating material only on the 10 nm Ag NPs. Additionally, the pure coating agents were separately tested for antibacterial potency (Table 2).

The primary size, $D_h$, PDI, Ag content of the NPs and zeta-potential as well as the dissolved part of the NPs were estimated by our collaboration partners at the CITM (more information in publication II). The stability of Ag NP suspensions in test conditions was assessed by UV-vis spectroscopy.

*Table 2. Ag NPs, soluble AgNO$_3$ and pure capping agents employed in the study. The number before the metal component indicates the primary size of the nano (n) compound.*

| Designation of the compound | Primary size, NP | Organic coating | Origin | Antibacterial efficiency evaluation on bacteria | Publication |
|---|---|---|---|---|---|
| **10nAg-CIT** | 10nAg$^0$ | citrate | CITM | *E. coli* MG1655 *S. aureus* 6538 | II |
| **10nAg-PVP** | 10nAg$^0$ | poly-vinylpyrrolidone | CITM | *E. coli* MG1655 *S. aureus* 6538 | II |
| **10nAg-AOT** | 10nAg$^0$ | bis-2-ethylhexyl sulfosuccinate | CITM | *E. coli* MG1655 *S. aureus* 6538 | II |
| **10nAg-Tween 80** | 10nAg$^0$ | polysorbate 80 | CITM | *E. coli* MG1655 *S. aureus* 6538 | II |
| **10nAg-CTAB** | 10nAg$^0$ | cetyltrimethyl-ammonium bromide | CITM | *E. coli* MG1655 *S. aureus* 6538 | II |
| **10nAg-PLL** | 10nAg$^0$ | poly-l-lysine | CITM | *E. coli* MG1655 *S. aureus* 6538 | II |
| **50nAg-CIT** | 50nAg$^0$ | citrate | CITM | *E. coli* MG1655 *S. aureus* 6538 | II |
| **50nAg-PVP** | 50nAg$^0$ | poly-vinylpyrrolidone | CITM | *E. coli* MG1655 *S. aureus* 6538 | II |
| **50nAg-AOT** | 50nAg$^0$ | bis-2-ethylhexyl sulfosuccinate | CITM | *E. coli* MG1655 *S. aureus* 6538 | II |
| **50nAg-Tween 80** | 50nAg$^0$ | polysorbate 80 | CITM | *E. coli* MG1655 *S. aureus* 6538 | II |
| **50nAg-CTAB** | 50nAg$^0$ | cetyltrimethyl-ammonium bromide | CITM | *E. coli* MG1655 *S. aureus* 6538 | II |
| **AgNO$_3$** | AgNO$_3$ | - | J.T. Baker | *E. coli* MG1655 *S. aureus* 6538 | II |
| **CIT** | - | citrate | Sigma-Aldrich | *E. coli* MG1655 *S. aureus* 6538 | II |
| **PVP** | - | poly-vinylpyrrolidone | Sigma-Aldrich | *E. coli* MG1655 *S. aureus* 6538 | II |
| **AOT** | - | bis-2-ethylhexyl sulfosuccinate | Sigma-Aldrich | *E. coli* MG1655 *S. aureus* 6538 | II |
| **Tween 80** | - | polysorbate 80 | Sigma-Aldrich | *E. coli* MG1655 *S. aureus* 6538 | II |
| **CTAB** | - | cetyltrimethyl-ammonium bromide | Sigma-Aldrich | *E. coli* MG1655 *S. aureus* 6538 | II |
| **PLL** | - | poly-l-lysine | Sigma-Aldrich | *E. coli* MG1655 *S. aureus* 6538 | II |

### 2.1.3 POM-ILs

The prototype POM-ILs ($Q^x$-IL) that feature Keggin-type anions $[\alpha\text{-}SiW_{11}O_{39}]^{8-}$ and quaternary ammonium cations ($Q^x$) as active cationic species were synthesized and characterized at the Institute of Materials Science of Aragón (ICMA) (Table 3). The binding of the POMs was confirmed by elemental analysis and the purity was determined by the FT-IR spectroscopy (Publication III, Supplementary Material).

For antibacterial testing, the respective compounds and benzalkonium chloride (BAC) were used as a positive control. The BAC was dissolved in dimethyl sulfoxide (DMSO) at 100 g/L concentration followed by sequential dilutions into half strength cation ($Ca^{2+}$ 25 mg/L/$Mg^{2+}$ 12.5 mg/L) adjusted Mueller Hinton Broth (CA-MHB). The samples were poorly dissolved at higher concentrations and further incubation at 37 °C overnight with shaking at 200 rpm was done.

*Table 3. POM-ILs ($Q^x$-IL, x=C= 6, 7, 8), corresponding salts ($Q^x$-Br, x=C= 6, 7, 8) to organic components and a positive control benzalkonium chloride (BAC) used in the study. x and C designate the carbon in the carbon chain of different alkyl chain lengths of quaternary ammonium cations.*

| Nomination of the compound | Metal component | Organic component with different carbon chain lengths | Origin | Antibacterial efficiency evaluation on bacteria | Publication |
|---|---|---|---|---|---|
| **$Q^6$-IL** | POM | quaternary ammonium C=6 | ICMA | *E. coli* MG1655<br>*S. aureus* RN4220<br>*P. aeruginosa* DS10–129 | III |
| **$Q^7$-IL** | POM | quaternary ammonium C=7 | ICMA | *E. coli* MG1655<br>*S. aureus* RN4220<br>*P. aeruginosa* DS10–129 | III |
| **$Q^8$-IL** | POM | quaternary ammonium C=8 | ICMA | *E. coli* MG1655<br>*S. aureus* RN4220<br>*P. aeruginosa* DS10–129 | III |
| **$Q^6$-Br** | - | quaternary ammonium bromide salt C=6 | ICMA | *E. coli* MG1655<br>*S. aureus* RN4220<br>*P. aeruginosa* DS10–129 | III |
| **$Q^7$-Br** | - | quaternary ammonium bromide salt C=7 | ICMA | *E. coli* MG1655<br>*S. aureus* RN4220<br>*P. aeruginosa* DS10–129 | III |
| **$Q^8$-Br** | - | quaternary ammonium bromide salt C=8 | ICMA | *E. coli* MG1655<br>*S. aureus* RN4220<br>*P. aeruginosa* DS10–129 | III |
| **BAC** | - | benzalkonium chloride | Appli Chem | *E. coli* MG1655<br>*S. aureus* RN4220<br>*P. aeruginosa* DS10–129 | III |

## 2.2 Antibacterial properties of metal-based NPs and POM-ILs

For evaluating bacterial susceptibility to the toxicants, several assays were deployed: Spot assay, Growth inhibition assay and Resazurin assay (viability). Additionally, the recombinant bioluminescent bacteria that produce light in the presence of intracellular metal were used for bioavailable metal quantification in Ag and CuO NP suspensions (publications I, II, manuscript).

### 2.2.1 Biosensor for intracellular Ag and Cu measurement

Genetically modified recombinant sensor bacteria are tools that enable to track toxicants such as genotoxic agents from the water [166] or heavy metals from the soil [167]. The whole cell bioengineered bacterial sensors that are modified to express luminescence encoding genes in the presence of e.g. bioavailable metals are described by Ivask *et al* [168].

Quantification of bioavailable silver and copper in the NP test suspensions was performed using recombinant luminescent sensor bacteria that respond dose-dependently to Ag and Cu that have entered the bacterial cells and that is measured by the increased bioluminescence with a luminometer (Figure 8). In parallel, constitutively luminescent bacteria *E. coli* MC1061 (pDNlux) were measured for luminescence. The results were calculated by dividing the induced bioluminescence from the Ag and CuO NP dispersions with a background bioluminescence and are presented in relative light units (RLUs) whereas the corresponding metal salts were considered as 100% soluble to normalise the measurement data.

Ag and Cu ions are transported and detoxified via similar pathways in *E. coli* [169]. CueR is a biological recognition element that activates a cascade of resistance systems in *E. coli* in response to Cu or Ag [8,77]. In the current thesis, the recombinant *E. coli* MC1061 bacterium (pSLcueR/pDNPcopAlux) was used to determine the intracellular concentration of Ag and Cu (publications I, II and manuscript). The essence of biosensors is that they provide quantitative analytical information in response to the external source [168]. The luminescence induction of the recombinant *E. coli* MC1061 to intracellular Ag is mediated via CueR activator protein and is regulated by CopA promoter (responsible for transcription of CopA ATPase that enables the transport of respective metal ions between the cytosol and periplasm [170]). The CopA promoter was inserted to the luxCDABE gene cluster, resulting in a construct that produced luminescence in response to bioavailable Ag and Cu (Figure 8) [171].
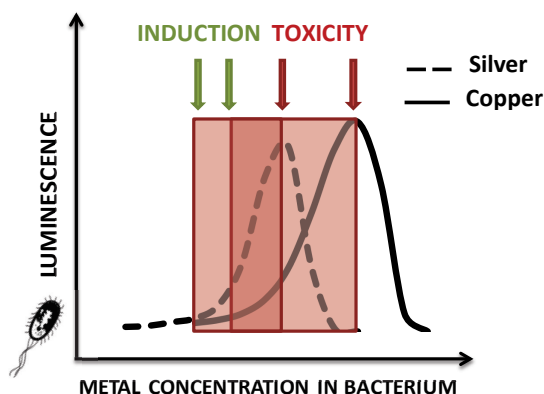
*Figure 8. Luminescence induction curves in response to bioavailable silver and copper inside the recombinant bacteria.*

## 2.3 Assays for antibacterial potency evaluation

The antibacterial potency of CuO I and CuO S NPs towards *E. coli* was assessed using a 2-h Spot assay that was developed by Kasemets *et al* [172] and by Suppi *et al* [173] (publication I). Briefly, the *E. coli* were grown into exponential phase and $10^6$ CFU/ml bacteria were exposed to the serial dilutions of test chemicals for 2 hours in DI water in the wells of 96-well polystyrene plates. 3 µl of the suspensions of the exposed bacteria were delivered to the toxicant-free agar plates and incubated for 24 h at 30° C. The minimal bactericidal concentration (MBC) was considered the first concentration of a toxicant that totally inhibited the growth of bacteria on the agar plates (Figure 7).

The antibacterial potency of Ag NPs (publication II) was evaluated on a 4-h and on a 24-h Spot assays deploying a similar method as described above. 4-h or 24-h exposures of *E. coli* and *S. aureus* to the Ag NPs were done in DI water to avoid the effects of complexation on the bioavailability of the NPs.

CuO P, CuO-COOH, CuO-NH$_2$ and CuO-PEG NPs were studied for antibacterial potency against *E. coli* using a 24-h Resazurin assay (manuscript). The test compounds were exposed to bacteria (prepared as described in ISO 20776-1:2006 [174]) for 24 hours in RPMI-1640 containing cell culture complete medium (CCM) supplemented with 10% fetal bovine serum (FBS). The resazurin was added to the cells. The viability indicator dye blue resazurin is reduced to pink resorufin in the respiration process of viable cells. The fluorescence intensity of treated and untreated samples was registered and used for viability (presented as % of live cells) and subsequently 50% effective dose (EC50) calculations (Figure 7).

Antibacterial potency of Q$^x$-Br and Q$^x$-IL and BAC were studied using a standard broth microdilution method as described in ISO 20776-1:2006 [174] (publication III). The *E. coli*, *S. aureus* and *P. aeruginosa* bacteria were exposed to the respective compounds in cation adjusted Mueller Hinton Broth (CA-MHB) supplemented with 1 vol-% of DMSO. The 1 % DMSO was not toxic to bacteria (data not shown). Bacterial growth was followed by the increase of absorbance at 600 nm registered after every 15 min (Figure 7). Based on the growth inhibition data, EC50 values were calculated. Also, the 20-h Spot assay on CA-MHB agar plates was deployed to determine MBC values. The antibacterial assays used in the study are summarized in Figure 9.

## 2.4 Safety of CuO NPs

For safety/toxicity analysis *in vitro*, three cell lines were used in this study: two human epithelial cell lines (Caco-2 and HaCaT) and one immune cell line (THP-1). All the cells were obtained from American Type Culture Collection (ATCC) and the cell culture was maintained according to ATCC guidance. Cells were grown on tissue culture treated plates at 37 °C in the air-jacketed incubator in the presence of 95% humidity and 5% $CO_2$.

In publication I, the toxicity of CuO I and CuO S NPs dispersed in different test media was measured with Caco-2 cells using Resazurin assay (Figure 9). The cells were seeded in Modified Eagles Medium (MEM) containing cell culture medium supplemented with 10% FBS. MEM is a basal medium often deployed in *in vitro* tissue culture studies [175]. The exposure to test chemicals was done for 24 h. Cells were washed and resazurin was added in the test medium. The fluorescence intensity was used for EC50 calculations.

The CuO P, CuO-$NH_2$, CuO-COOH and CuO-PEG NPs with $CuSO_4$ as a control were estimated for safety with HaCaT keratinocytes and differentiated THP-1 macrophages (dTHP-1) in Dulbecco's modification of Eagle medium (DMEM) supplemented with 10% FBS (manuscript). The substances were exposed to the cells for 24 h. Cells were washed, and the viability was assessed with resazurin in CCM. The fluorescence was measured, and the viability was calculated as described in publication I and manuscript.

CuO P, CuO-$NH_2$, CuO-COOH and CuO-PEG NPs with $CuSO_4$ as a soluble control were studied for safety also with dTHP-1 macrophages. THP-1 monocytes were differentiated in CCM containing RPMI-1640 supplemented with 10% FBS and 100 ng/mL PMA for 72 h achieving dTHP-1 macrophages. For viability estimation, the cells were exposed to Cu compounds for 24 h followed by addition of resazurin for 2 h. Alternatively, the supernatants from the cells influenced with 100 mg/L Cu compound suspensions were collected and quantified for the presence of TNF-α by enzyme linked immunosorbent assay (ELISA). The conditions for safety and TNF-α production evaluation are summarized in Figure 9 and more information can be found in manuscript.

## 2.5 Statistical analysis of the results

The 50% and the 20% effective concentration values (EC50 and EC20 respectively, mg/L) with 95% confidence intervals were calculated from dose-response data using MS Excel macro Regtox (http://www.normalesup.org/~vindimian/en_download.html) using optimal EC50 values obtained from the least squares best fit transformation of the data. The statistical significance between the EC values was calculated with equal variances at $p < 0.05$.

The analysis of variance between different groups (one-way ANOVA followed by a Tukey's honest significant difference post-hoc test) was done with R Language and Environment for Statistical Computing (http:// www.R-project.org).

Bioinformatics analysis of the toxic effects of CuO NPs to *E. coli*, HaCaT and dTHP-1 macrophages was done using the R Language and Environment for Statistical Computing and described by Jolliffe *et al* [176] whereas the principal component analysis (PCA) and an eigenvector analysis were implemented. The PCA was done to obtain an estimation of the multiple parameters that contributed to the variability of the toxic effects of CuO P, CuO-COOH, CuO-$NH_2$ and CuO-PEG NPs on different cells. In the analysis, the average EC50 values from the viability data were used (more information can be found in manuscript).
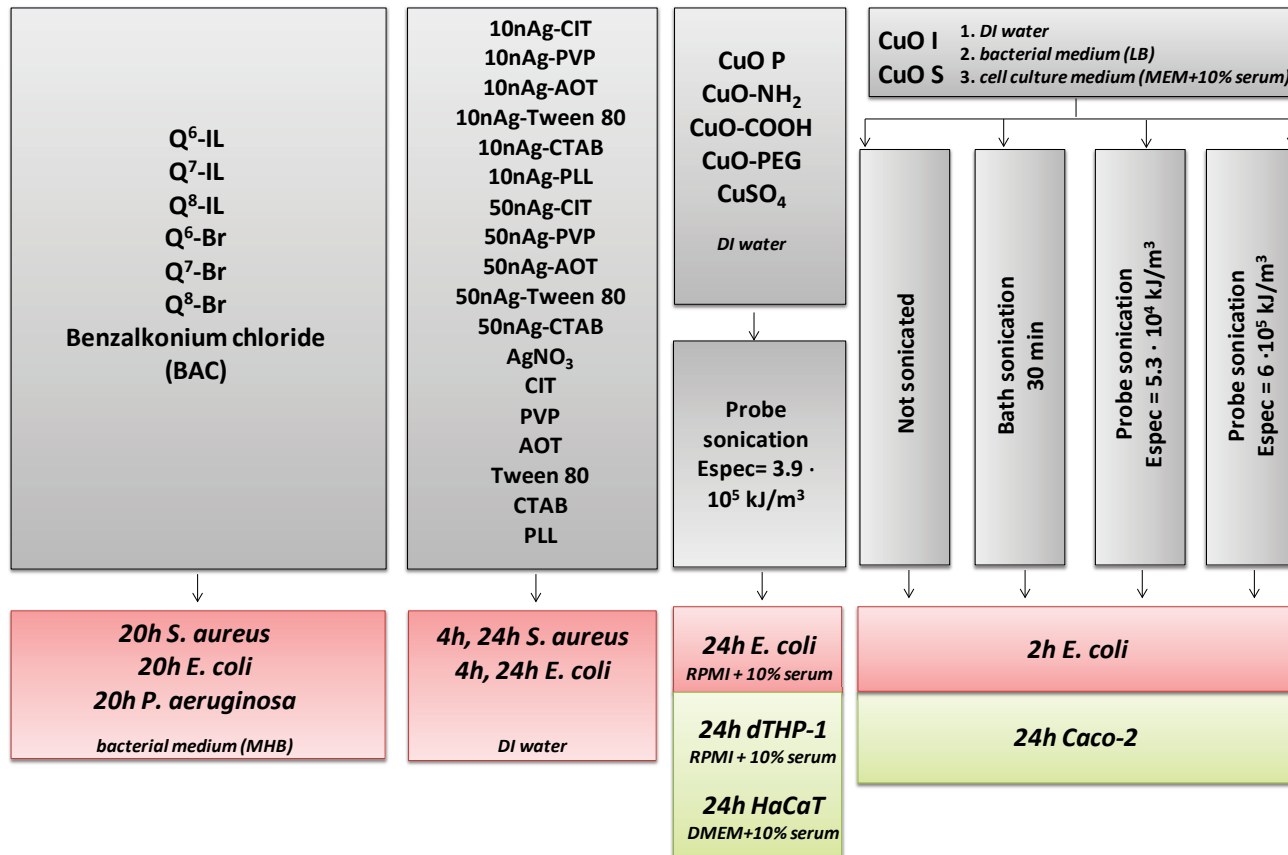
*Figure 9. Schematic representation of tests for evaluating physico-chemical properties (grey boxes), antibacterial potency (red boxes) and safety (green boxes) of chemicals in the study.*

# 3 Results and discussion

## 3.1 The physico-chemical characteristics of NPs

In the first part of the work (publication I), the sonication protocols for the dispersion of NPs were optimized for toxicity testing. The suspensions of uncoated CuO NPs of two origins (Sigma Aldrich and Intrinsiq Materials) were prepared without sonication or via bath sonication for 30 min or via different intensities of probe sonication corresponding to Espec = 5.3 * $10^4$ kJ/m$^3$ and Espec =6 * $10^5$ kJ/m$^3$. The sonication energy was chosen based on previous studies in nanotoxicology and the sonication efficiency was evaluated by the estimation of the polydispersity of the NP samples (expressed as polydispersity index, pdi) [48–50,177]. The suspensions were employed for antibacterial potency and for safety evaluations. Sonication was carried out in three testing environments: DI water, bacterial LB growth medium and MEM (Figure 9). The bioavailable Cu measurement was determined in LB bacterial growth medium. As shown in Figure 10B, the fraction of internalized ions increased with the increasing intensity of sonication energy confirming that the dissolution of CuO NPs is related to sonication intensity. The dissolution analysis of CuO in LB in abiotic conditions was in accordance with the bioavailability study showing higher bioavailability of NPs dispersed with higher sonication energy (Figure 10C).

The sonication in MEM medium supplemented with 10 % serum followed by viability assessment indicated that the toxicity to Caco-2 cells was substantially increased with sonicated NPs (Figure 10D). Also, the dissolution increased, and $D_h$ decreased for NPs that were dispersed by sonication in MEM compared to unsonicated samples (Figure 10A, C) showing the relevance of deploying sonication energy for preparation of suspensions of NPs.

The sonication facilitates the dispersion of NPs by decreasing the agglomeration of NPs [178]. The sonication in water environment did not substantially increase the dissolution of the NPs. Also, different parameters used for CuO NPs in water environment did not result in differences in toxicity to bacteria (the 2-h MBCs of sonicated and unsonicated CuO NPs in DI water were between 14-16 mg Cu/L, publication I). Also, the dissolution of the NPs in DI water in abiotic conditions was not different suggesting that the toxicity of CuO NPs is related to the dissolution of the CuO NPs and is not changed by applying sonication energy in DI water. There was no substantial difference between the behaviour of CuO NPs (antibacterial effects, toxicity) from various sources (Sigma Aldrich vs Intrinsiq Materials) (Figure 10B).

Relying on the observations that the dissolution behaviour was stable for particles dispersed in DI water, it was concluded that the stock suspensions should be made in DI water followed by dissolution in test media. This knowledge was used for subsequent analysis of CuO NPs` toxic effects.
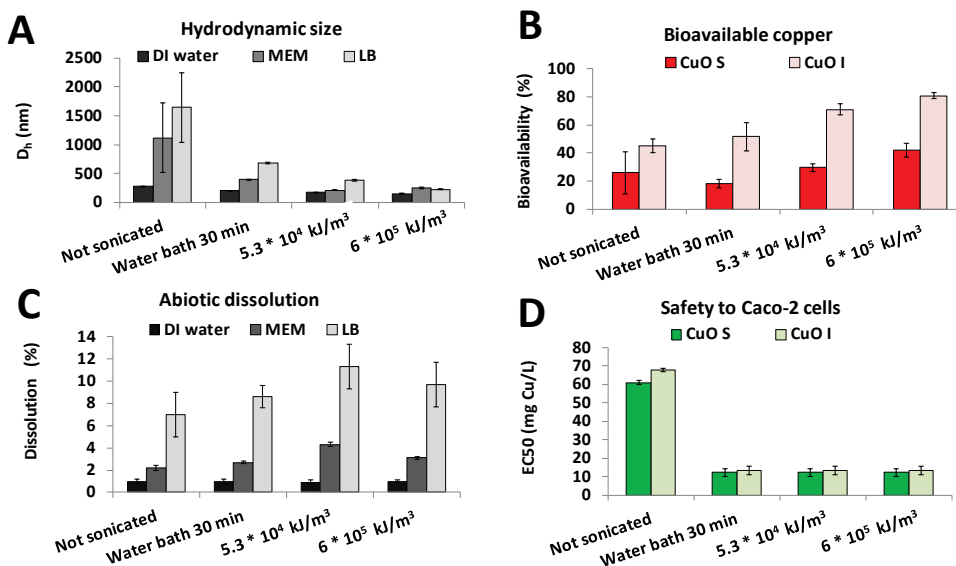
*Figure 10. Influence of sonication energy on CuO NPs physico-chemical properties and toxic effects. 0-h hydrodynamic size (A); 2-h bioavailable copper in recombinant* E. coli *bacterium (B); 0-h abiotic dissolution (C); and toxicity (EC50 mg Cu/l) of uncoated CuO NPs to Caco-2 cells (D). Hydrodynamic size ($D_h$) and abiotic dissolution were measured in three media: DI water, cell culture medium (MEM+10% serum) and bacterial growth medium LB. Error bars are the standard deviations of the three experiments with at least two technical replicates (publication I).*

### 3.1.1 The physico-chemical characteristics of CuO and Ag NPs

Next, a panel of 10 and 50 nm Ag NPs with coatings rendering positively or negatively charged NPs was investigated. The exposure of the Ag NPs to bacteria was carried out in DI water to decrease the possibility of interference by the components of the organic-rich test media [129]. Prior to toxicity evaluation, the physico-chemical properties of Ag NPs were characterized revealing that there was a clear difference between the two groups of Ag NPs: a group with primary sizes $D_h$ 6-17 nm (the average around 10 nm) and a group with primary sizes $D_h$ 33-59 nm (the average around 50 nm) (Figure 11A and Table 2 in publication II). The Ag NPs with PLL and CTAB coatings were positively charged whereas the other coating agents on NPs resulted in negative or neutral zeta-potentials (Figure 11C).

The stability of the Ag NPs was measured in testing conditions using the UV-vis method. The Ag NPs, indeed, were stable for 24 hours with the exception of 50 nm CTAB that tended to form aggregates and sedimented to the bottom of the vials (the forming of aggregates was confirmed by visual inspection and by decreased Ag characteristic peak of dispersed Ag NPs in the UV-vis measurements, Figure 12).

The CuO P, CuO-NH$_2$ were positively charged and the CuO-COOH and CuO-PEG negatively charged in DI water (Figure 11C). The surface charge was evenly negative for all the test compounds in the cell culture medium (Figure 11C, the insert) that might be due to the formation of a protein corona on the surface of NPs [179,180].
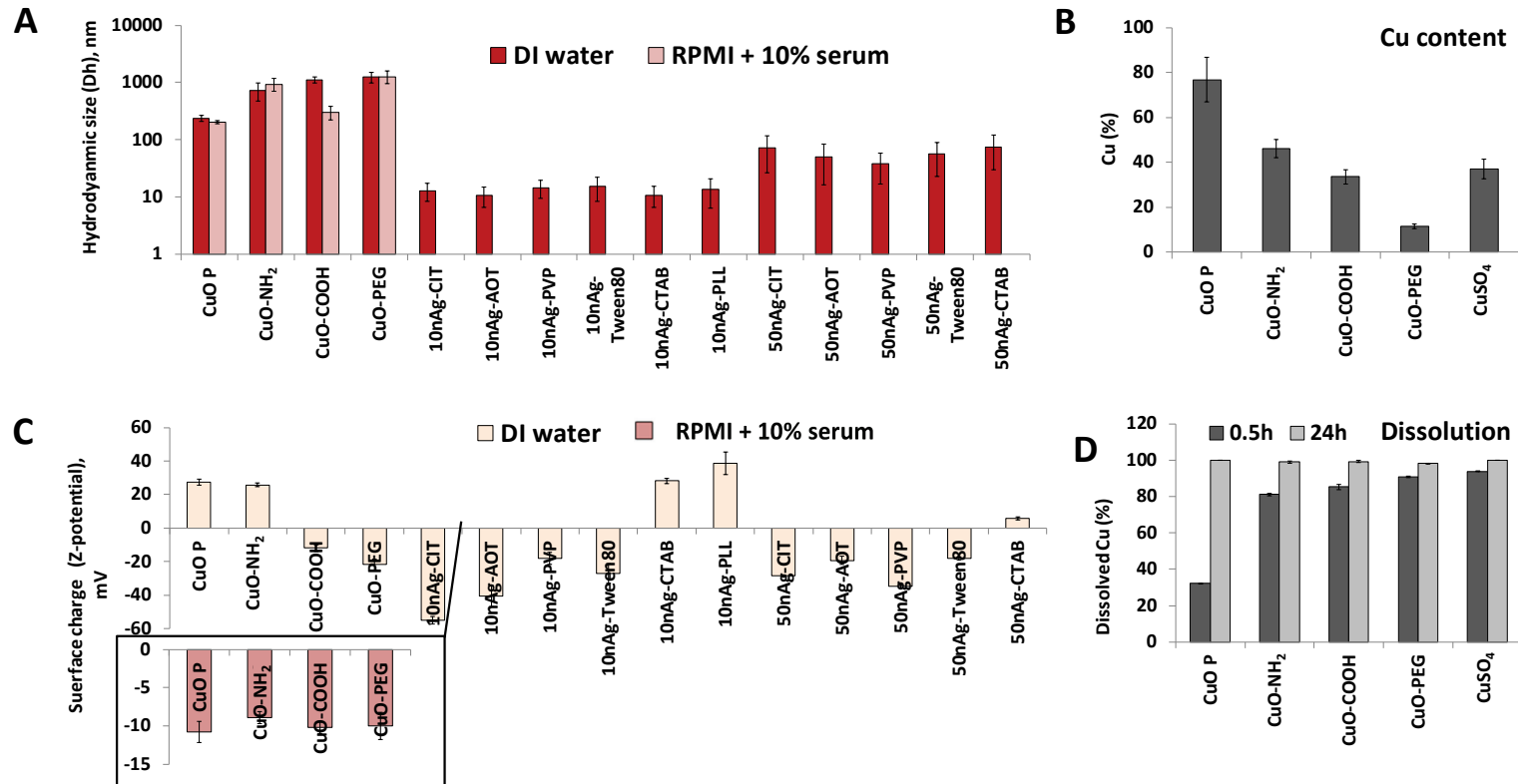
*Figure 11. Physico-chemical properties of CuO P, CuO-NH$_2$, CuO-COOH, CuO-PEG NPs and Ag NPs with different coatings measured in DI water and in cell culture medium (RPMI +10% FBS). Hydrodynamic size (D$_h$; please note the logarithmic scale) (A), Cu content of NPs (B), surface charge (zeta-potential) (C), and 0.5h and 24-h dissolution (D). The Ag NPs were evaluated for hydrodynamic size with a Malvern Z-sizer in bimodal mode (larger fraction is presented). The CuO NPs hydrodynamic size was evaluated in monomodal mode. Data from publications I, II and from manuscript.*
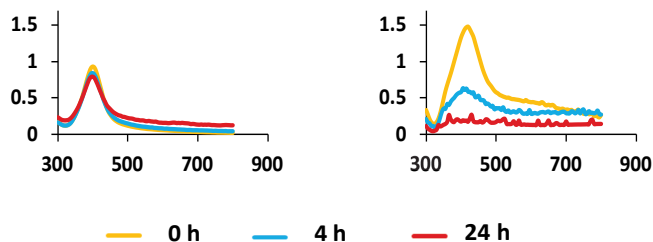
*Figure 12. An example of UV-vis spectra of 10 nm CTAB coated Ag NPs as compared to 50 nm CTAB Ag NPs at 10 mg Ag/mL concentration (publication II). On the diagram are the absorbance values derived from the scanning from 300 to 700 nm with a 10 nm gap at 0 h, 4-h and 24-h time points. The curves represent the average values from three experiments with two replicates. Ag peaks are 390–395 nm and 400–440 nm for 10 nm and 50 nm Ag NPs respectively.*

## 3.2 The antimicrobial potency of CuO, Ag NPs and POM-ILs

A panel of above-described Ag NPs and CuO NPs and POM-ILs were subsequently used to study toxic effects of these compounds on Gram-positive and Gram-negative bacteria. Table 4 summarizes the results of most of the antibacterial tests conducted in this thesis (publications II, III, manuscript). In the current thesis, different test media were used for toxicity assessment of CuO NPs, POM-ILs and Ag NPs. Organic-rich test media, for example, were used for testing of POM-ILs and DI water was used for testing of Ag NPs and of CuO NPs.

The Ag-based NPs were the most toxic of the tested compounds in our conditions. These results are partly in accordance with previously published data where out of NPs consisting from three metals (CuO, ZnO and Ag), the Ag NPs proved to be the most toxic to bacteria despite of the differences in test media components [76].

The Gram-positive *S. aureus* and the Gram-negative *E. coli* and *P. aeruginosa* were chosen as the main bacterial models because they are important causes of HAIs [5]. Ag NPs were most toxic to *E. coli* (Table 4). Overall, the toxicity of Ag NPs to *E. coli* was higher than to *S. aureus* (Table 4). Also, the 24-h MBC of AgNO$_3$ was 0.02 mg Ag/L to *E. coli* and 0.1 mg Ag/L to *S. aureus* showing results that are in agreement with previously published data using similar test format [173]. The difference between the susceptibilities of the test bacteria might rely on the cell wall composition. The Gram-negative bacteria have an outer layer of membrane and the cell wall with peptidoglycan only 3 nm thick. In the Gram-positive bacteria the peptidoglycan layer is 30 nm thick [181,182] that most probably impairs the passage of the toxic Ag ions through. The lower sensitivity of Gram-positive *S. aureus* has been confirmed by previous studies [181,183,184]. The higher leakage of proteins through the membranes of Gram-negative bacteria treated with Ag NPs have been shown by Kim *et al* [184]. The differences in the toxicity mechanisms of CuO and Ag NPs may relay in the destabilization of the Gram-negative and the Gram-positive bacterial membranes and the influence on the integrated membrane transportation systems for the metals. The outer membrane of Gram-negative bacteria contains selective and unselective porins that could be responsible for the transportation of smaller nanoparticles and metal ions. The Gram-positive bacteria contain similar membrane porins [104,185]. Also, the transporters are important in determining the passage of the metals through.

The metal ions can be internalised by unspecific routes to the cells, along the chemiosmotic gradient or via the inducible energy demanding routes that are necessary for their metabolic activity in a special situation such as e.g. starvation. In high concentrations of metal ions (e.g. Cu and Ag), the passage can be more unspecific. Additionally, in Gram-negative bacteria, the Cu is transported to the cytoplasm with CopA, CopC and CopD proteins [186][187]. In the Gram-positive bacteria the CopA and CopB ATPases are responsible for Cu metabolism. The first is for the uptake of metal in cytoplasm and the latter for efflux and detoxification. Silver has similar pathways as Cu in bacterial metabolism in Gram-positive bacteria mediated by P-type ATPases. Interestingly, however, the Gram-negative bacteria are more prone to develop resistance against Ag [188].

Table 4. Toxicity of the test compounds to the bacteria. The MBC values of Ag NPs and pure coating materials are averages from three to five experiments. The MBC values of different carbon chain lengths POM-ILs ($Q^x$-IL), corresponding salts ($Q^x$-Br) and CuO NPs are most representative values from parallel experiments. The red colour shows the lower, and the green colour the higher MBC values that correspond to more toxic and less toxic compounds respectively; the grey colour indicates the MBC values for the compounds that were not toxic at the tested concentrations. The data is summarized from publications II, III and manuscript.

| | | | TOXICITY (MBC) | | | | |
| | | | E. coli | | P. aeruginosa | S. aureus | |
| Compound | Test medium | MBC unit | 20h | 24h | 20h | 20h | 24h |
|---|---|---|---|---|---|---|---|
| CuO P | CCM | mg Cu/L | - | 72.2 | - | - | - |
| CuO-NH$_2$ | CCM | mg Cu/L | - | 9.7 | - | - | - |
| CuO-COOH | CCM | mg Cu/L | - | 49 | - | - | - |
| CuO-PEG | CCM | mg Cu/L | - | >35.4 | - | - | - |
| CuSO$_4$ | CCM | mg Cu/L | - | 66.6 | - | - | - |
| 10nAg-CIT | DI water | mg Ag/L | - | 0.1 | - | - | 0.4 |
| 10nAg-AOT | DI water | mg Ag/L | - | 0.1 | - | - | 0.2 |
| 10nAg-PVP | DI water | mg Ag/L | - | 0.1 | - | - | 0.3 |
| 10nAg-Tween 80 | DI water | mg Ag/L | - | 0.3 | - | - | 0.9 |
| 10nAg-CTAB | DI water | mg Ag/L | - | 0.1 | - | - | 0.5 |
| 10nAg-PLL | DI water | mg Ag/L | - | 0.1 | - | - | 0.4 |
| 50nAg-CIT | DI water | mg Ag/L | - | 0.2 | - | - | 0.6 |
| 50nAg-AOT | DI water | mg Ag/L | - | 0.3 | - | - | 2.1 |
| 50nAg-PVP | DI water | mg Ag/L | - | 0.3 | - | - | 0.4 |
| 50nAg-Tween 80 | DI water | mg Ag/L | - | 3.8 | - | - | 6.5 |
| 50nAg-CTAB | DI water | mg Ag/L | - | 0.6 | - | - | 3.4 |
| AgNO$_3$ | DI water | mg Ag/L | - | 0.02 | - | - | 0.1 |
| CIT | DI water | mg/L | - | >294 | - | - | >294 |
| AOT | DI water | mg/L | - | >445 | - | - | 44.5 |
| PVP | DI water | mg/L | - | 4000 | - | - | >4000 |
| Tween 80 | DI water | mg/L | - | >131 | - | - | >131 |
| CTAB | DI water | mg/L | - | 3.7 | - | - | 3.7 |
| PLL | DI water | mg/L | - | 3 | - | - | 3 |
| Q$^6$-IL | CA-MHB | mg/L | 1000 | - | >1000 | 10 | - |
| Q$^7$-IL | CA-MHB | mg/L | 50 | - | 100 | 2 | - |
| Q$^8$-IL | CA-MHB | mg/L | 100 | - | 100 | 5 | - |
| Q$^6$-Br | CA-MHB | mg/L | 1000 | - | 1000 | 10 | - |
| Q$^7$-Br | CA-MHB | mg/L | 25 | - | 100 | 2 | - |
| Q$^8$-Br | CA-MHB | mg/L | 100 | - | 100 | 10 | - |
| BAC | CA-MHB | mg/L | 50 | - | 100 | 6 | - |

The antimicrobial potency of CuO NPs was studied in similar testing conditions as Ag NPs for a shorter incubation time (2 h). The 2-h MBC of CuO I and CuO S in DI water to *E. coli* was 14-16 mg Cu/L showing toxicity that was two orders of magnitude lower compared to Ag NPs (publications I and II).

From literature is known that CuO NPs exhibit considerable toxicity to bacteria and mammalian cells. For example, the 24-h MBCs of uncoated CuO NPs incubated with bacteria in DI water was 1-10 mg/ L to Gram-negative *E. coli* and 0.1-1 mg/L to

Gram-positive *S. aureus* [173]. CuO NPs are also toxic to mammalian cells. The EC50 values of CuO NPs to human lung alveolar epithelial cells have been from 10 to 50 mg/L [107,189]. In the current thesis, the CuO NPs were functionalized with different surface coatings that could possibly change the toxic effects of CuO NPs (manuscript). The CuO-NH$_2$ was employed in this study representing positively charged NPs and CuO-COOH, CuO-PEG negatively charged NPs. The toxicity of uncoated CuO NPs and CuSO$_4$ salt to *E. coli* was evaluated in parallel (Figure 9). The antibacterial potency (MBC values based on Cu content of the CuO NP) of these compounds is summarized in Table 4. The toxicity of CuO NPs to *E. coli* was several orders of magnitude smaller than toxicity of Ag NPs. The coating of NPs was an important factor in toxicity because the CuO-NH$_2$ NPs were the most toxic of the tested compounds and the uncoated CuO NPs the least toxic of the NPs. Surprisingly, the soluble copper control was less toxic than the functionalized CuO NPs. Such behaviour of Cu compounds is considerably different from Ag compounds (Table 4).

In order to find new bactericidal agents, the antibacterial potency of POM-ILs was studied (publication III). In the current thesis, the POMs are anionic atomic clusters containing oxygen molecules, silica molecules and a transient metal tungsten (Figure 5A). Additionally, to make potentially more effective antibacterial agents, the POMs were attached to cationic organic chemicals namely quaternary ammonium compounds (Q$^x$) via hydrogen bonding (Figure 5B). Such a construct has both, anionic and cationic properties. Toxicity to three medically relevant bacteria: *S. aureus*, *E. coli* and *P. aeruginosa* were tested. The most susceptible bacterium to POM-ILs was *S. aureus* (20-h MBC 2-10 mg/L). This is different from Ag NPs that were more toxic to Gram-negative *E. coli*. The toxic effects of Q$^6$-IL on *E. coli* and *P. aeruginosa* were over 1000 mg/L while for Q$^7$ and Q$^8$ the values were between 50 and 100 mg/L. The toxicity of POM-ILs compared to BAC – a well-known antimicrobial compound - was in concordance with previously published literature showing MIC values 1-50 mg/L [190,191].

In addition, POM-ILs tested in the current thesis were the most potent antibacterial agents compared to the previously published data. The minimal inhibitory concentration values for *S. aureus* have been reported in previous studies to be over 400 mg/L [192]. Our preliminary data – the high toxicity of Q$^7$-IL to *S. aureus* – suggests that POM-ILs presented in this thesis are promising new antibacterials against *S. aureus* and potentially to other Gram-positive bacteria. Such phenomenon could lead to their application in water decontaminating filters or in topical surface coatings especially against *S. aureus* which is the second most prevailing HAI causing bacterium [5].

### 3.2.1 The role of dissolution in the toxic effects of CuO and Ag NPs

It is known from the literature that Ag ions can be the main causes of toxic effects of Ag NPs [78]. Stemming from this, we measured the extracellular Ag ions (AAS) and intracellular Ag ions (publication II). The intracellular fraction of Ag was evidenced by the increased bioluminescence of the biosensors. The per cent of internalized ions from NPs is calculated based on the internalized metal salt [167]. The results showed that the external fraction of ions released from Ag NPs was between 0.8 and 6.5 % and the bioavailable fraction was between 0.2 and 12.6 % (Figure 13A and B, respectively). In general, the smaller Ag NPs were more dissolved compared to larger Ag NPs. As expected, the extra- and intracellular fraction of Ag ions originating from Ag NPs correlated with toxicity of Ag NPs (Figure 13A and B, respectively) suggesting that the

toxic effects of Ag NPs studied in the current thesis are most probably due to Ag ions that destabilize and damage bacterial cell membranes [19,68,193,194].
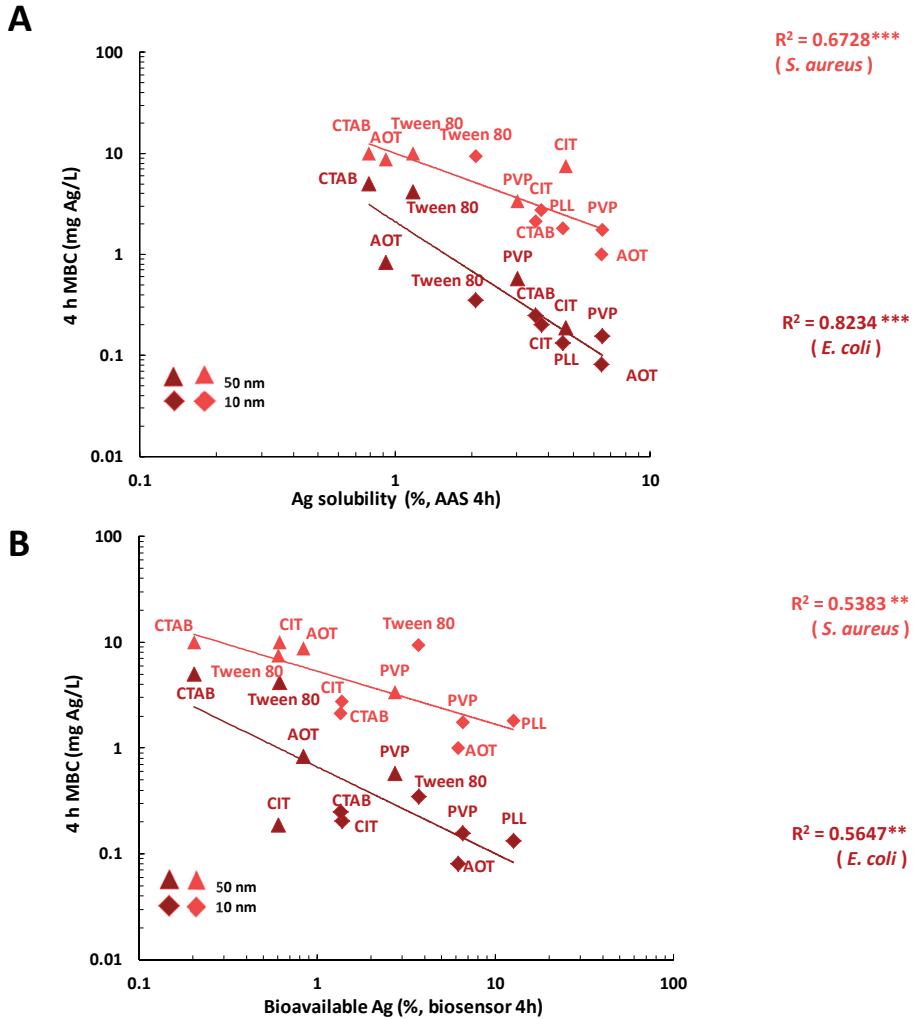


Figure 13.Correlation plots of 10 and 50 nm Ag NPs` toxicity with different coatings (4-h MBC) to E. coli and S. aureus with solubility (A) and with bioavailable fraction of Ag inside the bacteria (B). The data labels are the coating materials on the Ag NPs. The triangles on the correlation plots are the 50 nm Ag NPs and the rectangles are the 10 nm Ag NPs. (Please note the logarithmic scale of correlation plots.) The asterisks show statistical significance as follows: ** <0.01, ***<0.001 (publication II).

Essentially, the Gram-negative *E. coli* was considerably more susceptible to Ag NPs and silver ions compared to Gram-positive *S. aureus* at the 4-h time point whereas by 24 h the MBC values were more even (Figure 14) proving a more prominent time-dependent toxic effect of Ag NPs and AgNO$_3$ for *S. aureus* compared to *E. coli*.

The role of Cu ions in the toxicity mechanisms is under discussion. It has been shown previously that the dissolution of CuO NPs can be facilitated with organic components of the test medium [82]. It is suggested that at least part of the toxicity is attributed to the release of Cu ions [14,94,195,196]. In the current thesis, it was shown that the

higher toxicity of CuO S and CuO I NPs was explained by the higher fraction of dissolved Cu (as seen from the increase of bioavailable Cu). In addition, dissolution (and hence, toxicity) of CuO NPs can be affected by NP size [32], because smaller particles have larger specific surface area and therefore dissolve better as demonstrated with the Cu sensing biosensor analysis [14,32,197].

CuO P, CuO-NH$_2$, CuO-COOH and CuO-PEG, on the other hand were all dissolved by the 24-h time point (Figure 11D). The soluble CuSO$_4$ was evenly toxic to all test models (Figure 15A) suggesting that the dissolved Cu could have an impact on the toxic effects of Cu compounds. The toxicity and dissolution profiles of functionalized CuO NPs on the other hand were different. The most toxic compound CuO-NH$_2$ had a high fraction of bioavailable Cu. (Figure 2A in manuscript). Based on the results above, it is suggested that due to the moderate toxicity of Cu ions, the coating-dependent toxicity played important role for CuO NPs.

### 3.2.2 The coating-dependent toxic effects of Ag NPs

The Ag NPs are often coated to stabilize or disperse them better in suspensions that in turn can modulate toxicity [58]. In the current thesis, the antibacterial properties of a panel of 11 different Ag NPs with positive (coated with PLL and CTAB) and negative charge (coated with AOT, CIT, PVP and Tween 80) (Table 2) were investigated. As these coating materials are attached to the NPs non-covalently in an equilibrium process and are present in the NP dispersions, the toxic effects of pure coatings alone to bacteria in testing conditions relevant for this study were tested. There were no clear coating–dependent toxic effects of 10 nm Ag NPs on *E. coli* (Figure 14 left panels). Instead, the 50 nm Ag NPs covered with CIT, AOT and PVP coatings proved to be more toxic to *E. coli*.

*S. aureus* was less susceptible to Ag NPs than *E. coli* (Figure 14). The effects of coatings on the toxicity of Ag NPs to *S. aureus* were most pronounced in case of 50 nm NPs at 24-h endpoint (Figure 14). The membrane damage of 10 nm NPs to *S. aureus* was facilitated with the addition of PLL and CTAB on Ag NPs (Figure 5, publication II). PLL can cause the disruption of membranes and generation of ROS [198] while quaternary ammonium CTAB have been shown to permeabilize the bacterial cell membranes [199,200]. Citrate is a food preservative with mild antimicrobial effects [201,202] and AOT is an anionic surfactant that causes permeabilization of membranes [203].

Tween 80 and CTAB were the least favourable coatings on 50 nm Ag NPs in terms of antibacterial potency (Figure 14). The inefficient toxicity of CTAB coated larger Ag NPs, however, may be explained by their poor stability in suspensions as determined by the UV-vis analysis (Figure 12).
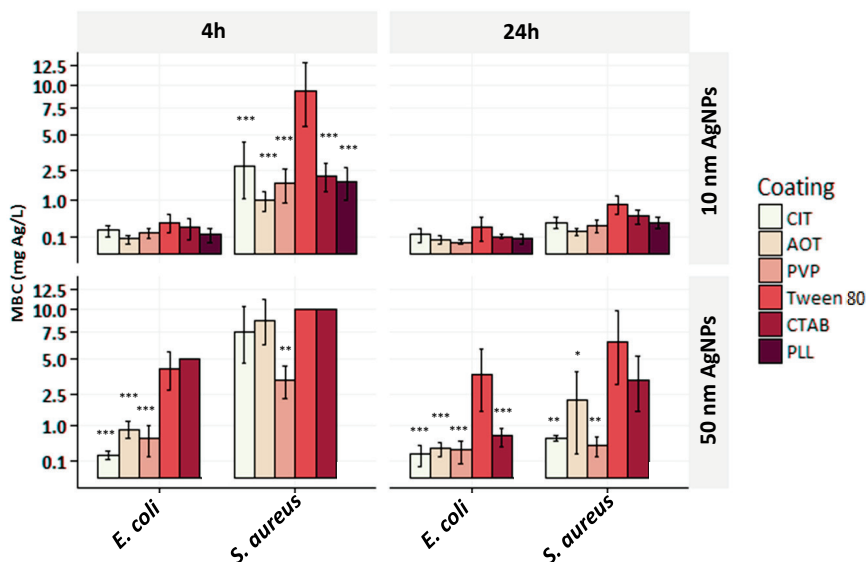
*Figure 14.Toxic effects of 10 and 50 nm Ag NPs on* E. coli *and* S. aureus *at 4- and 24-h time points. The MBC values are averages from three to five experiments and the whiskers are the standard deviations of the results. The asterisks show statistical significance compared to the least toxic compound in the group. The statistically significant differences are designated as follows: \*<0.05, \*\*<0.01, \*\*\*<0.001 (publication II).*

The toxic effects of pure coatings alone on the test bacteria are summarized in Table 4. Based on the determination of the concentration of PLL in the nano suspensions and based on the determination of the toxic concentration of PLL to bacteria, it was seen that the toxicity of PLL was orders of magnitude lower than the toxicity of Ag NPs dispersed with PLL(publication II). The toxicity assessment of pure dispersing materials as coatings in this thesis could give essential information for the synthesis of better Ag-based antibacterial agents that can be used synergistically with antibacterial chemicals and Ag NPs for biomedical applications.

### 3.2.3 The coating-dependent toxic effects of CuO NPs

To study the coating-dependent effects of CuO NPs, three types of functionalizations were chosen: amine ($-NH_2$), carboxyl (-COOH) and polyethylene glycol (PEG). As described in chapter 3.2, the coatings on CuO NPs had an impact on the toxic effects upon the bacteria. One explanation for this phenomenon is the possibility of the charge-dependent effect that might have a role in the toxicity of functionalized CuO NPs. In the current thesis, the amine functionalization or the absence of coating provided positively charged CuO NPs whereas the carboxyl and PEG coatings resulted in negatively charged CuO NPs (Figure 11C). The positively charged CuO NPs exerted superior toxicity to bacteria and mammalian cells (Figure 15A).

It was hypothesized that some of the coating-dependent properties of the CuO NPs can facilitate toxic effects on bacteria and decrease toxicity to humans (determined with human cell models). The evaluated EC50 values of the Cu compounds on bacteria and human cells in similar testing environments (Figure 9) showed that all the models were similarly susceptible to soluble $CuSO_4$ (toxicity 89.4 – 93.6 mg/L) (Figure 15A).

These results emphasize the importance of Cu ions in the toxicity mechanisms of all tested Cu compounds. Essentially, even though the CuO NPs were dissolved by 24 h in abiotic conditions (Figure 15A), we still noticed significant differences in the toxicity profile of these compounds against the cells.

From the tested NPs, the CuO-NH$_2$ proved to be the most toxic to all models (EC50 28.7 – 42.0 mg/L) (Figure 15A). The phenomenon of CuO-NH$_2$ high toxicity might be associated with the ability of CuO-NH$_2$ to induce the production of reactive oxygen species (ROS) (Figure 15B). Based on the previous data, it can be suggested that the –NH$_2$ functional groups themselves on NPs can be substantial causes of ROS by formation of NO radicals in water-based solvents [204]. Ammonium chloride was shown to be an inducer of ROS in cells as quantified with the sensitive H$_2$DCF probe [205]. ROS is an essential contributor to toxicity to both bacterial and mammalian cells [38,70]. The ROS from amino functional groups can trigger apoptosis in cells [206] and cause toxicity to bacteria [9,34]. In addition, contrary to all other CuO NPs and CuSO$_4$, CuO-NH$_2$ induced TNF-α in THP-1 cells. The proinflammatory cytokine TNF-α is an inflammation mediator and the TNF-α production can be associated with cell death [207].
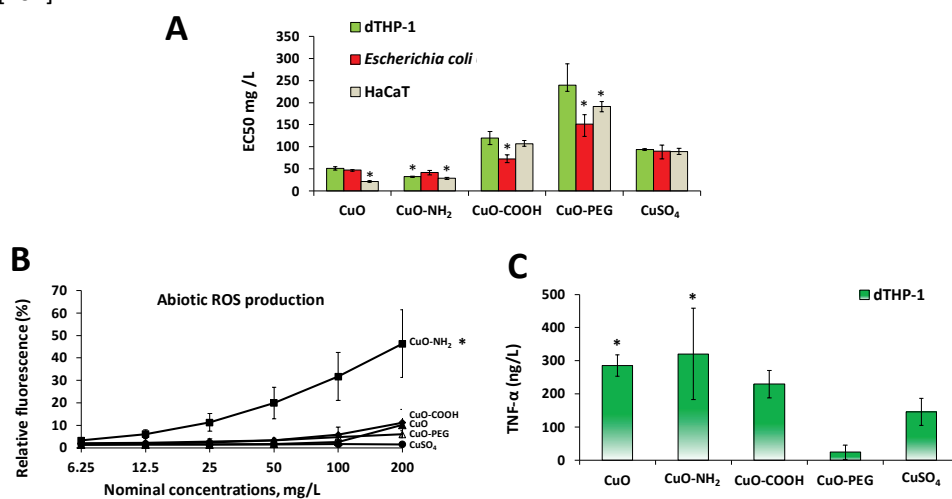


*Figure 15. Toxic effects of CuO P, CuO-NH$_2$, CuO-COOH and CuO-PEG NPs on dTHP-1 macrophages, HaCaT keratinocytes and* Escherichia coli *bacterium evaluated with Resazurin viability assay (A). The dose responsive production of reactive oxygen species in abiotic conditions (B). The ability to trigger proinflammatory cytokine TNF-α production in response to 100 mg/L Cu compounds in differentiated THP-1 macrophages (C). The error bars for the EC50 values are the 95% confidence intervals, in other cases error bars show standard deviation. Asterisks designate the statistically significant difference (p<0.05) compared to the least toxic effect in the group (A) or to the smallest result (B,C) (manuscript).*

Interestingly, however, it was observed that the pegylated and carboxyl-functionalized CuO NPs showed significantly less toxicity towards dTHP-1 and HaCaT cells compared to bacteria (Figure 15A). Notably, the carboxyl functionalization *per se* can modulate the toxicity. It has been shown previously that the carboxyl functionalized chemically inert polystyrene NPs resulted in less toxicity to human cells compared to NH$_2$ coated polystyrene NPs [206,208]. The PEG, on the other hand, is a widely used biocompatible coating and has been used on CuO NPs for biomedical applications [164].

Thus, uncoated CuO and CuO-NH$_2$ NPs were the most toxic to mammalian cells. Interestingly, both uncoated and NH$_2$-functionalized CuO NPs were positively charged and had the highest Cu content (Figure 11B), suggesting that these factors are important for toxicity.

**3.2.4 Multivariate analysis for safety and antibacterial efficiency evaluation of CuO NPs**

The multivariate analysis was done to evaluate the variability of coated and uncoated CuO NPs. For this, data from toxicity evaluation (Figure 15A) and from physico-chemical properties evaluation (Figure 11) were employed to model a scoresplot that comprises the eigenvectors (the arrows indicate the direction of the increasing size of the values) and the principal components analysis (PCA) resulting in NPs positions according to their variability (Figure 16).

Scores of the first two principal components comprised 94.4-95.5% of the variance. The multivariate analysis showed different clustering of more toxic CuO and CuO-NH$_2$ NPs from less toxic CuO-COOH and CuO-PEG NPs whereas the variability profile was not considerably changed between the test models (bacteria, HaCaT and differentiated THP-1) (Figure 16A,B and C). The properties contributing to increased toxic effects of the NPs were more positive zeta-potential, higher Cu content, higher 24-h dissolution, ability to induce the generation of abiotic ROS, higher production of TNF-α (dTHP-1 cells).
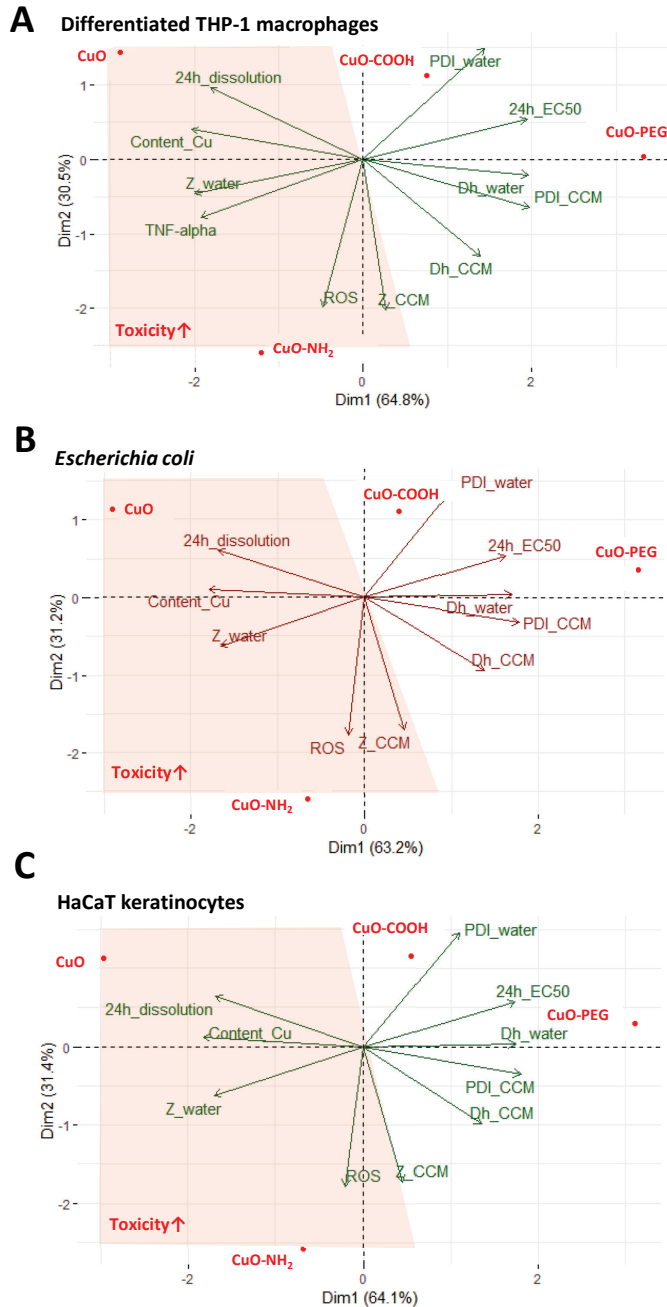
*Figure 16. Multivariate analysis of the properties contributing to the variability of the toxicity of CuO, CuO-NH2, CuO-COOH and CuO-PEG NPs to differentiated THP-1 macrophages (A),* E. coli *bacterium (B) and HaCaT keratinocytes (C). As input, the data from Figures 11 and 15 was used. The abbrevations of the labels are the following: Z_water - surface charge in DI water, Z_CCM - surface charge in cell culture medium, Dh_water - hydrodynamic size in DI water, Dh_CCM - hydrodynamic size in cell culture medium, PDI_CCM - PDI in cell culture medium, PDI_water - PDI in water, ROS - abiotic reactive oxygen species, Content_Cu - Copper content, 24h_EC50 – 24-h EC50 nominal values (mg/L), 24h_dissolution – 24-h dissolution. The more toxic compounds are highlighted in the red area. For visualization, the data was scaled by dividing the (centered) columns of x by their standard deviations (manuscript).*

**3.2.5 Toxicity mechanisms of POM-ILs to medically relevant bacteria**

For testing the antimicrobial properties of POM-ILs, the quaternary ammonium salts ($Q^x$-Br, x=6,7,8) without the POM component were used as controls in toxicity testing. The results showed that the EC50 values of POM-ILs and their corresponding salts were comparable (Table 4 and Figure 17). Relying on this, it was suggested that the antibacterial properties of the compounds were mainly due to the presence of ammonium cations. Additionally, the chain lengths of the cations determined the toxicity profile of the compounds. The toxicity of the compounds, however, might be related to their hydrophobicity It was seen that the POM-ILs with the carbon chain length C=6 of quaternary ammonium compounds were less toxic to all test bacteria. The ILs with longer alkyl chain lengths were more hydrophobic and possessed higher potential to damage bacterial membrane of marine bacterium *Vibrio fischeri* [209]. It is also proposed that the main causes of toxicity are the formation of ROS by transient metals (such as tungsten) or destabilization of the bacterial membranes by quaternary ammonium components of the ILs [210]. The quaternary ammonium compounds have been shown to disrupt the bacterial membranes due to the electrostatic interactions between the quaternary ammonium cations and anionic phospholipids in the membrane [190].

In conclusion, in the current thesis the highest antibacterial activity of POM-ILs to medically relevant bacteria is reported so far. Additionally, it was shown that the carbon chain lengths of cationic quaternary ammonium compounds influence the antibacterial properties of the prototype POM-ILs.
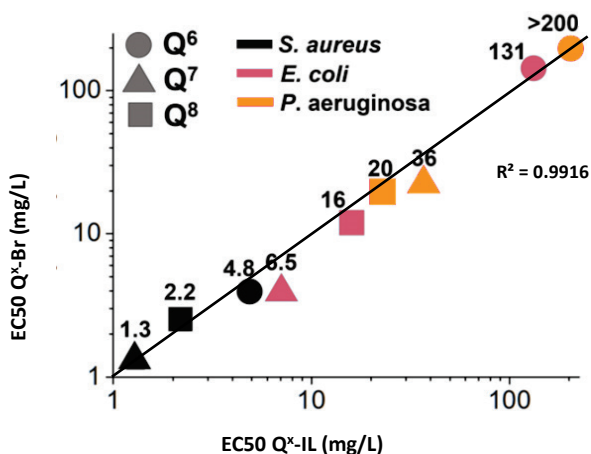


*Figure 17. Correlation plot of toxic effects of POM-ILs ($Q^x$-IL) and their corresponding reference compounds ($Q^x$-Br) on different test bacteria. The shapes represent the lengths of carbon chains (x=6,7,8) of cation quaternary ammonium components of POM-ILs and colours are the test-bacteria (publication III).*

# Conclusions

In this thesis, the bactericidal effects of CuO NPs, Ag NPs and polyoxometalate ionic liquids were studied. Altogether, 20 CuO and Ag NPs and POM-ILs, including 10 nm and 50 nm Ag NPs with various surface coatings, CuO NPs with different surface functionalizations and from various commercial sources and POM-ILs with various carbon chain lengths ($Q^x$-ILs) were characterized and tested. In parallel, the toxicity of 12 control compounds was evaluated. Given the presented toxicological profiles of NPs and POM-ILs in the current thesis, the results herein could be valuable for the manufacturers of the antimicrobial agents.

The main conclusions are the following:

1) In general, Ag NPs had superior antibacterial effect over the other tested compounds. The toxicity of Ag NPs was explained by dissolved Ag ions and less by the surface charge/coating of the Ag NPs.

2) Gram-negative bacterium *E. coli* was more susceptible to Ag NPs than Gram-positive *S. aureus*.

3) Compared to Ag NPs, different toxicity pattern was observed in the case of POM-ILs: Gram-positive *S. aureus* was more susceptible to POM-ILs than Gram-negative *E. coli* and *P. aeruginosa*. Remarkably, our studies showed the highest toxicity of tested POM compounds so far to *S. aureus* being comparable to the known antibacterial agent benzalkonium chloride. The antibacterial potency of POM-ILs depended on the carbon chain lengths of the quaternary ammonium cations rather than the POM anion components.

4) Coating materials and sizes of CuO NPs had substantial role in the toxicity to dTHP-1 macrophages, HaCaT keratinocytes and *E. coli* bacterium. Negatively charged and larger CuO NPs were less toxic to bacteria and mammalian cells *in vitro* as compared to the positively charged smaller CuO particles, whereas CuO-NH$_2$ were especially toxic to all test models (*E. coli* bacteria, HaCaT keratinocytes and dTHP-1 macrophages). Unexpectedly, CuO-COOH and CuO-PEG NPs proved to be significantly less toxic to human cells *in vitro* – HaCaT and dTHP-1 macrophages - compared to *E. coli* bacterium.

# List of figures

# List of tables

# References

[1]     H.A. Khan, F.K. Baig, R. Mehboob, Nosocomial infections: Epidemiology, prevention, control and surveillance, Asian Pac. J. Trop. Biomed. 7 (2017) 478–482. doi:10.1016/j.apjtb.2017.01.019.

[2]     C.L. Ventola, The antibiotic resistance crisis: part 1: causes and threats, P T. 40 (2015) 277–83.

[3]     T. Frieden, Antibiotic resistance threats in the United States, 2013, Centers Dis. Control Prev. (2013). doi:CS239559-B.

[4]     C.L. Ventola, The antibiotic resistance crisis: part 2: management strategies and new agents, P T. 40 (2015) 344–52.

[5]     P. Zarb, B. Coignard, J. Griskeviciene, A. Muller, V. Vankerckhoven, K. Weist, M.M. Goossens, S. Vaerenberg, S. Hopkins, B. Catry, D.L. Monnet, H. Goossens, C. Suetens, Point prevalence survey of healthcare-associated infections and antimicrobial use in European acute care hospitals, 2012. doi:10.2900/86011.

[6]     J.A. Lemire, J.J. Harrison, R.J. Turner, Antimicrobial activity of metals: Mechanisms, molecular targets and applications, Nat. Rev. Microbiol. 11 (2013) 371–384. doi:10.1038/nrmicro3028.

[7]     Z. Ma, F.E. Jacobsen, D.P. Giedroc, Coordination chemistry of bacterial metal transport and sensing, Chem. Rev. 109 (2009) 4644–4681. doi:10.1021/cr900077w.

[8]     L.A. Finney, T. V. O'Halloran, Transition metal speciation in the cell: Insights from the chemistry of metal ion receptors, Science (80-. ). 300 (2003) 931–936. doi:10.1126/science.1085049.

[9]     H. Palza, Antimicrobial polymers with metal nanoparticles, Int. J. Mol. Sci. 16 (2015) 2099–2116. doi:10.3390/ijms16012099.

[10]    M.J. Hajipour, K.M. Fromm, A.A. Ashkarran, D.J. De Aberasturi, I.R. De Larramendi, T. Rojo, Antibacterial properties of nanoparticles, Trends Biotechnol. 30 (2012) 499–511. doi:10.1016/j.tibtech.2012.06.004.

[11]    G. Grass, C. Rensing, M. Solioz, Metallic Copper as an Antimicrobial Surface, Appl. Environ. Microbiol. 77 (2011) 1541–1547. doi:10.1128/AEM.02766-10.

[12]    H. Karlsson, M.S. Toprak, B. Fadeel, Toxicity of Metal and Metal Oxide Nanoparticles, in: Handb. Toxicol. Met., 2015: pp. 75–112. doi:10.1007/s10531-012-0336-9.

[13]    A.E. Nel, L. Mädler, D. Velegol, T. Xia, E.M.V. Hoek, P. Somasundaran, F. Klaessig, V. Castranova, M. Thompson, Understanding biophysicochemical interactions at the nano-bio interface, Nat. Mater. 8 (2009) 543–557. doi:10.1038/nmat2442.

[14]    M. Heinlaan, A. Ivask, I. Blinova, H.C. Dubourguier, A. Kahru, Toxicity of nanosized and bulk ZnO, CuO and TiO2 to bacteria Vibrio fischeri and crustaceans Daphnia magna and Thamnocephalus platyurus, Chemosphere. 71 (2008) 1308–1316. doi:10.1016/j.chemosphere.2007.11.047.

[15]    W. Lu, D. Senapati, S. Wang, O. Tovmachenko, A.K. Singh, H. Yu, P.C. Ray, Effect of surface coating on the toxicity of silver nanomaterials on human skin keratinocytes, Chem. Phys. Lett. 487 (2010) 92–96. doi:10.1016/j.cplett.2010.01.027.

[16] S. Herrmann, L. De Matteis, J.M. de la Fuente, S.G. Mitchell, C. Streb, Removal of Multiple Contaminants from Water by Polyoxometalate-Supported Ionic Liquid Phases (POM-SILPs), Angew. Chemie Int. Ed. (2017) 1–5. doi:10.1002/anie.201611072.

[17] J. Jeevanandam, A. Barhoum, Y.S. Chan, A. Dufresne, M.K. Danquah, Review on nanoparticles and nanostructured materials: history, sources, toxicity and regulations, Beilstein J. Nanotechnol. 9 (2018) 1050–1074. doi:10.3762/bjnano.9.98.

[18] Regulation (EU) No 528/2012 of the European Parliament and of the Council of 22 May 2012 concerning the making available on the market and use of biocidal products, n.d.

[19] J.R. Morones-Ramirez, J.A. Winkler, C.S. Spina, J.J. Collins, Silver Enhances Antibiotic Activity Against Gram-Negative Bacteria, Sci. Transl. Med. 5 (2013) 1–11. doi:10.1126/scitranslmed.3006276.Silver.

[20] S. Gurunathan, J.W. Han, D.-N. Kwon, J.-H. Kim, Enhanced antibacterial and anti-biofilm activities of silver nanoparticles against Gram-negative and Gram-positive bacteria, Nanoscale Res. Lett. 9 (2014) 373. doi:10.1186/1556-276X-9-373.

[21] D.P. Gnanadhas, M. Ben Thomas, R. Thomas, A.M. Raichur, D. Chakravortty, Interaction of silver nanoparticles with serum proteins affects their antimicrobial activity in vivo, Antimicrob. Agents Chemother. 57 (2013) 4945–4955. doi:10.1128/AAC.00152-13.

[22] J.R. Morones-Ramirez, J.A. Winkler, C.S. Spina, J.J. Collins, Silver Enhances Antibiotic Activity Against Gram-negative Bacteria, 5 (2013). doi:10.1126/scitranslmed.3006276.Silver.

[23] P. Jena, S. Mohanty, R. Mallick, B. Jacob, A. Sonawane, Toxicity and antibacterial assessment of chitosan- coated silver nanoparticles on human pathogens and macrophage cells, Int. J. Nanomedicine. 2012 (2012) 1805–1818. doi:10.2147/IJN.S28077.

[24] J. Lellouche, A. Friedman, J.P. Lellouche, A. Gedanken, E. Banin, Improved antibacterial and antibiofilm activity of magnesium fluoride nanoparticles obtained by water-based ultrasound chemistry, Nanomedicine Nanotechnology, Biol. Med. 8 (2012) 702–711. doi:10.1016/j.nano.2011.09.002.

[25] S. Mohanty, S. Mishra, P. Jena, B. Jacob, B. Sarkar, A. Sonawane, An investigation on the antibacterial, cytotoxic, and antibiofilm efficacy of starch-stabilized silver nanoparticles, Nanomedicine Nanotechnology, Biol. Med. 8 (2012) 916–924. doi:10.1016/j.nano.2011.11.007.

[26] S. Kim, P.A. Thiessen, E.E. Bolton, J. Chen, G. Fu, A. Gindulyte, L. Han, J. He, S. He, B.A. Shoemaker, J. Wang, B. Yu, J. Zhang, S.H. Bryant, PubChem substance and compound databases, Nucleic Acids Res. 44 (2016) D1202–D1213. doi:10.1093/nar/gkv951.

[27] K. Blecher, A. Nasir, A. Friedman, The growing role of nanotechnology in combating infectious disease, Virulence. 2 (2011) 395–401. doi:10.4161/viru.2.5.17035.

[28] Y.W. Baek, Y.J. An, Microbial toxicity of metal oxide nanoparticles (CuO, NiO, ZnO, and Sb 2O 3) to Escherichia coli, Bacillus subtilis, and Streptococcus aureus, Sci. Total Environ. 409 (2011) 1603–1608. doi:10.1016/j.scitotenv.2011.01.014.

[29]  G. Ren, D. Hu, E.W.C. Cheng, M.A. Vargas-Reus, P. Reip, R.P. Allaker, Characterisation of copper oxide nanoparticles for antimicrobial applications, Int. J. Antimicrob. Agents. 33 (2009) 587–590. doi:10.1016/j.ijantimicag.2008.12.004.

[30]  M. Amiri, Z. Etemadifar, A. Daneshkazemi, M. Nateghi, Antimicrobial Effect of Copper Oxide Nanoparticles on Some Oral Bacteria and Candida Species, J. Dent. Biomater. J Dent Biomater J Dent Biomater. 444 (2017) 347–352.

[31]  R. Javed, M. Ahmed, I. ul Haq, S. Nisa, M. Zia, PVP and PEG doped CuO nanoparticles are more biologically active: Antibacterial, antioxidant, antidiabetic and cytotoxic perspective, Mater. Sci. Eng. C. 79 (2017) 108–115. doi:10.1016/j.msec.2017.05.006.

[32]  A. Azam, A.S. Ahmed, M. Oves, M.S. Khan, A. Memic, Size-dependent antimicrobial properties of CuO nanoparticles against Gram-positive and - negative bacterial strains, Int. J. Nanomedicine. 7 (2012) 3527–3535. doi:10.2147/IJN.S29020.

[33]  W.H. De Jong, E. De Rijk, A. Bonetto, W. Wohlleben, V. Stone, A. Brunelli, E. Badetti, A. Marcomini, I. Gosens, F.R. Cassee, Toxicity of copper oxide and basic copper carbonate nanoparticles after short-term oral exposure in rats, Nanotoxicology. 13 (2019) 50–72. doi:10.1080/17435390.2018.1530390.

[34]  R.Y. Pelgrift, A.J. Friedman, Nanotechnology as a therapeutic tool to combat microbial resistance, Adv. Drug Deliv. Rev. 65 (2013) 1803–1815. doi:10.1016/j.addr.2013.07.011.

[35]  S.M. Dizaj, F. Lotfipour, M. Barzegar-Jalali, M.H. Zarrintan, K. Adibkia, Antimicrobial activity of the metals and metal oxide nanoparticles, Mater. Sci. Eng. C. 44 (2014) 278–284. doi:10.1016/j.msec.2014.08.031.

[36]  C. Malarkodi, S. Rajeshkumar, K. Paulkumar, M. Vanaja, G. Gnanajobitha, G. Annadurai, Biosynthesis and Antimicrobial Activity of Semiconductor Nanoparticles against Oral Pathogens, Bioinorg. Chem. Appl. Spectrom. 2014 (2014) 1–10.

[37]  V. Aruoja, S. Pokhrel, M. Sihtmäe, M. Mortimer, L. Mädler, A. Kahru, Toxicity of 12 metal-based nanoparticles to algae, bacteria and protozoa, Environ. Sci. Nano. 2 (2015) 630–644. doi:10.1039/c5en00057b.

[38]  C. Kaweeteerawat, A. Ivask, R. Liu, H. Zhang, C.H. Chang, C. Low-Kam, H. Fischer, Z. Ji, S. Pokhrel, Y. Cohen, D. Telesca, J. Zink, L. Mädler, P.A. Holden, A. Nel, H. Godwin, Toxicity of metal oxide nanoparticles in Escherichia coli correlates with conduction band and hydration energies, Environ. Sci. Technol. 49 (2015) 1105–1112. doi:10.1021/es504259s.

[39]  Y.M. Zhang, C.O. Rock, Membrane lipid homeostasis in bacteria, Nat. Rev. Microbiol. 6 (2008) 222–233. doi:10.1038/nrmicro1839.

[40]  B.J. Shaw, R.D. Handy, Physiological effects of nanoparticles on fish: A comparison of nanometals versus metal ions, Environ. Int. 37 (2011) 1083–1097. doi:10.1016/j.envint.2011.03.009.

[41]  S. Ninganagouda, V. Rathod, D. Singh, J. Hiremath, A.K. Singh, J. Mathew, M. Ul-Haq, Growth kinetics and mechanistic action of reactive oxygen species released by silver nanoparticles from Aspergillus niger on Escherichia coli, Biomed Res. Int. 2014 (2014) 1–9. doi:10.1155/2014/753419.

[42]  L. Wang, C. Hu, L. Shoa, The-antimicrobial-activity-of-nanoparticles--present-situati, Int. J. Nanomedicine. 12 (2017) 1227–1249. doi:10.2147/IJN.S121956.

[43]    N.R. Bury, M. Grosell, A.K. Grover, C.M. Wood, ATP-dependent silver transport across the basolateral membrane of rainbow trout gills, Toxicol. Appl. Pharmacol. 159 (1999) 1–8. doi:10.1006/taap.1999.8706.

[44]    D.H. Nies, Microbial heavy-metal resistance, Appl Microbiol Biotechnol. 51 (1999) 730–750.

[45]    V. Labhasetwar, D.L. Leslie-Pelecky, Nanotoxicology, in: Biomed. Appl. Nanotechnol., John Wiley & Sons. Inc, 2007: pp. 227–249. doi:10.1002/9780470152928.

[46]    J.T. Seil, T.J. Webster, Antimicrobial applications of nanotechnology: Methods and literature, Int. J. Nanomedicine. 7 (2012) 2767–2781. doi:10.2147/IJN.S24805.

[47]    M.A. Dobrovolskaia, A.K. Patri, T.M. Potter, J.C. Rodriguez, J.B. Hall, S.E. McNeil, Dendrimer-induced leukocyte procoagulant activity depends on particle size and surface charge, Nanomedicine. 7 (2012) 245–256. doi:10.2217/nnm.11.105.

[48]    T. Meißner, K. Oelschlägel, A. Potthoff, Dispersion of nanomaterials used in toxicological studies: A comparison of sonication approaches demonstrated on TiO2 P25, J. Nanoparticle Res. 16 (2014) 1–13. doi:10.1007/s11051-013-2228-7.

[49]    J.S. Taurozzi, V.A. Hackley, M.R. Wiesner, Ultrasonic dispersion of nanoparticles for environmental, health and safety assessment issues and recommendations, Nanotoxicology. 5 (2011) 711–729. doi:10.3109/17435390.2010.528846.

[50]    P. Bihari, M. Vippola, S. Schultes, M. Praetner, A.G. Khandoga, C.A. Reichel, C. Coester, T. Tuomi, M. Rehberg, F. Krombach, Optimized dispersion of nanoparticles for biological in vitro and in vivo studies, Part. Fibre Toxicol. 5 (2008) 1–14. doi:10.1186/1743-8977-5-14.

[51]    J. Jiang, G. Oberdörster, P. Biswas, Characterization of size, surface charge, and agglomeration state of nanoparticle dispersions for toxicological studies, J. Nanoparticle Res. 11 (2009) 77–89. doi:10.1007/s11051-008-9446-4.

[52]    C. Bantz, O. Koshkina, T. Lang, H.J. Galla, C.J. Kirkpatrick, R.H. Stauber, M. Maskos, The surface properties of nanoparticles determine the agglomeration state and the size of the particles under physiological conditions, Beilstein J. Nanotechnol. 5 (2014) 1774–1786. doi:10.3762/bjnano.5.188.

[53]    Z. Magdolenova, D. Bilaniová, G. Pojana, L.M. Fjellsbø, A. Hudecova, K. Hasplova, A. Marcomini, M. Dusinska, Impact of agglomeration and different dispersions of titanium dioxide nanoparticles on the human related in vitro cytotoxicity and genotoxicity, J. Environ. Monit. 14 (2012) 455–464. doi:10.1039/c2em10746e.

[54]    J.P. Piret, J. Mejia, S. Lucas, C.C. Zouboulis, C. Saout, O. Toussaint, Sonicated and stirred copper oxide nanoparticles induce similar toxicity and pro-inflammatory response in N-hTERT keratinocytes and SZ95 sebocytes, J. Nanoparticle Res. 16 (2014) 1–18. doi:10.1007/s11051-014-2337-y.

[55]    P. Cronholm, K. Midander, H.L. Karlsson, K. Elihn, I.O. Wallinder, L. Möller, Effect of sonication and serum proteins on copper release from copper nanoparticles and the toxicity towards lung epithelial cells, Nanotoxicology. 5 (2011) 269–281. doi:10.3109/17435390.2010.536268.

[56]    P.C. Ray, Size and Shape Dependent Second Order Nonlinear Optical Properties of Nanomaterials and Its Application in Biological and Chemical Sensing, Chem Rev. 110 (2011) 5332–5365. doi:10.1021/cr900335q.Size.

[57] H.-J. Li, A.-Q. Zhang, Y. Hu, L. Sui, D.-J. Qian, M. Chen, Large-scale synthesis and self-organization of silver nanoparticles with Tween 80 as a reductant and stabilizer, Nanoscale Res. Lett. 7 (2012) 1–13. doi:10.1186/1556-276X-7-612.

[58] L. Kvítek, A. Panáček, J. Soukupová, M. Kolář, R. Večeřová, R. Prucek, M. Holecová, R. Zbořil, Effect of surfactants and polymers on stability and antibacterial activity of silver nanoparticles (NPs), J. Phys. Chem. C. 112 (2008) 5825–5834. doi:10.1021/jp711616v.

[59] M. Harada, K. Saijo, N. Sakamoto, K. Ito, Characterization of water/AOT/benzene microemulsions during photoreduction to produce silver particles, J. Colloid Interface Sci. 343 (2010) 423–432. doi:10.1016/j.jcis.2009.12.006.

[60] M. Marradi, F. Chiodo, I. García, S. Penadés, Glyconanoparticles as multifunctional and multimodal carbohydrate systems, Chem. Soc. Rev. 42 (2013) 4728–4745. doi:10.1039/c2cs35420a.

[61] J.M. de la Fuente, A.G. Barrientos, T.C. Rojas, J. Rojo, J. Canada, A. Fernandez, S. Penades, Gold Glyconanoparticles as Water-Soluble Polyvalent Models To Study Carbohydrate Interactions, Angew. Chem. Int. Ed. 40 (2001) 2258–2260. doi:10.1088/1674-1056/18/8/007.

[62] A.M. El Badawy, R.G. Silva, B. Morris, K.G. Scheckel, M.T. Suidan, T.M. Tolaymat, Surface charge-dependent toxicity of silver nanoparticles, Environ. Sci. Technol. 45 (2011) 283–287. doi:10.1021/es1034188.

[63] T. Gunasekaran, T. Nigusse, M.D. Dhanaraju, Silver nanoparticles as real topical bullets for wound healing, J. Am. Coll. Clin. Wound Spec. 3 (2011) 82–96. doi:10.1016/j.jcws.2012.05.001.

[64] M. Konop, T. Damps, A. Misicka, L. Rudnicka, Certain Aspects of Silver and Silver Nanoparticles in Wound Care: A Minireview, J. Nanomater. 2016 (2016) 1–10. doi:10.1155/2016/7614753.

[65] P. Dallas, V.K. Sharma, R. Zboril, Silver polymeric nanocomposites as advanced antimicrobial agents: Classification, synthetic paths, applications, and perspectives, Adv. Colloid Interface Sci. 166 (2011) 119–135. doi:10.1016/j.cis.2011.05.008.

[66] K. Juganson, A. Ivask, I. Blinova, M. Mortimer, A. Kahru, NanoE-Tox: New and in-depth database concerning ecotoxicity of nanomaterials, Beilstein J. Nanotechnol. 6 (2015) 1788–1804. doi:10.3762/bjnano.6.183.

[67] Z. Adamczyk, M. Oćwieja, H. Mrowiec, S. Walas, D. Lupa, Oxidative dissolution of silver nanoparticles: A new theoretical approach, J. Colloid Interface Sci. 469 (2016) 355–364. doi:10.1016/j.jcis.2015.12.051.

[68] D. McShan, P.C. Ray, H. Yu, Molecular Toxicity Mechanism of Nanosilver, 4 (2014) 116–127. doi:10.1126/scisignal.2001449.Engineering.

[69] S. Prabhu, E.K. Poulose, Silver nanoparticles: mechanism of antimicrobial action, synthesis, medical applications, and toxicity effects, Int. Nano Lett. 2 (2012) 1–10. doi:10.1186/2228-5326-2-32.

[70] A. Ivask, T. Titma, M. Visnapuu, H. Vija, A. Käkinen, M. Sihtmäe, S. Pokhrel, L. Mädler, M. Heinlaan, V. Kisand, R. Shimmo, A. Kahru, Toxicity of 11 Metal Oxide Nanoparticles to Three Mammalian Cell Types In Vitro, Curr. Top. Med. Chem. 15 (2015) 1914–1929. doi:10.2174/1568026615666150506150109.

[71] H. Líbalová, P.M. Costa, M. Olsson, L. Farcal, S. Ortelli, M. Blosi, J. Topinka, A.L. Costa, B. Fadeel, Toxicity of surface-modified copper oxide nanoparticles in a mouse macrophage cell line: Interplay of particles, surface coating and particle dissolution, Chemosphere. 196 (2018) 482–493. doi:10.1016/j.chemosphere.2017.12.182.

[72] A.K. Suresh, D.A. Pelletier, M.J. Doktycz, Relating nanomaterial properties and microbial toxicity, Nanoscale. 5 (2013) 463–474. doi:10.1039/c2nr32447d.

[73] R. Tantra, H. Bouwmeester, E. Bolea, C. Rey-Castro, C.A. David, J.M. Dogné, J. Jarman, F. Laborda, J. Laloy, K.N. Robinson, A.K. Undas, M. Van Der Zande, Suitability of analytical methods to measure solubility for the purpose of nanoregulation, Nanotoxicology. 10 (2016) 173–184. doi:10.3109/17435390.2015.1038661.

[74] D. McShan, P.C. Ray, H. Yu, Molecular toxicity mechanism of nanosilver, J. Food Drug Anal. 22 (2014) 116–127. doi:10.1016/j.jfda.2014.01.010.

[75] A. Jemec, A. Kahru, A. Potthoff, D. Drobne, M. Heinlaan, M. Geppert, S. Novak, K. Schirmer, R. Rekulapally, S. Singh, V. Aruoja, M. Sihtmäe, K. Juganson, A. Käkinen, D. Kühnel, An interlaboratory comparison of nanosilver characterisation and hazard identification : Harmonising techniques for high quality data, Environ. Int. 87 (2016) 20–32. doi:10.1016/j.envint.2015.10.014.

[76] O. Bondarenko, K. Juganson, A. Ivask, K. Kasemets, M. Mortimer, A. Kahru, Toxicity of Ag, CuO and ZnO nanoparticles to selected environmentally relevant test organisms and mammalian cells in vitro: A critical review, Arch. Toxicol. 87 (2013) 1181–1200. doi:10.1007/s00204-013-1079-4.

[77] A. Ivask, A. Elbadawy, C. Kaweeteerawat, D. Boren, H. Fischer, Z. Ji, C.H. Chang, R. Liu, T. Tolaymat, D. Telesca, J.I. Zink, Y. Cohen, P.A. Holden, H.A. Godwin, Toxicity mechanisms in Escherichia coli vary for silver nanoparticles and differ from ionic silver, ACS Nano. 8 (2014) 374–386. doi:10.1021/nn4044047.

[78] A. Ivask, I. Kurvet, K. Kasemets, I. Blinova, V. Aruoja, S. Suppi, H. Vija, A. Käkinen, T. Titma, M. Heinlaan, M. Visnapuu, D. Koller, V. Kisand, A. Kahru, Size-dependent toxicity of silver nanoparticles to bacteria, yeast, algae, crustaceans and mammalian cells in vitro, PLoS One. 9 (2014). doi:10.1371/journal.pone.0102108.

[79] S. Ahlberg, A. Antonopulos, J. Diendorf, R. Dringen, M. Epple, R. Flöck, W. Goedecke, C. Graf, N. Haberl, J. Helmlinger, F. Herzog, F. Heuer, S. Hirn, C. Johannes, S. Kittler, M. Köller, K. Korn, W.G. Kreyling, F. Krombach, J. Lademann, K. Loza, E.M. Luther, M. Malissek, M.C. Meinke, D. Nordmeyer, A. Pailliart, J. Raabe, F. Rancan, B. Rothen-Rutishauser, E. Rühl, C. Schleh, A. Seibel, C. Sengstock, L. Treuel, A. Vogt, K. Weber, R. Zellner, PVP-coated, negatively charged silver nanoparticles: A multi-center study of their physicochemical characteristics, cell culture and in vivo experiments, Beilstein J. Nanotechnol. 5 (2014) 1944–65. doi:10.3762/bjnano.5.205.

[80] J. Liu, Z. Wang, F.D. Liu, A.B. Kane, R.H. Hurt, Chemical transformations of nanosilver in biological environments, ACS Nano. 6 (2012) 9887–9899. doi:10.1021/nn303449n.

[81] L.-J.A. Ellis, E. Valsami-Jones, J.R. Lead, M. Baalousha, Impact of surface coating and environmental conditions on the fate and transport of silver nanoparticles in the aquatic environment, Sci. Total Environ. 568 (2016) 95–106. doi:10.1016/j.scitotenv.2016.05.199.

[82]   A. Käkinen, O. Bondarenko, A. Ivask, A. Kahru, The effect of composition of different ecotoxicological test media on free and bioavailable copper from CuSO4 and CuO nanoparticles: Comparative evidence from a Cu-selective electrode and a Cu-biosensor, Sensors. 11 (2011) 10502–10521. doi:10.3390/s111110502.

[83]   M.N. Hughes, R.K. Poole, Metal speciation and microbial growth--the hard (and soft) facts, J. Gen. Microbiol. 137 (1991) 725–734. doi:10.1099/00221287-137-4-725.

[84]   A. Semisch, J. Ohle, B. Witt, A. Hartwig, Cytotoxicity and genotoxicity of nano - and microparticulate copper oxide: Role of solubility and intracellular bioavailability, Part. Fibre Toxicol. 11 (2014) 1–16. doi:10.1186/1743-8977-11-10.

[85]   H. Gunshin, B. Mackenzie, U. V. Berger, Y. Gunshin, M.F. Romero, W.F. Boron, S. Nussberger, J.L. Gollan, M.A. Hediger, Cloning and characterization of a mammalian proton-coupled metal-ion transporter, Nature. 388 (1997) 6264–6268. doi:10.1038/41343.

[86]   H.P. van Leeuwen, W. Köster, eds., Physicochemical Kinetics and Transport at the Biointerface, John Wiley & Sons. Inc, 2004. doi:10.1002/0470094044.ch1.

[87]   R.D. Handy, F.B. Eddy, H. Baines, Sodium-dependent copper uptake across epithelia: A review of rationale with experimental evidence from gill and intestine, Biochim. Biophys. Acta - Biomembr. 1566 (2002) 104–115. doi:10.1016/S0005-2736(02)00590-4.

[88]   F. Ren, B.L. Logeman, X. Zhang, Y. Liu, D.J. Thiele, P. Yuan, X-ray structures of the high-affinity copper transporter Ctr1, Nat. Commun. 10 (2019) 1–9. doi:10.1038/s41467-019-09376-7.

[89]   A. Odermatt, R. Krapf, M. Solioz, Induction of the putative copper ATPases, CopA and CopB, of Enterococcus hirae by Ag+ and Cu2+, and Ag+ extrusion by CopB, Biochem. Biophys. Res. Commun. 202 (1994) 44–48. doi:10.1006/bbrc.1994.1891.

[90]   I. Fridovich, B. Freeman, Antioxidant defenses in the lung, Annu. Rev. Physiol. 48 (1986) 693–702. doi:10.1146/annurev.ph.48.030186.003401.

[91]   A. Ivask, O. Bondarenko, N. Jepihhina, A. Kahru, Profiling of the reactive oxygen species-related ecotoxicity of CuO, ZnO, TiO2, silver and fullerene nanoparticles using a set of recombinant luminescent Escherichia coli strains: Differentiating the impact of particles and solubilised metals, Anal. Bioanal. Chem. 398 (2010) 701–716. doi:10.1007/s00216-010-3962-7.

[92]   S. Käosaar, A. Kahru, P. Mantecca, K. Kasemets, Profiling of the toxicity mechanisms of coated and uncoated silver nanoparticles to yeast Saccharomyces cerevisiae BY4741 using a set of its 9 single-gene deletion mutants defective in oxidative stress response, cell wall or membrane integrity and endocyt, Toxicol. Vitr. 35 (2016) 149–162. doi:10.1016/j.tiv.2016.05.018.

[93]   M.S.P. Boyles, C. Ranninger, R. Reischl, M. Rurik, R. Tessadri, O. Kohlbacher, A. Duschl, C.G. Huber, Copper oxide nanoparticle toxicity profiling using untargeted metabolomics, Part. Fibre Toxicol. 13 (2016) 1–20. doi:10.1186/s12989-016-0160-6.

[94]   H.L. Karlsson, P. Cronholm, J. Gustafsson, L. Mo, Copper Oxide Nanoparticles Are Highly Toxic A Comparison between Metal Oxide Nanoparticles and Carbon Nanotubes - Chemical Research in Toxicology (ACS Publications), Chem. Res. Toxicol. 21 (2008) 1726–1732.

[95]  I. Bremner, Manifestations of copper excess, Am. J. Clin. Nutr. 67 (1998) 1069S–1073S. doi:10.1093/ajcn/67.5.1069S.

[96]  Y. Wang, W.G. Aker, H. Hwang, C.G. Yedjou, P.B. Tchounwou, A study of the mechanism of in vitro cytotoxicity of metal oxide nanoparticles using catfish primary hepatocytes and human HepG2 cells, Sci Total Environ. 409 (2011) 4753–4762. doi:10.1016/j.scitotenv.2011.07.039.A.

[97]  Z. Wang, N. Li, J. Zhao, J.C. White, P. Qu, B. Xing, CuO nanoparticle interaction with human epithelial cells: Cellular uptake, location, export, and genotoxicity, Chem. Res. Toxicol. 25 (2012) 1512–1521. doi:10.1021/tx3002093.

[98]  J.P. Piret, D. Jacques, J.N. Audinot, J. Mejia, E. Boilan, F. Noël, M. Fransolet, C. Demazy, S. Lucas, C. Saout, O. Toussaint, Copper(ii) oxide nanoparticles penetrate into HepG2 cells, exert cytotoxicity via oxidative stress and induce pro-inflammatory response, Nanoscale. 4 (2012) 7168–7184. doi:10.1039/c2nr31785k.

[99]  H.L. Karlsson, J. Gustafsson, P. Cronholm, L. Möller, Size-dependent toxicity of metal oxide particles-A comparison between nano- and micrometer size, Toxicol. Lett. 188 (2009) 112–118. doi:10.1016/j.toxlet.2009.03.014.

[100] Y. Rodhe, S. Skoglund, I. Odnevall Wallinder, Z. Potácová, L. Möller, Copper-based nanoparticles induce high toxicity in leukemic HL60 cells, Toxicol. Vitr. 29 (2015) 1711–1719. doi:10.1016/j.tiv.2015.05.020.

[101] O.M. Bondarenko, M. Sihtmäe, J. Kuzmičiova, L. Ragelienė, A. Kahru, R. Daugelavičius, Plasma membrane is the target of rapid antibacterial action of silver nanoparticles in Escherichia coli and Pseudomonas aeruginosa, Int. J. Nanomedicine. Volume 13 (2018) 6779–6790. doi:10.2147/IJN.S177163.

[102] K.B. Holt, A.J. Bard, Interaction of silver(I) ions with the respiratory chain of Escherichia coli: An electrochemical and scanning electrochemical microscopy study of the antimicrobial mechanism of micromolar Ag, Biochemistry. 44 (2005) 13214–13223. doi:10.1021/bi0508542.

[103] A. Panáček, L. Kvítek, R. Prucek, M. Kolár, R. Večeřová, N. Pizúrová, V.K. Sharma, T. Nevěčná, R. Zbořil, Silver Colloid Nanoparticles : Synthesis , Characterization, and Their Antibacterial Activity, J Phys. Chem. B. 110 (2006) 16248–16253. doi:10.1021/jp063826h.

[104] O. Choi, Z. Hu, Size dependent and reactive oxygen species related nanosilver toxicity to nitrifying bacteria, Environ. Sci. Technol. 42 (2008) 4583–4588. doi:10.1021/es703238h.

[105] Z.V. Feng, I.L. Gunsolus, T.A. Qiu, K.R. Hurley, L.H. Nyberg, H. Frew, K.P. Johnson, A.M. Vartanian, L.M. Jacob, S.E. Lohse, M.D. Torelli, R.J. Hamers, C.J. Murphy, C.L. Haynes, Impacts of gold nanoparticle charge and ligand type on surface binding and toxicity to Gram-negative and Gram-positive bacteria, Chem. Sci. 6 (2015) 5186–5196. doi:10.1039/c5sc00792e.

[106] O. Bondarenko, A. Ivask, A. Käkinen, I. Kurvet, A. Kahru, Particle-Cell Contact Enhances Antibacterial Activity of Silver Nanoparticles, PLoS One. 8 (2013). doi:10.1371/journal.pone.0064060.

[107] H.L. Karlsson, P. Cronholm, Y. Hedberg, M. Tornberg, L. De Battice, S. Svedhem, I.O. Wallinder, Cell membrane damage and protein interaction induced by copper containing nanoparticles-Importance of the metal release process, Toxicology. 313 (2013) 59–69. doi:10.1016/j.tox.2013.07.012.

[108]  S. Herrmann, M. Kostrzewa, A. Wierschem, C. Streb, Polyoxometalate ionic liquids as self-repairing acid-resistant corrosion protection, Angew. Chemie - Int. Ed. 53 (2014) 13596–13599. doi:10.1002/anie.201408171.

[109]  J. Li, Z. Chen, M. Zhou, J. Jing, W. Li, Y. Wang, L. Wu, L. Wang, Y. Wang, M. Lee, Polyoxometalate-Driven Self-Assembly of Short Peptides into Multivalent Nanofibers with Enhanced Antibacterial Activity, Angew. Chemie - Int. Ed. 55 (2016) 2592–2595. doi:10.1002/anie.201511276.

[110]  N.I. Gumerova, A. Rompel, Synthesis, structures and applications of electron-rich polyoxometalates, Nat. Rev. Chem. 2 (2018). doi:10.1038/s41570-018-0112.

[111]  S. Herrmann, C. Ritchie, C. Streb, Polyoxometalate - Conductive polymer composites for energy conversion, energy storage and nanostructured sensors, Dalt. Trans. 44 (2015) 7092–7104. doi:10.1039/c4dt03763d.

[112]  Y. Feng, Z. Han, J. Peng, J. Lu, B. Xue, L. Li, H. Ma, E. Wang, Fabrication and characterization of multilayer films based on Keggin-type polyoxometalate and chitosan, Mater. Lett. 60 (2006) 1588–1593. doi:10.1016/j.matlet.2005.11.069.

[113]  A. Bijelic, M. Aureliano, A. Rompel, The antibacterial activity of polyoxometalates: Structures, antibiotic effects and future perspectives, Chem. Commun. 54 (2018) 1153–1169. doi:10.1039/c7cc07549a.

[114]  S. Herrmann, L. De Matteis, J.M. de la Fuente, S.G. Mitchell, C. Streb, Removal of Multiple Contaminants from Water by Polyoxometalate Supported Ionic Liquid Phases (POM-SILPs), Angew. Chemie - Int. Ed. 56 (2017) 1667–1670. doi:10.1002/anie.201611072.

[115]  T. Yamase, N. Fukuda, Y. Tajima, Synergistic Effect of Polyoxotungstates in Combination with β-Lactam Antibiotics on Antibacterial Activity against Methicillin-Resistant Staphylococcus aureus, Biol.Pharm. Bull. 19 (1996) 459–465.

[116]  M. Inoue, T. Suzuki, Y. Fujita, M. Oda, N. Matsumoto, J. Iijima, T. Yamase, Synergistic effect of polyoxometalates in combination with oxacillin against methicillin-resistant and vancomycin-resistant Staphylococcus aureus: a high initial inoculum of 1×108 cfu/ml for in vivo test, Biomed. Pharmacother. 60 (2006) 220–226. doi:10.1016/j.biopha.2006.04.006.

[117]  A.G. Oomen, K. Günter, E.A.J. Bleeker, F. Van Broekhuizen, A. Sips, S. Dekkers, S.W.P. Wijnhoven, P.G. Sayre, Risk assessment frameworks for nanomaterials: Scope, link to regulations, applicability, and outline for future directions in view of needed increase in efficiency, NanoImpact. 9 (2018) 1–13. doi:10.1016/j.impact.2017.09.001.

[118]  R. Landsiedel, E. Fabian, L. Ma-Hock, W. Wohlleben, K. Wiench, F. Oesch, B. Van Ravenzwaay, Toxico-/biokinetics of nanomaterials, Arch. Toxicol. 86 (2012) 1021–1060. doi:10.1007/s00204-012-0858-7.

[119]  G. Oberdörster, E. Oberdörster, J. Oberdörster, Nanotoxicology: An emerging discipline evolving from studies of ultrafine particles, Environ. Health Perspect. 113 (2005) 823–839. doi:10.1289/ehp.7339.

[120]  J. Ai, E. Biazar, M. Jafarpour, M. Montazeri, A. Majdi, S. Aminifard, M. Zafari, H.R. Akbari, H.G. Rad, Nanotoxicology and nanoparticle safety in biomedical designs, Int. J. Nanomedicine. 6 (2011) 1117–1127. doi:10.2147/IJN.S16603.

[121]  W.G. Kreyling, M. Semmler-Behnke, J. Seitz, W. Scymczak, A. Wenk, P. Mayer, S. Takenaka, G. Oberdrster, Size dependence of the translocation of inhaled iridium and carbon nanoparticle aggregates fürom the lung of rats to the blood and secondary target organs, Inhal. Toxicol. 21 (2009) 55–60. doi:10.1080/08958370902942517.

[122] S. Yamago, H. Tokuyama, E. Nakamura, K. Kikuchi, S. Kananishi, K. Sueki, H. Nakahara, S. Enomoto, F. Ambe, In vivo biological behavior of a water-miscible fullerene: 14C labeling, absorption, distribution, excretion and acute toxicity, Chem. Biol. 2 (1995) 385–389. doi:10.1016/1074-5521(95)90219-8.

[123] A.T. Florence, Nanoparticle uptake by the oral route: Fulfilling its potential?, Drug Discov. Today Technol. 2 (2005) 75–81. doi:10.1016/j.ddtec.2005.05.019.

[124] E. Fabian, R. Landsiedel, L. Ma-Hock, K. Wiench, W. Wohlleben, B. Van Ravenzwaay, Tissue distribution and toxicity of intravenously administered titanium dioxide nanoparticles in rats, Arch. Toxicol. 82 (2008) 151–157. doi:10.1007/s00204-007-0253-y.

[125] W.M.S. Russell, R.L. Burch, The Principles of Humane Experimental Technique, Methuen Co., Ltd. (1959). doi:10.1017/CBO9781107415324.004.

[126] Regulation (EC) No 1223/2009 of the European Parliament and of the Council of 30 November 2009 on cosmetic products, n.d.

[127] M.E. Pittman, S.W. Edwards, C. Ives, H.M. Mortensen, AOP-DB: A database resource for the exploration of Adverse Outcome Pathways through integrated association networks, Toxicol. Appl. Pharmacol. 343 (2018) 71–83. doi:10.1016/j.taap.2018.02.006.

[128] D. Krewski, D. Acosta, M. Andersen, H. Anderson, J.C. Bailar, K. Boekelheide, R. Brent, G. Charnley, V.G. Cheung, S. Green, K.T. Kelsey, N.I. Kerkvliet, A.A. Li, L. McCray, O. Meyer, R.D. Patterson, W. Pennie, R.A. Scala, G.M. Solomon, M. Stephens, J. Yager, L. Zeise, Toxicity testing in the 21st century: A vision and a strategy, J. Toxicol. Environ. Heal. - Part B Crit. Rev. 13 (2010) 51–138. doi:10.1080/10937404.2010.483176.

[129] H. Johnston, G. Pojana, S. Zuin, N.R. Jacobsen, P. Moller, S. Loft, M. Semmler-Behnke, C. McGuiness, D. Balharry, A. Marcomini, H. Wallin, W. Kreyling, K. Donaldson, L. Tran, V. Stone, Engineered nanomaterial risk. Lessons learnt from completed nanotoxicology studies: Potential solutions to current and future challenges, Crit. Rev. Toxicol. 43 (2013) 1–20. doi:10.3109/10408444.2012.738187.

[130] P. Cronholm, H.L. Karlsson, J. Hedberg, T.A. Lowe, L. Winnberg, K. Elihn, I.O. Wallinder, L. Möller, Intracellular uptake and toxicity of Ag and CuO nanoparticles: A comparison between nanoparticles and their corresponding metal ions, Small. 9 (2013) 970–982. doi:10.1002/smll.201201069.

[131] A. Kunzmann, B. Andersson, T. Thurnherr, H. Krug, A. Scheynius, B. Fadeel, Toxicology of engineered nanomaterials: Focus on biocompatibility, biodistribution and biodegradation, Biochim. Biophys. Acta - Gen. Subj. 1810 (2011) 361–373. doi:10.1016/j.bbagen.2010.04.007.

[132] S. Arora, J. Jain, J.M. Rajwade, K.M. Paknikar, Cellular responses induced by silver nanoparticles: In vitro studies, Toxicol. Lett. 179 (2008) 93–100. doi:10.1016/j.toxlet.2008.04.009.

[133] E. Fröhlich, Comparison of conventional and advanced in vitro models in the toxicity testing of nanoparticles, Artif. Cells, Nanomedicine, Biotechnol. 46 (2018) 1–17. doi:10.1080/21691401.2018.1479709.

[134] J.S. Tsuji, A.D. Maynard, P.C. Howard, J.T. James, C. Lam, D.B. Warheit, A.B. Santamaria, Research Strategies for Safety Evaluation of Nanomaterials, Part IV : Risk Assessment of Nanoparticles, Toxicol. Sci. 89 (2006) 42–50. doi:10.1093/toxsci/kfi339.

[135] W.H. De Jong, P.J. Borm, Drug delivery and nanoparticles : Applications and hazards, Int. J. Nanomedicine. 3 (2008) 133–149.

[136] U. Zimper, J. Aaltonen, K. Krauel-Goellner, K.C. Gordon, C.J. Strachan, T. Rades, The Influence of Milling on the Dissolution Performance of Simvastatin, Pharmaceutics. 2 (2010) 419–431. doi:10.3390/pharmaceutics2040419.

[137] C. Buzea, I.I. Pacheco, K. Robbie, Nanomaterials and nanoparticles : Sources and toxicity, Biointerphases. 2 (2007) 17–71. doi:10.1116/1.2815690.

[138] V. Lievin-Le Moal, A.L. Servin, Pathogenesis of Human Enterovirulent Bacteria: Lessons from Cultured, Fully Differentiated Human Colon Cancer Cell Lines, Microbiol. Mol. Biol. Rev. 77 (2013) 380–439. doi:10.1128/MMBR.00064-12.

[139] N. Navabi, M.A. McGuckin, S.K. Lindén, Gastrointestinal Cell Lines Form Polarized Epithelia with an Adherent Mucus Layer when Cultured in Semi-Wet Interfaces with Mechanical Stimulation, PLoS One. 8 (2013) 1–15. doi:10.1371/journal.pone.0068761.

[140] C.A. Richmond, D.T. Breault, Move Over Caco-2 Cells: Human-Induced Organoids Meet Gut-on-a-Chip, Cmgh. 5 (2018) 634–635. doi:10.1016/j.jcmgh.2018.01.016.

[141] M. Natoli, B.D. Leoni, I. D'Agnano, F. Zucco, A. Felsani, Good Caco-2 cell culture practices, Toxicol. Vitr. 26 (2012) 1243–1246. doi:10.1016/j.tiv.2012.03.009.

[142] S. Gioria, J.L. Vicente, P. Barboro, R. La Spina, G. Tomasi, P. Urbán, A. Kinsner-Ovaskainen, R. François, H. Chassaigne, A combined proteomics and metabolomics approach to assess the effects of gold nanoparticles in vitro, Nanotoxicology. 10 (2016) 1743–5404. doi:10.3109/17435390.2015.1121412.

[143] B. Lehmann, HaCaT cell line as a model system for vitamin D3 metabolism in human skin, J. Invest. Dermatol. 108 (1997) 78–82. doi:10.1111/1523-1747.ep12285640.

[144] C. Hyde, B. Hollier, A. Anderson, D. Harkin, Z. Upton, Insulin-like growth factors (IGF) and IGF-binding proteins bound to vitronectin enhance keratinocyte protein synthesis and migration, J. Invest. Dermatol. 122 (2004) 1198–1206. doi:10.1111/j.0022-202X.2004.22527.x.

[145] J. López-García, M. Lehocký, P. Humpolíček, P. Sáha, HaCaT Keratinocytes Response on Antimicrobial Atelocollagen Substrates: Extent of Cytotoxicity, Cell Viability and Proliferation, J. Funct. Biomater. 5 (2014) 43–57. doi:10.3390/jfb5020043.

[146] A. Hoh, K. Maier, Comparative Cytotoxicity Test with Human Keratinocytes, HaCaT Cells, and Skin Fibroblasts to Investigate Skin-Irritating Substances, in: Cell Tissue Cult. Model. Dermatological Res., 1993: pp. 341–347. doi:10.1007/978-3-642-77817-9.

[147] S. Kar, A. Gajewicz, K. Roy, J. Leszczynski, T. Puzyn, Extrapolating between toxicity endpoints of metal oxide nanoparticles: Predicting toxicity to Escherichia coli and human keratinocyte cell line (HaCaT) with Nano-QTTR, Ecotoxicol. Environ. Saf. 126 (2016) 238–244. doi:10.1016/j.ecoenv.2015.12.033.

[148] S. Gordon, P.R. Taylor, Monocyte and macrophage heterogeneity, Nat. Rev. Immunol. 5 (2005) 953–964. doi:10.1038/nri1733.

[149] M.E. Lund, J. To, B.A. O'Brien, S. Donnelly, The choice of phorbol 12-myristate 13-acetate differentiation protocol influences the response of THP-1 macrophages to a pro-inflammatory stimulus, J. Immunol. Methods. 430 (2016) 64–70. doi:10.1016/j.jim.2016.01.012.

[150] M.B. Maeß, B. Wittig, A. Cignarella, S. Lorkowski, Reduced PMA enhances the responsiveness of transfected THP-1 macrophages to polarizing stimuli, J. Immunol. Methods. 402 (2014) 76–81. doi:10.1016/j.jim.2013.11.006.

[151] S. Aras, M. Raza Zaidi, TAMeless traitors: Macrophages in cancer progression and metastasis, Br. J. Cancer. 117 (2017) 1583–1591. doi:10.1038/bjc.2017.356.

[152] V. Kodali, M.H. Littke, S.C. Tilton, J.G. Teeguarden, L. Shi, C.W. Frevert, W. Wang, J.G. Pounds, B.D. Thrall, Dysregulation of Macrophage Activation Profiles by Engineered Nanoparticles, AscNano. 7 (2013) 6997–7010. doi:10.1021/nn402145t.

[153] C. Meindl, K. Öhlinger, J. Ober, E. Roblegg, E. Fröhlich, Comparison of fluorescence-based methods to determine nanoparticle uptake by phagocytes and non-phagocytic cells in vitro, Toxicology. 378 (2017) 25–36. doi:10.1016/j.tox.2017.01.001.

[154] C.E. Soma, C. Dubernet, G. Barratt, S. Benita, P. Couvreur, Investigation of the role of macrophages on the cytotoxicity of doxorubicin and doxorubicin-loaded nanoparticles on M5076 cells in vitro, J. Control. Release. 68 (2000) 283–289.

[155] J.Z. Rappoport, Focusing on clathrin-mediated endocytosis, Biochem. J. 412 (2008) 415–423. doi:10.1042/bj20080474.

[156] D. Fourches, D. Pu, C. Tassa, R. Weissleder, S.Y. Shaw, R.J. Mumper, A. Tropsha, Quantitative Nanostructure-Activity Relationship (QNAR) Modeling, ACS Nano. 4 (2011) 6903–6913. doi:10.1126/scisignal.2001449.Engineering.

[157] M.A. Dobrovolskaia, S.E. McNeil, Immunological properties of engineered nanomaterials, Nat. Nanotechnol. 2 (2007) 469–478. doi:10.1038/nnano.2007.223.

[158] J. Dausend, A. Musyanovych, M. Dass, P. Walther, H. Schrezenmeier, K. Landfester, V. Mailänder, Uptake mechanism of oppositely charged fluorescent nanoparticles in Hela cells, Macromol. Biosci. 8 (2008) 1135–1143. doi:10.1002/mabi.200800123.

[159] S. Zhang, J. Li, G. Lykotrafitis, G. Bao, S. Suresh, L. Ju, G. Lykotrafitis, G. Bao, S. Suresh, J. Li, G. Lykotrafitis, G. Bao, S. Suresh, Size Dependent Endocytosis of Nanoparticles, Adv. Mater. 21 (2009) 419–424. doi:10.1002/adma.200801393.Size-Dependent.

[160] Y. Min, M. Akbulut, K. Kristiansen, Y. Golan, J. Israelachvili, The role of interparticle and external forces in nanoparticle assembly, Nat. Mater. 7 (2008) 527–538. doi:10.1038/nmat2206.

[161] F. Zhao, Y. Zhao, Y. Liu, X. Chang, C. Chen, Y. Zhao, Cellular uptake, intracellular trafficking, and cytotoxicity of nanomaterials, Small. 7 (2011) 1322–1337. doi:10.1002/smll.201100001.

[162] R.F. Hamilton, S. Buckingham, A. Holian, The effect of size on Ag nanosphere toxicity in macrophage cell models and lung epithelial cell lines is dependent on particle dissolution, Int. J. Mol. Sci. 15 (2014) 6815–6830. doi:10.3390/ijms15046815.

[163] W. Zhang, P. Jiang, W. Chen, B. Zheng, Z. Mao, A. Antipov, M. Correia, E.H. Larsen, C. Gao, Genotoxicity of Copper Oxide Nanoparticles with Different Surface Chemistry on Rat Bone Marrow Mesenchymal Stem Cells, J. Nanosci. Nanotechnol. 16 (2016) 5489–5497. doi:10.1166/jnn.2016.11753.

[164] K. Giannousi, E. Hatzivassiliou, S. Mourdikoudis, G. Vourlias, A. Pantazaki, C. Dendrinou-Samara, Synthesis and biological evaluation of PEGylated CuO nanoparticles, J. Inorg. Biochem. 164 (2016) 82–90. doi:10.1016/j.jinorgbio.2016.09.003.

[165] O.M. Bondarenko, M. Heinlaan, M. Sihtmäe, A. Ivask, I. Kurvet, E. Joonas, A. Jemec, M. Mannerström, T. Heinonen, R. Rekulapelly, S. Singh, J. Zou, I. Pyykkö, D. Drobne, A. Kahru, Multilaboratory evaluation of 15 bioassays for (eco)toxicity screening and hazard ranking of engineered nanomaterials: FP7 project NANOVALID, Nanotoxicology. 10 (2016) 1229–1242. doi:10.1080/17435390.2016.1196251.

[166] M. Woutersen, B. Van Der Gaag, A.A. Boakye, J. Mink, R.S. Marks, A.J. Wagenvoort, H.A.M. Ketelaars, B. Brouwer, M.B. Heringa, Development and validation of an on-linewater toxicity sensor with immobilized luminescent bacteria for on-line surface water monitoring, Sensors. 17 (2017) 1–14. doi:10.3390/s17112682.

[167] A. Ivask, M. Virta, A. Kahru, Construction and use of specific luminescent recombinant bacterial sensors for the assessment of bioavailable fraction of cadmium, zinc, mercury and chromium in the soil, Soil Biol. Biochem. 34 (2002) 1439–1447. doi:10.1016/S0038-0717(02)00088-3.

[168] A. Ivask, T. Rõlova, A. Kahru, A suite of recombinant luminescent bacterial strains for the quantification of bioavailable heavy metals and toxicity testing, BMC Biotechnol. 9 (2009) 1–15. doi:10.1186/1472-6750-9-41.

[169] M. Solioz, J. V. Stoyanov, Copper homeostasis in Enterococcus hirae, FEMS Microbiol. Rev. 27 (2003) 183–195. doi:10.1016/S0168-6445(03)00053-6.

[170] C. Rensing, G. Grass, Escherichia coli mechanisms of copper homeostasis in a changing environment, FEMS Microbiol. Rev. 27 (2003) 197–213. doi:10.1016/S0168-6445(03)00049-4.

[171] H.J. Purohit, Biosensors as molecular tools for use in bioremediation, J. Clean. Prod. 11 (2003) 293–301. doi:org/10.1016/S0959-6526(02)00072-0.

[172] K. Kasemets, S. Suppi, K. Künnis-Beres, A. Kahru, Toxicity of CuO nanoparticles to yeast saccharomyces cerevisiae BY4741 wild-type and its nine isogenic single-gene deletion mutants, Chem. Res. Toxicol. 26 (2013) 356–367. doi:10.1021/tx300467d.

[173] S. Suppi, K. Kasemets, A. Ivask, K. Künnis-Beres, M. Sihtmäe, I. Kurvet, V. Aruoja, A. Kahru, A novel method for comparison of biocidal properties of nanomaterials to bacteria, yeasts and algae, J. Hazard. Mater. 286 (2015) 75–84. doi:10.1016/j.jhazmat.2014.12.027.

[174] ISO 20776-1:2006 Clinical Laboratory Testing and in Vitro Diagnostic Test Systems -- Susceptibility Testing of Infectious Agents and Evaluation of Performance of Antimicrobial Susceptibility Test Devices -- Part 1 2006., n.d.

[175] T. Yao, Y. Asayama, Animal-cell culture media: History, characteristics, and current issues, Reprod. Med. Biol. 16 (2017) 99–117. doi:10.1002/rmb2.12024.

[176] I.T. Jolliffe, J. Cadima, J. Cadima, Principal component analysis : a review and recent developments Subject Areas, Phil.Trans.R.Soc.A. 374 (2016) 1–16.

[177] N. Mandzy, E. Grulke, T. Druffel, Breakage of TiO2 agglomerates in electrostatically stabilized aqueous dispersions, Powder Technol. 160 (2005) 121–126. doi:10.1016/j.powtec.2005.08.020.

[178] E.J. Petersen, T.B. Henry, J. Zhao, R.I. MacCuspie, T.L. Kirschling, M.A. Dobrovolskaia, V. Hackley, B. Xing, J.C. White, Identification and avoidance of potential artifacts and misinterpretations in nanomaterial ecotoxicity measurements, Environ. Sci. Technol. 48 (2014) 4226–4246. doi:10.1021/es4052999.

[179] V. Mirshafiee, R. Kim, S. Park, M. Mahmoudi, M.L. Kraft, Impact of protein pre-coating on the protein corona composition and nanoparticle cellular uptake, Biomaterials. 75 (2016) 295–304. doi:10.1016/j.biomaterials.2015.10.019.

[180] C.D. Walkey, W.C.W. Chan, Understanding and controlling the interaction of nanomaterials with proteins in a physiological environment, Chem. Soc. Rev. 41 (2012) 2780–2799. doi:10.1039/c1cs15233e.

[181] M. López-Heras, I.G. Theodorou, B.F. Leo, M.P. Ryan, A.E. Porter, Towards understanding the antibacterial activity of Ag nanoparticles: Electron microscopy in the analysis of the materials-biology interface in the lung, Environ. Sci. Nano. 2 (2015) 312–326. doi:10.1039/c5en00051c.

[182] M.K. Rai, S.D. Deshmukh, A.P. Ingle, A.K. Gade, Silver nanoparticles: The powerful nanoweapon against multidrug-resistant bacteria, J. Appl. Microbiol. 112 (2012) 841–852. doi:10.1111/j.1365-2672.2012.05253.x.

[183] J.S. Kim, E. Kuk, K.N. Yu, J.-H. Kim, S.J. Park, H.J. Lee, S.H. Kim, Y.K. Park, Y.H. Park, C.Y. Hwang, Y.-K. Kim, Y.-S. Lee, D.H. Jeong, M.-H. Cho, Antimicrobial effects of silver nanoparticles, Nanomedicine. 3 (2007) 95–101. doi:10.1016/j.nano.2006.12.001.

[184] S.-H. Kim, H.-S. Lee, D.-S. Ryu, S.-J. Choi, D.-S. Lee, Antibacterial activity of silver-nanoparticles against Staphylococcus aureus and Escherichia coli, Korean J. Microbiol. Biotechnol. 39 (2011) 77–85.

[185] S. Galdiero, A. Falanga, M. Cantisani, R. Tarallo, M. Elena Della Pepa, V. D'Oriano, M. Galdiero, Microbe-Host Interactions: Structure and Role of Gram-Negative Bacterial Porins, Curr. Protein Pept. Sci. 13 (2013) 843–854. doi:10.2174/138920312804871120.

[186] E. Vargas, S. Gutiérrez, M.E. Ambriz, C. Cervantes, Chromosome-encoded inducible copper resistance in Pseudomonas strains, Antonie Van Leeuwenhoek. 68 (1995) 225–229. doi:10.1007/BF00871819.

[187] C. Lin, B.H. Olson, Occurrence of cop -like copper resistance genes among bacteria isolated from a water distribution system, Can. J. Microbiol. 41 (1995) 642–646. doi:10.1139/m95-087.

[188] A.A. de Lima e Silva, M.A.R. de Carvalho, S.A.L. de Souza, P.M.T. Dias, R.G. da Silva Filho, C.S. de M. Saramago, C.A. de M. Bento, E. Hofer, Heavy metal tolerance (Cr, Ag and Hg) in bacteria isolated from sewage, Brazilian J. Microbiol. 43 (2012) 1620–1631. doi:10.1590/S1517-83822012000400047.

[189] E. Moschini, M. Gualtieri, M. Colombo, U. Fascio, M. Camatini, P. Mantecca, The modality of cell-particle interactions drives the toxicity of nanosized CuO and TiO2in human alveolar epithelial cells, Toxicol. Lett. 222 (2013) 102–116. doi:10.1016/j.toxlet.2013.07.019.

[190] S. Buffet-Bataillon, P. Tattevin, M. Bonnaure-Mallet, A. Jolivet-Gougeon, Emergence of resistance to antibacterial agents: The role of quaternary ammonium compounds - A critical review, Int. J. Antimicrob. Agents. 39 (2012) 381–389. doi:10.1016/j.ijantimicag.2012.01.011.

[191] L. Furi, M.L. Ciusa, D. Knight, V. Di Lorenzo, N. Tocci, D. Cirasol, L. Aragones, J.R. Coelho, A.T. Freitas, E. Marchi, L. Moce, P. Visa, J.B. Northwood, C. Viti, E. Borghi, G. Orefici, I. Morrissey, M.R. Oggioni, Evaluation of reduced susceptibility to quaternary ammonium compounds and bisbiguanides in clinical isolates and laboratory-generated mutants of staphylococcus aureus, Antimicrob. Agents Chemother. 57 (2013) 3488–3497. doi:10.1128/AAC.00498-13.

[192] L. Grama, A. Man, D.L. Muntean, S.A.G. Florea, F. Boda, A. Curticăpean, Antibacterial activity of some saturated polyoxotungstates, Rev. Rom. Med. Lab. 22 (2014) 111–118. doi:10.2478/rrlm-2014-0007.

[193] N. Durán, C.P. Silveira, M. Durán, D.S.T. Martinez, Silver nanoparticle protein corona and toxicity: a mini-review., J. Nanobiotechnology. 13 (2015) 1–17. doi:10.1186/s12951-015-0114-4.

[194] K. Theophel, V.J. Schacht, M. Schlüter, S. Schnell, C.-S. Stingu, R. Schaumann, M. Bunge, The importance of growth kinetic analysis in determining bacterial susceptibility against antibiotics and silver nanoparticles., Front. Microbiol. 5 (2014) 1–10. doi:10.3389/fmicb.2014.00544.

[195] J.P. Ruparelia, A.K. Chatterjee, S.P. Duttagupta, S. Mukherji, Strain specificity in antimicrobial activity of silver and copper nanoparticles, Acta Biomater. 4 (2008) 707–716. doi:10.1016/j.actbio.2007.11.006.

[196] R.J. Griffitt, R. Weil, K.A. Hyndman, N.D. Denslow, K. Powers, D. Taylor, D.S. Barber, Exposure to copper nanoparticles causes gill injury and acute lethality in zebrafish (Danio rerio), Environ. Sci. Technol. 41 (2007) 8178–8186. doi:10.1021/es071235e.

[197] O. Bondarenko, A. Ivask, A. Käkinen, A. Kahru, Sub-toxic effects of CuO nanoparticles on bacteria: Kinetics, role of Cu ions and possible mechanisms of action, Environ. Pollut. 169 (2012) 81–89. doi:10.1016/j.envpol.2012.05.009.

[198] R. Ye, H. Xu, C. Wan, S. Peng, L. Wang, H. Xu, Z.P. Aguilar, Y. Xiong, Z. Zeng, H. Wei, Antibacterial activity and mechanism of action of ε-poly-l-lysine, Biochem. Biophys. Res. Commun. 439 (2013) 148–153. doi:10.1016/j.bbrc.2013.08.001.

[199] K. Rajagopal, P.K. Singh, R. Kumar, K.F. Siddiqui, CTAB-mediated, single-step preparation of competent Escherichia coli, Bifidobacterium sp: And Kluyveromyces lactis cells, Meta Gene. 2 (2014) 807–818. doi:10.1016/j.mgene.2014.10.002.

[200] S.L. Lai, C.-H. Chen, K.-L. Yang, Enhancing the Fluorescence Intensity of DNA Microarrays by Using Cationic Surfactants, Langmuir. 27 (2011) 5659–5664. doi:10.1021/la2004694.

[201] Y.L. Lee, T. Cesario, J. Owens, E. Shanbrom, L.D. Thrupp, Antibacterial activity of citrate and acetate, Nutrition. 18 (2002) 665–666. doi:10.1016/S0899-9007(02)00782-7.

[202] S. Nagaoka, S. Murata, K. Kimura, T. Mori, K. Hojo, Antimicrobial activity of sodium citrate against Streptococcus pneumoniae and several oral bacteria, Lett. Appl. Microbiol. 51 (2010) 546–551. doi:10.1111/j.1472-765X.2010.02932.x.

[203] G. Simonetti, N. Simonetti, A. Villa, Tetracycline in Combination with Sodium Dioctylsulfosuccinate Show Increased Antimicrobial Activity in Resistant Microorganisms, J. Chemother. 16 (2004) 38–44. doi:10.1179/joc.2004.16.1.38.

[204] L.P. Padhye, B. Hertzberg, G. Yushin, C.H. Huang, N -nitrosamines formation from secondary amines by nitrogen fixation on the surface of activated carbon, Environ. Sci. Technol. 45 (2011) 8368–8376. doi:10.1021/es201696e.

[205] C.R.K. Murthy, K. V. Rama Rao, G. Bai, M.D. Norenberg, Ammonia-induced production of free radicals in primary cultures of rat astrocytes, J. Neurosci. Res. 66 (2001) 282–288. doi:10.1002/jnr.1222.

[206] C. Loos, T. Syrovets, A. Musyanovych, V. Mailänder, K. Landfester, T. Simmet, Amino-functionalized nanoparticles as inhibitors of mTOR and inducers of cell cycle arrest in leukemia cells, Biomaterials. 35 (2014) 1944–1953. doi:10.1016/j.biomaterials.2013.11.056.

[207] S.L. Fink, B.T. Cookson, Apoptosis , Pyroptosis , and Necrosis : Mechanistic Description of Dead and Dying Eukaryotic Cells, Infect. Immun. 73 (2005) 1907–1916. doi:10.1128/IAI.73.4.1907.

[208] O. Lunov, T. Syrovets, C. Loos, G.U. Nienhaus, V. Mailänder, K. Landfester, M. Rouis, T. Simmet, Amino-functionalized polystyrene nanoparticles activate the NLRP3 inflammasome in human macrophages, ACS Nano. 5 (2011) 9648–9657. doi:10.1021/nn203596e.

[209] D.K.A. Kusumahastuti, M. Sihtmäe, I. V. Kapitanov, Y. Karpichev, N. Gathergood, A. Kahru, Toxicity profiling of 24 L-phenylalanine derived ionic liquids based on pyridinium, imidazolium and cholinium cations and varying alkyl chains using rapid screening Vibrio fischeri bioassay, Ecotoxicol. Environ. Saf. 172 (2019) 556–565. doi:10.1016/j.ecoenv.2018.12.076.

[210] M. Inoue, T. Suzuki, Y. Fujita, M. Oda, N. Matsumoto, T. Yamase, Enhancement of antibacterial activity of β-lactam antibiotics by [P2W18O62]6-, [SiMo12O40]4-, and [PTi2W10O40]7-against methicillin-resistant and vancomycin-resistant Staphylococcus aureus, J. Inorg. Biochem. 100 (2006) 1225–1233. doi:10.1016/j.jinorgbio.2006.02.004.

# Acknowledgements

# Abstract

## Toxicological Profiling of Copper Oxide and Silver Nanoparticles and Polyoxometalate Ionic Liquids with Medically Relevant Bacteria and Mammalian Cells *in vitro*

Engineered metal-based nanoparticles (NPs) are efficient antimicrobial agents, the toxic effects of which depend to a large extent on their physico-chemical properties. The NPs` small size gives them large active surface area that can be modified with different surface modifications. Even though, the toxic effects of metal-based NPs have been extensively studied in recent years, there are still knowledge gaps concerning their mechanisms of toxicity. Also, there is very little information on the antimicrobial effects of polyoxometalate ionic liquids (POM-ILs).

In this thesis, the antibacterial potency of 20 NPs (Ag NPs and CuO NPs) with different sizes and different surface coatings, and POM-ILs was evaluated with Gram-negative bacteria *Escherichia coli* or *Pseudomonas aeruginosa* and Gram-positive *Staphylococcus aureus*. In addition, safety of CuO NPs to mammalian cells *in vitro* was studied.

First, the impact of NP suspension preparation protocol on physico-chemical properties and safety of NPs was evaluated using CuO NPs as an example. The results showed that the sonication of the CuO NP solutions should be done in DI water followed by making dilutions in test media, because it results in better dispersed and less dissolved particles.

Next, Ag NPs, CuO NPs and POM-ILs were tested for antibacterial effects. In general, Ag NPs proved to be more potent antibacterials than CuO NPs and POM-ILs. Interestingly, *E. coli* was the most susceptible bacterium to Ag NPs. *S. aureus*, however, was more susceptible to POM-ILs than *E. coli* and *P. aeruginosa*.

The toxicity mechanisms of Ag NPs/CuO NPs and POM-ILs were different. Ag NPs` toxicity was mainly dependent on the released ions. The Ag NPs with smaller size (10 nm) and with bis-2-ethylhexyl sulfosuccinate (AOT) or poly-vinylpyrrolidone (PVP) as coatings proved to be more efficient antibacterials. In the case of CuO NPs functionalized with amine ($-NH_2$), carboxyl (-COOH) and polyethylene glycol (PEG), the $CuO-NH_2$ proved to be the most toxic to *E. coli* but also to mammalian cells: HaCaT keratinocytes and human differentiated THP-1 macrophages. The PEG and carboxyl functionalizations on CuO NPs were the most interesting because the CuO NPs with these coatings were less toxic to human cells as compared to bacteria. The multivariate analysis revealed that the higher toxicity of CuO NPs was associated with higher copper content, positive surface charge and higher reactive oxygen species production.

The antibacterial potency of POM-ILs, however, depended on the chain length of the organic constituent. Especially high antibacterial toxicity was seen for POM-IL with seven carbon atoms.

To conclude, the toxic effects of engineered metal-based antibacterials were systematically studied in the present thesis. Based on the results it is suggested (i) to tune antibacterial properties of Ag NPs by decreasing the size and applying coating agents; (ii) to adapt the chain lengths of quaternary ammonium compounds of POM-ILs and (iii) to apply special surface coating agents on CuO NPs for achieving better antibacterial potency and safety.

# Lühikokkuvõte

## Vaskoksiidi ja hõbeda nanoosakeste ning polüoksometalaat-ioonvedelike toksilisuse uuringud meditsiiniliselt oluliste bakterite ja imetajarakkudega *in vitro*

Bakteriaalsete nakkuste, sh antibiootikumiresistentsete bakterite levik maailmas on tõsine probleem, millele otsitakse pidevalt uudseid lahendusi. Väga suur on bakteriaalse infektsiooni oht haiglates, põhjuseks arvukad kirurgilised protseduurid ja tavapärasest rohkem levivad nakkused. Üks võimalus haiglainfektsioonide vähendamiseks on tõrjuda nende levikut innovatiivsete lahendustega materjaliteaduses.

Antud doktoritöös uuriti uudseid antibakteriaalseid aineid: metallilisi nanoosakesi ja polüoksometalaate. Definitsiooni järgi on vähemasti üks nanoosakese mõõde 1–100 nm. Väiksuse tõttu on nanoosakestel suur aktiivne eripind, mis annab neile erilised füüsikalised ja keemilised omadused. Antibakteriaalseid nanoosakesi kasutatakse haiglates pindade katmiseks ja tekstiilides, et vähendada nakkushaiguste levikut. Polüoksometalaadid on negatiivse laenguga metallilised nanosuuruses struktuurid, mida on võimalik modifitseerida, lisades juurde orgaanilisi antibakteriaalseid komponente. Polüoksometalaatidel on selles konfiguratsioonis mitmeid biomeditsiinilisi rakendusi nakkuste levikute piiramiseks, näiteks kasutamine pindade katmisel ja veefiltrites.

Antud doktoritöös uuriti kokku 20 nanoosakese ja polüoksometalaat-ioonvedelike antibakteriaalset toimet ja bioloogilist ohutust imetajarakkudega *in vitro* leidmaks inimesele ohutud tõhusad antibakteriaalsed ained. Eesmärgiks oli: 1) optimeerida vaskoksiidi nanoosakeste suspensiooni ettevalmistamist katseks; 2) uurida nanoosakeste bakterivastast toimet haiglanakkusi põhjustavate bakterite *Escherichia coli, Staphylococcus aureus* ja *Pseudomonas aeruginosa* suhtes; 3) uurida nanoosakese suuruse ja pinnamodifikatsioonide mõju antibakteriaalsele toimele; 4) uurida nanoosakeste füüsikalis-keemilistest omadustest tulenevat mõju bakteritele ja imetajarakkudele *in vitro*.

Töös kasutati vaskoksiidi (CuO) ja hõbeda (Ag) nanoosakesi ning volframi (W) baasil polüoksometalaate. Vask on tuntud bakteritsiidsete omaduste poolest ja on seetõttu laialdaselt kasutusel nii tööstuses kui ka tarbekaupades. Vaskoksiidi nanoosakeste antibakteriaalsete omaduste uuringud biomeditsiinilisteks rakendusteks on leidnud huvipinda just viimasel ajal. Hõbeda nanoosakesi kasutatakse juba laialdaselt erinevates antibakteriaalse toimega toodetes, kuid vähe on uuritud hõbeda nanoosakeste spetsiifiliste katete mõju bakteritele. Polüoksometalaadid on antud uuringus seotud orgaaniliste positiivselt laetud kvaternaarsete lämmastikega, mille tulemusena saadi nii positiivse kui ka negatiivse laenguga ioonsed ained.

Kõikidest testitud ainetest olid hõbeda nanoosakesed bakteritele kõige mürgisemad. Antud töös uuriti süstemaatiliselt eri pinnamodifikatsiooniga ja suurusega (10 nm ja 50 nm) hõbeda nanoosakeste mõju grampositiivsele bakterile *Staphylococcus aureus* ja gramnegatiivsele bakterile *Escherichia coli*. Selgus, et hõbeda nanoosakestel oli tugevam inaktiveeriv mõju põhilisele haiglanakkuse põhjustajavale gramnegatiivsele *E. coli* bakterile võrreldes grampositiivse *S. aureus* bakteriga ning see sõltus kõige rohkem nanoosakeste lahustuvusest. Huvipakkuvateks kattematerjalideks hõbeda nanoosakestele olid bis-2-etüülheksüül sulfosuktsinaat (AOT) ja polüvinüülpürrolidoon

(PVP), sest nende ainetega kaetud nanoosakesed lahustusid paremini ja olid seetõttu toksilisemad.

Huviväärne oli polüoksometalaatidega ioonsete vedelike tõhus bakterivastasus veel ühele valdavale haiglanakkuste põhjustajale – grampositiivsele *S. aureus´*ele. Polüoksometalaadid, mida antud doktoritöös kasutati, olid seni teadaolevalt taolistest ühenditest kõige efektiivsemad bakterivastased ained. Doktoritöös iseloomustatakse eri pikkusega süsinikuahelate osatähtsust nende ioonsete ainete toksilisuses bakteritele *S. aureus*, *E. coli* ja *P. aeruginosa*. Tulemused näitasid, et polüoksometalaatidega ioonsete ainete antibakteriaalsed omadused sõltusid positiivselt laetud orgaaniliste komponentide süsinikuahela pikkusest. Eriti heade antibakteriaalsete omadustega olid seitsme süsinikuaatomi ahelaga polüoksometalaat-ioonvedelikud.

Vaskoksiidi nanoosakeste bakterivastane toime oli nõrgem kui hõbeda nanoosakestel, seetõttu uuriti võimalusi selle parendamiseks, modifitseerides vaskoksiidi nanoosakesi erinevate orgaaniliste funktsionaalrühmadega, nagu karboksüül, ammoonium ja polüetüleenglükool. Uuringus kasutati *E. coli* bakterit mudelina bakterivastase toime hindamiseks ning inimese immuunrakke ja naha epiteelkoerakke mudelitena bioloogilise ohutuse määramiseks *in vitro*. Vaskoksiidi bakterivastaste omaduste testimiseks tuleb nanoosakesed esmalt dispergeerida veekeskkonnas, näiteks ultraheliga töötlemise teel, et saada homogeensed lahused. Ultraheli kasutatakse tihti, kuid samas ei ole hästi teada, kuidas selle energia mõjutab nanoosakeste toksilist toimet. Siinses doktoritöös kohandati meetodeid vaskoksiidi nanoosakeste ultraheliga töötlemiseks ning hinnati dispergeeritud nanoosakeste toksilist mõju *E. coli* bakteri ja inimese sooleepiteeli Caco-2 *in vitro* rakumudeli suhtes. Tulemused näitasid, et ultrahelitöötlus kahandas nanoosakeste suurust orgaanikarikastes söötmetes ja suurendas nende toksilisust. Saadud tulemuste põhjal on soovituslik kõigepealt nanoosakesed dispergeerida vees ultraheli abil ja seejärel teha lahused orgaanikarikastes testikeskkondades, sest nii saadi väiksemad nanoosakesed, mis lahustusid vähem. Antud andmeid kasutati edasi nanoosakeste proovide ettevalmistamiseks toksilisuse uuringuteks. Need näitasid, et ootuspäraselt mõjutasid katted oluliselt vaskoksiidi nanoosakeste bakterivastast toimet. Ilmnes, et sisalduva vase kogus (suurema vasesisaldusega nanoosakesed olid toksilisemad), nanoosakese suurus (suuremad olid vähem toksilised), laeng (positiivselt laetud olid toksilisemad) ja võime indutseerida reaktiivsete hapnikuühendite tootmist (ained, mis indutseerisid aktiivsemalt reaktiivseid hapnikuühendeid olid toksilisemad) avaldasid olulist mõju kõigile toksilisuse testimise rakumudelitele. Vaskoksiidi nanoosakesed, mida oli modifitseeritud ammooniumkattega, osutusid kõige mürgisemateks. Huvipakkuvaimad olid aga karboksüül- ja polüetüleenglükoolkattega vaskoksiidi nanoosakesed, mis olid efektiivsed antibakteriaalsed ained, kuid samas inimese rakkudele vähem mürgised kui bakteritele.

Kokku võttes tuuakse antud töös soovitusi, kuidas luua tõhusaid ja ohutuid metallilisi antibakteriaalseid nanoosakesi. Kõige mõjusamateks bakterivastasteks aineteks osutusid erinevate katetega hõbeda nanoosakesed, mille toksilisus sõltus enamasti lahustuvusest. Vaskoksiidi nanoosakeste toksilist toimet suurendas aga funktsionaliseerimine, eriti ammooniumiga. Polüoksometalaatidega ioonvedelike antibakteriaalsuses oli oluline katioonsete komponentide süsinikuahela pikkus (mürgiseimad olid seitsme süsinikuaatomiga ained).

# Appendix

**Publication I**

Käkinen, A., Kahru, A., Nurmsoo, H., **Kubo, A. L.**, Bondarenko, O. M. (2016). Solubility-driven toxicity of CuO nanoparticles to Caco2 cells and *Escherichia coli*: Effect of sonication energy and test environment. Toxicology in Vitro, 36, 172–179.
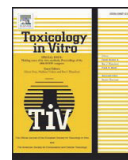
# Solubility-driven toxicity of CuO nanoparticles to Caco2 cells and *Escherichia coli*: Effect of sonication energy and test environment

Aleksandr Käkinen *, Anne Kahru, Helen Nurmsoo, Anna-Liisa Kubo, Olesja M. Bondarenko *

*Laboratory of Environmental Toxicology, National Institute of Chemical Physics and Biophysics, Akadeemia tee 23, Tallinn 12618, Estonia*

## ARTICLE INFO

## ABSTRACT

Due to small size and high surface energy nanoparticles (NPs) tend to agglomerate and precipitate. To avoid/diminish that, sonication of NPs stock suspensions *prior* toxicity testing is often applied. Currently, there is no standardized particle sonication protocol available leading to inconsistent toxicity data, especially if toxicity is driven by NPs' dissolution that may be enhanced by sonication.

In this study we addressed the effect of sonication on hydrodynamic size ($D_h$), dissolution and toxicity of copper oxide (CuO) NPs to mammalian cell line Caco-2 *in vitro* and bacteria *Escherichia coli* in the respective test environments (cell culture MEM medium, bacterial LB medium and deionised (DI) water). NPs were suspended using no sonication, water bath and probe sonication with different energy intensities.

Increased sonication energy (i) decreased the $D_h$ of CuO NPs in all three test environments; (ii) increased dissolution of NPs in MEM medium and their toxicity to Caco-2; (iii) increased dissolution of NPs in LB medium and their bioavailability to *E. coli*; and (iv) had no effect on dissolution and antibacterial effects of NPs in DI water. Thus, to reduce variations in dissolution and toxicity, we recommend sonication of NPs in DI water following the dilution into suitable test media.

© 2016 Elsevier Ltd. All rights reserved.

## 1. Introduction

The safety evaluation of industrial chemicals (*e.g.*, nanoparticles (NPs)) is a key issue in EU chemical regulation REACH (registration, evaluation, authorisation and restriction of chemicals). However, while the information on toxicity of NPs is rapidly expanding, the amount of high quality data remains limited (Krug, 2014; Oomen et al., 2014) leading to the inconsistent toxicity values for the same type of NPs (Bondarenko et al., 2013a). One reason for that are the variations in methodological settings that can significantly influence the physico-chemical characteristics of NPs and hence, their toxicity. The latter is especially crucial if toxicity is driven by dissolution of NPs (for example, CuO, Ag, ZnO) that depends on a variety of factors *e.g.*, test medium composition, temperature and time (Kasemets et al., 2009). During the recent years it has become evident that it is necessary to

systematically and accurately define and report physico-chemical characteristics (such as primary size, specific surface area, purity, crystalline structure) of NPs *prior* the test as well as in the test conditions (hydrodynamic size, zeta potential, dissolution) in order to interpret the results of the toxicity tests (Kahru and Ivask, 2013; Krug, 2014; Nel et al., 2013; Zhu et al., 2012). However, the preparation of NP dispersion and the influence of preparation method on the physico-chemical (such as aggregation/agglomeration and dissolution) and biological (toxicity) characteristics of NPs received considerably less attention. Currently, there is no common standardized protocol for the preparation of NP dispersions for the nanotoxicology studies (*e.g.*, solvent, additives, intensity of sonication).

Different approaches for the preparation of NP suspensions have been published over the last few years. To keep NPs in dispersion, the suspension of NPs is usually treated by vigorous stirring or ultrasound either using ultrasonication bath (providing low intensity energy input) or probe sonicator (higher intensity energy input). There are several studies showing that the particle dispergation and ultrasonication conditions can affect the properties of NPs in solution (dispersibility, hydrodynamic size, agglomeration, aggregation and dissolution) (Bihari et al., 2008; Jiang et al., 2009; Meißner et al., 2014; Taurozzi et al., 2012) and consequently, the toxicity (Cronholm et al., 2011; Magdolenova et al., 2012; Piret et al., 2014). Most of these previous studies focused on the effects of dispergation method on physico-chemical behaviour of $TiO_2$ NPs that are not dissolving. However, little is known about the effect of sonication procedure on the hydrodynamic size, dissolution and

---

subsequent toxicity of solubilisation-prone NPs such as CuO NPs. A few studies comparing the toxic effects of sonicated *vs* not sonicated CuO NPs (Cronholm et al., 2011; Midander et al., 2009) and sonicated *vs* stirred CuO NPs (Piret et al., 2014) inferred that CuO dispergation method may affect dissolution of NPs and hence, their toxicity. Indeed, previous studies have shown that dissolution is the most important factor in the toxicity of CuO NPs to various bacteria (Bondarenko et al., 2012; Juganson et al., 2015; Kaweeteerawat et al., 2015; Käkinen et al., 2011; Puzyn et al., 2011) as well to mammalian cells *in vitro* (Ivask et al., 2015; Karlsson et al., 2013, 2014; Zhang et al., 2012). This implies that variations in sonication protocol affecting the dissolution of NPs will most probably influence their cytotoxicity. As the dissolution of NPs depends on the surface properties such as surface reactivity, charge, composition and presence of surface defects (Midander et al., 2007a,b) that can be modulated during sonication process, we hypothesised that the CuO NP preparation method can significantly affect dissolution and toxicity of NPs to various cell types.

In the present study, we asked (i) to what extent the sonication protocol affects the toxicity of NPs in various test environments to different cell types and (ii) whether the sonication-induced changes in hydrodynamic size or/and dissolution contribute into this process. Two types of NPs, CuO from Sigma-Aldrich and CuO NPs from Intrinsiq Materials were dispersed using four different approaches i) no sonication, ii) sonication in water bath for 30-min or sonication with probe sonicator with specific energies ($E_{spec}$) iii) $5.3 \cdot 10^4$ kJ/m$^3$ and iv) Espec = $6 \cdot 10^5$ kJ/m$^3$. Three different test environments were used to prepare the CuO dispersions and test their toxicity and bioavailability to bacteria *Escherichia coli* and mammalian cell line Caco-2 *in vitro*. Both, bacteria (unicellular prokaryotic organisms with rigid cell wall and unable to particle internalisation by endocytosis) and mammalian cells (eukaryotic cells capable to particle endocytosis) are widely used as models in (nano)toxicology studies. However, most of the studies focus either on mammalian or bacterial cells and do not enable the direct comparison of the toxicity of NMs to these different cell types. It has been previously suggested that the toxicity and mechanism of action of CuO NPs to these two cell types are remarkably different due to presence or lack of particle-internalisation capability (Bondarenko et al., 2013a). It is generally accepted that the main mechanism of toxicity of metal-based dissolution-prone NMs (such as CuO) to bacteria is mediated *via* dissolved metal ions (Ivask et al., 2010; Sotiriou and Pratsinis, 2010; Bondarenko et al., 2012; Xiu et al., 2012). In contrast, additional particle-specific effects such as *e.g.*, size, shape and agglomeration status may be involved in the toxicity of NMs to mammalian cells (Lankoff et al., 2012; Piret et al., 2012; Karlsson et al., 2014). Thus, we hypothesised that sonication procedure may have different effects on bacterial *vs* mammalian cells through the modulation of agglomeration status and dissolution of CuO NMs.

## 2. Material and methods

### 2.1. Chemicals and nanoparticles

Autoclaved deionised (DI) water (18 MΩ, Millipore) was used throughout the study. CuO NPs were purchased from Sigma-Aldrich (CAS Number 1317-38-0) and from Intrinsiq Materials. NaCl, tryptone and yeast extract were from LabM. Minimum Essential Medium (MEM) with GlutaMAX, sodium pyruvate, non-essential amino acids (NEAA) and streptomycin-penicillin were from Gibco, Life Technologies; Fetal Bovine Serum (FBS) was from Biological Industries. Bacterial test medium LB was prepared by dissolving 10 g of tryptone, 5 g of yeast extract and 5 g of NaCl in 1 l of DI water (Sambrook et al., 1989), autoclaved (121 °C for 15 min) and stored at room temperature. Cell culture medium MEM contained 15% FBS, 1% NEAA, 1% sodium pyruvate, 100 µg/ml and 100 U/ml streptomycin-penicillin, respectively.

### 2.2. Preparation of nanoparticle stock suspensions

CuO NP stock suspensions (20 ml, 1 g Cu/l) were prepared using different dispersion methods (Fig. 1): no sonication, bath sonication (Branson 1510) and probe sonication (450 Ultrasonifier, Branson Ultrasonics Corporation) equipped with 3 mm microtip, either in DI water (pH = 5.8), LB (pH = 7) or MEM (pH = 7.2) media. Calorimetric determination of the delivered acoustic energy of probe sonicator was performed *prior* experiment to determine the specific energy $E_{spec}$ (Taurozzi et al., 2011) as described in supplementary information (Fig. S1). $E_{spec} = 5.3 \cdot 10^4$ kJ/m$^3$ corresponded to sonication of 20 ml of NP suspension for 3 min at 10% of probe sonicator power and $E_{spec} = 6 \cdot 10^5$ kJ/m$^3$ to 13 min 4 s at 25% of power. Probe sonication was performed in an ice bath to avoid heating of NP suspensions. Not sonicated NP suspension was shortly vortexed (1–2 s) to mix NPs before diluting the NP suspensions. The stock suspensions were used immediately after preparation.

### 2.3. Physico-chemical characterization of CuO stock suspension

#### 2.3.1. Hydrodynamic size, zeta potential and polydispersity of CuO NPs

Hydrodynamic size and polydispersity index (PDI) of CuO NPs were determined using dynamic light scattering (DLS) (Zetasizer Nano-ZS, Malvern Instruments, UK) at the concentration of 100 mg Cu/l at 0, 2 and 24 h after stock suspension preparation in DI water, LB or MEM. The measurements were carried out in triplicates using standard polypropylene plastic cuvettes of 1 cm path length. Zeta potential of CuO NPs in DI water was measured in triplicate using Zetasizer Nano-ZS and Disposable folder capillary cells.

#### 2.3.2. Dissolution of CuO NPs

Time dependent (0, 2 and 24 h) dissolution of CuO NPs in different test environments (DI water, LB, MEM) was determined using total reflection X-ray fluorescence (dissolution, Picofox S2, Bruker Corporation). For this CuO NPs stock solutions were diluted to 100 mg Cu/l in the respective medium, centrifuged at 20,000g for 30 min (Centrifuge Sigma 3-16PK). To measure dissolution, CuO NP suspensions were centrifuged immediately after dilution (0 h dissolution) or after 2 h or 24 h of incubation at 30 °C followed by centrifugation at 20,000g for 30 min. After centrifugation supernatants were collected and analysed by TXRF by mixing 40 µl of supernatant with 40 µl of reference element (2 mg/l Ga) and pipetting the 3 µl of the mixture to quarts sample holder (Analyslide Petri Dish, Pall Corporation). Three independent experiments were performed.

#### 2.3.3. Analysis of bioavailable copper

The quantification of bioavailable Cu was performed in LB medium using recombinant biosensor bacteria *E. coli* MC1061 (pSLcueR/pDNPcopAlux) in which bioluminescence is specifically induced by subtoxic concentrations of bioavailable Cu ions (Ivask et al., 2009) essentially as described by Bondarenko et al. (2013b). Bacteria were pre-grown overnight on a shaker (200 rpm, 30 °C) in 3 ml of LB medium supplemented with 100 µg/l of ampicillin and 100 µg/l of tetracycline to maintain the recombinant plasmids. 20 ml of fresh LB was inoculated with 1/50 diluted overnight culture, and bacteria were grown at 30 °C until exponential phase (OD$_{600}$ of 0.6) and diluted with LB medium until OD$_{600}$ = 0.1 (approximately 10$^6$ bacterial cells/ml).

100 µl of bacterial suspension was exposed to 100 µl of 0.01–30 mg Cu/l dilutions of CuSO$_4$ or CuO NPs in LB medium at 30 °C for 2 h. Dose–response curves of the Cu-biosensor were obtained by plotting the applied concentrations of Cu against the bioluminescence of Cu-biosensor (as fold induction) in respective samples. Fold induction was calculated by dividing the bioluminescence of Cu-biosensor in the sample to the background bioluminescence (0 mg Cu/l). Bioluminescence was measured using Orion II Luminometer (Berthold Detection Systems, Germany).
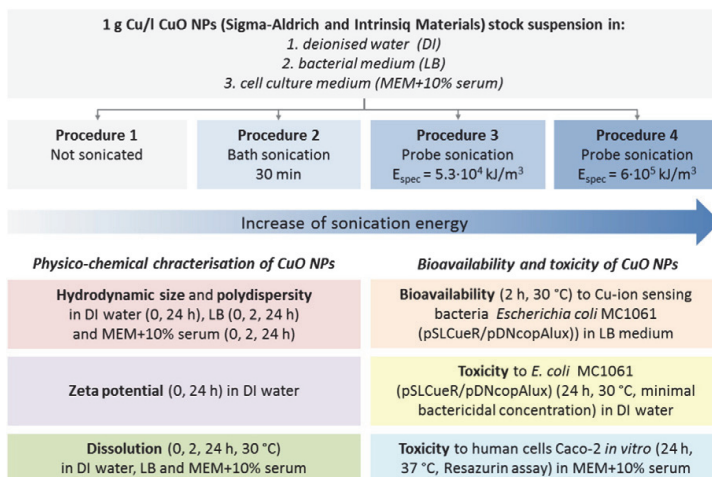
**Fig. 1.** Schematic illustration of preparation of CuO NPs stock suspensions, their physico-chemical characterization and toxicity testing.

Bioavailable Cu was determined by using the linear regression equations derived from the linear region of the dose response curves of Cu-biosensor to $CuSO_4$ and CuO NPs, whereas $CuSO_4$ was considered 100% bioavailable and was used as a standard (Bondarenko et al., 2013b). Four independent experiments in duplicates were performed.

### 2.3.4. Toxicity of CuO NPs to Escherichia coli

Minimal bactericidal concentration (MBC) of studied CuO NPs towards *E. coli* was determined essentially as described by Suppi et al. (2015). MBC was defined as the lowest tested nominal concentration of NPs which upon exposure in DI water at 30 °C for 2 h completely inhibited the formation of visible colonies of *E. coli* after sub-culturing on toxicant-free agarized LB medium. Briefly, *E. coli* MC1061 (pSLCueR/pDNcopAlux) was pre-grown overnight as described above. 20 ml of fresh LB was inoculated with 1/50 diluted overnight culture, and bacteria were grown until exponential phase ($OD_{600}$ of 0.6) at 30 °C, then washed (6000*g* 5 min) twice with DI water and diluted with DI water until $OD_{600}$ 0.1 (approximately $10^6$ bacterial cells/ml). 100 µl of diluted bacteria were added to 100 µl of CuO NPs (1–60 mg Cu/l) in DI water on a 96-well microplate (BD Falcon) and incubated in a thermostat at 30 °C for 2 h. After 2 h exposure 3 µl of suspension was pipetted on a toxicant free agarized LB growth medium (supplemented with antibiotics ampicillin 100 µg/l and tetracycline 10 µg/l) followed by incubation of the plates at 30 °C for 24 h. Six independent experiments in duplicate were performed.

### 2.3.5. Toxicity of CuO NPs to Caco-2 cells in vitro

Caco-2 cells were obtained from American Type Culture Collection (ATCC HTB-37). The cell culture was maintained according to ATCC guidance and cultured in MEM medium supplemented with 15% FBS, 1% NEAA, 1% sodium pyruvate, 100 µg/ml and 100 U/ml streptomycin-penicillin, respectively. Before the tests, cells were seeded on 96-well plates (Cellstar, Greiner) at density $5 \cdot 10^3$ cells per well and incubated for 24 h (37 °C, 95% humidity and 5% $CO_2$). After 24 h cells, exposed to 0–200 mg Cu/l CuO NPs and incubated for 24 h at 37 °C, 95% humidity and 5% $CO_2$. After 24 h exposure, cells were washed with PBS and resazurin (10 µg/ml final concentration) in the test medium was added, incubated for 2 h, and the fluorescence (530 nm excitation/590 nm emission) was measured using microplate reader (Multiskan, Thermo Scientific). In parallel, the possible interference of CuO NMs with resazurin assay was assessed by incubating NMs with resazurin without the cells. No interference was detected. Viability

(as % from untreated cells) was calculated by dividing the fluorescence value of CuO-treated cells with the fluorescence value of untreated cells. 24-h $EC_{50}$ was calculated using MS Excel macro Regtox. Three independent experiments in duplicate were performed.

### 2.3.6. Statistics

All experiments were performed at least in three independent replicates and at least in technical duplicate; the data are shown as average values ± S.D. One-way ANOVA method was used for statistical analysis, assuming equal variances at $p < 0.05$.

## 3. Results

Two types of CuO NPs were tested. CuO NPs from Sigma-Aldrich are commercially available and are widely used in nanotoxicology studies. CuO NPs from Intrinsiq Materials were used in EU FP7 flagship project NANOVALID (particle code: NNV-011). Primary particle size and specific surface area (SSA) were 30 nm and 25.5 $m^2$/g, respectively, for CuO NPs from Sigma-Aldrich (Ivask et al., 2010) and 24.5 nm and 23.4 $m^2$/g respectively, for CuO NPs from Intrinsiq Materials (Bondarenko et al., 2016). Both types of CuO NPs had no surface functionalization (coating). Thus, NPs were relatively similar in terms of primary size, SSA and coating.

Effect of sonication intensity on $D_h$, PDI and toxicity of CuO NPs was investigated in three different environments (DI water, MEM, LB) at different incubation time points (0, 2 and 24 h) after the sonication. The time points corresponded to the incubation times used in parallel for the biological assays (2 h for Cu-ion sensing *E. coli* bioavailability assay and 24 h for *E. coli* and Caco-2 toxicity tests). 30-min water bath sonication and probe sonication at $E_{spec} = 5.3 \cdot 10^4$ kJ/$m^3$ and $6 \cdot 10^5$ kJ/$m^3$ were selected on the basis of wide use in various nanotoxicology studies (Bihari et al., 2008; Mandzy et al., 2005; Meißner et al., 2014; Taurozzi et al., 2012); not sonicated CuO NPs were used in parallel for comparison.

From three test environments used, DI water is a traditional environment for the preparation of stock suspensions of NPs for ecotoxicological and some toxicological studies. Recently, DI water was shown as a suitable environment to study biocidal properties of metallic NPs towards various microorganisms (Suppi et al., 2015). Namely, the use of DI water instead of organics-containing media minimizes the effects of test medium components on bioavailability, toxicity and agglomeration of NPs (Johnston et al., 2013) and reduces the formation of reactive oxygen species (ROS) (Cohen et al., 2013).

LB medium was chosen as the traditional environment for the cultivation of microbes (Sambrook et al., 1989) that is widely used to study the potency of antibacterial compounds in various conventional assays such as bacterial growth inhibition tests. MEM supplemented with serum represented one of the traditional environments for the cultivation of mammalian cell cultures *in vitro*.

### 3.1. Effect of sonication on hydrodynamic size and polydispersity of CuO

The dependence of hydrodynamic size ($D_h$) and size distribution range (characterised by PDI values) of NPs from sonication procedure was similar for both types of CuO NPs: from Sigma-Aldrich (Fig. 2A–C) and Intrinsiq Materials (Fig. S2A–C).

Increasing sonication intensity decreased the $D_h$ of CuO NPs in all test environments whereas the most remarkable effects were observed in case of NP suspensions in DI water. For example, the $D_h$ of CuO NPs (Sigma-Aldrich) was 282 nm in case of not sonicated dispersion and 152 nm, when NPs were sonicated at the highest intensity ($E_{spec} = 6 \cdot 10^5$ kJ/m$^3$) (Fig. 2A). $D_h$ of not sonicated CuO NPs from Intrinsiq Materials was 213 nm (PDI = 0.21) and decreased to 140 nm (PDI = 0.14) after sonication at $E_{spec} = 6 \cdot 10^5$ kJ/m$^3$ (Fig. S2A, Table S1). Despite clear effect of sonication intensity on the $D_h$ of both types of CuO NPs in DI water, the effect on zeta potential was minor (Table S2).

In both organics-containing environments (LB and complete MEM) the $D_h$ and PDI of CuO NPs were higher than in DI water (Table S1). In complete MEM medium not sonicated CuO NPs from Sigma-Aldrich were highly polydispersed and agglomerated with the $D_h$ of 1120 nm and PDI = 0.82 at 0 h. The $D_h$ increased even more after 24 h exposure up to 1620 nm (PDI = 0.84) (Fig. 2B). The trends for CuO NPs from Intrinsiq Materials were similar (Fig. S2B, Table S1). Increased sonication intensity significantly dispersed both types of CuO NPs: both $D_h$ and PDI decreased immediately after sonication (0 h) and did not change significantly after 24 h incubation. Effect of sonication intensity on NP stability was observed visually confirming increased dispersibility of CuO suspensions in LB and MEM with enhanced sonication energy (Fig. S4).

Similarly to complete MEM, the $D_h$ and PDI of both types of CuO NPs in LB decreased with increasing sonication intensity immediately after sonication. However, when the $D_h$ of Sigma-Aldrich CuO NPs decreased in time (Fig. 2C), the $D_h$ of CuO NPs from Intrinsiq Materials increased after 24 h incubation (Fig. S2C). Statistical analysis showed no significant difference between $D_h$ of CuO NPs in different media tested in the current study ($p > 0.05$).

### 3.2. Effect of sonication of CuO NPs on dissolution

The dissolution of both CuO NPs in DI water (tested at CuO nominal concentration of 100 mg Cu/l and at 30 °C) was around 1% and did not depend on sonication intensity and incubation time (Figs. 2D, S2D). However, the dissolution of CuO in organics-containing media was higher, about 2–4% at 0 h in MEM medium and 7–11% in LB medium (Fig. 2E and F). Dissolution of CuO NPs increased around 3 times after 2 h incubation and around 10 times after 24 h incubation in both organic media. The difference between the CuO NPs sonicated with different intensities was especially remarkable after 24 h of incubation: for example, when the dissolution of not sonicated CuO NPs was 15.4%, the dissolution of CuO NPs in MEM medium sonicated with the highest intensity was 40%. The dissolution trends for CuO NPs from Intrinsiq Materials were similar although these NPs dissolved slightly more in MEM and LB media (Fig. S2E and F).

### 3.3. Effect of sonication of CuO NPs in LB medium on bioavailable copper

Effect of sonication on bioavailability of CuO (dissolution of CuO NPs detected by Cu ions-sensing bacteria) was analysed using sensor bacteria *E. coli* MC1061 (pSLcueR/pDNPcopAlux) after 2 h incubation time in LB medium at 30 °C. Clearly, the induction of bacterial luminescence by subtoxic concentration of CuO NPs depended on the sonication intensity used, confirming that dissolution of CuO NPs was the lowest for the not sonicated CuO and highest with the most intensively sonicated CuO NP sample (Fig. 3A). Taking into account the induction of bioluminescence by CuO NPs in bacteria (Fig. 3A), bioavailability of Cu from CuO NPs was quantified using this biological method (Fig. 3B). When the
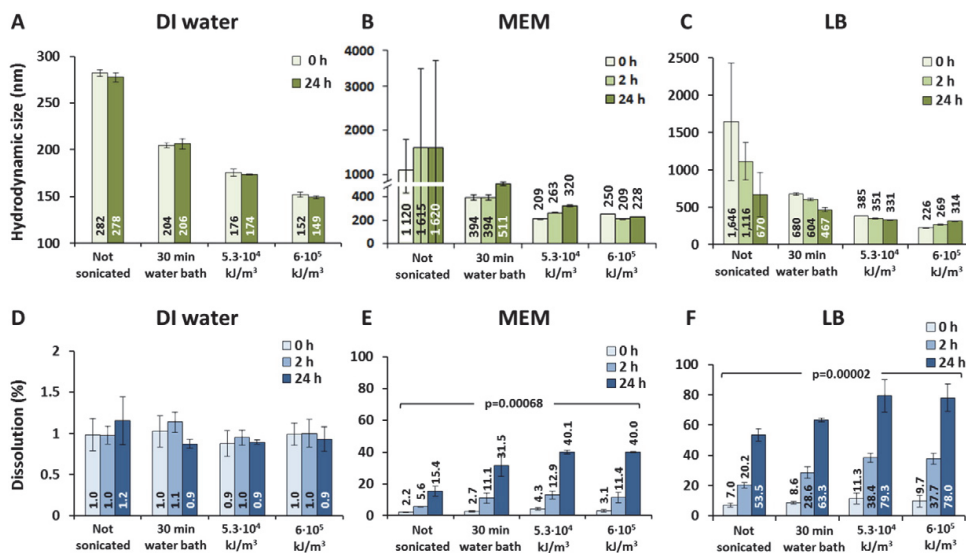


**Fig. 2.** Effect of sonication on hydrodynamic size (A–C) and dissolution (D–F) of CuO NPs (100 mg Cu/l, Sigma-Aldrich) in DI water (A and D), complete MEM medium (B and E) and LB medium (C and F) after 0, 2 h and 24 h of incubation at 30 °C. $n = 3 \pm$ standard deviation is shown. Note the different scales of Y-axis. *p*-values denote statistically significant differences between different time points (ANOVA).
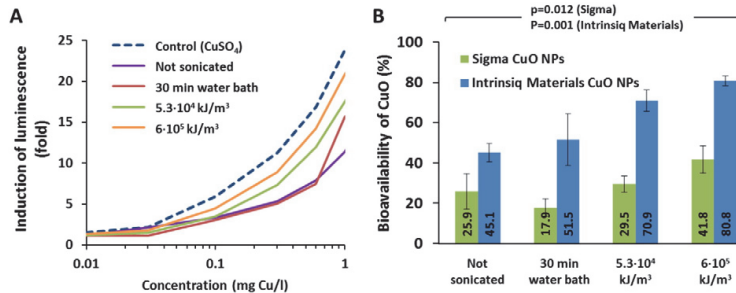
**Fig. 3.** Effect of sonication on bioavailability of copper from CuO NPs and CuSO$_4$ (100% soluble control) using Cu-sensing bacteria *Escherichia coli* MC1061 (pSLcueR/pDNPcopAlux). (**A**) Representative figure of induction of luminescence by CuO NPs and CuSO$_4$ in Cu ions-responsive bacteria *E. coli* in LB medium at 30 °C. (**B**) Bioavailable copper in differently treated CuO NPs from Sigma-Aldrich (■) and Intrinsiq Materials (■) (calculated from Fig. 3A as described in Materials and Methods, $n = 4 \pm$ standard deviation is shown). p-values denote statistically significant differences between different sonication methods (ANOVA).

bioavailability of not sonicated Sigma-Aldrich CuO NPs was 25.9%, the sonication at the highest intensity increased the bioavailability to sensor bacteria to 42%. Bioavailability of CuO NPs from Intrinsiq Materials had the same dependence on sonication procedure, but was approximately twice higher than for CuO NPs from Sigma-Aldrich (Fig. 3B).

When we compared the data on solubility of both CuO preparations analysed after 2 h of incubation in LB medium (Figs. 2F, S2F) with the bioavailability data measured using *E. coli* sensor bacteria after 2 h of incubation in LB medium, the correlation was not so remarkable, $R^2 = 0.61$, although the data pointed to the same direction (Fig. S3A). However, the correlation was more obvious in case of CuO NPs from Intrinsiq Materials ($R^2 = 0.98$; Fig. S3B) than CuO NPs from Sigma-Aldrich ($R^2 = 0.40$; Fig. S3C). This may be related to the smaller primary size of CuO NPs from Intrinsiq Materials (24.5 nm) compared to CuO NPs from Sigma-Aldrich (30 nm) leading to higher dissolution and bioavailability of the CuO NPs from Intrinsiq Materials compared to CuO NPs from Sigma-Aldrich.

*3.4. Effect of sonication on toxicity of CuO*

Effect of sonication of CuO on cytotoxicity was studied by determining (i) minimal bactericidal concentrations of differently sonicated CuO to bacteria *E. coli* in DI water (Fig. 4) and (ii) 24 h EC$_{50}$ values of CuO NP preparations to Caco-2 cells *in vitro* in complete MEM medium (Fig. 5).

MBC values for both types of CuO NPs to bacteria *E. coli* were the same (2 h MBC = 15 ± 10 mg Cu/l) regardless of the sonication protocol used (Fig. 4). Thus, sonication decreased the D$_h$ of CuO NPs in DI water (approximately 2-fold, Fig. 2A) but had no effect on dissolution (Fig. 2D) and toxicity to *E. coli* (Fig. 4A), suggesting that (i) toxicity of

CuO NPs to *E. coli* depended on dissolution and (ii) dissolution and toxicity of CuO NPs did not depend on hydrodynamic size.

The toxicity of both types of CuO NPs to Caco-2 cells *in vitro* increased with the sonication intensity (Fig. 5). Remarkably lower toxicity was observed for not sonicated CuO NPs (EC$_{50}$ = 61.0 and 67.8 mg Cu/l for CuO from Sigma-Aldrich and Intrinsiq Materials, respectively) that was assumingly caused by pronounced agglomeration (Figs. 2B, S2B; Table S1) and low dissolution of CuO NPs (Figs. 2E, S2E). Toxicity of CuO NPs sonicated for 30 min in water bath significantly increased – EC$_{50}$ were 12.3 and 13.3 mg Cu/l for NPs from Sigma-Aldrich and Intrinsiq Materials, respectively. CuO NPs sonicated with probe sonicator were slightly more toxic than CuO treated with water bath but this difference was small and statistically not significant. Overall, toxicity of both types of CuO to Caco-2 cells was comparable.

## 4. Discussion

Sonication of NP suspension *prior* toxicological studies are widely used for dispersion of particles (Handy, 2012; Murdock et al., 2008; Taurozzi et al., 2012). The recommended dispersion protocols used for various types of NPs are summarized by EU FP7 project NanoReg (2014). However, no standardized NP dispersion protocol is currently available and various authors use different methods. In general NP stock suspensions can be prepared using two different approaches: (i) one-tiered approach, where NPs are sonicated directly in the test medium that is used for the subsequent toxicity testing or (ii) two-tiered approach, which comprises the preparation of NP stock suspension in DI water and then dilution of this suspension to the test media (Meißner et al., 2014). Some authors prefer one-tiered approach and
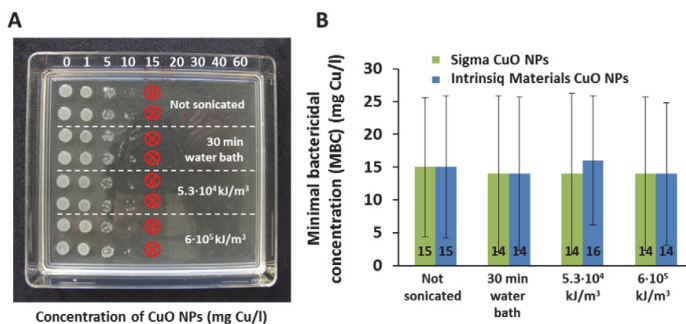


**Fig. 4.** (**A**) Representative photo of determination of minimal bactericidal concentration (MBC) of differently sonicated CuO NPs (Intrinsiq Materials) to *Escherichia coli* bacteria after 2-h exposure in DI water at 30 °C. (**B**) 2-h MBC values (mg Cu/l) of differently sonicated CuO NPs from Sigma-Aldrich (■) and Intrinsiq Materials (■) to *E. coli* bacteria after 2 h exposure in DI water. $n = 6 \pm$ standard deviation is shown.
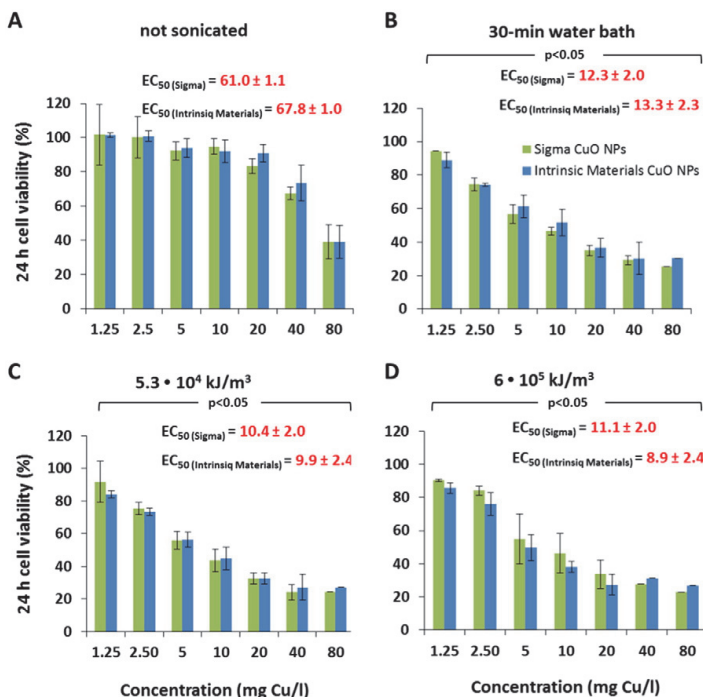
**Fig. 5.** The toxicity of CuO NPs from Sigma-Aldrich (■) and Intrinsiq Materials (■) to Caco-2 cells *in vitro* (24 h, Resazurin assay; MEM medium, 37 °C). NPs stock suspensions were prepared using four dispersion methods using different sonication regimes. n = 3 ± standard deviation is shown.

prepare the stock suspensions of NPs directly in test medium (Magdolenova et al., 2012; Meißner et al., 2014) whereas other researchers suggest first to prepare the stock suspensions in DI water (Cohen et al., 2013; PROSPEcT, 2010) or use bovine serum albumin (BSA) for the dispergation of NPs (Nanogenotox, 2011).

In this study we tested different sonication protocols and evaluated the effect of sonication on physico-chemical parameters and biological effects of CuO NPs. Specifically, we prepared CuO NPs stock suspensions using no sonication, 30-min water bath and probe sonication at two different specific energies. Both, water bath sonication and probe sonication are common in nanotoxicology studies. However, as the energy input resulting from probe sonication is higher than in case of bath sonication (Santos et al., 2009), we hypothesised that these two sonication methods might affect the hydrodynamic size, dissolution and hence, the toxicity of differently prepared CuO NPs.

Indeed, higher sonication intensities increased the toxicity of CuO NPs to Caco-2 cells, when sonicated directly in MEM medium (Fig. 5). The same tendency was observed for LB medium, where pronounced sonication yielded more bioavailable copper in Cu-sensing *E. coli* assay (Fig. 3). Remarkably, in DI water the toxicity of NPs was not affected by sonication intensity (Fig. 4). As the toxicity pattern of CuO NPs in different test environments was coherent with their dissolution (sonication enhanced dissolution in MEM and LB media and had no effect in DI water (Fig. 2)), we concluded that the effect of sonication on toxicity of CuO NPs was mediated by dissolution. The test environment-dependent effect of sonication intensity on dissolution is an important finding since dissolution is one of the key mechanisms of cytotoxicity of different metal containing NPs (reviewed in (Ivask et al., 2014)).

Interestingly, while higher sonication intensity decreased the hydrodynamic size of CuO NPs in DI water (Figs. 2A, S2A), no effect on dissolution (Figs. 2D, S2D) and toxicity (Fig. 4) was observed. This suggests that at least in DI water the hydrodynamic size of particles is less

important for dissolution and hence, toxicity than assumed previously in several nanotoxicological studies (Cronholm et al., 2011; Karlsson et al., 2009; Magdolenova et al., 2012; Midander et al., 2007b).

The enhanced dissolution on NPs in cell media compared to DI water is attributed to the organic compounds (mostly proteins) that form complexes with soluble Cu (Borm et al., 2006; Kober and Sugiura, 1912) and bind NP surface forming a protein layer of so-called 'protein corona' (Vroman et al., 1980; Bhattacharya et al., 2014; Monopoli et al., 2012), which can act as dispersant for NPs. Increased sonication intensity increases the number of single particles in suspension and thus, the total surface area available for the protein binding, decreasing the size and agglomeration of NPs. This leads to enhanced dissolution of CuO NPs in organics-containing media with increasing sonication intensity and, thus, causes higher cytotoxicity.

Summarizing, the sonication intensity can remarkably affect dissolution and toxicity of CuO NPs, when the preparation and sonication of NP stock is performed in organics containing media such as LB and MEM. In contrast, dissolution and toxicity of CuO NPs were not affected by sonication intensity in DI water. Hence, we recommend two-tiered approach for the preparation of NP dispersions, *i.e.*, the preparation of NP stock suspension in DI water and subsequent dilution into the test media. This approach is also supported by our previous study, where sonication of CuO NP stock suspensions in DI water and their further toxicity testing in three different cell culture media with different cell lines yielded comparable dissolution and toxicity data (Ivask et al., 2015).

## 5. Conclusions

Our results demonstrated that higher sonication intensity enhanced the bioavailability of CuO NPs to bacteria *E. coli* and toxicity to Caco-2 cells in organics-containing media *via* increased dissolution. Thus, the sonication intensity can influence the toxicity results, if CuO NPs are

prepared in test media or similar organics-containing environment (*e.g.*, serum). Furthermore, as dissolution in organics-containing media increased in time, CuO dispersions prepared in these media should be used for the testing immediately or equilibrated for the designated time to obtain reproducible toxicity data.

In contrast, in our study dissolution and cytotoxicity of CuO NPs in DI water did not depend on sonication protocol. Taking into account that the sonication of NPs in DI water also minimizes the generation of ROS, particle interactions and, unlike cell media, excludes the presence of proteins denaturated during sonication, we recommend the use of DI water as the first consideration, when preparing metal-based NP dispersions for toxicity testing.

## Transparency document

The Transparency document associated with this article can be found, in online version.

## Acknowledgements

## Appendix A. Supplementary data

Supplementary data to this article can be found online at http://dx.doi.org/10.1016/j.tiv.2016.08.004.

## References

Bhattacharya, K., Farcal, L., Fadeel, B., 2014. Shifting identities of metal oxide nanoparticles: focus on inflammation. MRS Bull. 39, 970–975.

Bihari, P., Vippola, M., Schultes, S., Praetner, M., Khandoga, A., Reichel, C., Coester, C., Tuomi, T., Rehberg, M., Krombach, F., 2008. Optimized dispersion of nanoparticles for biological *in vitro* and *in vivo* studies. Part. Fibre Toxicol. 5.

Bondarenko, O., Ivask, A., Käkinen, A., Kahru, A., 2012. Sub-toxic effects of CuO nanoparticles on bacteria: kinetics, role of Cu ions and possible mechanisms of action. Environ. Pollut. 169, 81–89.

Bondarenko, O., Juganson, K., Ivask, A., Kasemets, K., Mortimer, M., Kahru, A., 2013a. Toxicity of Ag, CuO and ZnO nanoparticles to selected environmentally relevant test organisms and mammalian cells in vitro: a critical review. Arch. Toxicol. 87, 1181–1200.

Bondarenko, O., Ivask, A., Käkinen, A., Kurvet, I., Kahru, A., 2013b. Particle-cell contact enhances antibacterial activity of silver nanoparticles. PLoS One 8 (5), e64060.

Bondarenko, O., Heinlaan, M., Sihtmäe, M., Ivask, A., Kurvet, I., Joonas, E., Jemec, A., Mannerström, M., Heinonen, T., Rekulapelly, R., Singh, S., Zou, J., Pyykkö, I., Drobne, D., Kahru, A., 2016. Multilaboratory evaluation of 15 bioassays for (eco)toxicity screening and hazard ranking of engineered nanomaterials: FP7 project NANOVALID. Nanotoxicology 28, 1–14.

Borm, P., Klaessig, F., Landry, T., Moudgil, B., Pauluhn, J., Thomas, K., 2006. Research strategies for safety evaluation of nanomaterials, part V: role of dissolution in biological fate and effects of nanoscale particles. Toxicol. Sci. 90, 23.

Cohen, J., Deloid, G., Pyrgiotakis, G., Demokritou, P., 2013. Interactions of engineered nanomaterials in physiological media and implications for *in vitro* dosimetry. Nanotoxicology 7, 417–431.

Cronholm, P., Midander, K., Karlsson, H., Elihn, K., Wallinder, I., Möller, L., 2011. Effect of sonication and serum proteins on copper release from copper nanoparticles and the toxicity towards lung epithelial cells. Nanotoxicology 5, 269–281.

Handy, R., 2012. Guidance from EU FP7 Project MARINA. TiO₂ Nanoparticle Stock Preparation. Final Version.

Ivask, A., Rõlova, T., Kahru, A., 2009. A suite of recombinant luminescent bacterial strains for the quantification of bioavailable heavy metals and toxicity testing. BMC Biotechnol. 9, 1–15.

Ivask, A., Bondarenko, O., Jepihhina, N., Kahru, A., 2010. Profiling of the reactive oxygen species related ecotoxicity of CuO, ZnO, TiO₂, silver and fullerene nanoparticles using a set of recombinant luminescent *Escherichia coli* strains: differentiating the impact of particles and solubilised metals. Anal. Bioanal. Chem. 398, 701–716.

Ivask, A., Juganson, K., Bondarenko, O., Mortimer, M., Aruoja, V., Kasemets, K., Blinova, I., Heinlaan, M., Slaveykova, V., Kahru, A., 2014. Mechanisms of toxic action of Ag, ZnO and CuO nanoparticles to selected ecotoxicological test organisms and mammalian cells *in vitro*: a comparative review. Nanotoxicology 8, 57–71.

Ivask, A., Titma, T., Visnapuu, M., Vija, H., Kakinen, A., Sihtmae, M., Pokhrel, S., Madler, L., Heinlaan, M., Kisand, V., Shimmo, R., Kahru, A., 2015. Toxicity of 11 metal oxide nanoparticles to three mammalian cell types *in vitro*. Curr. Top. Med. Chem. 15, 1914–1929.

Jiang, J., Oberdörster, G., Biswas, P., 2009. Characterization of size, surface charge, and agglomeration state of nanoparticle dispersions for toxicological studies. J. Nanopart. Res. 11, 77–89.

Johnston, H., Pojana, G., Zuin, S., Jacobsen, N., Moller, P., Loft, S., Semmler-Behnke, M., McGuiness, C., Balharry, D., Marcomini, A., Wallin, H., Kreyling, W., Donaldson, K., Tran, L., Stone, V., 2013. Engineered nanomaterial risk. Lessons learnt from completed nanotoxicology studies: potential solutions to current and future challenges. Crit. Rev. Toxicol. 43, 1–20.

Juganson, K., Ivask, A., Blinova, I., Mortimer, M., Kahru, A., 2015. Nano E-Tox: new and in-depth database concerning ecotoxicity of nanomaterials. Beilstein J. Nanotechnol. 6, 1788–1804.

Kahru, A., Ivask, A., 2013. Mapping the dawn of nanoecotoxicological research. Acc. Chem. Res. 46, 823–833.

Käkinen, A., Bondarenko, O., Ivask, A., Kahru, A., 2011. The effect of composition of different ecotoxicological test media on free and bioavailable copper from CuSO₄ and CuO nanoparticles: comparative evidence from a Cu-selective electrode and a Cu-biosensor sensors. 11, 10502–10521.

Karlsson, H., Gustafsson, J., Cronholm, P., Möller, L., 2009. Size-dependent toxicity of metal oxide particles- a comparison between nano- and micrometer size. Toxicol. Lett. 188, 112–118.

Karlsson, H., Cronholm, P., Hedberg, Y., Tornberg, M., De Battice, L., Svedhem, S., Wallinder, I., 2013. Cell membrane damage and protein interaction induced by copper containing nanoparticles-importance of the metal release process. Toxicology 313, 59–69.

Karlsson, H., Gliga, A., Calléja, F., Gonçalves, C., Wallinder, I., Vrieling, H., Fadeel, B., Hendriks, G., 2014. Mechanism-based genotoxicity screening of metal oxide nanoparticles using the ToxTracker panel of reporter cell lines. Part. Fibre. Toxicol. 11, 41.

Kasemets, K., Ivask, A., Dubourguier, H., Kahru, A., 2009. Toxicity of nanoparticles of ZnO, CuO and TiO₂ to yeast *Saccharomyces cerevisiae*. Toxicol. in Vitro 23, 455–464.

Kaweeteerawat, C., Ivask, A., Liu, R., Zhang, H., Chang, C., Low-Kam, C., Fischer, H., Ji, Z., Pokhrel, S., Cohen, Y., Telesca, D., Zink, J., Mädler, L., Holden, P., Nel, A., Godwin, H., 2015. Toxicity of metal oxide nanoparticles in *Escherichia coli* correlates with conduction band and hydration energies. Environ. Sci. Technol. 49, 1105–1112.

Kober, P., Sugiura, K., 1912. The copper complexes of amino-acids, peptides and peptones. J. Biol. Chem. 13, 1–13.

Krug, H., 2014. Nanosafety research- are we on the right track? Angew. Chem. Int. Ed. Eng. 53, 12304–12319.

Lankoff, A., Sandberg, W.J., Wegierek-Ciuk, A., Lisowska, H., Refsnes, M., Sartowska, B., Schwarze, P.E., Meczynska-Wielgosz, S., Wojewodzka, M., Kruszewski, M., 2012. The effect of agglomeration state of silver and titanium dioxide nanoparticles on cellular response of HepG2, A549 and THP-1 cells. Toxicol. Lett. 208, 197–213.

Magdolenova, Z., Bilaničová, D., Pojana, G., Fjellsbø, L., Hudecova, A., Hasplova, K., Marcomini, A., Dusinska, M., 2012. Impact of agglomeration and different dispersions of titanium dioxide nanoparticles on the human related *in vitro* cytotoxicity and genotoxicity. J. Environ. Monit. 14, 455–464.

Mandzy, N., Grulke, E., Druffel, T., 2005. Breakage of TiO₂ agglomerates in electrostatically stabilized aqueous dispersions. Powder Technol. 160, 121–126.

Meißner, T., Oelschlägel, K., Potthoff, A., 2014. Dispersion of nanomaterials used in toxicological studies: a comparison of sonication approaches demonstrated on TiO₂ P25. J. Nanopart. Res. 16, 2228.

Midander, K., Pan, J., Wallinder, I., Leygraf, C., 2007a. Metal release from stainless steel particles *in vitro*-influence of particle size. J. Environ. Monit. 9, 74–81.

Midander, K., Wallinder, I., Leygraf, C., 2007b. *In vitro* studies of copper release from powder particles in synthetic biological media. Environ. Pollut. 145, 51–59.

Midander, K., Cronholm, P., Karlsson, H., Elihn, K., Möller, L., Leygraf, C., Wallinder, I., 2009. Surface characteristics, copper release, and toxicity of nano- and micrometer-sized copper and copper(II) oxide particles: a cross-disciplinary study. Small 5, 389–399.

Monopoli, M., Åberg, C., Salvati, A., Dawson, K., 2012. Biomolecular coronas provide the biological identity of nanosized materials. Nat. Nanotechnol. 7, 779–786.

Murdock, R., Braydich-Stolle, L., Schrand, A., Schlager, J., Hussain, S., 2008. Characterization of nanomaterial dispersion in solution prior to *in vitro* exposure using dynamic light scattering technique. Toxicol. Sci. 102, 239–253.

Nanogenotox, 2011. Deliverable 3: final protocol for producing suitable manufactured nanomaterial exposure media. URL https://www.anses.fr/fr/system/files/nanogenotox_deliverable_5.pdf.

NanoReg, 2014. Guidance document. URL http://www.prppg.ufpr.br:8080/worknano/sites/default/files/Documentos/20140505_Technical_Guidance_document_for_characterization_in_toxicological_testing_V1.0.pdf.

Nel, A., Xia, T., Meng, H., Wang, X., Lin, S., Ji, Z., Zhang, H., 2013. Nanomaterial toxicity testing in the 21st century: use of a predictive toxicological approach and high-throughput screening. Acc. Chem. Res. 46, 607–621.

Oomen, A., Bos, P., Fernandes, T., Hund-Rinke, K., Boraschi, D., Byrne, H., Aschberger, K., Gottardo, S., Von der Kammer, F., Kühnel, D., Hristozov, D., Marcomini, A., Migliore, L., Scott-Fordsmand, J., Wick, P., Landsiedel, R., 2014. Concern-driven integrated approaches to nanomaterial testing and assessment-report of the NanoSafety cluster working group 10. Nanotoxicology 8, 334–348.

Piret, J.P., Vankoningsloo, S., Mejia, J., Noël, F., Boilan, E., Lambinon, F., Zouboulis, C.C., Masereel, B., Lucas, S., Saout, C., Toussaint, O., 2012. Differential toxicity of copper (II) oxide nanoparticles of similar hydrodynamic diameter on human differentiated intestinal Caco-2 cell monolayers is correlated in part to copper release and shape. Nanotoxicology 6, 789–803.

Piret, J., Mejia, J., Lucas, S., Zouboulis, C., Saout, C., Toussaint, O., 2014. Sonicated and stirred copper oxide nanoparticles induce similar toxicity and pro-inflammatory response in N-hTERT keratinocytes and SZ95 sebocytes. J. Nanopart. Res. 16, 2337.

PROSPEcT, 2010. Ecotoxicology test protocols for representative nanomaterials in support of the OECD sponsorship programme. Ecotoxicology test protocols for representative

nanomaterials in support of the OECD sponsorship programme. URL http://www.nanotechia.org/sites/default/files/files/PROSPECT_Dispersion_Protocol.pdf.

Puzyn, T., Rasulev, B., Gajewicz, A., Hu, X., Dasari, T., Michalkova, A., Hwang, H., Toropov, A., Leszczynska, D., Leszczynski, J., 2011. Using Nano-QSAR to predict the cytotoxicity of metal oxide nanoparticles. Nat. Nanotechnol. 6, 175–178.

Sambrook, J., Fritsc, E., Maniatis, T., 1989. Molecular Cloning: A Laboratory Manual. second ed. Cold Spring Harbor Laboratory Press, Plainview, NY, USA.

Santos, H., Lodeiro, C., Capelo-MartRnez, J., 2009. The Power of Ultrasound. In: Capelo-Martínez, J.-L. (Ed.), Ultrasound in Chemistry: Analytical Applications. WILEY-VCH, Weinheim, pp. 1–16.

Sotiriou, G.A., Pratsinis, S.E., 2010. Antibacterial activity of nanosilver ions and particles. Environ. Sci. Technol. 44, 5649–5654.

Suppi, S., Kasemets, K., Ivask, A., Künnis-Peres, K., Sihtmäe, M., Kurvet, I., Aruoja, V., Kahru, A., 2015. A novel method for comparison of biocidal properties of nanomaterials to bacteria, yeasts and algae. J. Hazard. Mater. 286, 75–84.

Taurozzi, J., Hackely, V., Wiesner, M., 2011. Ultrasonic dispersion of nanoparticles for environmental, health and safety assessment—issues and recommendations. Nanotoxicology 5, 711–729.

Taurozzi, J., Hackely, V., Wiesner, M., 2012. A standardised approach for the dispersion of titanium dioxide nanoparticles in biological media. Nanotoxicology 7, 389–401.

Vroman, L., Adams, A.L., Fischer, G.C., Munoz, P.C., 1980. Interaction of high molecular-weight kininogen, factor-Xii, and fibrinogen in plasma at interfaces. Blood 55, 156–159.

Xiu, Z.M., Zhang, Q.B., Puppala, H.L., Colvin, V.L., Alvarez, P.J.J., 2012. Negligible particle-specific antibacterial activity of silver nanoparticles. Nano Lett. 12, 4271–4275.

Zhang, H., Ji, Z., Xia, T., Meng, H., Low-Kam, C., Liu, R., Pokhrel, S., Lin, S., Wang, X., Liao, Y., Wang, M., Li, L., Rallo, R., Damoiseaux, R., Telesca, D., Mädler, L., Cohen, Y., Zink, J., Nel, A., 2012. Use of metal oxide nanoparticle band gap to develop a predictive paradigm for oxidative stress and acute pulmonary inflammation. ACS Nano 6, 4349–4368.

Zhu, M., Nie, G., Meng, H., Xia, T., Nel, A., Zhao, Y., 2012. Physicochemical properties determine nanomaterial cellular uptake, transport and fate. Acc. Chem. Res. 46, 622–631.

# Supplementary information for

# Solubility-driven toxicity of CuO nanoparticles to Caco2 cells and Escherichia coli: effect of sonication energy and test environment

Aleksandr Käkinen[*], Anne Kahru, Helen Nurmsoo, Anna-Liisa Kubo and Olesja M Bondarenko[*]

*Laboratory of Environmental Toxicology, National Institute of Chemical Physics and Biophysics, Akadeemia tee 23, Tallinn 12618, Estonia*

**\*Corresponding authors:** olesja.bondarenko@kbfi.ee, telephone/fax: +372 639 8362;

aleksandr.kakinen@kbfi.ee, telephone: +372 6398368, fax: +372 639 8362

**FIGURES**
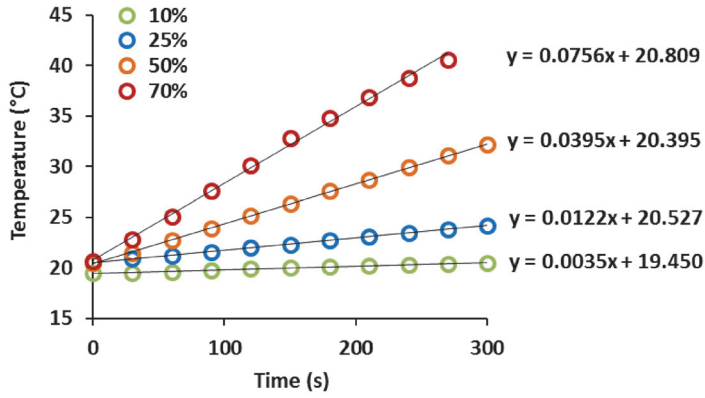


**Figure S1.** Calorimetric curves obtained for calorimetric determination of the delivered acoustic energy by direct sonication procedure at different power settings of the sonication probe (10, 25, 50 and 70% of the maximum usable theoretical power; 450 Ultrasonifier, Branson Ultrasonics Corporation, USA).

The specific energy $E_{spec}$ (kJ /m³) (**Equation 1**) is a function of the delivered acoustic power $P$ (W) (**Equation 2**) (the energy consumed for breaking the agglomerates of NPs but also for thermal losses and potential chemical reactions), time $t$ (s) and the sample volume $V$ (m³). $E_{spec}$ is independent of used ultrasonic device. It is calculated using the following equation:

$$E_{spec} = \frac{P \cdot t}{V}$$
(1)

The delivered acoustic power for sonication probe used in this study (450 Ultrasonifier, Branson Ultrasonics Corporation, USA) was determined calorimetrically by recording the temperature increase as a result from the ultrasonication of DI water over time (**Fig. S1**) and the delivered acoustic power was calculated using the following equation:

$$P = \frac{dT}{dt} m \cdot c_P$$
(2)

2

where $T$ is temperature (K), $t$ - time (s), $m$ - the mass of the liquid (here 300 g of DI water), and $c_P$ is the specific heat of the liquid (J g$^{-1}$ K$^{-1}$) at constant pressure. The specific heat of water with 4.18 J·g$^{-1}$·K$^{-1}$ (**Physik Formelsammlung)** was used. Due to the linear increase of the temperature over time $dT/dt$ was replaced by the difference quotient $\Delta T/\Delta t$ and was determined as the slope in **Fig. S1**. The procedure was performed at different power settings of the sonication probe (10, 25, 50 and 70% of the maximum usable theoretical power). The sonication process run for 5 min in continuous mode and the temperature was recorded every 30 s.

Example of calculation of delivered acoustic power for 10% of the maximum theoretical power (**Equation 3**) and specific energy $E_{spec}=5.3 \cdot 10^4$ kJ/m$^3$ (Sonication procedure 3; **Equation 4**) is presented below:

$$P = 0.0035 \cdot 300 \ (g) \cdot 4.18 \ \left(\frac{J}{g \cdot K}\right) = 4.4 \ (W \ or \ J/s) \tag{3}$$

$$E_{spec} = \frac{4.4 \left(\frac{J}{s}\right) \cdot 240(\text{s})}{0.00002 \ (m^3)} = 5.3 \cdot 10^4 \left(\frac{kJ}{m^3}\right) \tag{4}$$
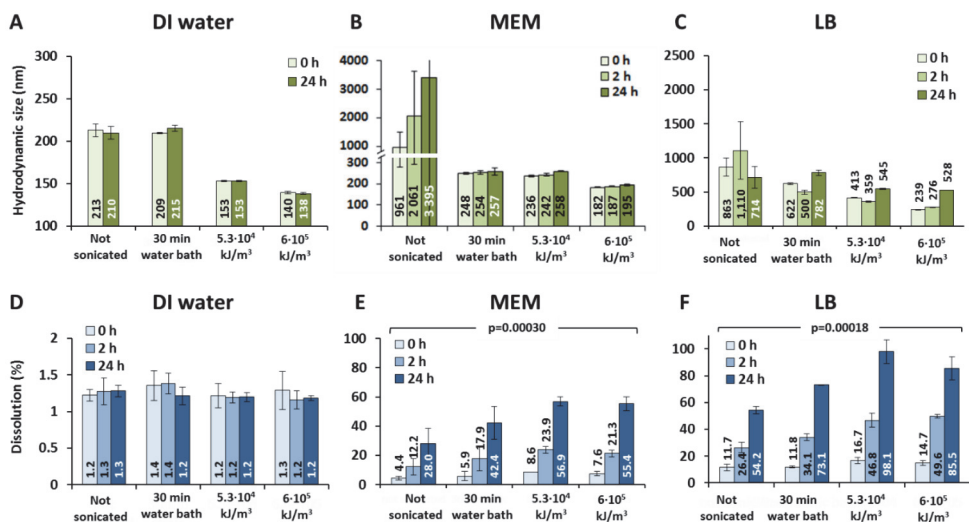
**Figure S2.** Effect of sonication on hydrodynamic size (A-C) and dissolution (D-F) of CuO NPs (100 mg Cu/l, 30 °C, Intrinsiq Materials) in DI water (A and D), complete MEM medium (B and E) and LB medium (C and F). n=3 ± standard deviation is shown. Note the different scales of Y-axis. p-values denote statistically significant differences between different time points (ANOVA).
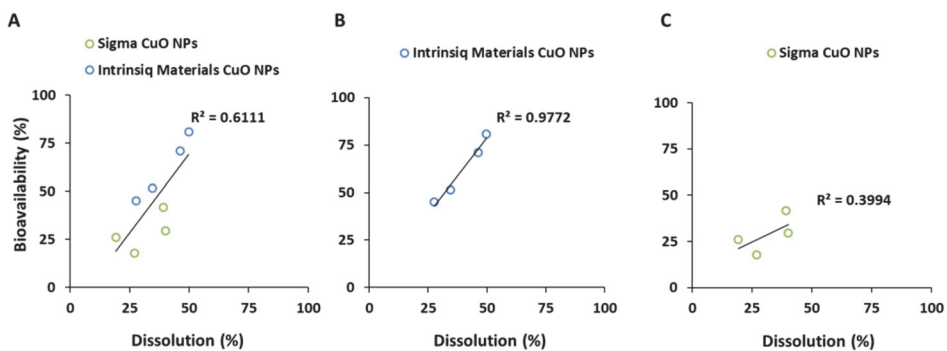


**Figure S3.** Dissolution (LB medium, 2 h, 30 °C) versus bioavailability (Cu-sensing bacteria; LB medium, 2 h, 30 °C) of CuO NPs from Sigma-Aldrich (**o;** panels A and C) and Intrinsiq Material (**o;** panels A and B) CuO NPs. Data are plotted from **Figures 2F**, **S2F** and **3B**.
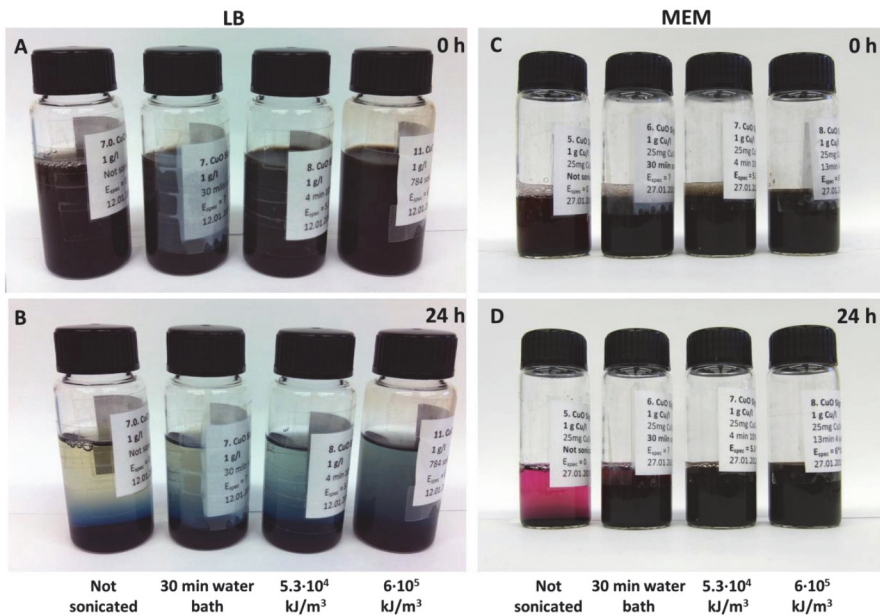
**Figure S4.** Effect of sonication energy on stability (0 and 24 h) of Sigma-Aldrich CuO NPs stock suspensions (1 g/l) prepared in (A-B) LB and (C-D) MEM media using four different approaches.

**TABLES**

**Table S1.** Polydispersity index (PDI) of Sigma-Aldrich and Intrinsiq Materials CuO NPs in three different media (DI water, bacterial LB medium and MEM cell medium) and at different time points (0, 2 and 24 h) at 100 mg/l.

| | Polydispersity index (PDI) | | | | | | | |
|---|---|---|---|---|---|---|---|---|
| | DI water | | LB | | | MEM | | |
| Time | 0 h | 24 h | 0 h | 2 h | 24 h | 0 h | 2 h | 24 h |
| Sigma-Aldrich CuO NPs | | | | | | | | |
| not sonicated | 0.22 | 0.23 | 0.82 | 0.79 | 0.58 | 0.82 | 0.77 | 0.84 |
| 30 min water bath | 0.17 | 0.17 | 0.28 | 0.30 | 0.39 | 0.39 | 0.39 | 0.51 |
| $5.3 \cdot 10^4$ kJ/m$^3$ | 0.17 | 0.17 | 0.32 | 0.23 | 0.31 | 0.21 | 0.20 | 0.29 |
| $6 \cdot 10^5$ kJ/m$^3$ | 0.14 | 0.15 | 0.22 | 0.25 | 0.30 | 0.17 | 0.17 | 0.22 |
| Intrinsiq Materials CuO NPs | | | | | | | | |
| not sonicated | 0.21 | 0.20 | 0.68 | 0.76 | 0.63 | 0.76 | 0.85 | 0.81 |
| 30 min water bath | 0.20 | 0.22 | 0.29 | 0.39 | 0.57 | 0.28 | 0.30 | 0.32 |
| $5.3 \cdot 10^4$ kJ/m$^3$ | 0.14 | 0.15 | 0.24 | 0.25 | 0.31 | 0.20 | 0.21 | 0.25 |
| $6 \cdot 10^5$ kJ/m$^3$ | 0.14 | 0.16 | 0.33 | 0.35 | 0.34 | 0.15 | 0.16 | 0.18 |

**Table S2**. Zeta potential of Sigma-Aldrich and Intrinsiq Materials CuO NPs in DI water at 0 and 24 hours.

| | Zeta potential (mV) | | | |
|---|---|---|---|---|
| | Sigma-Aldrich CuO NPs | | Intrinsiq Materials CuO NPs | |
| Time | 0 h | 24 h | 0 h | 24 h |
| not sonicated | 43.8 | 40.9 | 44.9 | 43.4 |
| 30 min water bath | 44.1 | 45.8 | 44.9 | 45.7 |
| $5.3 \cdot 10^4$ kJ/m$^3$ | 47.6 | 43.6 | 51.9 | 45.7 |
| $6 \cdot 10^5$ kJ/m$^3$ | 45.1 | 45.5 | 47.7 | 46.7 |

**Publication II**
**Kubo, A. L.**, Capjak, I., Vrček, I. V., Bondarenko, O. M., Kurvet, I., Vija, H., Kahru, A. (2018). Antimicrobial potency of differently coated 10 and 50 nm silver nanoparticles against clinically relevant bacteria *Escherichia coli* and *Staphylococcus aureus*. Colloids and Surfaces B: Biointerfaces, 170(February), 401–410.

# Antimicrobial potency of differently coated 10 and 50 nm silver nanoparticles against clinically relevant bacteria *Escherichia coli* and *Staphylococcus aureus*

Anna-Liisa Kubo[a], Ivona Capjak[b], Ivana Vinković Vrček[c], Olesja M. Bondarenko[a], Imbi Kurvet[a], Heiki Vija[a], Angela Ivask[a], Kaja Kasemets[a], Anne Kahru[a,d,*]

[a] *Laboratory of Environmental Toxicology, National Institute of Chemical Physics and Biophysics, Akadeemia tee 23, Tallinn 12618, Estonia*
[b] *Croatian Institute of Transfusion Medicine, Petrova 3, 10 000 Zagreb, Croatia*
[c] *Institute for Medical Research and Occupational Health, Ksaverska cesta 2, Zagreb, Croatia*
[d] *Estonian Academy of Sciences, Kohtu 6, Tallinn, Estonia*

## ARTICLE INFO

## ABSTRACT

Silver nanoparticles (nanoAg) are effective antimicrobials and promising alternatives to traditional antibiotics. This study aimed at evaluating potency of different nanoAg against healthcare infections associated bacteria: Gram-negative *Escherichia coli* and Gram-positive *Staphylococcus aureus*. A library of differently coated nanoAg of two different sizes (10 and 50 nm) were prepared using coating agents poly-L-Lysine (PLL), cetyltrimethyl-ammonium bromide (CTAB), citrate (CIT), polyvinyl-pyrrolidone (PVP), polysorbate 80 (Tween 80), and dioctyl-sodium sulfosuccinate (AOT). Stability evaluation by means of agglomeration and dissolution behaviour was performed for all nanoAg under conditions relevant for this study.

Antibacterial properties of nanoAg were addressed by determining their minimal bactericidal concentrations (MBC) in deionised (DI) water to minimise the influence of silver speciation on its bioavailability. In parallel, AgNO₃ was analysed as an ionic control.

Studied nanoAg were efficient antimicrobials being remarkably more potent towards *E. coli* than to *S. aureus* (4 h MBC values for different nanoAg ranged from 0.08 to 5.0 mg Ag/L and 1.0–10 mg Ag/L, respectively). The toxicity of all nanoAg to *S. aureus* (but not to *E. coli*) increased with exposure time (4 h vs 24 h). 10 nm sized nanoAg released more Ag-ions and were more toxic than 50 nm nanoAg. Coating-dependent toxicity was more prominent for 50 nm nanoAg coated with Tween 80 or CTAB rendering the least toxic nanoAg. Obtained results showed that the antimicrobial effects of nanoAg were driven by shed Ag-ions, depended on target bacteria, exposure time and were the interplay of NP size, solubility and surface coating.

## 1. Introduction

The increased microbial resistance to antibiotics is a worldwide problem that significantly affects public health issue due to healthcare-associated infections (HAIs). O'Neill recently forecasted that the antimicrobial resistant bacteria (AMR) belonging to both, Gram-negative and Gram-positive bacteria [1] will kill more people than cancer by 2020 [2]. Unfortunately, prevention of HAIs is challenging due to rapid proliferation of bacteria and their profound ability to accommodate within unfavourable environment and develop resistance to nearly all existing antibiotics [3]. The use of silver nanoparticles (nanoAg) is one of the possibilities to combat the antibacterial resistance [1]. High antibacterial efficacy of nanoAg has often been demonstrated to originate from the effect of solubilised Ag-ions on the microbial membranes, specifically on the thiol-groups of proteins leading to enzyme inhibition [4] including enzymes of the respiratory chain [5]. Different nanoAg-based formulations have been recommended for high-touch surfaces in healthcare environment to avoid proliferation of pathogenic bacteria [6]. Also, as the risks of HAIs are often related with catheterization, silver-impregnated catheters are widely applied in acute-care hospitals [7]. In contrast to conventional antibiotics, bacterial resistance against silver has been reported just in a few hospital cases [8]. Additionally, synergic action of nanoAg with antibiotics commonly used against *E. coli* and *S. aureus* could be an effective antimicrobial strategy [9]. NanoAg are nowadays used as biocidal additives in many fields and in various products including dental resin composites, bone

**Table 1**
Coating/stabilising agents used in this study.

| Name | Molecular structure | Molecular weight (g/mol) | Charge of the coating agent in deionised water | Conventional use |
|---|---|---|---|---|
| Trisodium citrate (CIT) | | 294.10 (dihydrate) | Negative | Buffering agent |
| Bis-2-ethylhexyl sulfosuccinate (AOT) | | 444.56 (Na-salt) | Negative | Anionic surfactant |
| Poly-vinylpyrrolidone (PVP) | | 40000 | Neutral | Nonionic polymer |
| Polysorbate 80 (Tween 80) | w+x+y+z=20 | 1310 | Neutral | Nonionic surfactant |
| Cetyltrimethyl-ammonium bromide (CTAB) | | 364.45 | Positive | Cationic surfactant |
| Poly-L-lysine (PLL) | | 3000 | Positive | Cationic polymer |
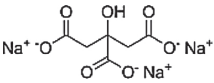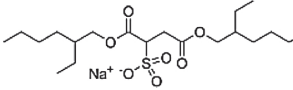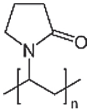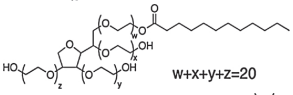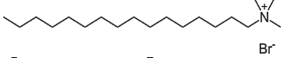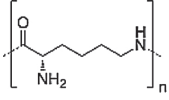
cements, medical devices, water filters, textiles, detergents, soaps, toothpastes, wet wipes, washing machines, refrigerators, and many others [10,11]. According to the Nanotechnology Products Database (www.statnano.com), nanoAg are used in 75% nano enabled products for medical applications. The design of Ag-enabled biomedical nanomaterials is commonly performed by modulating the physico-chemical properties of nanoAg such as size, shape and surface properties [12,13]. Surface functionalisation is one of the important strategies to improve colloidal stability, controlled release of Ag-ions or targeted delivery of nanoAg [14]. Moreover, surface characteristics of nanoparticles (NPs) influence the interactions between NPs and microbes. A plethora of chemicals such as polymers, anionic, cationic or non-ionic surfactants, ionic liquids and reducing agents can be used to modulate NP surface properties providing protective, stabilising or functional surface coatings [14]. For metal-based NPs, such coatings control size and shape of NPs already during synthesis by interacting with metal ions and affecting the equilibrium of synthesis reaction, particle nucleation and growth rate [15]. According to Kvitek et al. [16], the aqueous dispersions of NPs can be stabilised (i) with the assistance of steric repulsion by using polymers (such as PVP) or non-ionic surfactants (Tween 80, Triton X-100); or (ii) by electrostatic repulsion using anionic (SDS) or cationic surfactants (CTAB).

A search in the Web of Science research platform (performed on Sep 15th 2017) on the use of coating/capping agents for stabilisation of nanoAg intended for use in biomedicine yielded altogether 4298 papers (Fig. S1). Literature search revealed that citrate (CIT) and polyvinyl-pyrrolidone (PVP) were the most frequently used coating materials (4.5 and 4.2% of the studies, respectively) followed by cetyltrimethyl-ammonium bromide (CTAB), dioctyl-sodium sulfosuccinate (AOT), poly-L-lysine (PLL) and polyoxyethylene sorbitan monolaurate (Tween 80). Other studies (~90%) reported the use of very diverse coating materials including different polymers (like PEG, chitosan, PVC, PEA, PAA, polypropylen), mineral-based materials (like HAP, silica, and iron oxide), surfactants, different biomolecules (like β-cyclodextrin, chitosan, cellulose, cysteine) or their combination. Chemicals applied as surface coating agents can protect NPs from direct interaction with the

environment, oxidation [17], dissolution [18], or aggregation. However, stabilisation of NPs with functional coatings may significantly affect their biological activity. For example, Kvitek et al. [16] found a correlation between the stabilisation efficiency and increased antibacterial activity of SDS- and Tween 80-coated nanoAg concluding that non-aggregated NPs (but not spacious NPs aggregates) strongly interact with bacterial cell wall due to their high surface energy and mobility. Importantly, surface coating agent is not only attached to the NPs` surface, but exists also in free form in NPs suspensions [19]. Thus, the role (e.g., potential toxicity) of coating agents should be addressed during evaluation of biological impact or toxicity of coated/stabilised NPs. Yet, the information on contribution of surface coatings to overall NPs biological effects is scarce [19].

This study aimed to evaluate antibacterial activity of differently coated nanoAg of two different sizes: 10 nm (10 nAg) and 50 nm (50 nAg). For this purpose, a library of 11 different nanoAg was prepared employing neutral (PVP and Tween 80), positively (PLL and CTAB) and negatively charged surface coatings (AOT and CIT). Biocidal activity of these nanoAg was evaluated against two clinically relevant pathogens: Gram-negative *Escherichia coli* and Gram-positive *Staphylococcus aureus*. Additionally, antibacterial effects of coatings themselves were investigated. The role of possible nanoAg dissolution on their biocidal effects was assessed by quantifying the released Ag-ions from nanoAg surface.

## 2. Materials and methods

### 2.1. Synthesis of silver nanoparticles

Silver nitrate ($AgNO_3$) was used as a precursor of nanoAg. Capping/coating agents used for stabilisation of nanoAg are described in Table 1. CIT-coated 10 nAg were synthesised as described by Li et al. [20]. Other types of 10 nAg were synthesised by reducing $AgNO_3$ with $NaBH_4$ as described in [21]. 50 nAg coated with AOT, PVP, Tween 80 or CTAB were prepared via chemical reduction of the complex cation [Ag$(NH_3)_2$]$^+$ by *D*-glucose [22], while CIT-coated 50 nAg were prepared as

described by Munro et al. [23]. High purity deionised (DI) water obtained from a Milli-Q® system (Merck Millipore, Darmstadt, Germany) was used as solvent in all synthesis. Detailed protocols are in the Supplementary material (SM).

## 2.2. Physico-chemical characterisation of silver nanoparticles

The hydrodynamic size and surface charge of nanoAg were measured by dynamic light scattering (DLS) and electrophoretic light scattering (ELS), respectively, at 173 °C using Zetasizer Nano ZS (Malvern, UK) equipped with a green laser (532 nm). The hydrodynamic diameter ($d_H$) was obtained as a value at peak maximum of size volume distribution functions. The $d_H$ values for each sample are reported as an average of 10 measurements. The surface charge of the nanoAg was characterised by zeta ($\zeta$)-potential values, which was calculated from the measured electrophoretic mobility by means of the Henry equation using the Smoluchowski approximation. Each sample was measured 5 times and the results are expressed as average values. The data were processed by Zetasizer software 6.32 (Malvern Instruments).

Visualisation of nanoAg was carried out using a transmission electron microscope (TEM, Zeiss 902 A, Germany) operated in bright field mode at an acceleration voltage of 80 kV. Images were recorded with a Canon PowerShot S50 camera attached to the microscope. TEM samples were prepared by depositing a drop of the nanoAg suspension after 1 h of incubation at room temperature on a Formvar® coated copper grid (Agar Scientific Ltd.) and air-drying at room temperature. TEM images were used for measurement of primary size of nanoAg. Size was determined from the cross-sectional area of the particles which was converted to an equivalent spherical diameter by using ImageJ software. Primary particles were distinguished from nanoAg aggregates by tracing it manually. Altogether at least 70 particles per particle type were measured.

Total Ag concentration in nanoAg colloidal suspensions was determined in acidified solutions (10% (v/v) $HNO_3$) using an Agilent Technologies 7500 cx inductively coupled plasma mass spectrometer (ICPMS) (Waldbronn, Germany). An Ag standard solution (1000 mg/L in 5% $HNO_3$) from Merck (Darmstadt, Germany) was used for calibration.

Stability of nanoAg in DI water was studied by ultraviolet-visible (UV–vis) spectral analysis. The absorbance spectra were recorded by the Multiskan Spectrum spectrophotometer (Thermo Electron Corporation, Finland) at wavelengths of 200–800 nm (measurement step 10 nm) on the 96-well polystyrene microplates (BD Falcon, USA), 200 µl per well, after the nanoAg suspension preparation (0 h) and incubation for 4 and 24 h at 30 °C in the dark without shaking. Prior to the UV–vis measurements, the samples were shaken for 1 min.

## 2.3. Quantification of dissolved silver in abiotic conditions by chemical method

Suspensions of nanoAg (1 mg Ag/L) were incubated in DI water in conditions simulating the antibacterial test (but without bacteria added) on 12-well polystyrene plates (BD Falcon), 1.2 mL per well, for 4 h at 30 °C in the dark without shaking. Dissolved Ag-ions were separated from nanoAg by ultrafiltration [24] using Amicon-4 Ultra centrifugal filter units with 3 KDa cut-off (Merck Millipore, Darmstadt, Germany) and were quantified by graphite furnace atomic absorption spectrometry (AAS) (Perkin Elmer AAnalyst 600, Perkin Elmer, Shelton, USA) with Zeeman background correction. Standard Reference Material® 1643e Trace Elements in Water (NIST, USA) was used to confirm the reliability of analytical methods. The results were within ± 10% of the certified values.

## 2.4. Quantification of bioavailable silver using Ag-sensing bacteria

Quantification of bioavailable/intracellular silver in the test suspensions of nanoAg was performed according to Bondarenko et al. and Käosaar et al. [25,26] using recombinant luminescent sensor bacteria *E. coli* MC1061 (pSLcueR/pDNPcopAlux) responding dose-dependently by increased bioluminescence to Ag-ions that have entered bacterial cells [27]. In parallel, 'control' bacteria, *i.e.* constitutively luminescent bacteria *E. coli* MC1061 (pDNlux) [28] were used. Preparation of the test bacteria, test media and additional details of the assay are in SM.

## 2.5. Analysis of antibacterial efficiency of different nanoAg and their coatings

The antibacterial efficiency was evaluated using a spot assay as described in Kasemets et al. [29] and Suppi et al. [30] by estimating minimal bactericidal concentrations (MBC) of test compounds against *Escherichia coli* MG1655 (bacterial strain obtained from the *E. coli* genetic stock centre, Yale University) and *Staphylococcus aureus* (6538) (obtained from the American Type Culture Collection, ATCC). Briefly, after 4-h or 24-h exposure of test bacteria to the test compound in DI water, 3 µl of bacterial test suspension was pipetted as a 'spot' onto LB agar plates to assess the viability of the cells. In addition to the spot assay, the pure coatings were evaluated using bacterial growth inhibition assay according to ISO 20776-1 [31]. Preparation of test bacteria and details of the assays are in SM.

## 2.6. Flow cytometry analysis of nanoAg -bacteria interactions

Flow cytometry with BD Accuri™ (BD Biosciences) was used to determine the binding of nanoAg to bacterial cells essentially as described by Feng et al. [32]. Briefly, bacteria were exposed to nanoAg (2 or 8 mg Ag/L), 70% ethanol or AgNO₃ (0.2 mg Ag/L) at room temperature for 10 min without shaking. The bacteria were stained 15 min with 5 µM SYTO 9 (Invitrogen S34854 846177) or 7.5 µM propidium iodide (PI) (Fluka 81845) in the dark. For additional information, see SM.

## 2.7. Statistical analysis

R Language and Environment for Statistical Computing (http://www.R-project.org) was used for the analysis of variance (one-way ANOVA followed by a Tukey's honest significant difference post-hoc test) and a *t*-test in Microsoft Excel 2010 to determine statistically significant differences between the test values (nanoAg size, solubility, bioavailability, and MBC).

# 3. Results

## 3.1. Characterisation and stability evaluation of nanoAg

The library of nanoAg was prepared aiming two size groups: ~10 nm (further designated as 10 nAg) and ~50 nm (designated as 50 nAg). Six different coating agents were used for stabilisation of nanoAg (Table 1). The average primary size (TEM) of 10 nAg (irrespective of the coating) was 13 ± 5.8 nm and median size 12 nm, while 50 nAg had the average size 58 ± 39 nm and median size 49 nm (Fig. S2). 10 nAg and 50 nAg of the same coating were clearly distinguishable and different (Fig. S3).

NanoAg were characterised immediately after synthesis using DLS, ELS, and UV–vis spectrophotometry. Table 2 summarises data on $d_H$, polydispersity index (PdI) and $\zeta$-potential values. All 10 nAg were characterised by $d_H$ values in the range of 5.6–39.7 nm. The CIT-, AOT-PVP- and PLL- coated 10 nAg showed bimodal size distribution while Tween 80- and CTAB-coated 10 nAg had monomodal size distribution (Table 2). All 50 nAg, with the exception of Tween 80 coating, had bimodal size distribution. The CIT- and PVP-coated 50 nAg had

**Table 2**
Physico-chemical characteristics of differently coated silver nanoparticles (nanoAg) determined by transmission electron microscope (TEM), dynamic light scattering (DLS) and electrophoretic light scattering (ELS).

| Intended primary size | Surface coating | Primary size (average, TEM, nm) | $d_H$ [*] (nm) | Mean volume (%) | PdI[†] | ζ-potential (mV) |
|---|---|---|---|---|---|---|
| 10 nm | CIT[‡] | 12.9 ± 4.5 | 16.5 ± 0.8 | 97.6 | 0.17 | −55.2 ± 2.1 |
| | | | 39.7 ± 2.7 | 2.4 | | |
| | AOT[¥] | 10.8 ± 4.2 | 15.2 ± 5.3 | 96.6 | 0.15 | −40.6 ± 6.5 |
| | | | 12.6 ± 0.9 | 3.4 | | |
| | PVP[Ŀ] | 14.5 ± 5.2 | 15.0 ± 1.6 | 98.4 | 0.12 | −18.0 ± 3.7 |
| | | | 31.2 ± 3.5 | 1.6 | | |
| | Tween 80 | 15.2 ± 6.9 | 15.8 ± 0.3 | 100 | 0.09 | −27.2 ± 5.8 |
| | CTAB[#] | 10.8 ± 4.3 | 11.9 ± 1.6 | 100 | 0.08 | +28.2 ± 1.5 |
| | PLL[**] | 13.5 ± 7.1 | 5.6 ± 0.8 | 91.8 | 0.10 | +38.6 ± 6.9 |
| | | | 18.4 ± 1.6 | 8.2 | | |
| 50 nm | CIT | 72.7.0 ± 46 | 35.6 ± 3.2 | 91.8 | 0.27 | −28.6 ± 0.7 |
| | | | 148.1 ± 28.8 | 8.2 | | |
| | AOT | 50.4 ± 34 | 58.7 ± 28.0 | 62.8 | 0.31 | −19.3 ± 2.6 |
| | | | 12.4 ± 5.4 | 37.2 | | |
| | PVP | 37.6 ± 21 | 40.1 ± 8.2 | 76.1 | 0.34 | −34.8 ± 0.9 |
| | | | 7.6 ± 2.5 | 14.7 | | |
| | Tween 80 | 56.0 ± 33 | 54.5 ± 1.1 | 100 | 0.17 | −18.3 ± 0.9 |
| | CTAB | 75.3 ± 45 | 32.7 ± 15.6 | 56.7 | 0.38 | +5.9 ± 0.8 |
| | | | 180.1 ± 92.9 | 43.3 | | |

[*]$d_H$– hydrodynamic diameter, [†]PdI – polydispersity index, [‡]CIT – Trisodium citrate, [¥]AOT – Bis-2-ethylhexyl sulfosuccinate, [Ŀ]PVP – Poly-vinylpyrrolidone, Tween 80 – Polysorbate 80, [#]CTAB – Cetyltrimethyl-ammonium bromide, [**]PLL – Poly-ʟ-lysine. Primary sizes of NPs (nm) were measured from TEM images by using ImageJ software. DLS values indicate hydrodynamic diameter ($d_H$, nm) obtained from size distributions by volume. Light scattering methods provided in addition ζ-potential (mV) and polydispersity index (PdI). All parameters were obtained by diluting nanoAg in DI water to a concentration of 10 mg/L immediately after the synthesis, at 25 °C.

predominant NPs population of ∼ 40–60 nm size, while CTAB- and AOT-coated 50 nAg were more polydisperse, which is also obvious from measured PdI values. All attempts to prepare PLL-coated 50 nAg failed. Thus, this type of nanoAg was not included in this study.

All nanoAg were stable and well-dispersed in DI water for a period of 24 h with the exception of 50 nAg-CTAB that formed aggregates as evidenced also from the observed PdI 0.38 (Table 2; Fig. S2, D).

UV–vis absorption spectra of nanoAg showed the characteristic surface plasmon resonance (SPR) peaks for 10 nAg and 50 nAg at 390–395 nm and 400–440 nm, respectively (Fig. S4). Slight decrease in the intensity values of the SPR peaks can be explained by the nanoAg solubility [33]. Significant changes were observed only in the case of 50 nAg-CTAB, where the absorption band disappeared completely after 24 h of incubation due to significant agglomeration as evidenced also by DLS measurements (Fig. S4). Interestingly, the aggregation of 50 nAg-CTAB was facilitated only after dilution in DI water prior to the tests, whereas the stock solution of 50 nAg-CTAB (total Ag concentration of 1220 mg/L) prepared immediately after the synthesis, was stable for several months (data not shown). The poorer stability of 50 nAg-CTAB may be explained by their surface charge close to the neutral ζ-potential value.

### 3.2. Antibacterial properties of nanoAg against E. coli and S. aureus

Antimicrobial efficiency of nanoAg was evaluated using a spot assay and expressed as MBC.

4 h and 24 h MBC values are presented in Fig. 1 and Table S1 (SM).

Comparison of the antibacterial efficiency of differently sized nanoAg showed that 10 nAg were in general more potent antibacterial agents than 50 nAg to both *E. coli* (Fig. 1, upper panels) and *S. aureus* (Fig. 1, lower panels). However, in the case of CIT- and PVP-coated nanoAg the differences in size-dependent toxic effects were statistically not significant with the exception of 4 h-exposed *S. aureus* (Fig. 1; Table S1).

The toxicity of all studied nanoAg (except 50 nAg-Tween 80) towards *S. aureus* significantly increased with time, *i.e.*, 4 h *versus* 24 h (Fig. S5, lower panels). As a rule, the effect of prolonged incubation on toxicity was not observed in *E. coli*. Only 10 nAg-PVP, 50 nAg-CTAB and

50 nAg-AOT showed statistically different effect between 4 h and 24 h time points in *E. coli* (Fig. S5, upper panels). The same tendency, *i.e.* increase of toxic effect with time in case of *S. aureus,* was observed for AgNO$_3$ evidencing the role of released ionic Ag in nanoAg toxicity (Fig. S5, B; Table S1).

Comparison of the sensitivities of two different bacterial strains showed significantly higher susceptibility of Gram-negative *E. coli* than Gram-positive *S. aureus* to both nanoAg and ionic Ag (Fig S6). The difference was especially remarkable after 4 h of exposure, when MBC values for nanoAg to *E. coli* were in the range of 0.08–5 mg Ag/L and 1–10 mg Ag/L for *S. aureus* (Table S1). For both bacterial strains Ag-ions were remarkably more toxic than nanoAg. The 4 h MBC for Ag-ions to *E. coli* was 0.02 mg Ag/L and 0.16 mg Ag/L to *S. aureus* (Table S1). Thus, *E. coli* was up to 12-times more susceptible to nanoAg and 8-times more susceptible to Ag-ions than *S. aureus*. The same tendency was observed after 24 h of exposure, except for 50 nAg coated with AOT, PVP and Tween 80.

There was no clear trend on the effect of the coating on antibacterial efficacy. Among 10 nAg, the Tween 80-coated nanoAg induced the lowest toxic effects to *S. aureus* after 4 h exposure (Fig. 2), while *E. coli* was susceptible to all 10 nAg to a similar extent after 4 h. After 24 h of exposure, all studied 10 nAg exhibited similar antibacterial effects to both strains. Probably, the antibacterial effect was mainly driven by their small size. Results obtained for 50 nAg (Fig. 2, lower panels) implied that antimicrobial effect can be tuned using various coatings. Tween 80- and CTAB-coated 50 nAg showed lower antimicrobial potential as compared to CIT-, AOT- and PVP-coated 50 nAg.

### 3.3. The role of dissolved Ag-ions in antibacterial effects of nanoAg

Dissolution behaviour of nanoAg in DI water as determined by AAS showed that ionic Ag in nanoAg dispersions ranged from 0.8 to 6.5%. In general, 10 nAg released more Ag-ions (2.1–6.5%) than 50 nAg (0.8–3.0%) (Fig. 3). The highest content of Ag-ions was found in PVP and AOT-coated 10 nAg (∼6.5%), while CTAB-coated 50 nAg released the lowest amount of Ag-ions (0.8%).

Biosensor data showed that the Ag bioavailability was highest for PLL-coated 10 nAg (12.6%) and lowest for CTAB-coated 50 nAg (0.2%)
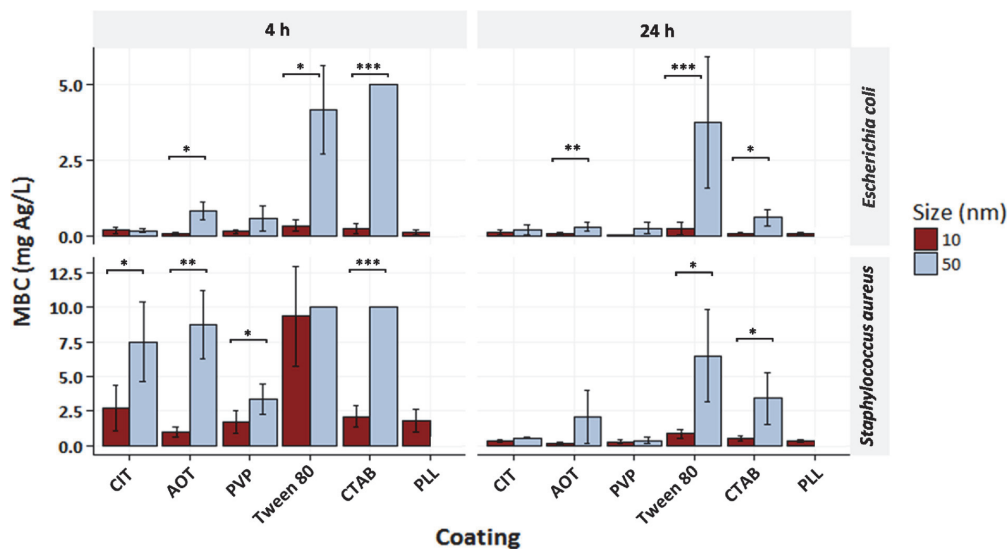
**Fig. 1.** Effect of particle size on minimal bactericidal concentration (MBC) of differently coated 10 nAg and 50 nAg to *Escherichia coli* (upper panels) and *Staphylococcus aureus* (lower panels). Data represent the average values of 3–5 experiments ± standard deviation (SD); ***p < 0.001, **p < 0.01, *p < 0.05. Data are plotted from Table S1.

(Fig. 3). Although the bioavailable fraction of Ag was, at first sight, comparable with its soluble fraction, biosensor and solubility data were significantly different for CIT-coated 10- and 50 nAg, CTAB-coated 10- and 50 nAg, Tween 80-coated 10- and 50 nAg and PLL-coated 10nAg (Fig. S7). For CIT-coated nanoAg, we hypothesize that CIT formed complexes with Ag-ions that were not bioavailable to Ag-sensor bacteria. In the case of PLL-coated 10 nAg, the bioavailability of dissolved

Ag was ca 3-fold higher than their solubility as measured by AAS, indicating that biological factors (*e.g.*, cell-nanoAg interactions) might contribute to their bioavailability. Plotting of nanoAg solubility and bioavailability against their respective MBC values, a good correlation (log-log $R^2$ = 0.54–0.82) between antibacterial efficacy and solubilisation/bioavailability of nanoAg was observed (Fig. 4) suggesting that the antibacterial effect was mainly driven by shed Ag-ions.
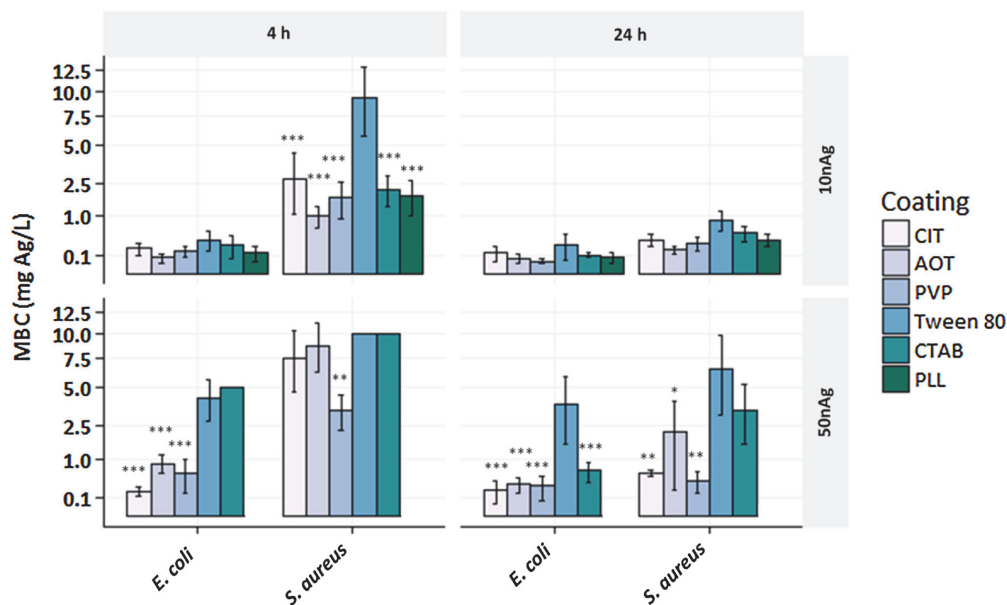


**Fig. 2.** The effect of coating on antimicrobial potency of 10 nAg (upper panels) and 50 nAg (lower panels) to *E. coli* and *S. aureus* exposed for 4 h (left panels) and 24 h (right panels). The statistical significance was compared to the least toxic compound (Tween 80) in the group: ***p < 0.001, **p < 0.01, *p < 0.05.
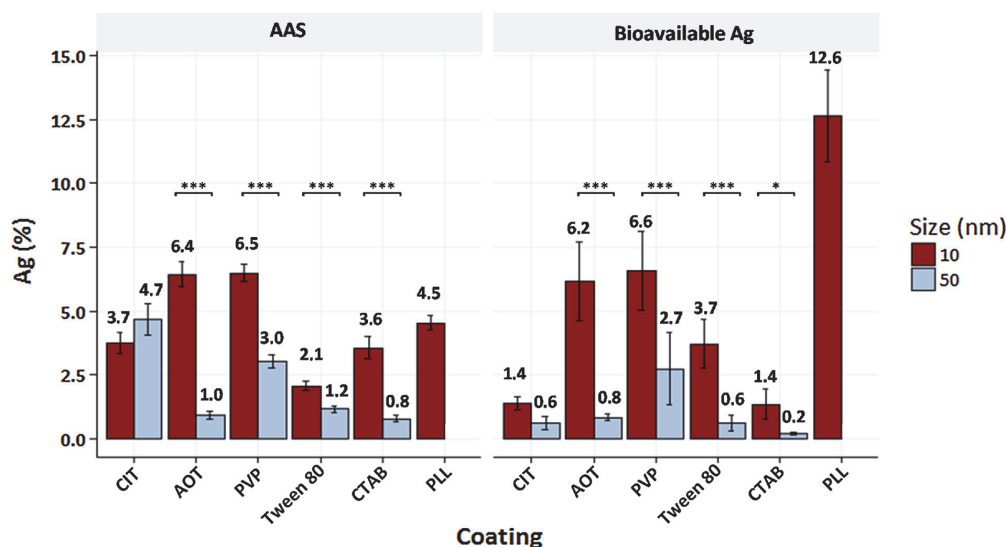
**Fig. 3.** Solubility (measured by AAS) and bioavailability (determined by Ag-sensing bacteria) of different nanoAg and expressed as % of initial Ag content in nanoAg. Average values of at least three measurements ± SD are presented. Solubility analyses was performed at 1 mg Ag/L. Asterisks designate the statistical difference between 10 nAg and 50 nAg (***p < 0.001, **p < 0.01, *p < 0.05).

### 3.4. Antibacterial effects of coating agents

It is well-known that some of the coating materials used throughout this study, such as cationic polymer PLL [34] and cationic surfactant CTAB [35], can be inherently antibacterial. Thus, toxicity of pure AOT, CIT, CTAB, PLL, PVP and Tween 80 coatings was tested.

As shown in Table S2, all coating agents, except positively charged CTAB and PLL were not toxic to both bacterial strains up to the maximal tested concentrations (4000 mg/L).

Cationic polymer PLL and cationic surfactant CTAB proved toxic in both antibacterial assays with the EC$_{50}$ values comparable to the toxicity of well-known cationic biocide benzalkonium chloride (MBC to both bacteria ranged between 1.3–2.5 mg/L, Tables S2 and S3). Our data were in agreement with previous articles on inherent toxicity of PLL and CTAB [34,35]. The toxicity of these coatings was similar to both strains with some exceptions. The antibacterial effects of PLL and AOT against *S. aureus* increased remarkably in time, which was not observed for *E. coli* (Table S2). Bacterial growth inhibition assay following ISO 20776-1 standard showed the toxicity of coatings to dividing cells (Table S3). The PVP, CIT and Tween 80 were not toxic to bacteria up to their maximal tested concentrations, while MBC and MIC values indicated slightly toxic effect of AOT to *S. aureus*, but not to *E. coli*. Similar to results obtained from the spot assay (Table S2), PLL and CTAB were inhibitory to both bacteria, with higher antimicrobial potency against Gram-positive *S. aureus* than against Gram-negative *E. coli* (Table S3).

Although the proportion of the coating in the formulations of nanoAg was small, we calculated, whether the toxic coatings PLL or CTAB may have contributed to the net toxicity of the 50 nAg-PLL and 50 nAg-CTAB (see SM). The calculations showed that the bactericidal concentrations of pure coatings (Table S2) were orders of magnitude higher than their concentration at the respective nanoAg MBCs (Table S1) indicating that the toxicity of those coatings was not contributing to the net antibacterial effects of respective nanoAg.

### 3.5. Flow cytometry analysis of particle-cell contact

Interaction of different nanoAg types with bacteria was evaluated using flow cytometry analysis. Bacterial cells were exposed to 2 and 8 mg/L nanoAg for 10 min. The SSC shift of SYTO 9-stained cell population was measured to study binding of nanoAg to cells [36], while fluorescence intensity after PI staining was indicating cell viability by determining the number of dead cells and cells with damaged membranes (Fig. S8).

PI staining indicated that viability of control cells (non-treated) was 91.7% for *E. coli* and 96.2% for *S. aureus* (Fig. 5, B). For all nanoAg, no binding to both bacterial strains was observed at lower nanoAg concentration (2 mg Ag/L, data not shown). Higher applied nanoAg concentration (8 mg Ag/L) led to binding of four different nanoAg types to *E. coli*, but binding above 10% was observed only for 10 nAg-PLL (Fig. 5, A). In the case of *S. aureus*, 10 nAg-PLL and all 50 nAg interacted with cells (Fig. 5, A).

The effect of nanoAg on cellular viability (10 min exposure) is shown in Fig. 5, B. In general, the damaging effects of nanoAg were smaller to *S. aureus* than to *E. coli*, while CTAB-coated 10 nAg showed highest toxic potential for *S. aureus* (Fig. 5, B). Interestingly, this was not reflected in the MBC values (Table S1). Thus, apparently some cells with damaged membranes (PI positive cells) were able to form colonies even after 4 h exposure to nanoAg. Remarkably, in the case of *S. aureus*, CTAB and PLL-coated nanoAg decreased cellular viability more than other nanoAg types of comparable sizes (Fig. 5, B). For example, the 50 nAg-CTAB damaged 35.3% of *S. aureus* cells, whereas the damage caused by other 50 nAg was below 16%. Thus, positively charged coating contributed to the membrane damage of *S. aureus* but not of *E. coli*. While *E. coli* cells were readily killed by Ag-ions released from nanoAg and cell-particle contact did not play the major role, cell-particle contact and particle charge obviously played significant role to the nanoAg effects on *S. aureus* cell damage.

### 4. Discussion

This study was conducted to provide systematic data on
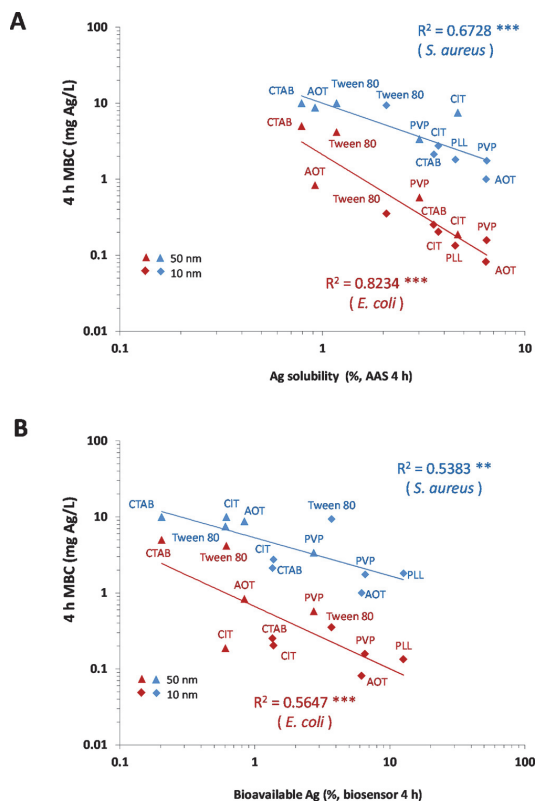
**Fig. 4.** Antibacterial effect (4 h MBC) of differently coated 10 nAg and 50 nAg to *Escherichia coli* and *Staphylococcus aureus versus* (A) solubility of nanoAg (%) as quantified by AAS and *versus* (B) bioavailability of nanoAg as quantified by Ag-sensing biosensor bacteria. A log-log correlation and respective correlation coefficients ($R^2$) are presented. The statistical significance of the calculated correlation coefficients (r) was estimated at different confidence levels (P) and designated as follows: $\lvert r \rvert > 0$, *P = 90%, **P = 95%, *** P = 99%, respectively.

antimicrobial potency of nanosilver by synthesising a library of differently coated nanoAg of two different sizes (10 and 50 nm). As microbial models, we chose *E. coli* and *S. aureus* representing Gram-negative and Gram-positive potentially pathogenic bacteria, respectively. Selection of these bacterial strains was based on the fact that the most often isolated bacteria in 15 000 HAI cases in 29 EU/EEA Member States were *E. coli* (15.9%) and *S. aureus* (12.3%) in the period between 2011–2012 [37]. *S. aureus* also belongs to the six problematic pathogens associated with multi-drug-resistant infections [38].

To evaluate the effect of NPs' surface properties, different surface coatings were employed in preparation of nanoAg library. Effect of Ag-ions (in the form of AgNO$_3$) was determined for comparative purposes.

Antibacterial evaluation of the nanoAg was performed in DI water to diminish the effects of organic components from the growth media on the colloidal stability (aggregation/agglomeration, protein adsorption, dissolution) of nanoAg [25,26,39–41]. The importance of absence of interfering compounds affecting speciation of silver for the interpretation of the toxic effects of silver NPs was stressed also in the recent review by Le Ouay and Stellacci [42].

Obtained data confirmed the main paradigm of nanotechnology, *i.e.* the small particle size yielded higher antimicrobial potency. Thus, 10 nAg were more toxic to tested bacteria than 50 nAg, irrespective of

the coatings used for their stabilisation. As expected, nanoAg were less potent towards both *E. coli* and *S. aureus* as compared to Ag-ions (Table S1; Fig. S6). In addition, *S. aureus* was less susceptible than *E. coli* to all nanoAg types (Fig. S6), being in agreement with our previously published data from the similar test format [39]. Contrary to the effect observed for *E. coli*, the antibacterial effects of both nanoparticulate and ionic Ag forms to *S. aureus* increased with time (Table S1; Fig. S5). The difference in nanoAg toxicity between Gram-negative and -positive bacteria was especially remarkable after shorter (4 h) as compared to longer (24 h) exposure times (Fig. S6, B). The difference in toxicological profile of different nanoAg (and Ag-ions) for Gram-negative and -positive bacteria might be due to the fact that peptidoglycan layer in the cell walls of Gram-positive bacteria is 30 nm thick, while this layer is only 2–3 nm thick in the Gram-negative bacteria [1]. The thicker peptidoglycan layer may act as a barrier protecting the cell from penetration of nanoAg or/and Ag-ions into the cytoplasm ensuring the lower sensitivity of Gram-positive as compared to Gram-negative bacteria [43,44]. The difference in the thickness of this layer may also explain the longer time needed to gain equal antibacterial efficiency of nanoAg/Ag-ions against *S. aureus* than against *E. coli* (Fig. S5; Table S1). In addition, high sensitivity of Gram-negative bacteria towards nanoAg can be explained with the higher leakage of proteins from Ag destabilised membrane of *E. coli* as compared to *S. aureus* [45].

As expected, the antibacterial effects of nanoAg were in good correlation with the release of Ag-ions from the nanoAg surface (Fig. 4). Indeed, higher antibacterial potency of 10 nAg compared to 50 nAg was correlated with the higher % of free Ag-ions in the 10 nAg dispersions compared to 50 nAg (Figs. 3 and 4) being in good agreement with previously published data [46]. Ag-ions may additionally destabilise and rupture bacterial cell membranes [47–51]. For example, Ivask et al. demonstrated that the most nanoAg-affected proteins in *E. coli* were clusters of membrane proteins [33]. It has been reported that after disrupting the membranes, nanoAg inactivated the enzymes of respiration chain [5,52], released Ag-ions affected DNA and intracellular proteins, caused formation of intracellular reactive oxygen species (ROS) and enhanced the penetration of nanoAg into the cell [53].

Although there was a good correlation between the release of Ag-ions from nanoAg and their antibacterial action (Fig. 4), not all toxic effects were explained by Ag-ions. We hypothesise that toxicity may also have arisen from the toxicity of coatings themselves or from binding of nanoAg to the cells allowing higher local concentrations of released Ag-ions. Indeed, some of the coating agents can destabilise the bacterial membranes [54] and act as antimicrobials [55] leading to synergistic effect of coated nanoAg. For example, CTAB may permeabilise bacterial membranes [56,57], while PLL, a widely used food preservative, can disrupt bacterial membranes, generate ROS [58] and prevent *E. coli* growth at concentrations as low as ~70 μM [59]. Our data revealed that both coating agents, PLL and especially CTAB (but no other coatings tested in this study) were toxic to bacteria (Tables S2 and S3). However, the bactericidal concentrations of coatings were generally orders of magnitude higher than their concentrations in nanoAg toxicity test, indicating that the toxicity of coatings was not the obvious cause for the increased nanoAg toxicity.

Another important factor for observed effects could be the surface charge. The bacterial cell surface has negative surface charge as demonstrated in earlier studies [60] and confirmed also by us: the ζ potential of *S. aureus* and *E. coli* surface was −42 and −52 mV, respectively. Interestingly, CTAB and PLL-coated nanoAg with positive surface charge (Table 1) that were initially expected to be more antibacterial than nanoAg with negative surface charge, due to their higher potential for attachment to negatively charged bacterial cells, didn't demonstrate superior antimicrobial effects (Fig. 2). Thus, our data disagree with previously reported data on remarkably increased toxicity of nanoAg coated by positively charged branched PEI to *E. coli* [33]. However, positively charged nanoAg were superior in damaging membranes of *S. aureus* upon short exposures (Fig. 5, B), showing that
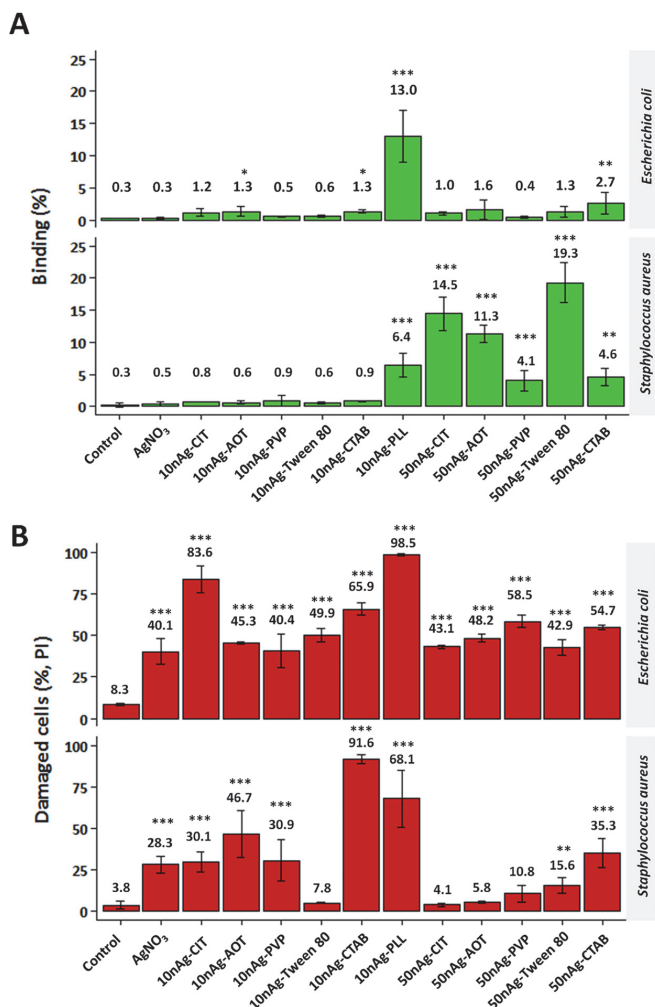
**Fig. 5.** Flow cytometry analysis of interactions between different nanoAg (8 mg Ag/L) or AgNO$_3$ (0.2 mg Ag/L) and bacteria determined by the SSC shift of SYTO 9-stained cells (A) and effect of nanoAg (8 mg Ag/L) or AgNO$_3$ (0.2 mg Ag/L) on viability of bacterial cells measured by propidium iodide (PI) stained cells (B). Asterisks show the statistical difference compared to control: ***p < 0.001, **p < 0.01, *p < 0.05.

positive charge is important but not a deciding factor for the actual bactericidal effect. Analogously, *E. coli* cells interacted with positively charged PLL-coated nanoAg (Fig. 5, A), which significantly increased their bioavailability for *E. coli* (Fig. 3). However, the direct charge-related effect of this interaction on toxicity was negligible, compared to the toxic effects caused by shed Ag-ions. Thus, in our experimental conditions, the role of nanoAg coatings in modulation of the release of Ag-ions (Fig. 3) was way more important than their NP-cell interactions directing effects. As a rule, within the same size category, the CTAB- and Tween 80-coated nanoAg were least soluble and least toxic to both bacterial strains, while PVP-, CIT- and AOT-coated nanoAg were most soluble and most efficient antibacterials (Fig. 4).

Thus, the strongest modulator of the antimicrobial effect was particle size which determined also dissolution behaviour of nanoAg: smaller nanoAg were significantly more toxic being more soluble. The effect of coating agents on antibacterial activity of nanoAg was only indirect modulator of nanoAg toxicity, mainly due to modulation of

their solubility. This was particularly obvious in the case of 50 nAg and *S. aureus*. We also do not exclude a synergistic toxic effect of released Ag-ions and coatings.

## 5. Conclusions

To design efficient antimicrobial silver-based nanomaterials, focus should be set on the fine-tuning of solubilisation of NPs. For this purpose, the selection of smaller size of nanoAg could be recommended. If Gram-negative bacteria (*E. coli*) are the target, all types of coating/capping agents seem to be applicable. However, for Gram-positive bacteria (*S. aureus*), Tween 80 and similar agents should be avoided. In the case of Gram-positive bacteria, more time might be needed for the antibacterial action of nanoAg than for the Gram-negative bacteria due to the differences in the cell wall composition between these two bacteria types. Finally and contrary to the common view, positively charged nanoAg did not exhibit superior antibacterial properties

compared to the negatively charged nanoAg, suggesting that solubility might be more important determinant of antibacterial acitivity than the surface charge as such.

## Conflict of interest

The authors declare no conflict of interest.

## Acknowledgements

## Appendix A. Supplementary Material

Supplementary Material related to this article can be found, in the online version, at doi:https://doi.org/10.1016/j.colsurfb.2018.06.027.

## References

[1] M.K. Rai, S.D. Deshmukh, A.P. Ingle, A.K. Gade, Silver nanoparticles: the powerful nanoweapon against multidrug-resistant bacteria, J. Appl. Microbiol. 112 (2012) 841–852, http://dx.doi.org/10.1111/j.1365-2672.2012.05253.x.

[2] J. O'Neill, Antimicrobial resistance: tackling a crisis for the health and wealth of nations, Rev. Antimicrob. Resist. (2014) 1–16, http://dx.doi.org/10.1038/510015a.

[3] C.L. Ventola, The antibiotic resistance crisis: part 1: causes and threats, PTA Peer-Rev. J. Formul. Manag. 40 (2015) 277–283. Article.

[4] S.Y. Liau, D.C. Read, W.J. Pugh, J.R. Furr, A.D. Russell, Interaction of silver nitrate with readily identifiable groups: relationship to the antibacterial action of silver ions, Lett. Appl. Microbiol. 25 (1997) 279–283, http://dx.doi.org/10.1046/j.1472-765X.1997.00219.x.

[5] K.B. Holt, A.J. Bard, Interaction of silver(I) ions with the respiratory chain of Escherichia coli: an electrochemical and scanning electrochemical microscopy study of the antimicrobial mechanism of micromolar Ag, Biochemistry 44 (2005) 13214–13223, http://dx.doi.org/10.1021/bi0508542.

[6] M. Ahonen, A. Kahru, A. Ivask, K. Kasemets, S. Kõljalg, P. Mantecca, I.V. Vrček, M.M. Keinänen-Toivola, F. Crijns, Proactive approach for safe use of antimicrobial coatings in healthcare settings: opinion of the cost action network AMiCI, Int. J. Environ. Res. Public Health 14 (2017), http://dx.doi.org/10.3390/ijerph14040366.

[7] P. Dallas, V.K. Sharma, R. Zboril, Silver polymeric nanocomposites as advanced antimicrobial agents: classification, synthetic paths, applications, and perspectives, Adv. Colloid Interface Sci. 166 (2011) 119–135, http://dx.doi.org/10.1016/j.cis.2011.05.008.

[8] J.L. Hobman, L.C. Crossman, Bacterial antimicrobial metal ion resistance, J. Med. Microbiol. 64 (2015) 471–497, http://dx.doi.org/10.1099/jmm.0.023036-0.

[9] A.R. Shahverdi, A. Fakhimi, H.R. Shahverdi, S. Minaian, Synthesis and effect of silver nanoparticles on the antibacterial activity of different antibiotics against Staphylococcus aureus and Escherichia coli, Nanomed. Nanotechnol. Biol. Med. 3 (2007) 168–171, http://dx.doi.org/10.1016/j.nano.2007.02.001.

[10] S. Prabhu, E.K. Poulose, Silver nanoparticles: mechanism of antimicrobial action, synthesis, medical applications, and toxicity effects, Int. Nano Lett. 2 (2012) 32, http://dx.doi.org/10.1186/2228-5326-2-32.

[11] M.E. Vance, T. Kuiken, E.P. Vejerano, S.P. McGinnis, M.F. Hochella, D.R. Hull, Nanotechnology in the real world: redeveloping the nanomaterial consumer products inventory, Beilstein J. Nanotechnol. 6 (2015) 1769–1780, http://dx.doi.org/10.3762/bjnano.6.181.

[12] D. Yohan, B.D. Chithrani, Applications of nanoparticles in nanomedicine, J. Biomed. Nanotechnol. 10 (2014) 2371–2392, http://dx.doi.org/10.1166/jbn.2014.2015.

[13] J. Piella, N.G. Bastús, V. Puntes, Size-controlled synthesis of sub-10-nanometer citrate-stabilized gold nanoparticles and related optical properties, Chem. Mater. 28 (2016) 1066–1075, http://dx.doi.org/10.1021/acs.chemmater.5b04406.

[14] V. Labhasetwar, D.L. Leslie-Pelecky, Biomedical Applications of Nanotechnology, (2007), http://dx.doi.org/10.1002/9780470152928.

[15] P.C. Ray, Size and shape dependent second order nonlinear optical properties of nanomaterials and their application in biological and chemical sensing, Chem. Rev. 110 (2010) 5332–5365, http://dx.doi.org/10.1021/cr900335q.

[16] L. Kvítek, A. Panáček, J. Soukupová, M. Kolář, R. Večeřová, R. Prucek, M. Holecová, R. Zbořil, Effect of surfactants and polymers on stability and antibacterial activity of silver nanoparticles (NPs), J. Phys. Chem. C 112 (2008) 5825–5834, http://dx.doi.org/10.1021/jp711616v.

[17] W. Lu, D. Senapati, S. Wang, O. Tovmachenko, A.K. Singh, H. Yu, P.C. Ray, Effect of surface coating on the toxicity of silver nanomaterials on human skin keratinocytes, Chem. Phys. Lett. 487 (2010) 92–96, http://dx.doi.org/10.1016/j.cplett.2010.01.027.

[18] Z. Adamczyk, M. Oćwieja, H. Mrowiec, S. Walas, D. Lupa, Oxidative dissolution of silver nanoparticles: a new theoretical approach, J. Colloid Interface Sci. 469

(2016) 355–364, http://dx.doi.org/10.1016/j.jcis.2015.12.051.

[19] Y. Zhang, B. Newton, E. Lewis, P.P. Fu, R. Kafoury, P.C. Ray, H. Yu, Cytotoxicity of organic surface coating agents used for nanoparticles synthesis and stability, Toxicol. In Vitro 29 (2015) 762–768, http://dx.doi.org/10.1016/j.tiv.2015.01.017.

[20] H. Li, H. Xia, D. Wang, X. Tao, Simple synthesis of monodisperse, quasi-spherical, citrate-stabilized silver nanocrystals in water, Langmuir 29 (2013) 5074–5079, http://dx.doi.org/10.1021/la400214x.

[21] I. Vinković Vrček, I. Pavičić, T. Crnković, D. Jurašin, M. Babič, D. Horák, M. Lovrić, L. Ferhatović, M. Ćurlin, S. Gajović, Does surface coating of metallic nanoparticles modulate their interference with in vitro assays? RSC Adv. 5 (2015) 70787–70807, http://dx.doi.org/10.1039/C5RA14100A.

[22] J. Soukupová, L. Kvítek, A. Panáček, T. Nevěčná, R. Zbořil, Comprehensive study on surfactant role on silver nanoparticles (NPs) prepared via modified tollens process, Mater. Chem. Phys. 111 (2008) 77–81, http://dx.doi.org/10.1016/j.matchemphys.2008.03.018.

[23] C.H. Munro, W.E. Smith, M. Garner, J. Clarkson, P.C. White, Characterization of the surface of a citrate-reduced colloid optimized for use as a substrate for surface-enhanced resonance raman scattering, Langmuir 11 (1995) 3712–3720, http://dx.doi.org/10.1021/la00010a021.

[24] A. Colombo, M. Saibene, E. Moschini, P. Bonfanti, M. Collini, K. Kasemets, P. Mantecca, Teratogenic hazard of BPEI-coated silver nanoparticles to Xenopus laevis, Nanotoxicology 11 (2017) 405–418, http://dx.doi.org/10.1080/17435390.2017.1309703.

[25] O. Bondarenko, K. Juganson, A. Ivask, K. Kasemets, M. Mortimer, A. Kahru, Toxicity of Ag, CuO and ZnO nanoparticles to selected environmentally relevant test organisms and mammalian cells in vitro: a critical review, Arch. Toxicol. 87 (2013) 1181–1200, http://dx.doi.org/10.1007/s00204-013-1079-4.

[26] S. Käosaar, A. Kahru, P. Mantecca, K. Kasemets, Profiling of the toxicity mechanisms of coated and uncoated silver nanoparticles to yeast Saccharomyces cerevisiae BY4741 using a set of its 9 single-gene deletion mutants defective in oxidative stress response, cell wall or membrane integrity and endocyt, Toxicol. In Vitro 35 (2016) 149–162, http://dx.doi.org/10.1016/j.tiv.2016.05.018.

[27] A. Ivask, O. Bondarenko, N. Jepihhina, A. Kahru, Profiling of the reactive oxygen species-related ecotoxicity of CuO, ZnO, TiO2, silver and fullerene nanoparticles using a set of recombinant luminescent Escherichia coli strains: differentiating the impact of particles and solubilised metals, Anal. Bioanal. Chem. 398 (2010) 701–716, http://dx.doi.org/10.1007/s00216-010-3962-7.

[28] A. Leedjärv, A. Ivask, M. Virta, A. Kahru, Analysis of bioavailable phenols from natural samples by recombinant luminescent bacterial sensors, Chemosphere 64 (2006) 1910–1919, http://dx.doi.org/10.1016/j.chemosphere.2006.01.026.

[29] K. Kasemets, S. Suppi, K. Künnis-Beres, A. Kahru, Toxicity of CuO nanoparticles to yeast Saccharomyces cerevisiae BY4741 wild-type and its nine isogenic single-gene deletion mutants, Chem. Res. Toxicol. 26 (2013) 356–367, http://dx.doi.org/10.1021/tx300467d.

[30] S. Suppi, K. Kasemets, A. Ivask, K. Künnis-Beres, M. Sihtmäe, I. Kurvet, V. Aruoja, A. Kahru, A novel method for comparison of biocidal properties of nanomaterials to bacteria, yeasts and algae, J. Hazard. Mater. 286 (2015) 75–84, http://dx.doi.org/10.1016/j.jhazmat.2014.12.027.

[31] ISO 20776-1:2006 Clinical Laboratory Testing and in Vitro Diagnostic Test Systems – Susceptibility Testing of Infectious Agents and Evaluation of Performance of Antimicrobial Susceptibility Test Devices – Part 1 2006.

[32] Z.V. Feng, I.L. Gunsolus, T.A. Qiu, K.R. Hurley, L.H. Nyberg, H. Frew, K.P. Johnson, A.M. Vartanian, L.M. Jacob, S.E. Lohse, M.D. Torelli, R.J. Hamers, C.J. Murphy, C.L. Haynes, Impacts of gold nanoparticle charge and ligand type on surface binding and toxicity to Gram-negative and Gram-positive bacteria, Chem. Sci. 6 (2015) 5186–5196, http://dx.doi.org/10.1039/C5SC00792E.

[33] A. Ivask, A. Elbadawy, C. Kaweeteerawat, D. Boren, H. Fischer, Z. Ji, C.H. Chang, R. Liu, T. Tolaymat, D. Telesca, J.I. Zink, Y. Cohen, P.A. Holden, H.A. Godwin, Toxicity mechanisms in Escherichia coli vary for silver nanoparticles and differ from ionic silver, ACS Nano 8 (2014) 374–386, http://dx.doi.org/10.1021/nn4044047.

[34] T. Yoshida, T. Nagasawa, Epsilon-poly-L-lysine: microbial production, biodegradation and application potential, Appl. Microbiol. Biotechnol. 62 (2003) 21–26, http://dx.doi.org/10.1007/s00253-003-1312-9.

[35] K. Nakata, T. Tsuchido, Y. Matsumura, Antimicrobial cationic surfactant, cetyltrimethylammonium bromide, induces superoxide stress in Escherichia coli cells, J. Appl. Microbiol. 110 (2011) 568–579, http://dx.doi.org/10.1111/j.1365-2672.2010.04912.x.

[36] J.T. Buchman, A. Rahnamoun, K.M. Landy, X. Zhang, A.M. Vartanian, L.M. Jacob, C.J. Murphy, R. Hernandez, C.L. Haynes, Using an environmentally-relevant panel of Gram-negative bacteria to assess the toxicity of polyallylamine hydrochloride-wrapped gold nanoparticles, Environ. Sci. Nano 5 (2018) 279–288, http://dx.doi.org/10.1039/C7EN00832E.

[37] European Centre for Disease Prevention and Control, Point Prevalence Survey of Healthcare Associated Infections and Antimicrobial Use in European Acute Care Hospitals, ECDC, Stockholm, 2013.

[38] H.W. Boucher, G.H. Talbot, J.S. Bradley, J.E. Edwards, D. Gilbert, L.B. Rice, M. Scheld, B. Spellberg, J. Bartlett, Bad bugs, no drugs: no ESKAPE! An update from the infectious diseases society of America, Clin. Infect. Dis. 48 (2009) 1–12, http://dx.doi.org/10.1086/595011.

[39] S. Suppi, K. Kasemets, A. Ivask, K. Künnis-Beres, M. Sihtmäe, I. Kurvet, V. Aruoja, A. Kahru, A novel method for comparison of biocidal properties of nanomaterials to bacteria, yeasts and algae, J. Hazard. Mater. 286 (2015) 75–84, http://dx.doi.org/10.1016/j.jhazmat.2014.12.027.

[40] A. Jemec, A. Kahru, A. Potthoff, D. Drobne, M. Heinlaan, S. Böhme, M. Geppert, S. Novak, K. Schirmer, R. Rekulapally, S. Singh, V. Aruoja, M. Sihtmäe, K. Juganson,

A. Käkinen, D. Kühnel, An interlaboratory comparison of nanosilver characterisation and hazard identification: harmonising techniques for high quality data, Environ. Int. 87 (2016) 20–32, http://dx.doi.org/10.1016/j.envint.2015.10.014.

[41] N. Durán, C.P. Silveira, M. Durán, D.S.T. Martinez, Silver nanoparticle protein corona and toxicity: a mini-review, J. Nanobiotechnol. 13 (2015) 55, http://dx.doi.org/10.1186/s12951-015-0114-4.

[42] B. Le Ouay, F. Stellacci, Antibacterial activity of silver nanoparticles: a surface science insight, Nano Today. 10 (2015) 339–354, http://dx.doi.org/10.1016/j.nantod.2015.04.002.

[43] M. López-Heras, I.G. Theodorou, B.F. Leo, M.P. Ryan, A.E. Porter, Towards understanding the antibacterial activity of Ag nanoparticles: electron microscopy in the analysis of the materials-biology interface in the lung, Environ. Sci. Nano 2 (2015) 312–326, http://dx.doi.org/10.1039/C5EN00051C.

[44] J.S. Kim, E. Kuk, K.N. Yu, J.H. Kim, S.J. Park, H.J. Lee, S.H. Kim, Y.K. Park, Y.H. Park, C.Y. Hwang, Y.K. Kim, Y.S. Lee, D.H. Jeong, M.H. Cho, Antimicrobial effects of silver nanoparticles, Nanomed. Nanotechnol. Biol. Med. 3 (2007) 95–101, http://dx.doi.org/10.1016/j.nano.2006.12.001.

[45] S. Kim, H. Lee, D. Ryu, Antibacterial activity of silver-nanoparticles against Staphylococcus aureus and Escherichia coli, Korean J. Microbiol. Biotechnol. 39 (2011) 77–85.

[46] A. Ivask, I. Kurvet, K. Kasemets, I. Blinova, V. Aruoja, S. Suppi, H. Vija, A. Käkinen, T. Titma, M. Heinlaan, M. Visnapuu, D. Koller, V. Kisand, A. Kahru, Size-dependent toxicity of silver nanoparticles to bacteria, yeast, algae, crustaceans and mammalian cells in vitro, PLoS One 9 (2014), http://dx.doi.org/10.1371/journal.pone.0102108.

[47] D. McShan, P.C. Ray, H. Yu, Molecular toxicity mechanism of nanosilver, J. Food Drug Anal. 22 (2014) 116–127, http://dx.doi.org/10.1016/j.jfda.2014.01.010.

[48] N. Durán, M. Durán, M.B. de Jesus, A.B. Seabra, W.J. Fávaro, G. Nakazato, Silver nanoparticles: a new view on mechanistic aspects on antimicrobial activity, Nanomed. Nanotechnol. Biol. Med. 12 (2016) 789–799, http://dx.doi.org/10.1016/j.nano.2015.11.016.

[49] K. Theophel, V.J. Schacht, M. Schlüter, S. Schnell, C.-S. Stingu, R. Schaumann, M. Bunge, The importance of growth kinetic analysis in determining bacterial susceptibility against antibiotics and silver nanoparticles, Front. Microbiol. 5 (2014) 544, http://dx.doi.org/10.3389/fmicb.2014.00544.

[50] J.R. Morones-Ramirez, J.A. Winkler, C.S. Spina, J.J. Collins, Silver enhances antibiotic activity against Gram-negative bacteria, Sci. Transl. Med. 5 (2013), http://dx.doi.org/10.1126/scitranslmed.3006276.Silver.

[51] S. Gurunathan, J.W. Han, D.-N. Kwon, J.-H. Kim, Enhanced antibacterial and anti-biofilm activities of silver nanoparticles against Gram-negative and Gram-positive bacteria, Nanoscale Res. Lett. 9 (2014) 373, http://dx.doi.org/10.1186/1556-276X-9-373.

[52] S. Ninganagouda, V. Rathod, D. Singh, J. Hiremath, A.K. Singh, J. Mathew, M. Ul-Haq, Growth kinetics and mechanistic action of reactive oxygen species released by silver nanoparticles from Aspergillus niger on Escherichia coli, Biomed. Res. Int. 2014 (2014), http://dx.doi.org/10.1155/2014/753419.

[53] M.A. Ansari, H.M. Khan, A.A. Khan, M.K. Ahmad, A.A. Mahdi, R. Pal, S.S. Cameotra, Interaction of silver nanoparticles with Escherichia coli and their cell envelope biomolecules, J. Basic Microbiol. 54 (2014) 905–915, http://dx.doi.org/10.1002/jobm.201300457.

[54] G. Kaur, S.K. Mehta, Developments of polysorbate (Tween) based microemulsions: preclinical drug delivery, toxicity and antimicrobial applications, Int. J. Pharm. 529 (2017) 134–160, http://dx.doi.org/10.1016/j.ijpharm.2017.06.059.

[55] C.K. Nielsen, J. Kjems, T. Mygind, T. Snabe, R.L. Meyer, Effects of tween 80 on growth and biofilm formation in laboratory media, Front. Microbiol. 7 (2016) 1–10, http://dx.doi.org/10.3389/fmicb.2016.01878.

[56] K. Rajagopal, P.K. Singh, R. Kumar, K.F. Siddiqui, CTAB-mediated, single-step preparation of competent Escherichia coli, Bifidobacterium sp. and Kluyveromyces lactis cells, Meta Gene 2 (2014) 807–818, http://dx.doi.org/10.1016/j.mgene.2014.10.002.

[57] S.L. Lai, C.-H. Chen, K.-L. Yang, Enhancing the fluorescence intensity of DNA microarrays by using cationic surfactants, Langmuir 27 (2011) 5659–5664, http://dx.doi.org/10.1021/la2004694.

[58] R. Ye, H. Xu, C. Wan, S. Peng, L. Wang, H. Xu, Z.P. Aguilar, Y. Xiong, Z. Zeng, H. Wei, Antibacterial activity and mechanism of action of ε-poly-ʟ-lysine, Biochem. Biophys. Res. Commun. 439 (2013) 148–153, http://dx.doi.org/10.1016/j.bbrc.2013.08.001.

[59] K. Colville, N. Tompkins, A.D. Rutenberg, M.H. Jericho, Effects of poly(ʟ-lysine) substrates on attached Escherichia coli bacteria, Langmuir 26 (2010) 2639–2644, http://dx.doi.org/10.1021/la902826n.

[60] P.K. Stoimenov, R.L. Klinger, G.L. Marchin, K.J. Klabunde, Metal oxide nanoparticles as bactericidal agents, Langmuir 18 (2002) 6679–6686, http://dx.doi.org/10.1021/la0202374.

**Supplementary Material for:**


**Antimicrobial potency of differently coated 10 and 50 nm silver nanoparticles against clinically relevant bacteria *Escherichia coli* and *Staphylococcus aureus***

Anna-Liisa Kubo[1], Ivona Capjak[2], Ivana Vinković Vrček[3], Olesja M. Bondarenko[1], Imbi Kurvet[1], Heiki Vija[1], Angela Ivask[1], Kaja Kasemets[1], Anne Kahru[1,4]


[1]Laboratory of Environmental Toxicology, National Institute of Chemical Physics and Biophysics, Akadeemia tee 23, Tallinn 12618, Estonia;

[2] Croatian Institute of Transfusion Medicine, Petrova 3, 10 000 Zagreb, Croatia;

[3] Institute for Medical Research and Occupational Health, Ksaverska cesta 2, Zagreb, Croatia;

[4] Estonian Academy of Sciences, Kohtu 6, Tallinn, Estonia


*Corresponding author* (anne.kahru@kbfi.ee, Akadeemia tee 23, Tallinn 12618, Phone: +3725210963)

# Table of Contents

# Materials and Methods

## Synthesis of differently coated silver nanoparticles

*Chemicals*

If not otherwise stated, chemicals used were of ≥ 99% purity and obtained from Sigma-Aldrich Chemie GmbH (Munich, Germany). Bovine serum albumin (product number A-7906, Sigma-Aldrich Chemie GmbH, Steinheim, Germany) was used as received without further purification. The plastic and glassware used for chemical analysis were from Sarstedt (Belgium). All dilutions were made with high purity deionised (DI) water (18.2 MΩ-cm) obtained from a Milli-Q® system (Merck Chemicals GmbH, Darmstadt, Germany). The glassware was cleaned with 10% (v/v) $HNO_3$ and rinsed thoroughly with DI water before use.

All the experiments were carried out at laboratory temperature (approx. 20°C) protected from light. Silver nitrate ($AgNO_3$) was used as a precursor of nanoAg. Unlike other silver salts, silver nitrate is chemically stable and provides nitrate ion as dominant anion in the reaction mixture. The synthesis of differently coated nanoAg was conducted using structurally different capping agents: trisodium citrate dihydrate (CIT), sodium bis(2-ethylhexyl) sulfosuccinate (AOT), cetyltrimethyl-ammonium bromide (CTAB), poly(vinylpyrrolidone) (PVP), poly(L-lysine) (PLL), and polysorbate 80 (Tween 80).

*Synthesis of spherical 10 nm-sized nanoAg using AOT, PVP, Tween 80, PLL and CTAB as coating/stabilising agents*

NanoAg of 10 nm-size (10nAg) were synthesised by reducing $AgNO_3$ with $NaBH_4$ following the protocol described elsewhere [1]. Briefly, the solutions of coating agents were prepared by dissolving appropriate amounts of coating material in DI water. Then, 5 mL of 90 mM $AgNO_3$ was added drop-wise and dissolved by constant stirring on a magnetic stirrer plate (IKA Werke, Germany). To this solution, 5 mL of 160 mM $NaBH_4$ solution was added drop-wise (~1 drop/sec). The final concentrations of AOT, CTAB, PVP, PLL, and Tween 80 were 0.5 mM, 0.5 mM, 0.3 %(v/v), 0.05 %(v/v) and 0.5 mM, respectively. The reaction mixture was mixed vigorously at room temperature for 45 min. After the synthesis, silver colloids were

centrifuged at 15 000 × $g$ for 20 min. After decanting the supernatant, the residue was suspended in DI water and kept at 4°C in the dark.


*Synthesis of spherical 10 nm-sized citrate-coated nanoAg*

CIT-coated nanoAg were synthesised according to the procedure described by Li *et al* [2]. Briefly, 0.2 mL of the aqueous 0.1 mM solution of ascorbic acid (AsA) was added into 190 mL of boiling DI water. After 1 min, a CIT-AgNO$_3$ mixture (3.8 mL of the aqueous solution of 35.4 mM sodium citrate and 1.2 mL of 50 mM AgNO$_3$) was injected into the boiling aqueous solutions of AsA. The final concentrations of reactants were 0.673 mM for sodium citrate, 0.3 mM for AgNO$_3$ and 0.1 μM for AsA. The colour of the reaction solution quickly changed from colourless to yellow. The transparent and yellow reaction solution was further boiled for 1 h under stirring to warrant formation of uniform quasi-spherical nanoAg. Purification of nanoAg was performed by centrifugation of colloidal solution 2 times at 11 000 × $g$ for 30 min. Supernatant was decanted and precipitate was redispersed in DI water by sonication. After purification, CIT-coated nanoAg were kept at 4°C in the dark.


*Synthesis of spherical 50 nm-sized nanoAg using AOT, PVP, Tween 80 and CTAB as*

*coating/stabilizing agents*

NanoAg were prepared via chemical reduction of the complex cation [Ag(NH$_3$)$_2$]$^+$ by *D*-glucose [3]. The initial concentrations of the reagents in the reaction system were as follows: 1 mM AgNO$_3$; 10 mM ammonia and 10 mM *D*-glucose (reducing agent). Surfactants were added to the reaction system prior to the reducing agent. The final concentrations of AOT, CTAB, PVP and Tween 80 were 0.5 mM, 0.5 mM, 0.3% (w/v), and 0.5 mM, respectively.

Briefly, the solutions of coating agents were prepared by dissolving appropriate amounts of coating material in DI water. Then, 2.22 mL of 90 mM AgNO$_3$ was added drop-wise and dissolved by constant stirring on a magnetic stirrer plate (IKA Werke, Germany). To this solution, a 0.133 mL of 15 M NH$_3$ was added in one portion and then 4 mL of 0.5 M glucose was added drop-wise (~ 1 drop/sec). The reaction velocity is

strongly influenced by pH and therefore the value was maintained at about 11.5 by the addition of NaOH (0.6 mL of 1M), which enabled to keep the reaction time within several minutes.

The reaction mixture was mixed vigorously at room temperature for 45 min. After the synthesis, silver colloids were centrifuged at 15 000 × $g$ for 20 min. After decanting the supernatant, the residue was suspended in ultrapure water and kept at 4°C in the dark.

*Synthesis of spherical 50 nm-sized CIT-coated nanoAg*

Synthesis of citrate coated nanoAg of 50 nm was prepared following sythesis protocol described by Munro *et al* [4]. To 190 mL of MQ water, 2.22 mL of 90 mM AgNO$_3$ was added and heated rapidly to boiling under stirring. Immediately after boiling, 4 mL of 250 mM sodium citrate solution was rapidly added, and heating was reduced, but the solution was kept at 80°C for 90 min with continuous stirring. After the synthesis, silver colloids were centrifuged at 15 000 × $g$ for 20 min. After decanting the supernatant, the residue was suspended in ultrapure water and kept at 4°C in the dark.

# Cultivation of Ag-sensor bacteria *E. coli* MC1061 (pSLcueR/pDNPcopAlux) and control bacteria *E. coli* MC1061 (pDNlux)

The sensor-bacteria were grown overnight in Luria-Bertani (LB) medium (yeast extract (Lab M, UK) 5 g/L; tryptone (Lab M, UK) 10 g/L; NaCl (Sigma-Aldrich, USA) 5 g/L) supplemented with 100 mg/L ampicillin (Sigma-Aldrich, USA) and 10 mg/L tetracycline (Sigma-Aldrich) and control bacteria were grown in LB medium supplemented with 10 mg/L tetracycline. Overnight cultures were diluted 1:50 in fresh LB medium and cultivated up to the exponential growth phase (optical density (OD) at 600nm=0.6 according to Jenway 6300 spectrophotometer (UK), 1 cm path cuvette) on the orbital shaker (Thermo Scientific Forma Orbital Shaker 420, USA) at 200 rpm, 30°C. Then, the bacterial suspension was washed twice with DI water by centrifugation at 2600 × g for 5 min and finally suspended in 40 mM MOPS buffer (Sigma-Aldrich) supplemented with 0.1% glucose (Sigma-Aldrich) and 0.01% Casamino acids (Lab M, UK) adjusting the

culture density to the $OD_{600nm}$=0.1 ($2\times10^7$ CFU/mL; CFU – cell forming unit determined by the plating and counting of colonies on the LB agar plates).

## Analysis of the toxicity of coating materials using bacterial growth inhibition assay (ISO 20776-1)

The bacterial growth inhibition assay was adapted from the reference method ISO 20776-1 for antimicrobial susceptibility testing [5]. The coating materials were diluted in cation-adjusted Mueller-Hinton Broth (CA-MHB, Oxoid Microbiology Products) containing 300 g dehydrated infusion from beef, 17.5 g casein hydrolysate, 1.5 g starch, 25 mg $Ca^{2+}$ and 12.5 mg $Mg^{2+}$ per 1 litre in two-fold dilutions. The overnight inoculum of bacteria was diluted with fresh medium to a density of ~$5x10^5$ CFU/mL.

The incubation mixtures were prepared by combining the bacterial suspension (50 µL) and test compound solution (50 µL) in 96-well transparent polystyrene microplates (BD Falcon) followed by incubation at 37°C for 20 hours in the dark in aerobic conditions with minor shaking after every 15 min. Bacterial growth was monitored by measuring optical density (OD at 600 nm) with Spectramax Paradigm spectrophotometer (Molecular Devices).

The minimal inhibitory concentration (MIC) of the compound was determined as the lowest tested concentration where no visible growth of bacteria was observed after 20 h. For that, after 20 h incubation of bacteria with the coating materials, 3 µL of sample from each test or control well was pipetted as a 'spot' onto the toxicant-free Mueller-Hinton (Oxoid CM0337; 25 mg $Ca^{2+}$/L and 12.5 mg $Mg^{2+}$/L added) agar plates which were incubated at 30°C for 24 h and colonies were counted. The experiments in one replication were repeated twice.

## Quantification of dissolved silver in abiotic conditions using chemical method

For the quantification of the solubility of nanoAg in abiotic conditions simulating the antibacterial test (but without bacteria added). Concentration of Ag-ions was determined in the ultra-filtered solutions

using graphite furnace atomic absorption spectrometry (GFAAS) (Perkin Elmer AAnalyst 600, Perkin Elmer) with Zeeman background correction in the laboratory of the Institute of Medical Research and Occupational Health, Zagreb, Croatia. The reliability of analytical methods was evaluated using Standard Reference Material® 1643e Trace Elements in Water (NIST). The results of our analysis were within ± 10% of the certified values.

## Quantification of bioavailable silver using Ag-sensing bacteria

For quantification of bioavailable silver, 100 µL of each nanoAg suspension (0.0001–20 mg Ag/L) in DI water (each concentration in duplicate) were mixed with 100 µL suspensions of Ag-sensing bacteria *E. coli* MC1061 (pSLcueR/pDNPcopAlux)  in 40 mM MOPS buffer supplemented with 0.1% glucose and 0.01% acid hydrolysate of casein. Incubation of sensor bacteria with silver compounds was performed in white 96-well polypropylene (PP) microplates (Greiner Bio-One) at 30°C for 4 h in the dark. For calibration of the biosensor, 100 µL of $AgNO_3$ dilutions in DI water (0.000015-0.016 mg Ag/L) were mixed with 100 µL of sensor bacteria and incubated as described above. Bacterial bioluminescence was measured by a Orion II Plate Luminometer (Berthold Detection Systems). In order to account for sample turbidity, nanoAg exposures were also performed with constitutively bioluminescent bacteria  *E. coli* MC1061 (pDNlux) ('control bacteria') and their bioluminescence after 4 h was measured to take into account possible turbidity/colour and toxic effects of nanoAg. Based on these data, Kf (correlation factor) was calculated as follows:

$$Kf = \frac{Bioluminescence\ of\ control\ bacteria\ without\ Ag\ (background)}{Bioluminescence\ of\ control\ bacteria\ upon\ exposure\ to\ Ag}$$

$$Induction, fold = \frac{Bioluminescence\ of\ sensor\ bacteria\ upon\ exposure\ to\ Ag}{Bioluminescence\ of\ sensor\ bacteria\ without\ Ag\ (background)}\ \ x\ Kf$$

Bioavailable Ag (%) from nanoAg was quantified by comparing the linear parts of the bioluminescence induction response curves of nanoAg and AgNO$_3$, considering AgNO$_3$ 100% bioavailable. Experiments were performed at least three times and average values ± standard deviation (SD) are presented.

## Analysis of antibacterial efficiency of nanoAg and their coatings

The test bacteria *Escherichia coli* MG1655 and *Staphylococcus aureus* (ATCC 6538) were cultivated from a few colonies from LB agar plates and grown overnight in liquid LB medium on a shaker at 30°C and 200 rpm. Next, the bacterial suspension was diluted in fresh LB medium (1:50) and grown up to exponential growth phase that was determined as OD value of ~0.6 at 600 nm spectrophotometrical measurement (Jenway 6300). The bacterial culture was washed twice by centrifugation and resuspended in DI water (2600 x g, 5 min) and diluted to obtain the OD$_{600nm}$= 0.1 that equals to 10$^7$ CFU/mL in the case of *E. coli* MG1655, and 6x10$^7$ CFU/mL for *S. aureus* 6538. 100 µL of the bacterial suspension and 100 µL of toxicants in DI water were mixed in the wells of 96-well polystyrene microplates (BD Falcon).  NanoAg was tested between 0.01 and 40 mg Ag/L using two-fold dilutions, nanoAg coating materials were tested between 0.3 and 8000 mg/L using 10-fold dilutions and AgNO$_3$ as an ionic Ag control was tested between 0.004 and 0.5 mg Ag/L using two-fold dilutions. The microplates were incubated without shaking in the dark at 30°C for 4 h and 24 h. After the incubation, 3 µL of exposed and unexposed culture (control) was pipetted onto toxicant-free LB-agar plates (as a spot) and incubated at 30°C for 24 h. MBC was determined as the lowest tested concentration of the test compound which completely inhibited the growth of visible colonies within the spot on agar plates. Three individual experiments in duplicates were performed, average MBC values ± SD were presented.

The pure coatings were also studied for their antimicrobial effects in bacterial growth inhibition assay according to ISO 20776-1 [5] and  described above. Growth inhibition assay was not applied for the characterisation of antimicrobial properties of nanoAg because the components of Mueller-Hinton broth used as test medium complex silver ions leading to decrease in bioavailability of Ag-compounds [6].

*Estimation of pure coatings toxicity at the MBC values of nanoAg*

Since CTAB and PLL were the most toxic of tested coatings, we calculated the potential toxic effects of PLL and CTAB coatings at 50nAg-PLL and 50nAg-CTAB MBC values. The 4 h MBC of 50nAg-CTAB to *E. coli* and *S. aureus* was 5 and 10 mg Ag/L, respectively (Table S1), meaning that at MBC concentrations the master stock of 50nAg-CTAB was diluted 244 and 122 times, respectively. Taking into account that the concentration of CTAB in the master stock of 50nAg-CTAB was 36.4 mg/L, the concentration of CTAB was 36.4/244=0.15 mg/L at MBC of *E. coli* and 36.4/122=0.3 mg/L of *S. aureus.* Analogously, the PLL concentration in the suspension of 10nAg-PLL at 4 h MBC was 0.02 and 0.26 mg/L for *E. coli* and *S. aureus*, respectively.

## Flow cytometry analysis of nanoAg-bacteria interactions

For flow cytometry, exponentially growing bacterial cells were prepared as described peviously and diluted in DI water up to the density $OD_{600nm}$= 0.2 (equals to 2 x $10^7$ CFU/mL for *E. coli* MG1655, and $10^8$ CFU/mL for *S. aureus* 6538). The bacterial suspensions were incubated with nanoAg (2 or 8 mg Ag/L) or $AgNO_3$ (0.2 mg Ag/L) at room temperature for 10 min without shaking, followed by staining with 5 µM SYTO 9 (Invitrogen S34854 846177) or 7.5 µM propidium iodide (PI) (Fluka 81845) in the dark. SYTO 9 is a green fluorescent dye that binds to the DNA of live and dead bacteria enabling to discriminate cell debris from bacterial cells. PI is a DNA-binding red fluorescent dye that diffuses through the membranes of damaged cells, allowing to determine the dead bacteria. 70% ethanol was used as a positive control for PI (yielding 95-100% PI-positive *E. coli* and *S. aureus* cells, data not shown). Flow cytometry analysis was conducted with BD Accuri ™ C6 Flow Cytometer Instrument (BD Biosciences ) using 488 nm excitation laser and 533 nm wavelength filter for SYTO 9 and 585 nm wavelength filter for PI. In addition, side-scatter signals (SSC) were collected while 20 000 events were counted in each run. Unexposed bacterial population was used to 'draw' the gates as shown in Figure S8. The percentage of bacterial cells interacting with differently coated nanoAg was determined by quantifying the shift in SSC and fluorescence intensity of SYTO 9-stained cells

and referred as 'NPs binding'. The percentage of damaged bacterial cells was determined quantifying the fluorescence intensity of PI-stained cells after exposure to nanoAg. Flow cytometry experiments were repeated three times.

# Figures
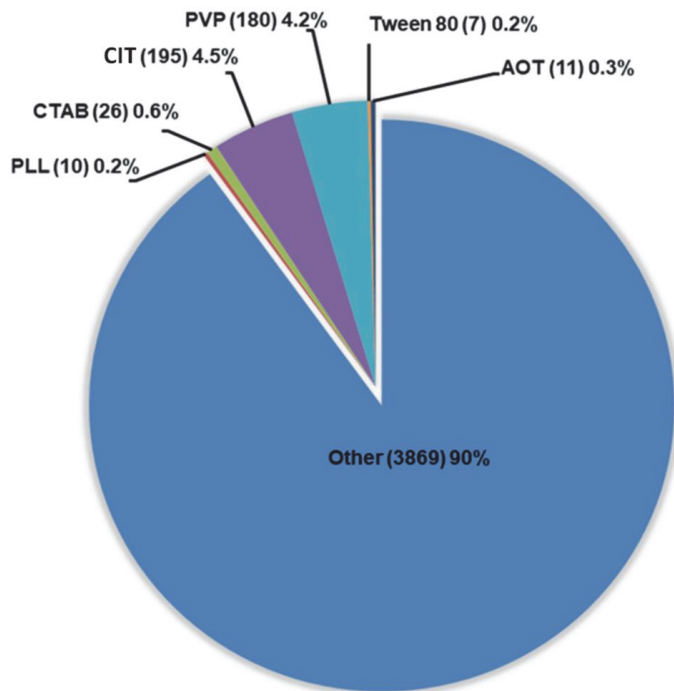


**Figure S1.** Number of publications in which different organic coatings/capping agents were used for synthesis and/or stabilisation of nanoAg to be used for medical or biocidal purposes. Publications were searched on 15.09.2017 in ISI WoS using search terms 'silver nanoparticle' and 'coating OR capping OR stabili*' and 'biocidal OR medic* OR antimicrobial OR antibacterial'. Highlighted are only coating agents that were used in the current study.
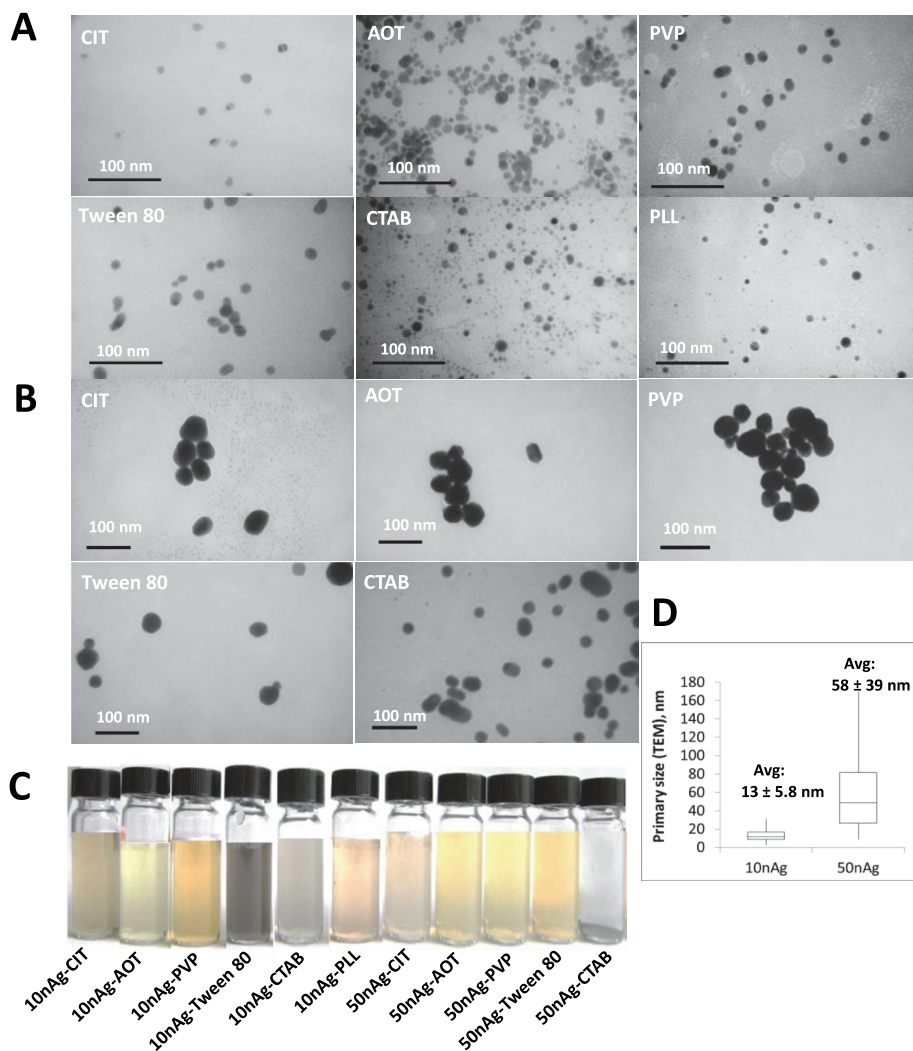
**Figure S2.** Transmission electron micrographs (TEM) of 10 nm silver nanoparticles (A) and of 50 nm silver nanoparticles (nanoAg) (B) coated with citrate (CIT), sodium bis(2-ethylhexyl)-sulfosuccinate (AOT), poly(vinylpyrrolidone) (PVP), Tween 80, poly-L-lysine (PLL), and cetyl trimethylammonium bromide (CTAB) in DI water. Appearance of nanoAg suspensions in DI water (10 mg Ag/L) (C). Boxplots of primary sizes of all 10 nm and all 50 nm nanoAg (measured from TEM pictures) (D).
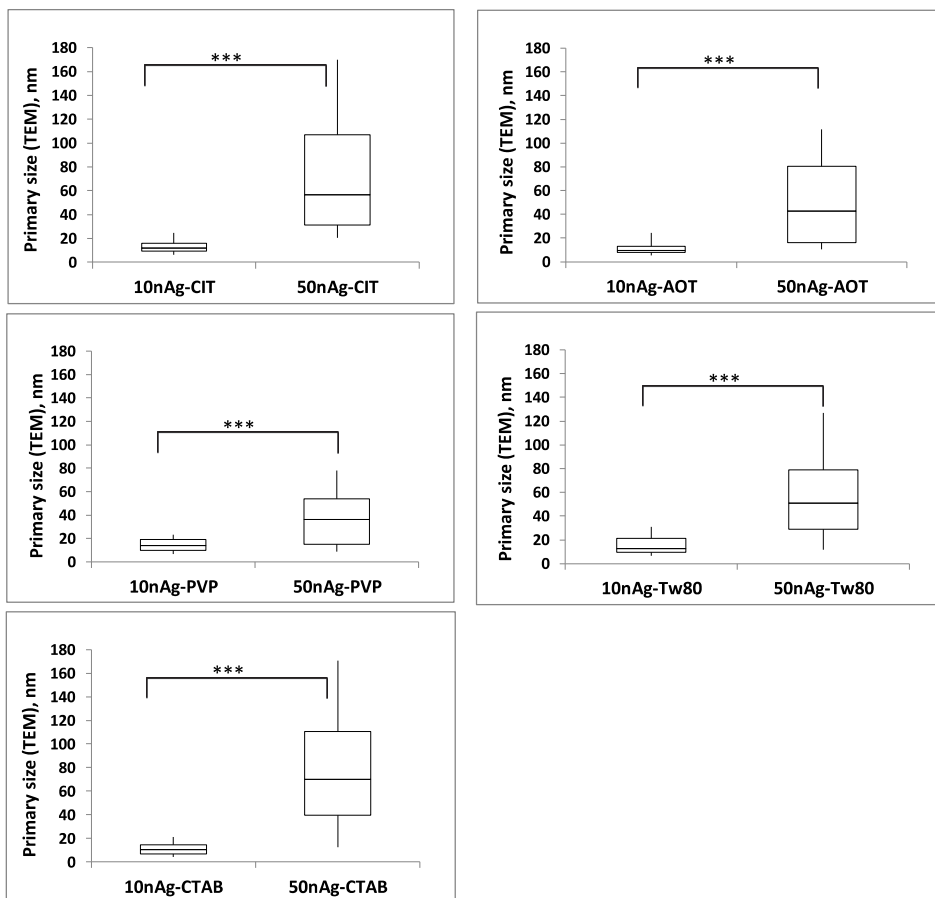
**Figure S3.** Primary size of differently coated nanoAg of two different sizes: 10 nm (10nAg) and 50 nm (50nAg) (measured from the TEM pictures by ImageJ software). Values between 25th and 75th percentile (1st and 3d quartile) form the box and the line inside of the box shows the median value of variables. 'Whiskers' show the scale of the minimum and maximum values. The average sizes for each particle type are in Table 2. The asterisks show the statistical significance: ***p<0.001.
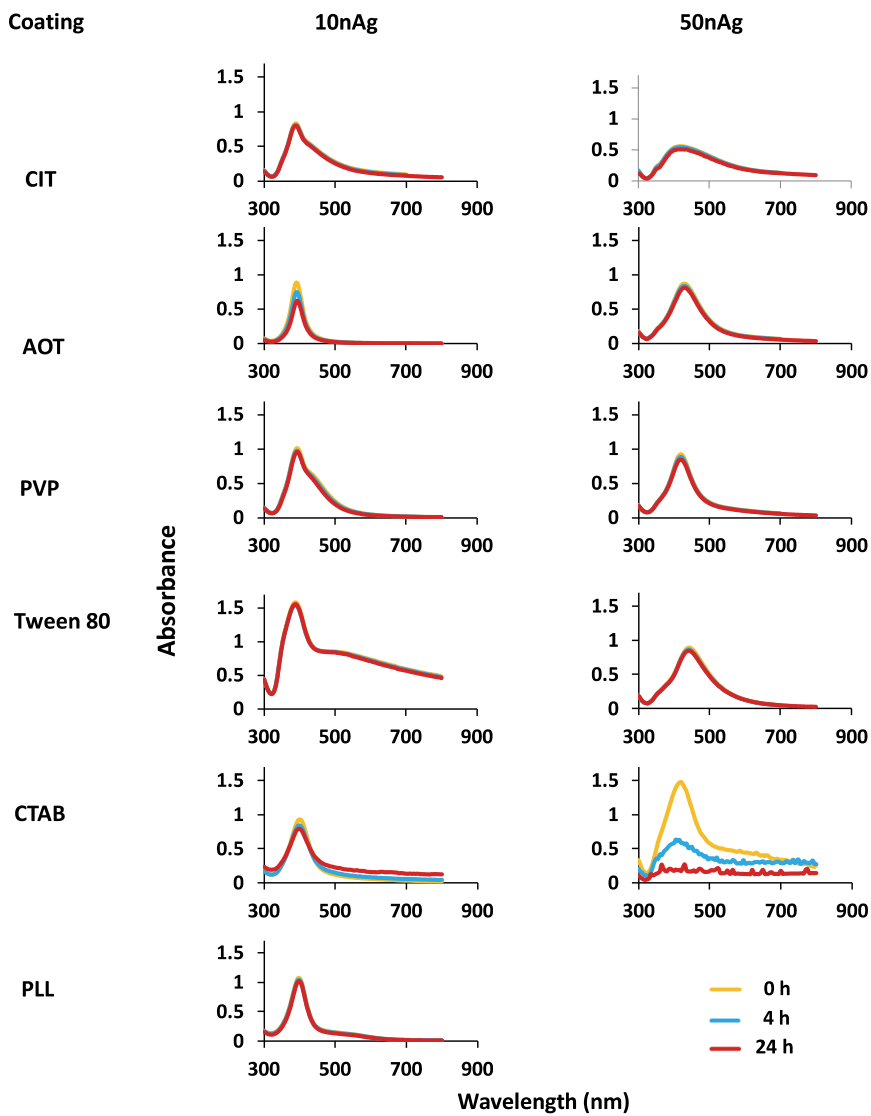
**Figure S4**. UV-Vis absorption spectra of 10nAg and 50nAg in DI water (20-40 mg Ag/L) after suspension

preparation (0 h) and after incubation for 4 h and 24 h at 30°C.
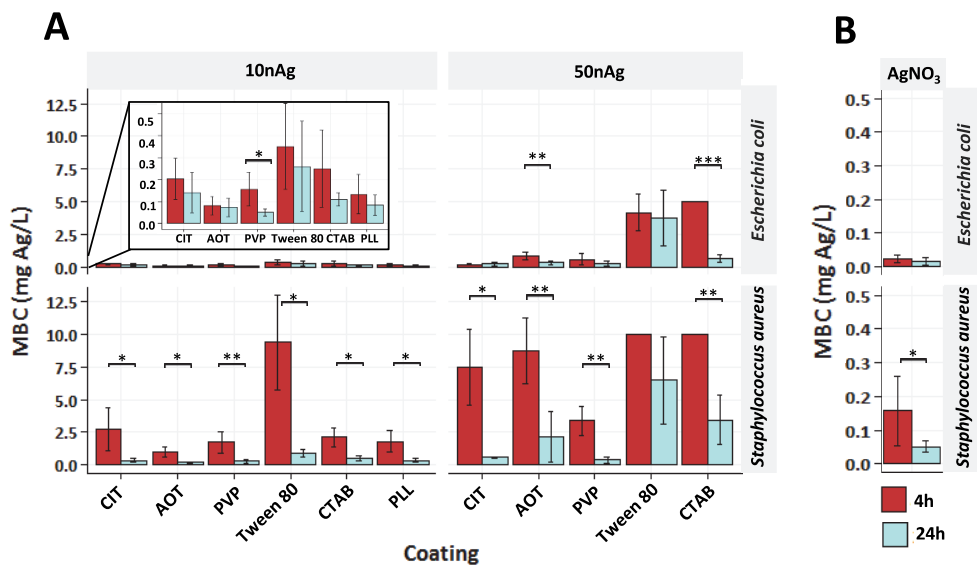
**Figure S5.** Effect of incubation time on minimal bactericidal concentrations (MBC) of differently coated (A) 10nAg and 50nAg and (B) AgNO$_3$ to *Escherichia coli* (upper panels) and *Staphylococcus aureus* (lower panels). 4 h (dark columns) and 24 h (light columns) incubation are compared. Data represent the average values of 3 to 5 experiments ± standard deviation (SD); ***p<0.001, **p<0.01, *p<0.05. Note that the *E. coli* data for 10 nm nanoAg are enlarged in the inset of the respective panel and that AgNO$_3$ data are plotted using different Y-axis scale. Data are plotted from Table S1.
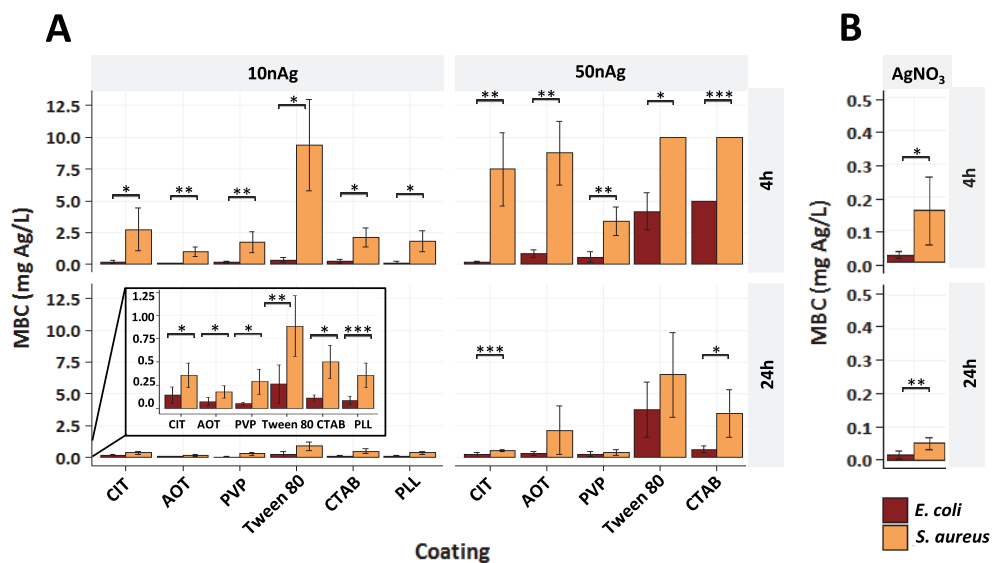
**Figure S6.** Antibacterial effect (MBC) of differently coated (A) 10nAg and 50nAg and (B) AgNO₃ to *Escherichia coli* (dark columns) and *Staphylococcus aureus* (light columns). MBC values after 4 h incubation (upper panels) and 24 h (lower panels) incubation are shown. Data represent the average values of 3 to 5 experiments ± SD; \*\*\*p<0.001, \*\*p<0.01, \*p<0.05. Note that AgNO₃ data are plotted using different Y-axis scale. Data are plotted from Table S1.
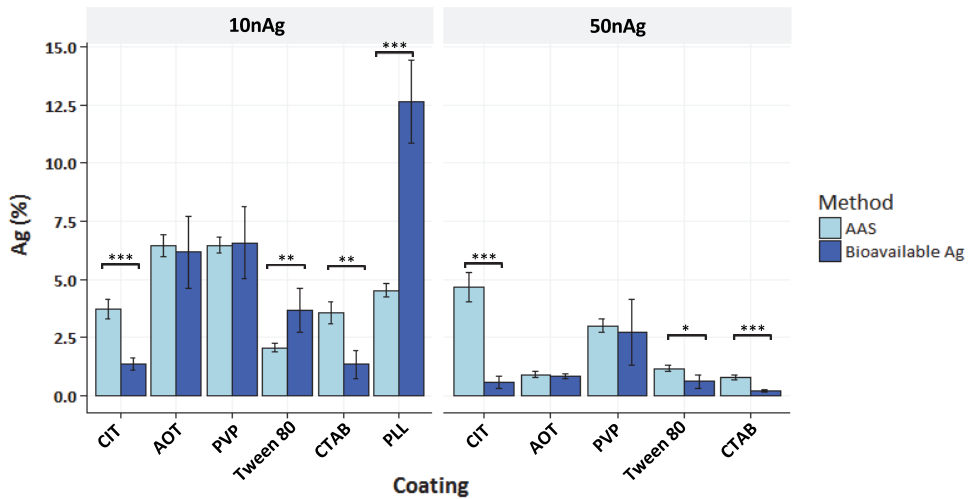
**Figure S7.** Comparison of solubility (AAS) and bioavailability (Ag-sensing biosensor bacteria) of 10nAg and 50nAg. Solubility (AAS) was analysed at 1 mg Ag/L. Average of at least three measurements ± SD are presented. Asterisks show the statistical difference of the values obtained with AAS and biosensor analysis: ***$p < 0.001$, **$p < 0.01$, *$p < 0.05$. Data are plotted from Figure 3.
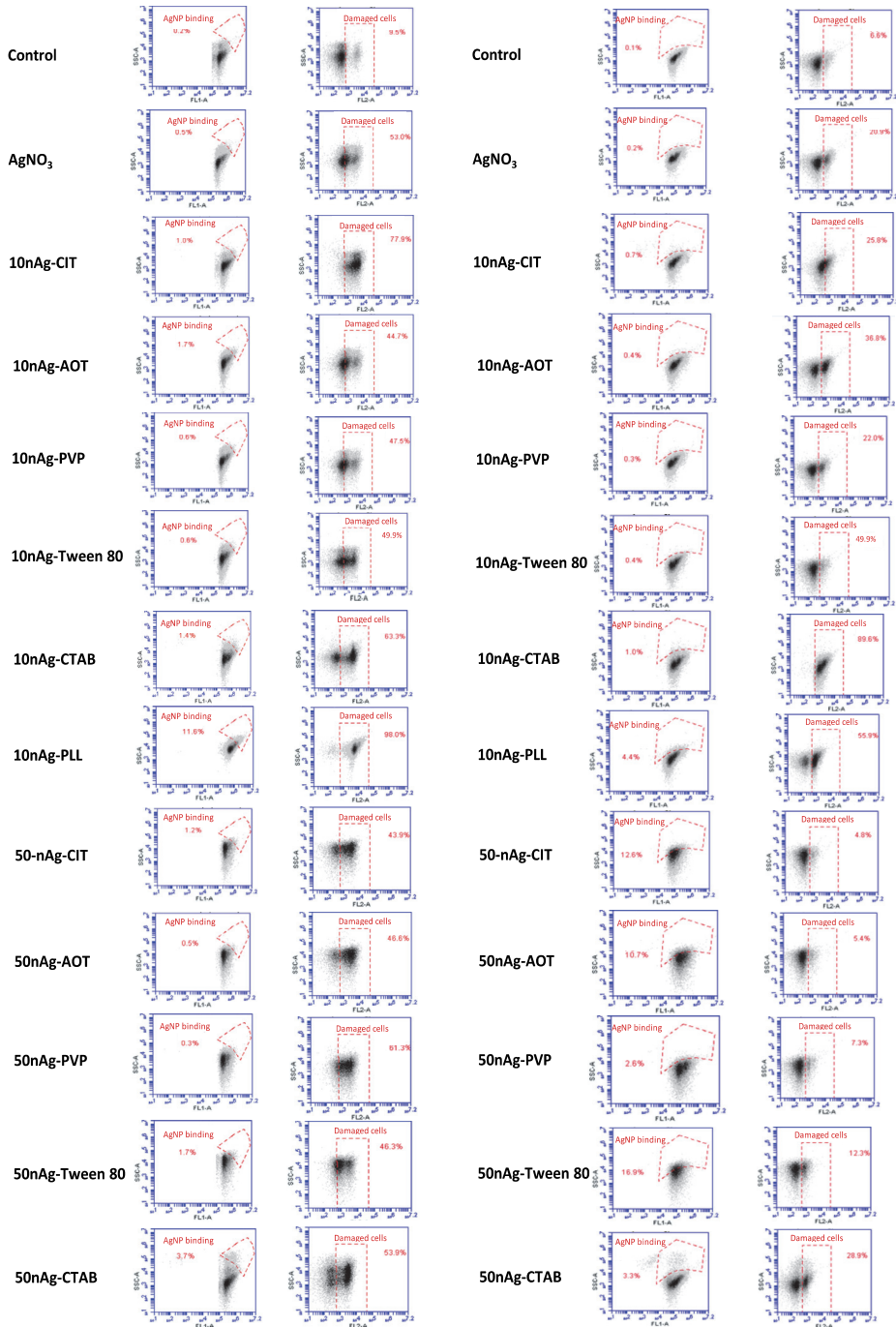
**Figure S8.** Representative flow cytographs of nanoAg binding (revealed by shift in side scatter signal, SSC) to *E. coli* and *S. aureus* and visualisation of bacterial death or membrane damage by propidium iodide (PI)

staining. NanoAg were added to bacteria at 8 mg Ag/L and AgNO$_3$ at 0.2 mg Ag/L for 10 min following staining for 15 min. On each panel, the left side graph shows nanoAg binding based on side scatter shift of SYTO 9-stained cells and right side graph shows cellular death (PI signal) versus SSC signal.

# Tables

**Table S1.**

The antimicrobial potency (minimal bactericidal concentration, MBC) of differently coated 10 nm and 50 nm nanoAg and AgNO$_3$ for *E. coli* and *S. aureus* after 4 h and 24 h of incubation in DI water.

| Toxicants | *Escherichia coli* MG1655 | | *Staphylococcus aureus* 6538 | |
|---|---|---|---|---|
| | 4 h MBC ± SD (mg Ag/L) | 24 h MBC ± SD (mg Ag/L) | 4 h MBC ±SD (mg Ag/L) | 24 h MBC ± SD (mg Ag/L) |
| AgNO$_3$ | 0.02±0.01 | 0.02±0.01 | 0.16±0.10 | 0.05±0.02 |
| 10nAg-CIT | 0.20±0.09 | 0.14±0.09 | 2.75±1.66 | 0.35±0.13 |
| 10nAg-AOT | 0.08±0.04 | 0.07±0.04 | 1.00±0.35 | 0.18±0.07 |
| 10nAg-PVP | 0.16±0.11 | 0.05±0.02 | 1.75±0.82 | 0.29±0.14 |
| 10nAg-Tween 80 | 0.35±0.20 | 0.26±0.21 | 9.38±3.61 | 0.89±0.33 |
| 10nAg-CTAB | 0.25±0.18 | 0.11±0.03 | 2.13±0.75 | 0.50±0.18 |
| 10nAg-PLL | 0.13±0.09 | 0.08±0.05 | 1.81±0.80 | 0.35±0.13 |
| 50nAg-CIT | 0.19±0.07 | 0.21±0.17 | 7.50±2.89 | 0.56±0.07 |
| 50nAg-AOT | 0.83±0.29 | 0.31±0.15 | 8.75±2.50 | 2.13±1.92 |
| 50nAg-PVP | 0.58±0.41 | 0.28±0.21 | 3.38± 1.11 | 0.38±0.22 |
| 50nAg-Tween | 4.17±1.44 | 3.75±2.17 | 10.00± 0.00 | 6.50±3.35 |
| 50nAg-CTAB | 5.00±0.00 | 0.63±0.27 | 10.00±0.00 | 3.44±1.88 |

The data are average of 3-5 replicate experiments. Heat-mapping: from red to green as from more toxic to less toxic

**Table S2**

The minimal bactericidal concentration (MBC, mg/L) of pure coating materials used for synthesis of

nanoAg.

| Test bacterium | E. coli | | S. aureus | |
|---|---|---|---|---|
| Coating/endpoint | 4 h MBC | 24 h MBC | 4 h MBC | 24 h MBC |
| CIT* | >294 | >294 | >294 | >294 |
| AOT¥ | >445 | >445 | 445 | 44.5 |
| PVPⱢ | 4000 | 4000 | >4000 | >4000 |
| Tween 80§ | >131 | >131 | >131 | >131 |
| CTAB‖ | 3.7 | 3.7 | 3.7 | 3.7 |
| PLL¶ | 3.0 | 3.0 | 300 | 3.0 |
| BAC# | 2.5 | 1.3 | 2.5 | 1.3 |

*CIT – Trisodium citrate, ¥AOT - Bis-2-ethylhexyl sulfosuccinate, ⱢPVP - Poly-vinylpyrrolidone, §Tween 80 - Polysorbate 80, ‖CTAB - Cetyltrimethyl-ammonium bromide, ¶PLL - Poly-L-lysine, #BAC - Benzalkonium choride (a positive control). Exposure of test bacteria to coating materials was made in DI water.

**Table S3**

The minimal bactericidal concentration (MBC) and minimal inhibitory concentration (MIC) of pure coating materials used for coating/capping of tested nanoAg.

| Coating | *Escherichia coli* MG1655 | | *Staphylococcus aureus* 6538 | |
|---|---|---|---|---|
| | 20 h MBC (mg/L) | 20 h MIC (mg/L) | 20 h MBC (mg/L) | 20 h MIC (mg/L) |
| CIT* | >294 | >294 | >294 | >294 |
| AOT† | >445 | >445 | 111 | 111 |
| PVP‡ | >2000 | >2000 | >2000 | >2000 |
| Tween 80§ | >131 | >131 | >131 | >131 |
| CTAB‖ | 36.5 | 36.5 | 1.9 | 1.9 |
| PLL¶ | 75 | 75 | 30 | 30 |
| BAC# | 71 | 71 | 7.1 | 1.4 |

*CIT – Trisodium citrate, †AOT - Bis-2-ethylhexyl sulfosuccinate, ‡PVP - Poly-vinylpyrrolidone, §Tween 80 - Polysorbate 80, ‖CTAB - Cetyltrimethyl-ammonium bromide, ¶PLL - Poly-*L*-lysine, #BAC-Benzalkonium chloride (positive control). Testing was following bacterial growth inhibition assay ISO 20776-1 [5] and was performed in Mueller-Hinton Broth.

# References

[1]     I. Vinković Vrček, I. Pavičić, T. Crnković, D. Jurašin, M. Babič, D. Horák, M. Lovrić, L. Ferhatović, M. Ćurlin, S. Gajović, Does surface coating of metallic nanoparticles modulate their interference with in vitro assays?, RSC Adv. 5 (2015) 70787–70807. doi:10.1039/C5RA14100A.

[2]     H. Li, H. Xia, D. Wang, X. Tao, Simple synthesis of monodisperse, quasi-spherical, citrate-stabilized silver nanocrystals in water, Langmuir. 29 (2013) 5074–5079. doi:10.1021/la400214x.

[3]     J. Soukupová, L. Kvítek, A. Panáček, T. Nevěčná, R. Zbořil, Comprehensive study on surfactant role on silver nanoparticles (NPs) prepared via modified Tollens process, Mater. Chem. Phys. 111 (2008) 77–81. doi:10.1016/j.matchemphys.2008.03.018.

[4]     C.H. Munro, W.E. Smith, M. Garner, J. Clarkson, P.C. White, Characterization of the Surface of a Citrate-Reduced Colloid Optimized for use as a Substrate for Surface-Enhanced Resonance Raman Scattering, Langmuir. 11 (1995) 3712–3720. doi:10.1021/la00010a021.

[5]     ISO 20776-1:2006 Clinical Laboratory Testing and in Vitro Diagnostic Test Systems -- Susceptibility Testing of Infectious Agents and Evaluation of Performance of Antimicrobial Susceptibility Test Devices -- Part 1 2006., n.d.

[6]     K. Nakata, T. Tsuchido, Y. Matsumura, Antimicrobial cationic surfactant, cetyltrimethylammonium bromide, induces superoxide stress in Escherichia coli cells, J. Appl. Microbiol. 110 (2011) 568–579. doi:10.1111/j.1365-2672.2010.04912.x.

**Publication III**

**Kubo, A. L.**, Kremer, L., Herrmann, S., Mitchell, S. G., Bondarenko, O. M., Kahru, A., Streb, C. (2017). Antimicrobial activity of polyoxometalate ionic liquids against clinically relevant pathogens. ChemPlusChem, 82(6), 867–871.

# Antimicrobial Activity of Polyoxometalate Ionic Liquids against Clinically Relevant Pathogens

Anna-Liisa Kubo+,[a] Lea Kremer+,[b] Sven Herrmann,[b] Scott G. Mitchell,[c] Olesja M. Bondarenko,[a] Anne Kahru,*[a, d] and Carsten Streb*[b]

The activity of a new class of antimicrobials—polyoxometalate ionic liquids (POM-ILs)—is systematically investigated. The prototype POM-ILs feature Keggin-type anions ($\alpha$-$SiW_{11}O_{39}^{8-}$) and tetraalkylammonium ions as active cationic species. Antimicrobial tests of the POM-ILs against important human pathogens show that variation of the alkyl chain length of the cation leads to significant changes in antimicrobial activity against the medically relevant Gram-negative bacteria *Escherichia coli* and *Pseudomonas aeruginosa*, and especially against the Gram-positive *Staphylococcus aureus*. Owing to the unique materials properties of the POM-ILs, such as high viscosity and water immiscibility, applications of antimicrobial surface coatings against airborne pathogens or for water decontamination can be envisaged. Furthermore, the combination of antimicrobially active cations with POM anions might afford new POM-ILs with two active components.

## Introduction

The ability of pathogenic bacteria to develop resistance against common antimicrobials is a major public health concern.[1] Chemists and pharmaceutical researchers worldwide are searching for alternative materials with potential antimicrobial or biocidal activity, particularly for use in clinical patient care, decentralized public health scenarios and water decontamination. In addition to new organic compounds (such as organo-ammonium cations),[2–4] including peptides,[5] metal oxides have attracted significant interest over the past decade, as they offer alternative modes of antimicrobial action.[6–8] A main advantage to using metal oxides is their vast variety in terms of particle size, structure and chemical composition, so that they can be deployed in various scenarios,[9] ranging from in vivo diagnostics and therapeutics[10, 11] through to applications in colloids,[8] as surface coatings[12–14] or embedded in various solid matrices.[15–17]

One particularly suitable sub-class of metal oxides are molecular metal oxide anions, the so-called polyoxometalates (POMs).[18] POMs are high-valent, early transition-metal oxide clusters, the size, structure and reactivity of which can be tuned by using established chemical procedures. Over recent decades, tungstate and molybdate POMs in particular have been investigated as potentially bioactive compounds[19, 20] and their use as antimicrobial,[21] antiviral,[22] antitumor,[23] and anti-amyloid-fibril agents (related to Alzheimer's disease)[24] has been reported.

One key advantage of anionic POMs is that a functional cation can easily be introduced as a second reactive component to afford multifunctional compounds. A prime example of this concept is the use of polyoxometalate ionic liquids (POM-ILs).[25] POM-ILs are obtained by combining a POM anion of choice with a bulky organocation such as an organoammonium or organophosphonium ion. The resulting compounds retain the properties of both the cationic and anionic species and can therefore be chemically tuned by separate modification of each component.[15, 25, 26] This has led to applications in self-separating epoxidation catalysts,[27] industrial catalysts for large-scale petrochemistry[28] or self-repairing anti-corrosion coatings.[12]

Recently, we reported a multifunctional POM-IL water purification filter that utilizes the key properties of this compound class.[12, 15] To that end, the water-insoluble POM-IL $[N(C_7H_{15})_4]_8[\alpha\text{-}SiW_{11}O_{39}]$ was immobilized on commercial porous silica,[29–31] affording a POM-supported ionic-liquid phase (POM-SILP). The POM-IL was based on antimicrobial tetraalkylammonium cations[4, 32] and POM anions featuring vacant metal-binding sites.[33] The resulting POM-SILP was used for the filtration of contaminated water and it was shown that toxic metal ions

[a] A.-L. Kubo,+ Dr. O. M. Bondarenko, Dr. A. Kahru
National Institute of Chemical Physics and Biophysics
Laboratory of Environmental Toxicology
Akadeemia tee 23; Tallinn 12618 (Estonia)
E-mail: anne.kahru@kbfi.ee

[b] L. Kremer,+ Dr. S. Herrmann, Prof. Dr. C. Streb
Institute of Inorganic Chemistry I
Ulm University
Albert-Einstein-Allee 11, 89081 Ulm (Germany)
E-mail: Carsten.streb@uni-ulm.de

[c] Dr. S. G. Mitchell
Instituto de Ciencia de Materiales de Aragon (ICMA-CSIC)
CISC-Universidad de Zaragoza
50019 Zaragoza (Spain)

[d] Dr. A. Kahru
Estonian Academy of Sciences
Kohtu 6, Tallinn 10130 (Estonia)

[+] These authors contributed equally to this work.

Supporting information (containing synthesis and the characterization of POM-ILs) and the ORCID identification number(s) for the author(s) of this article can be found under https://doi.org/10.1002/cplu.201700251.

(e.g., Ni$^{2+}$, Pb$^{2+}$), radionuclides (e.g., UO$_2^{2+}$), as well as organic pollutants (e.g., dyes) and microbes (*E. coli*) were effectively removed (Figure 1).[15]
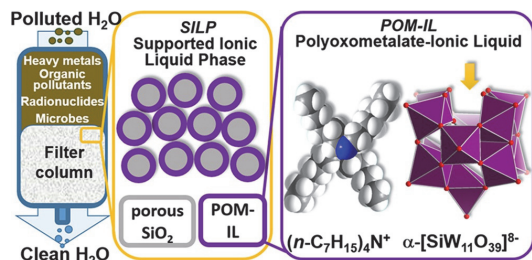


**Figure 1.** The concept of polyoxometalate-supported ionic-liquid phase (POM-SILP) water purification, showing the filter, which consists of a lipophilic POM-IL immobilized on porous silica. The IL components (antimicrobial tetraalkylammonium cations and polyoxometalate anions) show capabilities for the uptake of toxic heavy metals (e.g., Pb$^{2+}$, UO$_2^{2+}$), organic pollutants (e.g., trityl dyes) and microbial contaminants (e.g., *E. coli*). Reproduced from reference [15] by permission from Wiley-VCH.

Notably, the removal of microbes from water by filtration is still particularly challenging and often, physical filtration is used, in which small pores prevent passage of the microbes.[34] In contrast, the method described above uses truly antimicrobial surfaces, not only to remove but also to destroy microbes, thus providing an additional layer of security in water purification.[15] Thus, in the future, combining antimicrobial organic cations and antimicrobial POM anions might lead to synergistic POM-ILs that provide two active components with different antimicrobial modes of action.

## Results and Discussion

Here, we built on this concept and expanded our initial studies to assess the activity of several POM-ILs against well-known Gram-negative (*Escherichia coli*, *Pseudomonas aeruginosa*) and Gram-positive (*Staphylococcus aureus*) bacterial strains. These microbes are often implicated in hospital-acquired infections and thus serve as useful models to assess the biocidal efficacy of new materials.[35,36] Importantly, *P. aeruginosa* and *S. aureus* belong to a group of six problematic pathogens associated with drug-resistant infections, as identified by the Infectious Diseases Society of America.[37] For these pathogens, novel therapies against them are urgently required and their removal from contaminated water, air and surfaces is a major challenge.[37] These particular pathogens are also part of a wider global problem—increasing microbial resistance against antibiotics—that can lead to public healthcare crises and uncontrolled spread of infectious diseases.[38] Although the antibacterial effects of classical POMs have been reported previously,[21,39–42] to the best of our knowledge, this is the first systematic study on the antimicrobial activity of POM-ILs.

Here we report the antimicrobial activity of POM-ILs based on the tetraalkylammonium cations N(C$_6$H$_{13}$)$_4^+$ (**Q$^6$**), N(C$_7$H$_{15}$)$_4^+$

(**Q$^7$**) and N(C$_8$H$_{17}$)$_4^+$ (**Q$^8$**) and lacunary Keggin anions ($\alpha$-SiW$_{11}$O$_{39}^{8-}$). Our study showed that 1) all POM-ILs synthesized were active against medically relevant Gram-negative bacteria (*E. coli* and *P. aeruginosa*) and especially against Gram-positive *S. aureus*, and 2) antimicrobial activity can be tuned by modification of the cation alkyl chain length.

POM-IL synthesis was achieved using a cation metathesis reaction from the literature,[12,15] in which an aqueous solution of K$_8$[$\alpha$-SiW$_{11}$O$_{39}$] was extracted with a toluene phase containing the required stoichiometric amount of the respective cation, present as a bromide salt (**Q$^x$-Br**, $x = 6$, 7, 8). Separation, vacuum drying and lyophilization of the toluene phase gave the respective pure POM-IL (**Q$^x$-IL**, $x = 6$, 7, 8) in near-quantitative yield. Characterization by elemental analysis, FTIR and UV/Vis spectroscopy and differential scanning calorimetry confirmed the formation and purity of the respective POM-IL (see the Supporting Information and Table 1).

**Table 1.** POM-IL characterization parameters.

| POM-IL | Melting point [°C] | Yield [%] |
|---|---|---|
| **Q$^6$-IL** | room-temperature IL | 94 |
| **Q$^7$-IL** | 68 | 95 |
| **Q$^8$-IL** | 70 | 94 |

Next, we examined the antimicrobial performance of **Q$^6$-IL**, **Q$^7$-IL** and **Q$^8$-IL** against Gram-negative *E. coli* and *P. aeruginosa* and Gram-positive *S. aureus*. As reference compounds, we chose the three corresponding, water-insoluble ammonium bromide salts **Q$^6$-Br**, **Q$^7$-Br** and **Q$^8$-Br**. In addition, the most common antimicrobial quaternary ammonium salt, benzalkonium chloride (BAC), was used as a positive control.[43]

Antimicrobial activities were examined by incubating the each bacterial strain in an aqueous growth medium (cation-adjusted Mueller–Hinton broth, CA-MHB, $T = 37$ °C) containing the respective antibacterial compound (introduced as a DMSO solution, DMSO concentration in the broth: 1 vol %). Bacterial growth was monitored spectrophotometrically and referenced against control experiments using antibacterial-free growth medium (also containing 1 vol % DMSO). Tests were performed at different antimicrobial agent concentrations following the procedures established in ISO 20776-1:2006.[44] This allowed us to determine the respective EC$_{50}$ (half-maximal effective concentration), MIC (minimal inhibitory concentration) and MBC (minimal biocidal concentration) values (for details see the Experimental Section and the Supporting Information). In our studies, antibacterial activity was observed for all three POM-ILs tested—**Q$^6$IL**, **Q$^7$IL** and **Q$^8$IL**. Notably, the lowest MIC and MBC values were measured for *S. aureus*, a bacterial strain often associated with life-threatening infections at hospitals (Table 2).[45]

Notably, the longer-chain POM-ILs **Q$^7$-IL** and particularly **Q$^8$-IL**, as well as the reference compounds **Q$^7$-Br** and **Q$^8$-Br** showed superior antimicrobial efficacy against the bacterial strains examined compared with **Q$^6$-IL** and **Q$^6$-Br** (Table 2). For

**Table 2.** Minimal inhibitory concentration (MIC) and minimal biocidal concentration (MBC) of POM-ILs and reference compounds tested against *S. aureus* RN4220, *P. aeruginosa* DS10-129 and *E. coli* MG1655.[a]

| Compound | MIC/MBC [mg L$^{-1}$] *S. aureus* | MIC/MBC [mg L$^{-1}$] *P. aeruginosa* | MIC/MBC [mg L$^{-1}$] *E. coli* |
|---|---|---|---|
| **Q$^6$-IL** | 10/10 | > 1000/ > 1000 | 1000/1000 |
| **Q$^6$-Br** | 10/10 | > 1000/1000 | 500/1000 |
| **Q$^7$-IL** | 2/2 | 100/100 | 25/50 |
| **Q$^7$-Br** | 2/2 | 50/100 | 25/25 |
| **Q$^8$-IL** | 5/5 | 100/100 | 100/100 |
| **Q$^8$-Br** | 5/10 | 100/100 | 50/100 |
| **BAC**[b] | 3/6 | 100/100 | 50/50 |

[a] Incubation for 20 h at 37 °C in CA-MHB medium containing 1 vol% DMSO. [b] Benzalkonium chloride.



**Figure 2.** Toxicity (EC$_{50}$ [mg L$^{-1}$], growth inhibition) of POM-ILs **Q$^x$-IL** and the reference compounds **Q$^x$-Br** ($x$ = 6, 7, 8) against *S. aureus*, *E. coli* and *P. aeruginosa*. The EC$_{50}$ values for the POM-IL compounds are given as data labels. * EC$_{50}$ > 200 mg L$^{-1}$.

*P. aeruginosa* and *E. coli*, **Q$^7$-IL** and **Q$^8$-IL** showed MIC values of 25–100 mg L$^{-1}$, whereas for **Q$^6$-IL**, MIC values of 1000 mg L$^{-1}$ were observed. Furthermore, the MIC of BAC against different bacteria was 3–100 mg L$^{-1}$ (Table 2) which is consistent with the literature data.[32, 46]

Remarkably, the Gram-positive bacterium *S. aureus* was especially sensitive to all types of POM-IL tested and MIC values as low as 2–10 mg L$^{-1}$ were observed. Thus, the POM-ILs reported are significantly more potent antimicrobials than the POMs studied so far, for which MIC values for *S. aureus* typically were greater than 400 mg L$^{-1}$ (reported for several polyoxotungstates against various strains of *S. aureus*; Table 3).[39–42] These in-

**Table 3.** Selected literature studies on POM compounds with antimicrobial activity.

| Compound | Bacterial strain | MIC/MBC [mg L$^{-1}$] | Reference |
|---|---|---|---|
| $K_6[P_2W_{18}O_{62}]\cdot14\,H_2O$ | *S. aureus*[a] | 500/15 500 | [42] |
| $K_4[PMo_{12}O_{40}]\cdot3\,H_2O$ | *S. aureus*[a] | 800/6500 | [42] |
| $K_7[PTi_2W_{10}O_{40}]\cdot6\,H_2O$ | *S. aureus*[a] | 38 200/76 500 | [42] |
| $K_9H_5[\alpha\text{-}Ge_2Ti_6W_{18}O_{77}]\cdot16\,H_2O$ | *S. aureus*[b] | 2900/– | [41] |
| $Na_{12}[Fe_3(H_2O)_3(BiW_9O_{33})_2]\cdot34\,H_2O$ | *S. aureus*[c] | 1600/– | [40] |

[a] Methicillin-resistant *S. aureus* (MRSA), strain ATCC43300. [b] Vancomycin-resistant *S. aureus* (VRSA), strain Mu50. [c] *S. aureus* strain ATCC6538P.

itial data suggest that POM-ILs are promising new antimicrobials against *S. aureus* and possibly other Gram-positive bacteria that can rapidly develop resistance to antibiotics, leading to so-called "superbugs" such as methicillin-resistant *S. aureus* (MSRA).[47]

Based on bacterial growth inhibition data taken from the logarithmic growth phase, EC$_{50}$ values were determined for **Q$^6$-IL**, **Q$^7$-IL**, and **Q$^8$-IL**, as well as for the reference compounds **Q$^6$-Br**, **Q$^7$-Br**, and **Q$^8$-Br**. As shown in Figure 2, Tables 2 and 4, the higher antimicrobial activity of the longer-chain alkylammonium cations as well as the high sensitivity of *S. aureus* to POM-ILs is clearly demonstrated.

As the MIC, MBC, and EC$_{50}$ values (based on bacterial growth inhibition) of the POM-ILs and reference compounds were
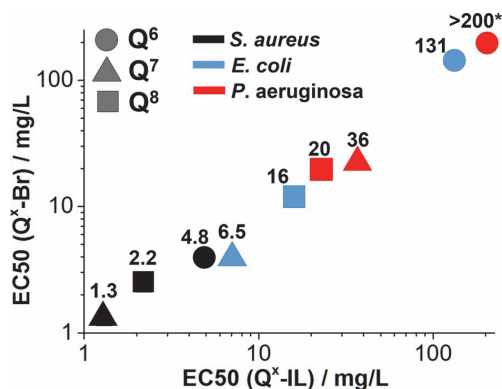
comparable (Tables 2 and 4 and Figure 2), we propose that the antibacterial activity of the compounds is mostly related to the presence of tetraalkylammonium cations. This is further substantiated by a comparison with previous studies on antimicrobial POMs in which significantly lower activity was noted (Table 3), as those POMs contained only inorganic alkali metal cations. Interestingly, however, it has been shown for *S. aureus* that polyoxotungstates can cross the bacterial cell wall and reach the cytoplasmic membrane, so that further development of POM anions for antibacterial activity warrants investigation.[42] Although the antimicrobial activity of POMs is currently not well understood,[21] more progress has been made for tetraalkylammonium salts, the biocidal effect of which has been explained by disruption of the cell membrane due to electrostatic interactions between the alkylammonium cations and the anionic phospholipid headgroups in the cell membrane.[32]

**Table 4.** Toxicity of antimicrobial compounds, EC$_{50}$±SD [mg L$^{-1}$], based on bacterial growth inhibition.[a]

| Compound | EC$_{50}$ [mg L$^{-1}$] *S. aureus* | EC$_{50}$ [mg L$^{-1}$] *P. aeruginosa* | EC$_{50}$ [mg L$^{-1}$] *E. coli* |
|---|---|---|---|
| **Q$^6$-IL** | 4.8 ± 0.69 | > 200 | 131 ± 25 |
| **Q$^6$-Br** | 3.9 ± 0.41 | > 200 | 138 ± 48 |
| **Q$^7$-IL** | 1.3 ± 0.55 | 36.0 ± 11.9 | 6.5 ± 0.08 |
| **Q$^7$-Br** | 1.3 ± 0.26 | 20.0 ± 7.9 | 3.9 ± 0.03 |
| **Q$^8$-IL** | 2.2 ± 0.83 | 20.1 ± 5.7 | 15.8 ± 1.1 |
| **Q$^8$-Br** | 2.4 ± 0.55 | 16.8 ± 6.3 | 11.8 ± 3.3 |
| **BAC**[b] | 1.7 ± 0.32 | 43.6 ± 12.5 | 32.5 ± 6.1 |

[a] Incubation with *S. aureus* RN4220, *P. aeruginosa* DS10-129 or *E. coli* MG1655 for 20 h at 37 °C in CA-MHB medium containing 1 vol% DMSO. [b] Benzalkonium chloride.

## Conclusion

We report the antimicrobial activity of three prototype POM-ILs against clinically important Gram-positive and Gram-nega-

tive bacteria. High activity of the POM-ILs against *E. coli, P. aeruginosa,* and particularly against *S. aureus*, is reported and we showed that variation of the tetraalkylammonium cation chain length can be used to modulate the antimicrobial activity, by which longer chains result in higher activity. Future studies will further investigate the exact interaction between the POM-ILs and the bacterial cell wall using electron microscopy. Furthermore, antibacterial surface coatings and water filters utilizing advanced POM-ILs will be examined based on the results of this study. This may lead to new multifunctional composites to address public health challenges.

## Experimental Section

Antimicrobial activity tests were performed using a standard broth microdilution method described in ISO 20776-1:2006.[44] Antimicrobial activity was analyzed by incubating the bacteria with different concentrations of each compound (introduced as a DMSO solution to give a final DMSO concentration of 1 vol%) in CA-MHB at 37 °C. Bacterial growth was monitored by the increase of the absorbance at 600 nm measured at 30 min intervals. Bacterial growth upon exposure to different concentrations of each compound was compared to bacterial growth in the pure medium with 1% DMSO (nontoxic at that concentration). Based on these data, $EC_{50}$ and MIC values [mg L$^{-1}$] were determined. MCB values were determined after 20 h of incubation by transferring bacterial suspension (3 µL) to CA-MHB agar plates, which were incubated at 30 °C for 24 h. For further details, see the Supporting Information.

## Acknowledgements

## Conflict of interest

The authors declare no conflict of interest.

**Keywords:** antimicrobial agents · ionic liquids · materials chemistry · metal oxides · polyoxometalates

[1] World Health Organization, *Antimicrobial Resistance: 2014 Global Report on Surveillance*, World Health Organization, **2014**.
[2] C. He, D. A. Parrish, J. M. Shreeve, *Chem. Eur. J.* **2014**, *20*, 6699–6706.
[3] M. B. Harney, R. R. Pant, P. A. Fulmer, J. H. Wynne, *ACS Appl. Mater. Interfaces* **2009**, *1*, 39–41.
[4] P. J. Lutz, *Disinfecting Use of Quaternary Ammonium Carbonates*. U.S. Patent No. 6080789., **2000**.
[5] M. Zasloff, *Nature* **2002**, *415*, 389–395.
[6] A. Simon-Deckers, S. Loo, M. Mayne-L'Hermite, N. Menguy, C. Reynaud, B. Gouget, M. Carriere, *Environ. Sci. Technol.* **2009**, *43*, 8423–8429.
[7] P. K. Stoimenov, R. L. Klinger, G. L. Marchin, K. J. Klabunde, *Langmuir* **2002**, *18*, 6679–6686.
[8] S. M. Dizaj, F. Lotfipour, M. Barzegar-Jalali, M. H. Zarrintan, K. Adibkia, *Mater. Sci. Eng. C* **2014**, *44*, 278–284.
[9] J. Xie, S. Lee, X. Chen, *Adv. Drug Delivery Rev.* **2010**, *62*, 1064–1079.

[10] D. Ficai, O. Oprea, A. Ficai, A. M. Holban, *Curr. Proteomics* **2014**, *11*, 139–149.
[11] A. Espinosa, R. Di Corato, J. Kolosnjaj-Tabi, P. Flaud, T. Pellegrino, C. Wilhelm, *ACS Nano* **2016**, *10*, 2436–2446.
[12] S. Herrmann, M. Kostrzewa, A. Wierschem, C. Streb, *Angew. Chem. Int. Ed.* **2014**, *53*, 13596–13599; *Angew. Chem.* **2014**, *126*, 13814–13817.
[13] C. Zollfrank, K. Gutbrod, P. Wechsler, J. P. Guggenbichler, *Mater. Sci. Eng. C* **2012**, *32*, 47–54.
[14] J. Hasan, R. J. Crawford, E. P. Ivanova, *Trends Biotechnol.* **2013**, *31*, 295–304.
[15] S. Herrmann, L. De Matteis, J. M. de la Fuente, S. G. Mitchell, C. Streb, *Angew. Chem. Int. Ed.* **2017**, *56*, 1667–1670; *Angew. Chem.* **2017**, *129*, 1689–1692.
[16] S. Herrmann, C. Ritchie, C. Streb, *Dalton Trans.* **2015**, *44*, 7092–7104.
[17] Y. Ji, L. Huang, J. Hu, C. Streb, Y.-F. Song, *Energy Environ. Sci.* **2015**, *8*, 776–789.
[18] Special issue on polyoxometalates (Eds.: L. Cronin, A. Müller), *Chem. Soc. Rev.* **2012**, *41*, 7325–7648.
[19] B. Hasenknopf, *Front. Biosci.* **2005**, *10*, 275–287.
[20] T. Yamase, *J. Mater. Chem.* **2005**, *15*, 4773–4782.
[21] a) T. Yamase, N. Fukuda, Y. Tajima, *Biol. Pharm. Bull.* **1996**, *19*, 459–465; b) J. Li, Z. Chen, M. Zhou, J. Jing, W. Li, Y. Wang, L. Wu, L. Wang, Y. Wang, M. Lee, *Angew. Chem. Int. Ed.* **2016**, *55*, 2592–2595; *Angew. Chem.* **2016**, *128*, 2638–2641.
[22] D. A. Judd, J. H. Nettles, N. Nevins, J. P. Snyder, D. C. Liotta, J. Tang, J. Ermolieff, R. F. Schinazi, C. L. Hill, *J. Am. Chem. Soc.* **2001**, *123*, 886–97.
[23] L. Fu, H. Gao, M. Yan, S. Li, X. Li, Z. Dai, S. Liu, *Small* **2015**, *11*, 2938–2945.
[24] N. Gao, H. Sun, K. Dong, J. Ren, T. Duan, C. Xu, X. Qu, *Nat. Commun.* **2014**, *5*, 3422.
[25] S. Herrmann, A. Seliverstov, C. Streb, *J. Mol. Eng. Mater.* **2014**, *2*, 1440001–1440008.
[26] S. Herrmann, J. T. Margraf, T. Clark, C. Streb, *Chem. Commun.* **2015**, *51*, 13702–13705.
[27] Y. Leng, J. Wang, D. Zhu, X. Ren, H. Ge, L. Shen, *Angew. Chem. Int. Ed.* **2009**, *48*, 168–171; *Angew. Chem.* **2009**, *121*, 174–177.
[28] W. Huang, W. Zhu, H. Li, H. Shi, G. Zhu, H. Liu, G. Chen, *Ind. Eng. Chem. Res.* **2010**, *49*, 8998–9003.
[29] A. Riisager, R. Fehrmann, S. Flicker, R. van Hal, M. Haumann, P. Wasserscheid, *Angew. Chem. Int. Ed.* **2005**, *44*, 815–819; *Angew. Chem.* **2005**, *117*, 826–830.
[30] A. Riisager, R. Fehrmann, M. Haumann, P. Wasserscheid, *Eur. J. Inorg. Chem.* **2006**, 695–706.
[31] *Supported Ionic Liquids* (Eds.: R. Fehrmann, A. Riisager, M. Haumann), Wiley-VCH Verlag, Weinheim, **2014**.
[32] S. Buffet-Bataillon, P. Tattevin, M. Bonnaure-Mallet, A. Jolivet-Gougeon, *Int. J. Antimicrob. Agents* **2012**, *39*, 381–389.
[33] T. J. R. Weakley, S. A. Malik, *J. Inorg. Nucl. Chem.* **1967**, *29*, 2935–2944.
[34] A. L. Lim, R. Bai, *J. Membr. Sci.* **2003**, *216*, 279–290.
[35] A. I. Hidron, J. R. Edwards, J. Patel, T. C. Horan, D. M. Sievert, D. A. Pollock, S. K. Fridkin, *Infect. Control Hosp. Epidemiol.* **2008**, *29*, 996–1011.
[36] K. M. Docherty, C. F. Kulpa, Jr., *Green Chem.* **2005**, *7*, 185–189.
[37] H. W. Boucher, G. H. Talbot, J. S. Bradley, J. E. Edwards, D. Gilbert, L. B. Rice, M. Scheld, B. Spellberg, J. Bartlett, *Clin. Infect. Dis.* **2009**, *48*, 1–12.
[38] R. M. Klevens, J. R. Edwards, C. L. Richards, T. C. Horan, R. P. Gaynes, D. A. Pollock, D. M. Cardo, *Public Health Rep.* **2007**, *122*, 160–166.
[39] L. Grama, A. Man, D.-L. Muntean, G. Florea, Ş. Andrei, F. Boda, A. Curticăpean, *Rev. Romana Med. Lab.* **2014**, *22*, 111–118.
[40] S. Balici, M. Niculae, E. Pall, M. Rusu, D. Rusu, H. Matei, *Rev. Chim.* **2016**, *67*, 485–490.
[41] M. Inoue, T. Suzuki, Y. Fujita, M. Oda, N. Matsumoto, T. Iijima, T. Yamase, *Biomed. Pharmacother.* **2006**, *60*, 220–226.
[42] M. Inoue, T. Suzuki, Y. Fujita, M. Oda, N. Matsumoto, T. Yamase, *J. Inorg. Biochem.* **2006**, *100*, 1225–1233.
[43] G. McDonnell, A. D. Russell, *Clin. Microbiol. Rev.* **1999**, *12*, 147–179.
[44] ISO 20776-1:2006 Clinical laboratory testing and in vitro diagnostic test systems—Susceptibility testing of infectious agents and evaluation of performance of antimicrobial susceptibility test devices—Part 1: reference method for testing the in vitro activity of antimicrobial agents against rapidly growing aerobic bacteria involved in infectious diseases, **2006**.

[45] S. R. Harris, E. J. Feil, M. T. G. Holden, M. A. Quail, E. K. Nickerson, N. Chantratita, S. Gardete, A. Tavares, N. Day, J. A. Lindsay, J. D. Edgeworth, H. de Lencastre, J. Parkhill, S. J. Peacock, S. D. Bentley, *Science* **2010**, *327*, 469–474.

[46] L. Furi, M. L. Ciusa, D. Knight, V. Di Lorenzo, N. Tocci, D. Cirasola, L. Aragones, J. R. Coelho, A. T. Freitas, E. Marchi, *Antimicrob. Agents Chemother.* **2013**, *57*, 3488–3497.

[47] M. C. Enright, D. A. Robinson, G. Randle, E. J. Feil, H. Grundmann, B. G. Spratt, *Proc. Natl. Acad. Sci. USA* **2002**, *99*, 7687–7692.

# CHEMPLUSCHEM

# Supporting Information

# Antimicrobial Activity of Polyoxometalate Ionic Liquids against Clinically Relevant Pathogens

Anna-Liisa Kubo+,[a] Lea Kremer+,[b] Sven Herrmann,[b] Scott G. Mitchell,[c] Olesja M. Bondarenko,[a] Anne Kahru,*[a, d] and Carsten Streb*[b]

**Table of Contents**

# 1. Instrumentation

**Elemental analysis**: Elemental analysis was performed on a Euro Vector Euro EA 3000 Elemental Analyzer.

**FT-IR spectroscopy:** FT-IR spectroscopy was performed on a Bruker FT-IR Spectrometer IFS113v. Samples were prepared as KBr pellets. Signals are given as wavenumbers in $cm^{-1}$ using the following abbreviations: vs = very strong, s = strong, m = medium, w = weak and b = broad.

**UV-Vis spectroscopy:** UV-Vis spectroscopy was performed on a Shimadzu UV-2401PC spectrophotometer, Varian Cary 50 spectrophotometer. All measurements were carried out using standard cuvettes ($V$ = 3 ml, $d$ = 10.0 mm).

**Inductively Coupled Plasma Atomic Emission Spectroscopy (ICP-AES)**: ICP-AES was performed on a Horiba Jobin Yvon Ultima2 referenced against calibrating standards of the respective elements.

**^{1}H-NMR-spectroscopy** was performed on a Bruker AVANCE 400 MHz instrument using deuterated solvents and using residual solvent signals for calibration. Signals are given in $\delta$ (ppm).

**General remarks:** All reagents and chemicals were supplied by SIGMA ALDRICH, FISHER CHEMICALS, ABCR CHEMICALS and ACROS ORGANICS. The materials were used without further purification. $K_8[\alpha\text{-}SiW_{11}O_{39}]\cdot 13H_2O$ was synthesized as described in [1].Unless described otherwise the reactions were conducted under ambient atmosphere.

## 2. Synthesis and characterization

### 2.1 Synthesis of $Q^6_8[\alpha\text{-SiW}_{11}O_{39}]$

The synthesis is a modified version of the synthesis described in reference [1]. $K_8[\alpha\text{-SiW}_{11}O_{39}]$ x 13 $H_2O$ (5.03 g, 1.56 mmol) was dissolved in water (100 ml) and heated to 50 °C. Tetrahexylammonium bromide (8 eq.; 5.42 g, 12.48 mmol) was dissolved in toluene (100 ml) and added to the first solution. The biphasic reaction mixture was stirred vigorously for 5 min at 50 °C. The organic phase was separated and the aqueous phase was extracted twice with toluene. The combined organic phases were evaporated and the resulting POM-IL was solvent stripped once with 100 mL toluene (100 ml) and twice with chloroform (100 ml). The pure POM-IL was dried under vacuum for several days.

**Yield:** 8.07 g (1.46 mmol, 93.9% based on $K_8[\alpha\text{-SiW}_{11}O_{39}]$ x 13 $H_2O$).

**$^1$H-NMR** (CDCl$_3$, 400.16 MHz): $\delta$ [ppm] = 3.62 − 3.22 (2 H$_1$, m), 1.59 − 1.52 (2 H$_2$, m), 1.31 − 1.28 (2 H$_3$, m), 1.19 − 1.10 (4 H$_{4/5}$, m), 0.71 (3 H$_6$, t, $^3J_{HH}$ = 6.9 Hz).

**IR** (KBr pellet): $\nu$ [cm$^{-1}$] = 2957 (s), 2930 (s), 2862 (m), 2361 (w), 2339 (w), 1483 (m), 1467 (m), 1380 (w), 1146 (w), 1051 (w), 997 (m), 953 (m), 899 (s), 807 (s), 784 (s), 747 (s), 531 (w).

**Elemental analysis** in wt.-% (calcd values in brackets): C: 41.69 (41.84), H: 7.67 (7.61), N: 2.04 (2.03), W: 37.02 (36.69), Si: 0.58 (0.50).

### 2.2 Synthesis of $Q^7_8[\alpha\text{-SiW}_{11}O_{39}]$

$K_8[\alpha\text{-SiW}_{11}O_{39}]$ x 13 $H_2O$ (7.55 g, 2.37 mmol) was dissolved in water (150 ml) and heated to 50 °C. Tetraheptylammonium bromide (8 eq.; 9.28 g, 18.91 mmol) was dissolved in toluene (240 ml) and added to the first solution. The biphasic reaction mixture was stirred vigorously for 25 min at 50 °C. The organic phase was separated and the aqueous phase was extracted with toluene (100 ml). The combined organic phases were evaporated and the resulting POM-IL was solvent stripped with toluene (100 ml) and twice with chloroform (100 ml). The resulting POM-IL was dried under vacuum for several days.

**Yield:** 13.43 g (2.25 mmol, 95.1% based on $K_8[\alpha\text{-SiW}_{11}O_{39}]$ x 13 $H_2O$).

**$^1$H-NMR** (CDCl$_3$, 400.16 MHz): $\delta$ [ppm] = 3.38 − 3.34 (2 H$_1$, m), 1.73 − 1.65 (2 H$_2$, m), 1.45 − 1.26 (8 H$_{3-6}$, m), 0.87 (3 H$_7$, t, $^3J_{HH}$ = 6.8 Hz).

**IR** (KBr pellet): $\nu$ [cm$^{-1}$] = 3448 (br, w), 2957 (s), 2926 (s), 2855 (s), 1628 (w), 1465 (s), 1379 (m), 1067 (w), 997 (m), 954 (s), 899 (s), 782 (s), 740 s), 532 (m).

**Elemental analysis** in wt.-% (calcd values in brackets): C: 45.31 (45.14), H: 8.71 (8.12), N: 2.00 (1.88), W: 34.25 (33.93), Si: 0.55 (0.47)

**2.3 Synthesis of $Q^8_8[\alpha\text{-}SiW_{11}O_{39}]$**

$K_8[\alpha\text{-}SiW_{11}O_{39}]$ x 13 $H_2O$ (7.51 g, 2.36 mmol) was dissolved in water (150 ml) and heated to 50 °C. Tetraoctylammonium bromide (8 eq.; 10.32 g, 18.87 mmol) was dissolved in toluene (240 ml) and added to the first solution. The biphasic reaction mixture was stirred vigorously for 25 min at 50 °C. The organic phase was separated and the aqueous phase was extracted twice with toluene (150 ml). The combined organic phases were evaporated and the resulting POM-IL was solvent stripped with toluene (100 ml) and twice with chloroform (100 ml). The resulting POM-IL was dried under vacuum for several days.

**Yield:** 14.23 g (2.22 mmol, 94.1 % based on $K_8[\alpha\text{-}SiW_{11}O_{39}]$ x 13 $H_2O$).

**$^1$H-NMR** (CDCl$_3$, 400.16 MHz): $\delta$ [ppm] = 3.39 − 3.35 (2 $H_1$, m), 1.73 − 1.65 (2 $H_2$, m), 1.47 − 1.25 (10 $H_{3-7}$, m), 0.86 (3 $H_8$, t, $^3J_{HH}$ = 7.2 Hz).

**IR** (KBr pellet): $\nu$ [cm$^{-1}$] = 2956 (s), 2924 (vs), 2853 (s), 2362 (w), 1627 (w), 1464 (m), 1379 (w), 997 (m), 954 (m), 900 (s), 807 (s), 532 (m).

**Elemental analysis** in wt.-% (calcd values in brackets): C: 48.09 (47.97), H: 8.76 (8.55), N: 1.89 (1.75), W: 32.01 (31.55), Si: 0.48 (0.44)

## 3. Bacterial growth analysis upon exposure to antimicrobials

**General remarks:** the bacterial growth analysis (broth microdilution method) was adapted from the reference method ISO 20776-1 for antimicrobial susceptibility testing.[2] The test was conducted with bacteria *Escherichia coli* MG1655, *Pseudomonas aeruginosa* DS10–129 and *Staphylococcus aureus* RN4220. The cation-adjusted Mueller-Hinton Broth (CA-MHB, Oxoid Microbiology Products) containing per 1 litre: dehydrated infusion from beef 300 g, casein hydrolysate 17.5 g, starch 1.5 g, $Ca^{2+}$ 25 mg and $Mg^{2+}$ 12.5 mg. The bacteria were first cultivated overnight in 3 ml of CA-MHB medium at 30°C with shaking at 200 rpm, and then diluted with fresh medium to a bacterial density of ~5x10$^5$ CFU/mL in the test (verified by viable plate counts on agarised medium).

**Sample preparation:** the respective antimicrobial compound (**Q$^x$-IL**, **Q$^x$-Br** and **BAC**, benzalkonium chloride) were prepared by dissolving the respective compound in DMSO ([compound] = 100 g/L) and diluting into CA MHB to give the desired final concentration. This was followed by incubation at 37 °C overnight on a shaker at 200 rpm. All test samples and controls were adjusted to contain a final concentration of 1 vol-% DMSO to ensure comparability. Control experiments showed that this concentration of DMSO does not affect the bacterial growth. The pH of the dilutions in CA-MHB was neutral. The incubation mixtures were prepared by combining the bacteria suspension (50 µL) and test compound solution (50 µL) in 96 well transparent microtiter plates (BD Falcon) at 37° C for 20 hours in the dark in aerobic conditions with minor shaking every 15 min. Wells containing 50 µL of control broth and 50 µL of bacterial culture in CA-MHB were included for each tested strain and served as non-treated controls.

**Bacterial growth control:** bacterial growth was followed by measuring optical density ($OD_{600}$ nm) with a Spectramax Paradigm spectrophotometer (Molecular Devices, USA).  Three different parameters were determined from the experiments for all  compounds tested and all bacterial strains examined (EC50, MIC and MBC, mg/L). EC50 values for the tested compounds were calculated from the dose-effect curves of bacterial log-phase growth (between 3h and 10h of incubation, depending on the bacterial strain (Fig. S1), i.e. inhibition of the growth rates of chemical-exposed bacteria *versus* bacterial growth in the control broth. The EC50 values (concentration of the chemical that reduced bacterial growth by 50%)  were calculated using MS Excel macro Regtox (http://www.normalesup.org/~vindimian/en_download.html).

The minimal inhibitory concentration (MIC) was determined as the lowest analysed concentration where no visible growth of bacteria was observed. For the evaluation of the MBC value, after 20 h incubation of bacteria with test chemicals, 3 µL of sample from each test or control well was pipetted onto the toxicant-free Mueller-Hinton (Oxoid CM0337; 25 mg/L Ca and 12,5 mg/L Mg added) agar plates. The inoculated agar plates were incubated at 30 ᵒC for 24 h. The concentration of chemical in the incubation medium that yielded no visible growth/colonies of the exposed organism after sub-culturing on toxicant-free agar medium was defined as minimum biocidal concentration (MBC). Each concentration of the tested chemicals and control culture was analysed in duplicate and at least three replications of the tests for each bacterial strain were performed.
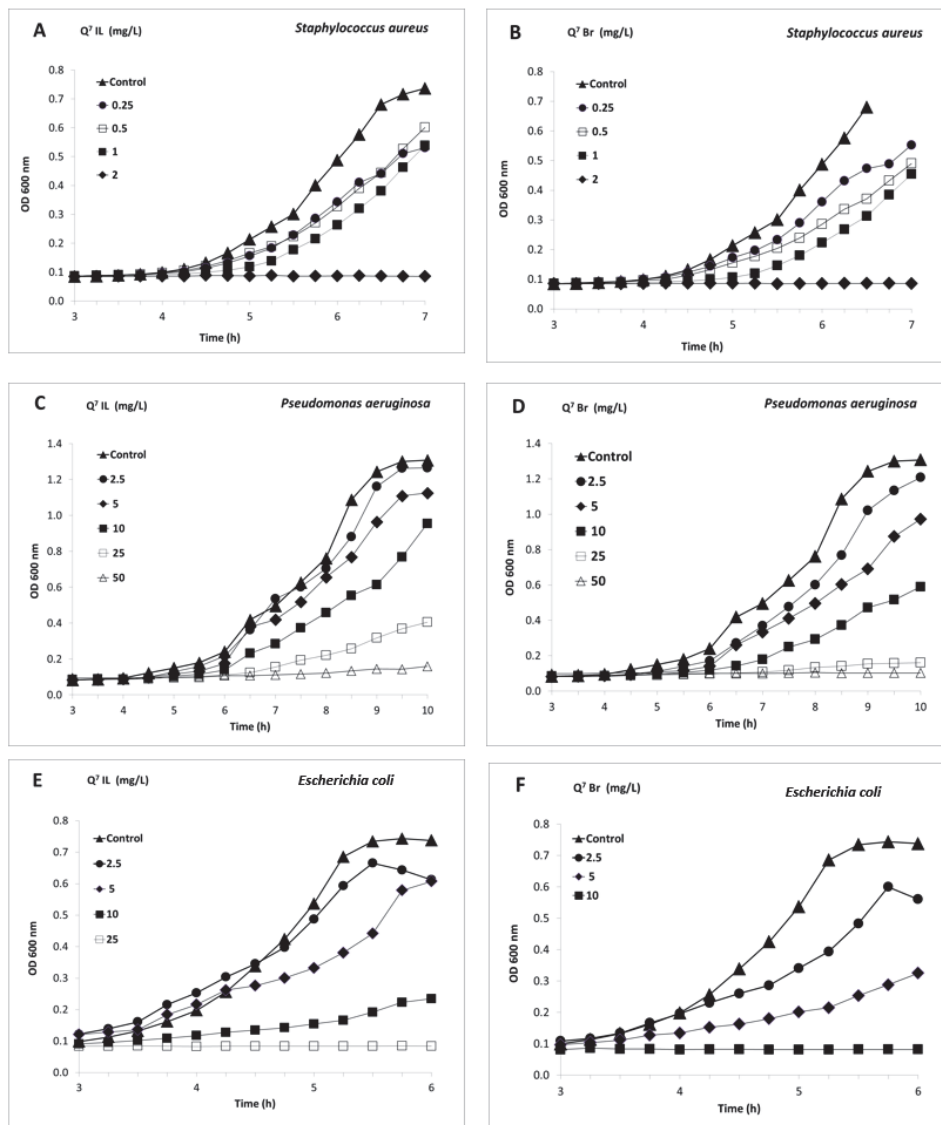
**Figure S1.** Inhibition of growth of *Staphylococcus aureus* (A, B), *Pseudomonas aeruginosa (C, D) and Escherichia coli* (E, F) by $Q^7IL$ (left panels) and $Q^7Br$ (right panels): dose-response curves. Concentration range used is indicated in the respective panel.

## 4. References

[1]    S. Herrmann, L. De Matteis, J. M. de la Fuente, S. G. Mitchell, C. Streb, *Angew. Chem. Int. Ed.* **2017**, *56*, 1667–1670.

[2]    *ISO 20776-1:2006 Clinical Laboratory Testing and in Vitro Diagnostic Test Systems -- Susceptibility Testing of Infectious Agents and Evaluation of Performance of Antimicrobial Susceptibility Test Devices - Part 1,* **2006**.

**Manuscript**
**Kubo, A. L.**, Vassiljev, G., Vija, H., Kristall, J., Tõugu, V., Kahru, A., Bondarenko, O. M. Towards (immuno)safety of antibacterial nanomaterials: surface functionalization of CuO with carboxyl- or polyethylene decreases their cytotoxicity to human cells in vitro (manuscript in preparation).

**Towards (immuno)safety of antibacterial nanomaterials: surface functionalization of CuO with carboxyl- or polyethylene decreases their cytotoxicity to human cells *in vitro***

A-L. Kubo[1], G. Vasiljev[1,2], H. Vija[1], J. Kristall[3], V. Tõugu[3], A. Kahru[1,4], O. M. Bondarenko[1*]

[1] *Laboratory of Environmental Toxicology, National Institute of Chemical Physics and Biophysics, Tallinn, Estonia.*
[2] *Department of Natural Sciences, TalTech, Tallinn, Estonia.*
[3] *Department of Chemistry and Biotechnology, School of Science, TalTech, Tallinn, Estonia.*
[4] *Estonian Academy of Sciences, Kohtu 6, Tallinn, Estonia.*

*Corresponding author

Contact: Tel./Fax: +372 6398382,  E-mail: olesja.bondarenko@kbfi.ee

## ABSTRACT

Clinical use of CuO nanoparticles (NPs) as antibacterials can be hampered by their toxicity to human cells, whereas NP surface functionalization may reduce unspecific cytotoxicity, while retaining antibacterial properties.

This study is the first report on the toxicity and mechanisms of differently functionalized CuO NPs (primary size 7.3-18.1 nm) to bacteria *vs* human cells *in vitro*. Toxicity of unfunctionalized CuO or CuO functionalized with amino groups (CuO-NH2), carboxyl groups (CuO-COOH) or polyethylene glycol (CuO-PEG) was tested to bacteria *Escherichia coli* and to mammalian cell lines (THP-1-derived macrophages and HACAT keratinocytes *in vitro*) in similar conditions.

CuO-COOH and CuO-PEG were more toxic to bacteria compared to mammalian cells, showing the best therapeutic window for potential use in humans. Chemical analysis of intracellular Cu and confocal microscopy revealed that at equitoxic concentrations, mammalian cells internalized 2-7 times more CuO-COOH NPs compared to the other CuO NPs, indicating COOH-specific uptake mechanisms that neutralized the toxicity. In contrast, CuO-NH2 NPs were the most toxic to mammalian cells followed by CuO, CuO-COOH and CuO-PEG NPs. The multivariate analysis revealed that small hydrodynamic size, high Cu dissolution, positive zeta-potential and induction of reactive oxygen species and TNF-α were contributing most to toxicity of both, CuO-NH2 and unfunctionalized CuO NPs.

## INTRODUCTION

Increasing resistance of bacteria to conventional antibiotics necessitates the development of alternative antimicrobials such as silver and copper-based antimicrobials, including in nano-formulations.  In fact, copper is known since long time as a metal with antibacterial effect that

1

can be used to inhibit bacterial spreads by employing Cu on copper surfaces[1], in aqueous suspension[2] and in textiles[3]. For living organisms, including human cells, copper is an essential microelement present in all tissues and is necessary for e.g. functioning of the innate and adaptive immune system[4,5] and is the necessary component of the key enzymes[6]. Previous studies have shown that CuO NPs supported the wound healing[7] and bone regeneration[8]. For instance, mesoporous silica NPs containing 2.5 to 5% Cu were suggested for the use in bone regeneration, since they up-regulated the genes contributing to osteogenic and angiogenic factors and were not toxic in the range of 10–500 mg/l (i.e., 0.5–25 mg Cu/l) to murine macrophages RAW 264.7, whereas Cu significantly contributed to the beneficial properties of these NPs[8].

Given the mentioned properties, CuO NPs are ideal candidates for the use in medicine as wound dressings and/or internal implants by combining two functions: antimicrobial activity and increased wound healing or osteogenesis. However, the excessive copper is toxic to the human cells and plays a role in the pathogenesis of several neurological diseases such as e.g. Alzheimer disease[9], Parkinson disease[10], amyotrophic lateral sclerosis, and Wilson disease[11]. Chronic copper overdose can cause hemolytic anemia, liver and renal damage[12]. Thus, the balance between the beneficial and adverse concentrations of copper and especially CuO NPs in human body should be respected.

In case of biomedical use as antibacterials, CuO NPs may induce cytotoxicity, since they will contact closely with the human cells such as skin keratinocytes (in case of wound dressings) and immune cells (in case of implants) residing in the blood and tissues and aiming to protect the body from foreign microorganisms and particles (including NPs). Previous studies have shown that pristine (unfunctionalized) CuO NPs were toxic to murine macrophage cell line RAW264.7[13] and other human cell models *in vitro* such as epidermal keratinocytes NHEK[14], lung adenocarcinoma cells A549[15], hepatoma cell line HepG2[16], epithelial colon carcinoma cells Caco-2[17] and differentiated Caco-2 *(in vitro* model for the cells of small intestine)[18] with the range of EC50 values of 13 – 100 mg/l[19]. Warningly, the antibacterial concentrations of CuO NPs are in the range of 20 – 280 mg/l, implying that the therapeutic value of the existing (mostly unfunctionalized) CuO NPs as antibacterials is rather limited, since the CuO NPs effective in killing bacteria were also toxic to the human cells *in vitro*[19,20].

Functionalization of synthetic NPs with various surface groups enables to modulate the interaction of NPs with cells, and thus, change the safety profiles of NPs[21,22]. In most of the cases, NPs introduced into the body are first encountered by the cells of mononuclear phagocyte system such as macrophages. The uptake of NPs by macrophages occures *via* different routes including phagocytosis for bigger (>250 nm) NPs and receptor-mediated endocytosis for smaller (~60-120 nm) NPs[23,24], and is mostly dependent on the opsonization of NPs (i.e., adsorption of bio-corona of proteins and other biomolecules onto their surface)[21,25–27]. To minimize opsonization and to reduce the uptake of NPs by macrophages, NPs can be functionalized with different polymers such as polyethylene glycol (PEG), chitosan or dextran[28–30]. The introduction of functional groups enables to modify the surface charge of NPs that changes the uptake of NPs by cells and the toxicity of NPs. In general, NPs functionalized with positively charged groups such as cationic polyethylenimine (PEI), branched PEI or amino group (NH2) proved more toxic to mammalian cell lines including murine macrophage cell line RAW264.7[13], epithelial cells BEAS-2B and human monocytes THP-1[31].

2

Given the surface functionalization of metal-based NPs may help to overcome their unspecific cytotoxicity and improve their therapeutic potential as antimicrobials, it is crucial to compare the impact of different surface functionalization on the antibacterial activity of NPs *vs* safety to the human cells. Indeed, the use of CuO NPs in the wound dressings and implants implies the determination of a therapeutic window: a concentration range of CuO NPs effective as antibacterials but safe to the human cells. While there are many articles on biological effects of unfunctionalized CuO, the information on differently functionalized CuO NPs is extremely limited[19,32]. Although there are various protocols available for the synthesis of CuO NPs functionalized with e.g., peptides, antibodies and oligonucleotides[33], these NPs were mostly intended for bioanalytical applications and were not tested for the biological effects. Our search in pubmed (performed in December 2018) using the keywords „copper nano* tox*" identified totally 164 research articles, and only five of these articles addressed the biological effects of differently functionalized CuO NPs with the focus on the „green" coatings such as chitosan[34], plant latex[35], albumin[36] and a set of coatings including citrate, sodium ascorbate, polyvinylpyrrolidone and polyethylenimine[13]. None of the studies compared the antibacterial properties of NPs with their safety to human cells *in vitro* or *in vivo*.

This study is the first report on the antimicrobial toxicity *vs* safety towards human cells of CuO NPs with different surface functionalizations: unfunctionalized CuO, CuO-$NH_2$, CuO-COOH, CuO-PEG NPs and $CuSO_4$ as an ionic control. THP-1-derived macrophages were used as a model for immunotoxicity, HACAT keratinocytes *in vitro* as the model for human skin cells and *Escherichia coli* as model bacteria. Toxicity of Cu compounds to these three cell types was tested in the same conditions using RPMI medium supplemented with 10% FBS and Alamar blue cell viability assay as the toxicity endpoint. In addition, we compared the potential mechanisms of toxicity of studied Cu compounds to different types of cells with the focus on reactive oxygen species (ROS), dissolution, cellular internalization of CuO and their ability to induce cellular inflammation.

**Materials and Methods**

**Chemicals**
All the purchased chemicals were at least of analytical grade. Dulbecco`s phosphate buffered saline (DPBS, Biognost), Alamar blue (AppliChem), lipopolysaccharide (LPS, Invivogen), $CuSO_4$ (Alfa Aesar), 2',7'-dichlorodihydrofluorescein diacetate (H2DCF-DA, Life Technologies), phosphate buffered saline (PBS pH=7.2, Biognost), tryptone (LabM), yeast extract (LabM), agar (LabM) and NaCl (Sigma-Aldrich) were used.

**Nanoparticles**
Four types of differently functionalized CuO NPs were obtained *via* the consortium of EU FP7 project NANOSOLUTIONS (https://nanosolutionsfp7.com/) as a kind gift from Prof. Bengt Fadeel (Karolinska Institutet, Sweden). CuO NPs were provided as dry powders, and the suspensions were prepared each time freshly before the tests at concentrations 1000-2000 mg compound/l in endotoxin free bi-distilled water (DI water). Ten milliliters of CuO NP suspensions were vortexed and sonicated using probe sonication (Branson 450 Sonifier, USA) for 5 min with acoustic power of 13 W corresponding to the specific energy of $3.9 \cdot 10^5$ kJ/m³ (Käkinen *et al* [17]).

Hydrodynamic size (Dh), polydispersity index (pdi) and zeta potential (Z-potential) were measured in 100 mg/l suspensions in DI water or cell culture medium using Malvern zetasizer (Zetasizer Nano-ZS, Malvern Instruments, UK).

Endotoxin content in CuO dispersions was assessed using the chromogenic limulus amoebocyte lysate (LAL) assay (Charles River Endosafe, Charleston, SC) according to the manufacturer's instructions and was found to be below the detection limit.

Cu content was determined using total reflection X-ray fluorescence (TXRF, Picofox S2, Bruker Corporation) from 100 mg/l suspensions.

For dissolution analysis, 100 mg/l CuO NPs or $CuSO_4$ in cell culture medium were centrifuged at 320 000 x g for 30 min ( Bekman Coulter ultracentrifuge) immediately (0-h dissolution) or after 24 h of incubation at 37 °C with 5% $CO_2$ and 95% humidity. After centrifugation, supernatants were collected and analysed by TXRF.


**Human cells**

Cell lines were obtained from American Type Culture Collection (ATCC) and cultured according to ATCC guidance. The cells were subcultured up to 20 passages, and the toxicity tests were performed after at least 2 passages.

The human monocytic leukemia cell line THP-1 (ATCC TIB-202) was grown in Roswell Park Memorial Institute medium with L-glutamine (RPMI-1640, Corning) supplemented with 10% fetal bovine serum (FBS, Corning), 100 mM sodium pyruvate solution (Na-Pyr, Gibco) and 1% solution containing 10000 U/ml Penicillin and 10000 µg/ml Streptomycin (PEST, Gibco) that is further referred as the complete cell culture medium (CCM). THP-1 cells (growing in suspension) were subcultured by adding fresh CCM. Before the assays, THP-1 cells were differentiated into macrophage like cells by culturing them with 100 ng/ml phorbol myristate acetate (PMA, Invivogen) in CCM for 3 days. For that, THP-1 cells were seeded into 96-well plates (Corning Falcon) at density of $10^5$ cells per well and incubated with 100 ng/ml phorbol myristate acetate (PMA) for 3 days at 37 °C and 5% $CO_2$.

The human HACAT cell line, immortalized keratinocytes (ATCC PCS-200-011), were grown in Dulbecco`s modified Eagle`s medium with 4.5 g/l glycose, L-glutamine and sodium pyruvate (DMEM, Corning) supplemented with 10% FBS and 1% PEST. Before the tests, cells were seeded into 96-well plates at density of $10^4$ cells per well and uncubated for 1 day at 37°C, 5% $CO_2$ and 95% humidity.


**Bacterial cells**

*Escherichia coli* MG1655 (obtained from the *E. coli* genetic stock centre, Yale University) and recombinant bioluminescent *E. coli* MC1061 (pSLcueR/pDNPcopAlux) were stored on agarized Luria-Bertani medium (LB, 1% tryptone, 0.5% yeast extract, 0.5% NaCl, 1.5% agar) and before the toxicity tests cultivated in 3 ml of LB medium at 30°C with shaking at 200 rpm overnight. In case of recombinant bacteria, LB was supplemented with 100 µg/l ampicillin and 10 µg/l tetracycline to retain the bioluminescence-encoding plasmid.

**Toxicity assays**

Toxicity of Cu compounds to bacterial and human cells was performed in similar conditions (24-h incubation at 37°C, Alamar Blue assay as the endpoint and CCM as the exposure medium for THP-1 and *E. coli* cells) with the minor differences: 1) PEST was removed from *E. coli* exposure medium; 2) human cells were incubated in humidified conditions (with 5% $CO_2$). Details on the test conditions are summarized in Table S1.

For the toxicity assay with bacteria, *E. coli* cells were grown in LB medium overnight followed by removal of LB by centrifugation, and resuspension of bacterial cells in CCM without PEST to ~$5x10^5$ colony forming units (CFU/ml). 100 µl of bacterial suspension was exposed to 100 µl of either cell culture medium (control) or 6.25 to 400 mg/l CuO suspensions/$CuSO_4$ in CCM in transparent 96-well plates for 24 h at 37°C. Bacterial viability was estimated using Alamar Blue assay. For that cells exposed to 6.25 to 400 mg/l CuO NPs or $CuSO_4$ were washed, and Alamar Blue (final concentration of 150 ug/mL) in CCM without PEST was added to the cells for 2 h at 37°C. After incubation, fluorescence was read by Fluoroscan (Fluoroskan Ascent FL, Thermo Labsystems) with excitation at 530 nm and emission at 590 nm. The metabolic activity (viability) of exposed cells was expressed in % by comparing their fluorescence with that of the untreated cells. The $EC_{50}$ values were values calculated as described in the statistical analysis section. Tests were performed in five biological experiments in duplicates. To access possible interference of NPs, NPs were incubated abiotically with the Alamar Blue and showed no unspecific reactions.

For the toxicity assay with human cells, cell culture medium was removed, cells were washed with PBS and exposed to 100 µl of either cell culture medium or 6.25 to 400 mg/l CuO suspensions/$CuSO_4$ in cell culture medium for 24 h at 37°C and 5% $CO_2$. After exposure, the supernatant was removed, cells were washed once with PBS and incubated with 100 µl solution of 150 µg/ml Alamar Blue (Applichem) for 2 h at 37°C and with 5% $CO_2$. Alamar Blue Biosensor assay was performed as described above for bacterial cells.

**Bioavailability of Cu to bacteria**

Quantification of intracellular Cu ions was performed using recombinant biosensor bacteria *E. coli* MC1061 (pSLcueR/pDNPcopAlux) in which Cu ion-inducible promoter *copA* is genetically coupled to the bioluminescence-encoding genes *luxCDABE* [21]. Thus, bioluminescence of this recombinant *E. coli* increases in response to sub-toxic concentrations of intracellular Cu ions in a dose-dependent manner. In the toxic concentration range, the bioluminescence of bacteria gradually decreases.

Overnight bacterial cell culture was diluted 1:20 into fresh LB medium supplemented with 100 µg/l ampicillin and 10 µg/l tetracycline, grown till OD=0.5-0.8 and diluted in CCM without PEST to OD=0.1 corresponding to final concentration of $10^6$ CFU/ml. 100 µl of the appropriate dilution (3.1 to 100 mg/l) of Cu compounds in CCM without PEST were pipetted into each well of the white 96-well microplates and 100 µl of bacterial culture in CCM without PEST was added. The test plates were incubated at 37 °C for 2 h, and bioluminescence was measured using Orion II plate luminometer (Berthold Detection Systems). Fold increase in bioluminescence in response to Cu compounds was calculated as a function of increased bioluminescence of biosensor in the sample (CuO and $CuSO_4$ dilutions in CCM without PEST) compared to the background (CCM without PEST).

**Measurement of reactive oxygen species**

The ability of CuO NPs and $CuSO_4$ to generate ROS was measured in abiotic conditions in DI water with $H_2DCFA$-DA as described by Aruoja et al[37]. 100 µl of 6.25 to 200 mg/l CuO NPs and $CuSO_4$ and 100 µl of $H_2DCF$ were incubated at room temperature for 60 minutes. Fluorescence (excitation at 485 nm and emission at 527 nm) was quantified using a microplate fluorometer (Fluoroskan Ascent FL, Thermo Labsystems, Finland). The ability of Cu compounds to induce ROS was expressed in % in relation to the control.

**Chemical analysis of cell-associated Cu**

THP-1 monocytes were seeded to 96 well plates (Corning Falcon) at density 100 000 cells/well and differentiated with 100 ng/mL PMA for 72 h. Cells were exposed to Cu compounds in CCM at $EC_{20}$ concentrations for 24 h (27.3 mg/l for CuO NPs, 22.2 mg/l for $CuO-NH_2$, 90.6 mg/l for CuO-COOH, 211.4 mg/l for CuO-PEG and 85.4 mg/l for $CuSO_4$).

HACAT cells were seeded to 96 well plates at density 10 000 cells/well and allowed to attach for 24 h. Cells were exposed to Cu compounds at $EC_{20}$ concentrations (11.6 mg/l for CuO NPs, 14.9 mg/l for $CuO-NH_2$, 73.7 mg/l for CuO-COOH, 142.0 mg/l for CuO-PEG and 57.6 mg/l for $CuSO_4$) for 24 h.

After 24 h exposure, cells were washed, detached and washed again twice with PBS by centrifugation at 150 x g for 5 min. 10 µl cell suspension was mixed with 10 µl trypan blue and the cell number and cell viability was determined. Supernatant was aspirated and the pellet was lyophilized. The Cu content was quantified with TXRF, normalised on total cell number basis and designated as „cell-associated Cu" referring to the sum of the following fractions: intracellular Cu and extracellular Cu bound to the cell surface.

**Measurement of TNF-α**

Differentiated THP-1 cells at density 100 000 cells/well were exposed to CuO NPs and $CuSO_4$ at concentrations from 25 to 400 mg/l in CCM. After 24-h exposure supernatants were collected, centrifuged for 10 min at 10 000 x g and stored frozen at -80°C. TNF-α was measured on 96-well plates using Enzyme-Linked Immunosorbent Assay (ELISA) kit (Invitrogen 88-7346) according to manufacturer's instructions.

**Microscopy**

For the automatic photographing, THP-1 cells were differentiated in 24-well plates, exposed to NPs (24-h $EC_{20}$ concentrations), washed, stained with Giemsa Stain (Sigma-Aldrich) according to manufacturer's instructions and visualized using Automated Digital Morphology System CellaVision®. Before the analysis differentiated THP-1 were mixed with red blood cells to improve the cell recognition by the automatic software.

For confocal microscopy, THP-1 cells were differentiated on glass coverslips in 12-well plates, stained with Cell Mask Orange (Invitrogen) cell membrane (CMO) according to manufacturer protocol, fixed with 4 % paraformaldehyde (Sigma) and stained with 1:300 diluted DAPI (Sigma). Finally, the coverslips were rinsed and mounted with ProLong® Gold antifade reagent (Life Technologies) for 12-24 h at RT in dark. Cells and NPs were visualized using a confocal microscope Zeiss Duo 510 META with 63X oil immersion objective 1.4 NA. To set up the reflectance optical configuration, the main beam splitter was set to NT80/20 and

the channel was set up for reflectance using the 488 nm laser. CMO was excited with 561 nm laser and DAPI was visualized with 405 nm laser. Z-stacks from the coverslip to the top of the cell were acquired at a step size of 320 nm. For three-dimensional (3D) reconstruction Imaris 6.4.2 software was used.

**Statistical analysis**

All tests were performed in at least three individual experiments in duplicates.

The $EC_{50}$ values were calculated using MS Excel macro Regtox (http://www.normalesup.org/~vindimian/en_download.html) and the results are presented with 95% confidence intervals. The statistical significance between the $EC_{50}$ values were estimated assuming equal variances at $p < 0.05$.

The principal component analysis (PCA) and a heatmap and dendrogram were done with R Language and Environment for Statistical Computing (http:// www.R-project.org). PCA was used to obtain a multiparametric estimation of the variables that contributed to the toxicity (average nominal $EC_{50}$ values) of CuO NPs and $CuSO_4$. Scores of the first two PCs which accounted for 87-95% of the variance were used to generate the biplots. Data were scaled by dividing the (centered) columns of x by their standard deviations. Heatmaps and dendrograms were generated using heatmap function (incorporating Euclidean distance and complete method). Data were transformed by dividing the (centered) columns of x by their standard deviations.

**RESULTS**

**Physico-chemical characterization of CuO NPs**

The primary sizes of CuO NPs were measured by transmission electron microscopy (TEM) and the presence of the different functional groups on the of NPs was verified with different characterization techniques including X-ray Photoelectron Spectroscopy (XPS), Fourier Transform Infrared Spectroscopy (FTIR), Thermogravimetric Analysis (TGA) and C,H,N elemental analysis in the previous publications[38,39]. Previous study showed that CuO NPs had comparable irregular morphology and primary particle dimeter of 7.3 – 18.1 nm mostly forming the agglomerates of a few hundred nanometers according to transmission electron microscopy[39].

In the current study hydrodynamic size (Dh), polydispersity index (pdi), Z-potential in MQ water and in test medium as well as Cu content in CuO NPs were measured (Table 1). Hydrodynamic size of NPs was in the range of 204 nm (CuO NPs) to 1268 nm (CuO-PEG). The pdi values did not exceed 0.35 in the MQ and increased to 0.45-0.88 in the test medium, confirming the tendency of NPs, especially CuO-PEG (pdi=0.88), to agglomerate in the test medium. The Z-potential reflecting the particle charge was positive for CuO and CuO-NH$_2$ and negative for CuO-COOH and CuO-PEG in MQ water. In the test medium, the Z-potential of NPs rendered negative for all the particles ranging from -8.9 mV (CuO-NH$_2$) to -10.8 mV (CuO), most likely due to the adsorption of the serum proteins (the Z-potential of the test medium alone was -10.4 mV) as suggested before by Ivask et al *(2015)* or the interference of the serum proteins with the measurements. Measured total Cu content was the highest for CuO (76.8%), followed by CuO-NH$_2$ (46.2%), CuO-COOH (33.6%) and CuO-PEG (11.7%). The measured total Cu content in $CuSO_4$ was 37.1± 4.5 % being in agreement with the

calculated amount of Cu in CuSO$_4$ (39.8%) and Cu content in CuO was $76.8 \pm 5.7$ % being in agreement with the calculated amount of Cu in CuO (79.9%).

Table 1. Physico-chemical characteristics of Cu compounds.

| Cu compounds | Primary diameter[1], nm | Hydrodynamic diameter (Dh) in DI water[2] nm (pdi[3]) | Dh in test medium[2], nm (pdi) | Z-potential in DI water[2], nm | Z-potential in test medium[2], nm | Cu content[4], % |
|---|---|---|---|---|---|---|
| CuO NPs | $18.1 \pm 4$ | $237 \pm 31$ (0.25) | $204 \pm 13$ (0.45) | $27.5 \pm 1.8$ | $-10.8 \pm 1.4$ | $76.8 \pm 5.7$ |
| CuO-NH$_2$ NPs | $9.2 \pm 2.4$ | $733 \pm 252$ (0.24) | $936 \pm 229$ (0.67) | $25.8 \pm 1.3$ | $-8.9 \pm 0.8$ | $46.2 \pm 4.0$ |
| CuO-COOH NPs | $8.4 \pm 1.2$ | $1124 \pm 128$ (0.35) | $303 \pm 84$ (0.70) | $-12.0 \pm 2.2$ | $-10.2 \pm 0.8$ | $33.6 \pm 3.2$ |
| CuO-PEG NPs | $7.3 \pm 1.5$ | $1244 \pm 254$ (0.35) | $1268 \pm 315$ (0.88) | $-21.9 \pm 3.3$ | $-10.0 \pm 1.8$ | $11.7 \pm 1.0$ |
| CuSO$_4$ | NA[¥] | NA | NA | NA | NA | $37.1 \pm 4.5$ |

[1] Published by Zhang et al. (2016); [2]Measured by Malvern Zetasizer from 100 mg/l suspensions; [3]Polydispersity index; [4]Analyzed by Picofox from 100 mg/l suspensions.

**Toxicity of Cu compounds**

Viability of cells measured by Resazurin assay after 24-h exposure to CuO NPs and CuSO$_4$ is shown in Figure S1. Clear dose-response to all compounds in all cell types was observed. At nominal concentrattions, uncoated CuO and especially CuO-NH$_2$ NPs were the most toxic to all cell types having significant effect on cellular viability already at concentrations of 25-50 mg/l (Figure S1).

Figure 1 depicts the average nominal 24-h EC$_{50}$ values calculated on the basis of the dose-response curves from Figure S1 and dendrogram showing the clustering of these EC$_{50}$ values. When the toxicity (24-h EC$_{50}$) of CuSO$_4$ was the same for all cell types, the toxicity of NPs to different cells varied significantly.

Namely, uncoated CuO and CuO-NH$_2$ were more toxic to human cells *in vitro* than to bacteria, whereas negatively charged NPs − CuO-COOH and CuO-PEG – were significantly more toxic to bacteria compared to human cells (Figure 1A). Dendrogram analysis pointed out several clusters: the most toxic NPs − uncoated CuO and CuO-NH$_2$ − clustered together, whereas CuO and CuSO$_4$ formed another cluster and the least toxic CuO-PEG NPs a separate cluster (Figure 2B).
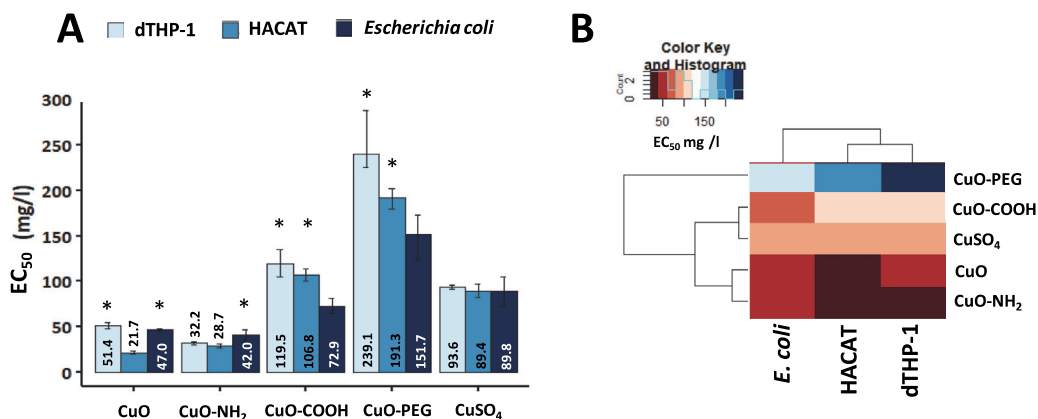
**Figure 1.** *The average nominal 24-h EC$_{50}$ values (mg/l) with 95% confidence intervals (A) and dendrogram showing the clustering of average nominal 24-h EC$_{50}$ values of Cu compounds to bacteria Escherichia coli (E. coli), HACAT keratinocytes and differentiated THP-1 cells (dTHP-1) (B). The asterisks designate the statistically significant differences (p<0.05) compared with the most susceptible cells in the group.*

When the 24-h EC$_{50}$ values of Cu compounds were re-calculated on Cu content (from Table 1), CuO-NH$_2$ remained the most toxic NPs to all cell types, followed by CuO-PEG and CuO (Figure S2). Since Cu-content adjusted 24-h EC$_{50}$ values for CuO-NH$_2$ were about twice lower than the EC$_{50}$ values for ionic control CuSO$_4$, we hypothesized that the toxicity of CuO-NH$_2$ NPs can not be solely explained by dissolved Cu and additional toxicity mechanisms played a role. Thus, we determined the ability of Cu compounds to induce ROS and inflammation and studied in details their interactions with bacterial and human cellls *in vitro* with the focus on NP localization and uptake mechanisms.

**Mechanisms of toxicity of Cu compounds**

*Bioavailability and dissolution of Cu compounds*

Recombinant bioluminescent *E. coli* increasing the bioluminescence in response to bioavailable Cu ions was applied to determine the role of internalized Cu ions in antibacterial potency of Cu compounds. In parallel, chemical analysis was used to reveal dissolution of CuO (Figure 2). When *E. coli* biosensor was exposed to Cu compounds on Cu content basis, the bioluminescence response of bacteria to CuSO$_4$, CuO-COOH and CuO-PEG  was not different, indicating that CuO-COOH and CuO-PEG exhibited antibacterial effects through bioavailable ionic Cu (Figure 2A). Although the response of biosensor to CuSO$_4$ was significantly different (Figure 2A), this was caused by slower dissolution of CuO (release of Cu ions) as revealed by chemical analysis (Figure 2B). In contrast, CuO-NH$_2$ NPs were different from all the other Cu compounds by killing bacteria at remarkably lower concentration that cannot be predicted from Cu content and dissolved Cu analysis, indicating that CuO-NH$_2$ exhibit specific Cu-independent antibacterial mechanism.
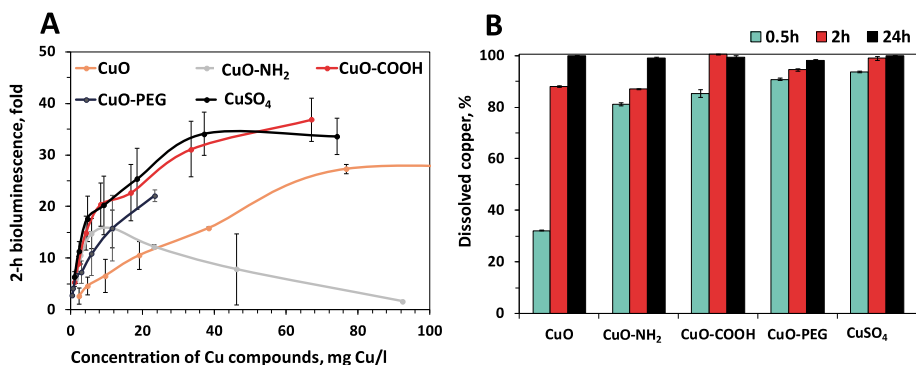
*Figure 2.* *Induction of bioluminescence in* E. coli *biosensor in response to Cu compounds (A) and abiotic dissolution of Cu compounds 100 mg/L, 37ºC (in CCM without PEST after 0.5-, 2- and 24-h incubation (B). Note that on x-axis the concentration of Cu compounds is recalculated on Cu basis.*

### Ability of Cu compounds to induce ROS and inflammation

CuO-NH$_2$ NPs were the most potent inducers of ROS (46-fold induction at concentration 200 mg/l), whereas other NPs were lower ROS inducers (6- to 11-fold). CuSO$_4$ did not induce ROS at any concentration (Figure 3A). CuO-NH$_2$ NPs were also the most potent inducers of TNF-α in differentiated THP-1 cells followed by CuO, CuO-COOH, CuSO$_4$ and CuO-PEG (Figure 3B). Using light microscopy we also noticed extensive vacuolization in the cells exposed to CuO and especially CuO-NH$_2$ NPs (Figure 3C) that was suggested to be a sign of inflammation and cell death[40] and may indicate distinct mechanism of toxicity of CuO-NH$_2$ NPs also in mammalian cells (macrophages) *in vitro*.
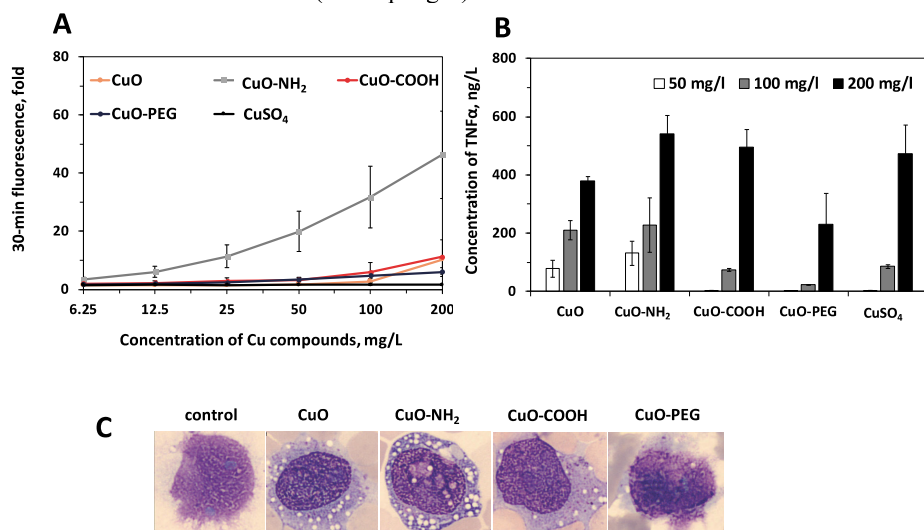




*Figure 3.* *Fluorescence of H$_2$DCFA-DA induced by Cu compounds reflecting the ability of Cu compounds to produce reactive oxygen species in abiotic conditions (A), concentration of TNF-α in the supernatants of differentiated THP-1 cells exposed to Cu compounds for 24 h (B) and representative light microscopy pictures of differentiated THP-1 cells exposed to equitoxic nominal concentrations (24-h EC$_{20}$) of Cu compounds for 24 h (C).*

*Measurement of cell-associated Cu from Cu compounds*

To dissect the mechanisms of toxicity of Cu compounds, differentiated THP-1 and HACAT cells were exposed to equitoxic (24-h $EC_{20}$) concentrations of Cu compounds, washed and analysed for Cu content. Supposedly, Cu content was mostly referring to intracellular Cu. However, it cannot be excluded that some fraction of CuO NPs or dissolved Cu was tightly bound to cell membranes and detected by our analysis. Thus, the measured fraction was designated as „cell-associated Cu", combining intracellular Cu and CuO NPs and possible membrane-bound Cu. We suggested that if the toxicity of Cu compounds was caused solely by Cu ions, the amount of cell-associated Cu in cells exposed to equitoxic concentrations of Cu compounds will be equal. In case the toxicity was caused by additional factors (as expected for $CuO-NH_2$), the amount of cell-associated Cu will be lower compared to the other CuO NPs and $CuSO_4$.

As expected, there was statistically significantly less Cu in the both differentiated THP-1 and HACAT cells exposed to $CuO-NH_2$ (Figure 4). Surprisingly, we also observed that about two- and seven-fold higher amounts of cell-associated Cu were detected in case of CuO-COOH compared to other NPs in both HACAT and differentiated THP-1 cells, respectively, suggesting that both cell lines had exceptional capacity to tolerate cell-associated Cu from CuO-COOH. Therefore, we conducted the confocal microscopy study to confirm this result and visualize the precise localization of CuO NPs inside the cells and on cellular membranes.
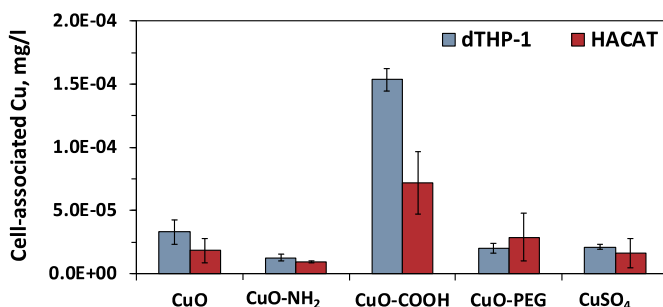


***Figure 4.*** *Cell-associated Cu determined by TXRF in differentiated THP-1 (dTHP-1) and HACAT cells exposed to equitoxic concentrations (24-h $EC_{20}$) of Cu compounds for 24 h.*

*Cellular localization of Cu compounds in mammalian cells*

Differentiated THP-1 cells were exposed to equitoxic (24-h $EC_{20}$) concentrations of Cu compounds as in previous experiments and visualized with confocal microscopy (Figures 5 and S3). Reflective mode of the microscope was optimized to vizualize CuO NPs. Confocal microscopy images confirmed that there were significantly more Cu inside the cells in case of CuO-COOH NPs. By combining Z-stacks into three-dimensional image, we observed that most of the CuO-COOH particles were inside the cells, whereas in case of $CuO-NH_2$ more particles localized on the cellular membranes (Figure 5). Thus, the resistance of THP-1 macrophages to internal Cu was exceptionally high for CuO-COOH NPs and low for $CuO-NH_2$ NPs.
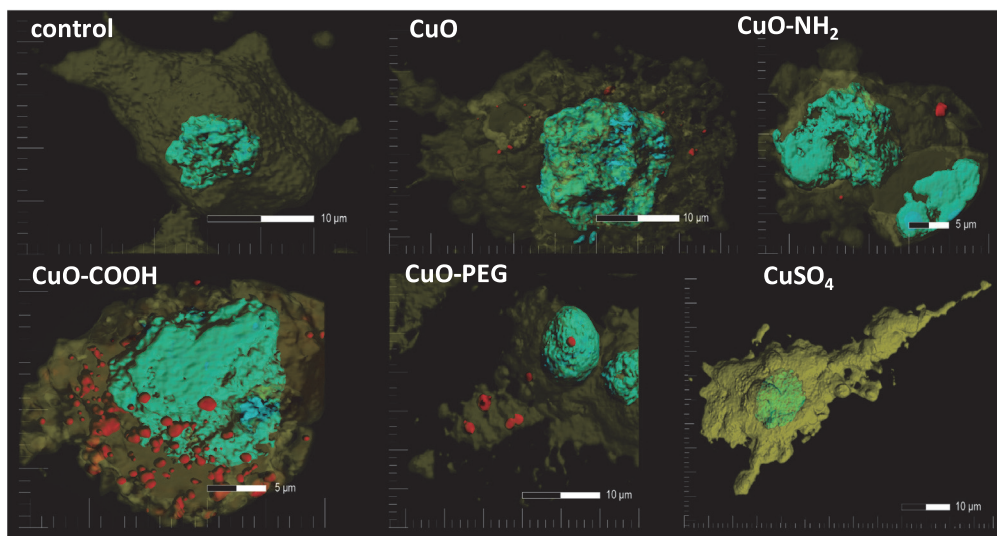
***Figure 5.*** *Representative confocal microscopy figures of differentiated THP-1 macrophages exposed to Cu compounds (24-h EC$_{20}$ concentrations) for 24 h.*

## Multivariate analysis

Finally, the multivariate analysis was performed to evaluate the variability of different properties of CuO NPs and thus, to estimate their contribution into toxicity. For this, toxicity data (Figure 1A) and physico-chemical characterization data (Figures 1-4) were fitted into scoresplot that comprises the eigenvectors. The principal components analysis (PCA) was applied resulting in NP positions according to their variability (Figure 6).

Since arrows indicated the direction of the increase of the values, 24-h EC50 vector denoted the direction of lower toxicity (increasing EC$_{50}$ value) that was the most characteristic for CuO-COOH and CuO-PEG (Figure 6). To estimate the contribution of different physico-chemical parameters into NP toxicity, we focused on the properties localizing in the area opposed to the EC$_{50}$ value vector. As seen, the properties contributing to increased toxic effects of unfunctionalized CuO and CuO-NH$_2$ NPs were more positive Z-potential, higher Cu content, higher 24-h dissolution, ability to produce more abiotic ROS and in case of THP-1 cells also higher production of TNF-α.

**A** Differentiated THP-1 macrophages

**B** HACAT keratinocytes

**C** *Escherichia coli*
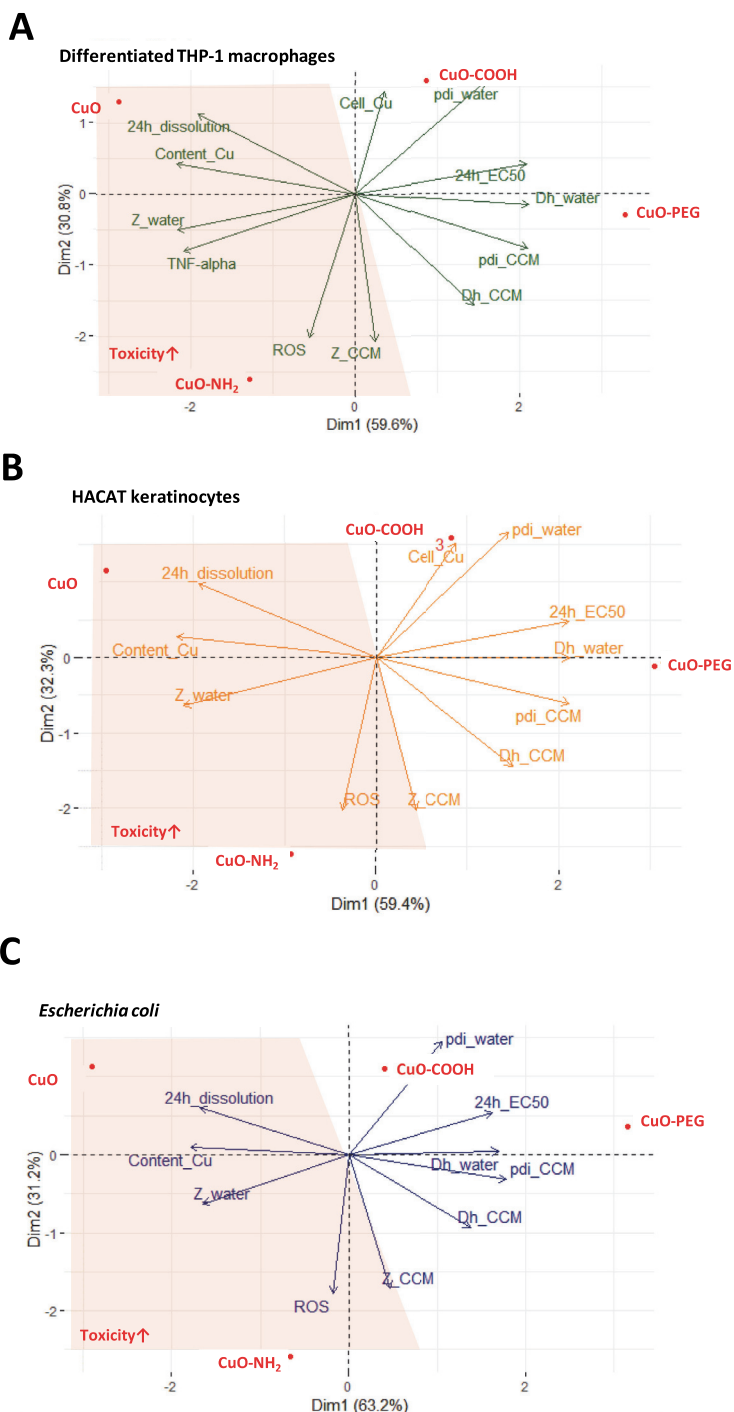
***Figure 6.*** *Multivariate analysis of the properties contributing to the variability of the toxicity of CuO, CuO-NH₂, CuO-COOH and CuO-PEG NPs to differentiated THP-1 macrophages (A), E. coli bacterium (B) and HACAT keratinocytes (C). As input, the data from Figures 11*

13

*and 15 was used. The abbreviations of the labels are the following: Z_water - surface charge in DI water, Z_CCM - surface charge in cell culture medium, Cell_Cu – cell-associated Cu, Dh_water - hydrodynamic size in DI water, Dh_CCM - hydrodynamic size in cell culture medium, PDI_CCM - PDI in cell culture medium, PDI_water - PDI in water, ROS - abiotic reactive oxygen species, Content_Cu - Copper content, 24h_EC50 – 24-h $EC_{50}$ nominal values (mg/l), 24h_dissolution – 24-h dissolution. The more toxic compounds are highlighted in the red area. For visualization, the data was scaled by dividing the (centred) columns of x by their standard deviations.*

**DISCUSSION**

Antibacterial metal-based NPs such as Ag and CuO are purposely designed to inhibit the undesired growth of bacteria and are widely applied in medical and commercial products. Warningly, it was shown that the toxicity range of CuO and Ag NPs to bacterial and mammalian cells *in vitro* may overlap, indicating potential hazard of these NPs to human cells[41][19]. Toxicity of CuO NPs was also demonstrated *in vivo*: oxidative DNA damage and the changes in epigenome (methylation of global DNA) were observed in mice instilled with 2.5 mg/kg CuO NPs[42]. In another study, similar concentrations (2.5 and 5 mg/kg) of CuO induced myofibroblast activation, extracellular matrix deposition and expression of the progressive fibrosis marker in the lung tissues, indicating that inhalation of CuO NPs could induce pulmonary fibrosis in C57BL/6 mice[43]. Despite of wide commercial use and toxicity of antibacterial Ag and CuO NPs demonstrated *in vitro* and *in vivo*, there were no attempts to identify antimicrobial metal-based NPs that would exhibit sufficient antibacterial activity and at the same time reduced toxicity to human cells.

In the current study, we compared the toxicity and revealed the mechanisms of toxicity of unfunctionalized CuO NPs, CuO-COOH, CuO-NH₂ , CuO PEG and soluble CuSO₄ to bacteria *Escherichia coli* and to human cells: HACAT keratinocytes and macrophages differentiated from THP-1 monocytes *in vitro*. Our main aim was to identify the NP surface functionalizations that would improve the safety profile of CuO NPs to mammalian cells *in vitro*, while retaining antibacterial activity. We showed for the first time, that the effect of the surface functionalizations of CuO NPs on toxicity is different for bacteria and human cells. Namely, while the toxicity of ionic CuSO₄ was nearly identical to bacterial and human cells, CuO-COOH and CuO-PEG were significantly more toxic to bacteria than to human cells *in vitro*. In contrast, CuO-NH₂ was more toxic to human cells than to bacterial cells.

The effects of COOH vs NH₂ functionalizations on the toxicity of NPs to mammalian cells *in vitro* was previously addressed  using e.g. polystyrene NPs and nanotubes. For example, it was shown that polystyrene-NH₂ and not polystyrene-COOH induced lysosomal leakage and inflammasome activation and IL-1β production in primary human monocyte-derived macrophages[44]. In another study carbon nanotubes functionalized with negatively charged COOH and PEG groups decreased the production of pro-fibrogenic cytokines and growth factors in human cell lines BEAS-2B and THP-1 compared to carbon nanotubes functionalized with NH₂ or PEI[31]. It was demonstrated that cationic NPs (such as NH₂-functionalized NPs) localize in the lysosomes of RAW 264.7 macrophages, whereas NH₂ groups supposedly bind protons and lead to the lysosomal rupture and inflammation[45]. These results are in line with our findings, showing that NH₂ functionalization makes CuO NPs especially toxic to human cells. Interestingly, from the studied NPs, CuO-NH₂ were also the

most toxic to bacteria, indicating additional universal mechanisms of toxicity unrelated to the NP uptake, lysosomal damage and inflammation (that are not existing in bacteria). Most probably, unspecific toxicity component of CuO-NH$_2$ was mediated *via* ROS (Figure 3A) and binding to the extracellular membranes (Figure 5).

CuO-COOH and CuO-PEG NPs can be advised as antibacterials, since they were significantly more toxic to bacteria than to human cells *in vitro*. It is well-known that functionalization of NPs with PEG prevents the adsorption of proteins and, thus, the uptake of NPs by macrophages[46] that most likely explains the reduced toxicity of CuO-PEG NPs to mammalian cells in our study. The reason, why mammalian cells are able to tolarate high intracellular concentration of CuO-COOH NPs remains to be addressed. We speculate that COOH functionalization guides the NPs to the specific receptors and non-inflammogenic pathway, since it is known that NP interactions with the cell receptors impact their cellular localization, inflammatory properties and toxicity [45,47].

## CONCLUSIONS

This study is the first report on the antimicrobial toxicity vs safety of CuO NPs with different surface functionalizations to bacteria *vs* human cells *in vitro*. We showed that CuO-NH$_2$ was significantly more toxic to THP-1 cells than to *E. coli* cells, probably because of its ability to induce inflammation (TNF-α) and ROS. The best therapeutic window was observed for CuO-COOH and CuO-PEG that can be recommended as antimicrobials.

Summarizing, we showed that the antibacterial toxicity *vs* safety profile of CuO NPs can be tuned with the surface functionalizations, and the effect of the surface functionalizations is different for bacteria and human cells. This knowledge can be used for the synthesis of more efficient and safer antimicrobials. Special attention should be paid to the specific targeting of bacterial cells, since the toxicity mechanisms of CuO NPs to bacterial and mammalian cells seem to be largely unspecific.

**Competing interests**
The authors declare no competing interests.

# References

1. Rosenberg, M., Vija, H., Kahru, A., Keevil, C. & Ivask, A. Rapid in situ assessment of Cu-ion mediated effects and antibacterial efficacy of copper surfaces. *Sci. Rep.* (2018). doi:10.1038/s41598-018-26391-8

2. Bastos, C. A. P. *et al.* Ligand-Doped Copper Oxo-hydroxide Nanoparticles are Effective Antimicrobials. *Nanoscale Res. Lett.* (2018). doi:10.1186/s11671-018-2520-7

3. Teli, M. D. & Sheikh, J. Modified bamboo rayon-copper nanoparticle composites as antibacterial textiles. *Int. J. Biol. Macromol.* **61,** 302–307 (2013).

4. Percival, S. S. Neutropenia Caused by Copper Deficiency: Possible Mechanisms of Action. *Nutr. Rev.* (1995). doi:10.1111/j.1753-4887.1995.tb01503.x

5. Percival, S. S. Copper and immunity. *Am. J. Clin. Nutr.* **67,** 1064–1068 (1998).

6. O'Dell, B. L. Biochemistry of copper. *Medical Clinics of North America* (1976). doi:10.1016/S0025-7125(16)31853-3

7. Borkow, G. *et al.* Molecular mechanisms of enhanced wound healing by copper oxide-impregnated dressings. *Wound Repair Regen.* **18,** 266–275 (2010).

8. Shi, M. *et al.* Copper-doped mesoporous silica nanospheres, a promising immunomodulatory agent for inducing osteogenesis. *Acta Biomater.* **30,** 334–344 (2016).

9. Brewer, G. J. Copper toxicity in the general population. *Clin. Neurophysiol.* **121,** 459–460 (2010).

10. Montes, S., Rivera-mancia, S., Diaz-ruiz, A., Tristan-lopez, L. & Rios, C. Review Article Copper and Copper Proteins in Parkinson's Disease. *Hindawi Publ.* **2014,** (2014).

11. Desai, V. & Kaler, S. G. Role of copper in human neurological disorders. *Am. J. Clin. Nutr.* **88,** 855S–858S (2008).

12. Aschner, M. Anand, S. Bloom, J. et. al. *Cassarett and Doull's Toxicology The Basic Science of Poisons. Toxicology* (2008). doi:10.1036/0071470514

13. Líbalová, H. *et al.* Toxicity of surface-modified copper oxide nanoparticles in a mouse macrophage cell line: Interplay of particles, surface coating and particle dissolution. *Chemosphere* **196,** 482–493 (2018).

14. Murugan, K., Choonara, Y. E., Kumar, P., du Toit, L. C. & Pillay, V. Cellular internalisation kinetics and cytotoxic properties of statistically designed and optimised neo-geometric copper nanocrystals. *Mater. Sci. Eng. C* **78,** 376–388 (2017).

15. Karlsson, H. L., Cronholm, P., Gustafsson, J. & Mo, L. Copper Oxide Nanoparticles Are Highly Toxic A Comparison between Metal Oxide Nanoparticles and Carbon Nanotubes - Chemical Research in Toxicology (ACS Publications). *Chem. Res. Toxicol.* **21,** 1726–1732 (2008).

16. Piret, J. P. *et al.* Pan-European inter-laboratory studies on a panel of in vitro cytotoxicity and pro-inflammation assays for nanoparticles. *Arch. Toxicol.* **91,** 2315–2330 (2017).

17. Käkinen, A., Kahru, A., Nurmsoo, H., Kubo, A. L. & Bondarenko, O. M. Solubility-driven toxicity of CuO nanoparticles to Caco2 cells and Escherichia coli: Effect of sonication energy and test environment. *Toxicol. Vitr.* (2016). doi:10.1016/j.tiv.2016.08.004

18. Ude, V. C. *et al.* Impact of copper oxide nanomaterials on differentiated and undifferentiated

Caco-2 intestinal epithelial cells; assessment of cytotoxicity, barrier integrity, cytokine production and nanomaterial penetration. *Part. Fibre Toxicol.* **14,** 1–16 (2017).

19.    Bondarenko, O. *et al.* Toxicity of Ag, CuO and ZnO nanoparticles to selected environmentally relevant test organisms and mammalian cells in vitro: A critical review. *Arch. Toxicol.* **87,** 1181–1200 (2013).

20.    Bondarenko, O. M. *et al.* Multilaboratory evaluation of 15 bioassays for (eco)toxicity screening and hazard ranking of engineered nanomaterials: FP7 project NANOVALID. *Nanotoxicology* **10,** 1229–1242 (2016).

21.    Nel, A. E. *et al.* Understanding biophysicochemical interactions at the nano-bio interface. *Nat. Mater.* **8,** 543–557 (2009).

22.    Kubo, A.-L. *et al.* Antimicrobial potency of differently coated 10 and 50 nm silver nanoparticles against clinically relevant bacteria Escherichia coli and Staphylococcus aureus. *Colloids Surfaces B Biointerfaces* **170,** (2018).

23.    Vonarbourg, A., Passirani, C., Saulnier, P. & Benoit, J. P. Parameters influencing the stealthiness of colloidal drug delivery systems. *Biomaterials* **27,** 4356–4373 (2006).

24.    Dobrovolskaia, M. A. & McNeil, S. E. Immunological properties of engineered nanomaterials. *Nature Nanotechnology* (2007). doi:10.1038/nnano.2007.223

25.    Ke, P. C., Lin, S., Parak, W. J., Davis, T. P. & Caruso, F. A Decade of the Protein Corona. *ACS Nano* **11,** 11773–11776 (2017).

26.    Gatto, F. & Bardi, G. Metallic Nanoparticles: General Research Approaches to Immunological Characterization. *Nanomaterials* **8,** 753 (2018).

27.    Gallud, A. *et al.* Macrophage activation status determines the internalization of mesoporous silica particles of different sizes: Exploring the role of different pattern recognition receptors. *Biomaterials* **121,** 28–40 (2017).

28.    Sheng, Y. *et al.* Long-circulating polymeric nanoparticles bearing a combinatorial coating of PEG and water-soluble chitosan. *Biomaterials* **30,** 2340–2348 (2009).

29.    Jenkins, S. I. *et al.* 'Stealth' nanoparticles evade neural immune cells but also evade major brain cell populations: Implications for PEG-based neurotherapeutics. *J. Control. Release* **224,** 136–145 (2016).

30.    Wonder, E. *et al.* Competition of charge-mediated and specific binding by peptide-tagged cationic liposome–DNA nanoparticles in vitro and in vivo. *Biomaterials* **166,** 52–63 (2018).

31.    Li, R. *et al.* The Surface Charge and Cellular Processing of Covalently Functionalized Multiwall Carbon Nanotubes Determine Pulmonary Toxicity. **34,** 283–293 (2014).

32.    Juganson, K., Ivask, A., Blinova, I., Mortimer, M. & Kahru, A. NanoE-Tox: New and in-depth database concerning ecotoxicity of nanomaterials. *Beilstein J. Nanotechnol.* **6,** 1788–1804 (2015).

33.    Tauran, Y., Brioude, A., Coleman, A. W., Rhimi, M. & Kim, B. Molecular recognition by gold, silver and copper nanoparticles. *World J. Biol. Chem.* **4,** 35 (2013).

34.    Worthington, K. L. S. *et al.* Chitosan coating of copper nanoparticles reduces in vitro toxicity and increases inflammation in the lung. *Nanotechnology* (2013). doi:10.1088/0957-4484/24/39/395101

35.    Valodkar, M., Jadeja, R. N., Thounaojam, M. C., Devkar, R. V. & Thakore, S. Biocompatible

synthesis of peptide capped copper nanoparticles and their biological effect on tumor cells. *Mater. Chem. Phys.* **128,** 83–89 (2011).

36. Azizi, M., Ghourchian, H., Yazdian, F., Dashtestani, F. & AlizadehZeinabad, H. Cytotoxic effect of albumin coated copper nanoparticle on human breast cancer cells of MDA-MB 231. *PLoS One* **12,** 1–21 (2017).

37. Aruoja, V. *et al.* Toxicity of 12 metal-based nanoparticles to algae, bacteria and protozoa. *Environ. Sci. Nano* **2,** 630–644 (2015).

38. Savolainen, K. & Vartio, A. *Biological Foundation for the Safety Classification of Engineered Nanomaterials (ENM): Systems Biology Approaches to Understand Interactions of ENM with Living Organisms and the Environment.* (2017).

39. Zhang, W. *et al.* Genotoxicity of Copper Oxide Nanoparticles with Different Surface Chemistry on Rat Bone Marrow Mesenchymal Stem Cells. *J. Nanosci. Nanotechnol.* **16,** 5489–5497 (2016).

40. Shubin, A. V., Demidyuk, I. V., Komissarov, A. A., Rafieva, L. M. & Kostrov, S. V. Cytoplasmic vacuolization in cell death and survival. *Oncotarget* **7,** (2016).

41. Greulich, C. *et al.* The toxic effect of silver ions and silver nanoparticles towards bacteria and human cells occurs in the same concentration range. *RSC Adv.* (2012). doi:10.1039/c2ra20684f

42. Lu, X. *et al.* In vivo epigenetic effects induced by engineered nanomaterials: A case study of copper oxide and laser printer-emitted engineered nanoparticles. *Nanotoxicology* (2016). doi:10.3109/17435390.2015.1108473

43. Lai, X. *et al.* Intranasal delivery of copper oxide nanoparticles induces pulmonary toxicity and fibrosis in C57BL/6 mice. *Sci. Rep.* **8,** 1–12 (2018).

44. Loos, C. *et al.* Amino-functionalized nanoparticles as inhibitors of mTOR and inducers of cell cycle arrest in leukemia cells. *Biomaterials* **35,** 1944–1953 (2014).

45. Xia, T., Kovochich, M., Liong, M., Zink, J. I. & Nel, A. E. Cationic polystyrene nanosphere toxicity depends on cell-specific endocytic and mitochondrial injury pathways. *ACS Nano* (2008). doi:10.1021/nn700256c

46. Nguyen, V. H. & Lee, B. J. Protein corona: A new approach for nanomedicine design. *International Journal of Nanomedicine* (2017). doi:10.2147/IJN.S129300

47. Dobrovolskaia, M. A. & McNeil, S. E. Immunological properties of engineered nanomaterials. *Nat. Nanotechnol.* (2007). doi:10.1038/nnano.2007.223

SUPPLEMENTARY INFORMATION for


**Towards (immuno)safety of antibacterial nanomaterials: surface functionalization of CuO with carboxyl- or polyethylene decreases their cytotoxicity to human cells *in vitro***

A-L. Kubo[1], G. Vassiljev[1,2], H. Vija[1], J. Kristall[3], V. Tõugu[3], A. Kahru[1,4], O. M. Bondarenko[1*]

[1] *Laboratory of Environmental Toxicology, National Institute of Chemical Physics and Biophysics, Tallinn, Estonia.*
[2] *Department of Natural Sciences, TalTech, Tallinn, Estonia.*
[3] *Department of Chemistry and Biotechnology, School of Science, TalTech, Tallinn, Estonia.*
[4] *Estonian Academy of Sciences, Kohtu 6, Tallinn, Estonia.*


*Corresponding author

Contact: Tel./Fax: +372 6398382,  E-mail: olesja.bondarenko@kbfi.ee

**Table S1.** Details on testing conditions for Cu compounds.

| Test | Method | Exposure media for Cu compounds | Time (h) | 95% humidity and 5% $CO_2$ | Temperature (°C) |
|---|---|---|---|---|---|
| | | ***Tests with human cells*** | | | |
| **HACAT viability** | Alamar Blue assay | DMEM[#], 4.5 g/l glycose, L-glutamine, sodium pyruvate, 10% FBS[‡], 1% PEST[l] | 24 | yes | 37 |
| **dTHP-1 viability** | Alamar Blue assay | CCM[Δ] (RPMI-1640[◻], 100 mM sodium pyruvate, 10% FBS, 1% PEST) | 24 | yes | 37 |
| **Cell-associated Cu, HACAT** | TXRF[¥] | DMEM, 4.5 g/l glycose, L-glutamine, sodium pyruvate, 10% FBS, 1% PEST | 24 | yes | 37 |
| **Cell-associated Cu, dTHP-1** | TXRF | CCM | 24 | yes | 37 |
| **NP cellular localization, dTHP-1** | Microscopy | CCM | 24 | yes | 37 |
| **TNF-α production, dTHP-1** | ELISA[£] | CCM | 24 | yes | 37 |
| | | ***Tests with bacterial cells*** | | | |
| ***E. coli* viability** | Alamar Blue assay | CCM without PEST | 24 | no | 37 |
| **Bioavailability of Cu to *E. coli*** | Cu ion biosensor *E. coli*[±] | CCM without PEST | 2 | no | 37 |
| | | ***Tests in abiotic conditions*** | | | |
| **Abiotic ROS** | H$_2$DCF fluorescence | DI-water[↑] | 0.5 | no | RT[⊕] |
| **Abiotic dissolution** | TXRF | CCM | 0.5, 2, 24 | yes | 37 |

¥ - Cu quantification with total reflection X-ray fluorescence analysis, £ - Enzyme-Linked Immunosorbent Assay, ± - *E. coli* MC1061 (pSLcueR/pDNPcopAlux), ‡-Fetal bovine serum, l-10000 U/ml Penicillin and 10000 µg/ml Streptomycin, #-Dulbecco's modified Eagle's medium, ◻-Roswell Park Memorial Institute medium with L-glutamine, ↑- endotoxin free bi-distilled water, Δ- complete cell culture medium, ⊕- room temperature
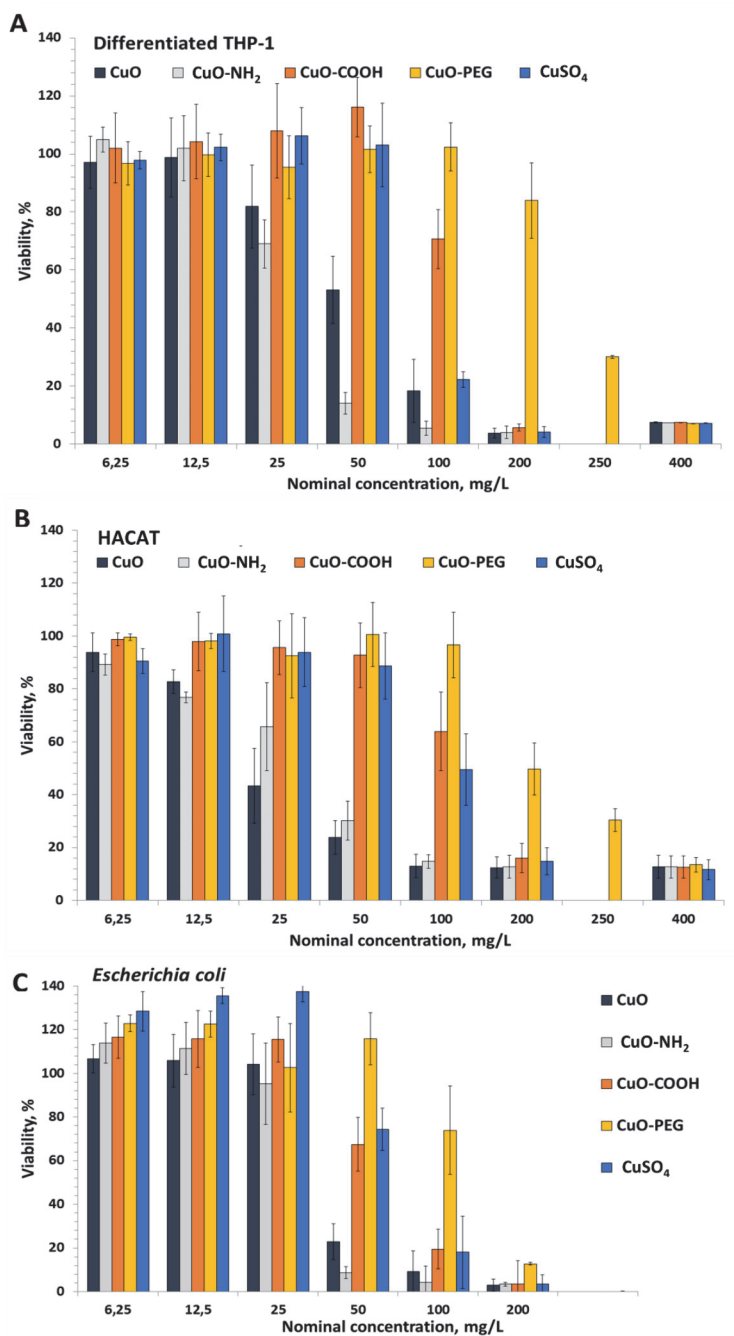
**Figure S1.** Viability of differentiated THP-1 (A), HACAT keratinocytes (B) and *Escherichia coli* (C) after 24-h incubation with CuO NMs in RPMI1640 medium supplemented with 10% fetal bovine serum.
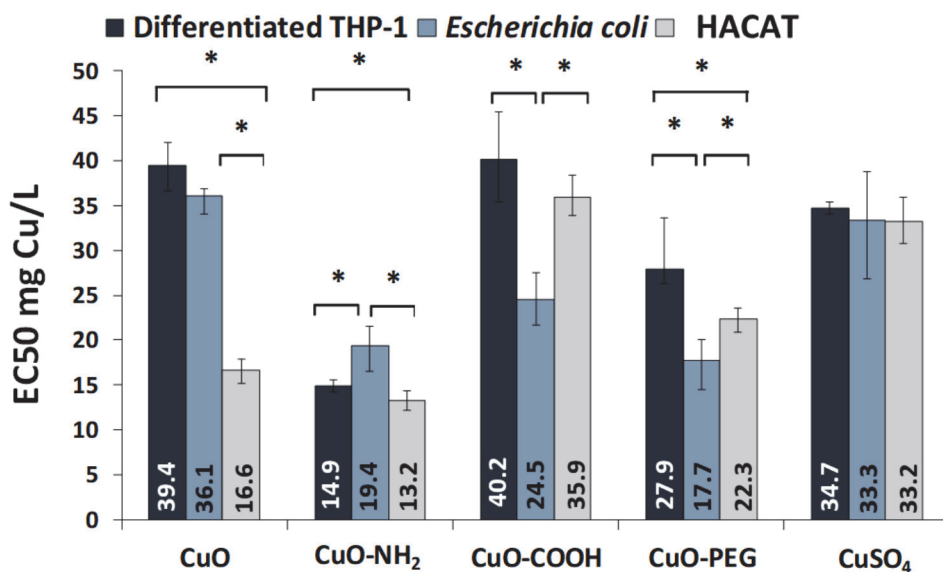
**Figure S2.** The average Cu-adjusted 24-h $EC_{50}$ values (mg Cu/L) of Cu compounds with 95% confidence intervals.
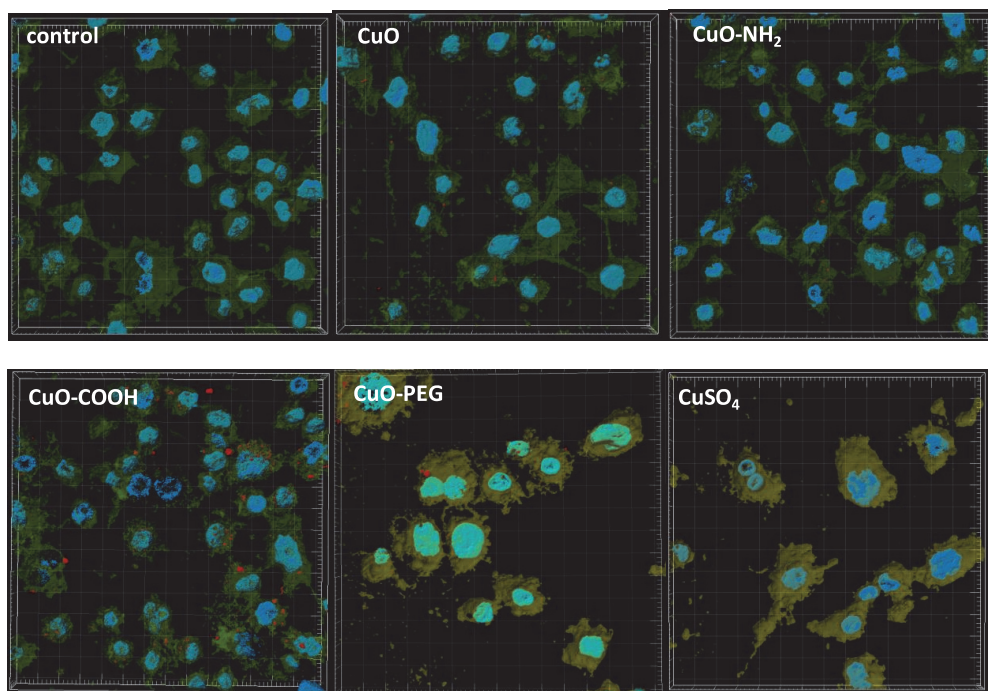
**Figure S3.** Representative confocal microscopy figures of differentiated THP-1 macrophages exposed to Cu compounds (24-h $EC_{20}$: 27.3 mg/l for CuO NPs, 22.2 mg/l for CuO-NH$_2$, 90.6 mg/l for CuO-COOH, 211.4 mg/l for CuO-PEG and 85.4 mg/l for CuSO$_4$) for 24 h.

# *Curriculum vitae*

**Name:** Anna-Liisa Kubo (maiden name Prangli)
**Date of birth:** 13th of August, 1984
**Place of birth:** Tallinn, Estonia
**Citizenship:** Estonian
**Contact information:**

National Institute of Chemical Physics and Biophysics (NICPB)
Laboratory of Environmental Toxicology
Akadeemia tee 23, 12618 Tallinn
Tel: +3725121279 , e-mail: anna-liisa.kubo@kbfi.ee

**Education:**

| | |
|---|---|
| 2010- | PhD student at Tallinn University of Technology, School of Science |
| 2005-2007 | MSc, University of Tartu, Faculty of Medicine, Department of Immunology |
| 2002-2005 | BSc, University of Tartu, Faculty of Biology and Geography |
| 1990-2002 | High school certificate, Tallinn School No. 21 |

**Special courses:**

- TalTech course „Developmental Biology Minisymposium" in Tallinn, September 2018
- EUROTOX2018 congress in Brussels, Belgium, September 2018
- Co-organizer of a NICPB and TalTech workshop: "From Nanotoxicology to Nanomedicine" in Tallinn, September 2018
- TalTech course "Practical Statistics in R and R-Studio" in Tallinn, June 2018
- VACTRAIN and Riga Stradins University course "Openings for Cancer Immunotherapy" in Riga, May 2018
- Co-organized a joint seminar of the COST and AMiCI Core Group and WG3 meeting in Tallinn, November 2017
- ecopa and SSCT workshop: "Up to date in vitro approaches in regulatory risk assessment and disease modelling" in Helsinki, June 2017
- TalTech IGIP course "Expression and academic writing" in Tallinn, spring semester 2017
- Cancer Biology Laboratory course „Targeted nanosystems for imaging and therapy" in Tartu, May 2017
- JRC Summerschool on alternative approaches for safety assessment "The path from science to protection of human health and the environment" in Ispra Italy, May 2017
- EUROTOX2017 congress in Bratislava, Slovakia, 2017
- ESTIV course " Applied in vitro Toxicology" in Belvaux-Luxembourg, January 2017
- Karolinska Institutet course "Safety Assessment in Drug Discovery and Development" in Stockholm, September 2016

- COST MODENA course " Assessing the dose of nanomaterials in toxicological studies: Advanced approaches utilising experimentation and modelling" in Tallinn, May 2016
- Federation of European Toxicologists and European Societies of Toxicology (EUROTOX) course "Principles of Toxicology" in Zagreb, Croatia, April 2016

**Professional employment:**

| | |
|---|---|
| 2016- | Junior Reseacher, NICPB, Laboratory of Environmental Toxicology |
| 2010-2012 | Molecular Biologist, HansaBioMed |
| 2008-2010 | Laboratory Specialist, Tallinn Diagnostics Centre |
| 2007-2008 | Researcher, Celecure AS |
| 2004-2007 | Laboratory Assistant, University of Tartu, Faculty of Medicine, Dept. of Immunology |

**Awards:**

2018    ESFUSA Estonian Students Fund in USA scholarship
2018    DoRa Pluss 1.1 to participate at EUROTOX2018 Congress
2017    ESFUSA Estonian Students Fund in USA scholarship
2017    DoRa Pluss 1.1 to participate at EUROTOX2017 Congress
2017    European Consensus Platform for Alternatives (ecopa) travel grant to participate at the ecopa SSCT workshop
2005    Poster award at the John Humphrey course/conference of EFIS on Innate and Adaptive Immune Responses to Pathogens. October 5-8, 2005, Vilnius

# Elulookirjeldus

**Nimi:** Anna-Liisa Kubo (neiupõlvenimi Prangli)
**Sünniaeg:** 13. august 1984
**Sünnikoht:** Tallinn, Eesti
**Kodakondsus:** Eesti
**Kontaktandmed:**

Keemilise ja Bioloogilise Füüsika Instituut (KBFI)
Keskkonnatoksikoloogia labor
Akadeemia tee 23, 12618 Tallinn
tel: +3725121279 , e-mail: anna-liisa.kubo@kbfi.ee

**Hariduskäik:**

| | |
|---|---|
| 2010- | doktorant, Tallinna Tehnikaülikool, loodusteaduskond |
| 2005-2007 | MSc, Tartu Ülikool, arstiteaduskond, immunoloogia õppetool |
| 2002-2005 | BSc, Tartu Ülikool, bioloogia- ja geograafiateaduskond |
| 1990-2002 | keskkoolitunnistus, Tallinna 21. Kool |

**Täiendusõpe:**

- Osalesin EUROTOX2018 konverentsil Brüsselis, Belgias (september 2018).
- Osalesin KBFI ja TalTech ühisseminari korraldamises "From Nanotoxicology to Nanomedicine" Tallinnas (september 2018).
- Osalesin TalTech kursusel „Developmental Biology Minisymposium" Tallinnas (september 2018).
- Osalesin TalTech kursusel „Practical Statistics in R and R-Studio". Tallinnas (juuni 2018).
- Osalesin VACTRAIN ja Riia Stradinši Ülikooli kursusel "Openings for Cancer Immunotherapy" Riias (mai 2018).
- Osalesin COST, AMiCI juhtgrupi ja WG3 kohtumisel Tallinnas (november 2017).
- Osalesin ecopa ja SSCT seminaril: "Up to date in vitro approaches in regulatory risk assessment and disease modelling" Helsingis (juuni 2017).
- Osalesin EUROTOX2017 konverentsil Slovakkias, Bratislavas (september 2017).
- Osalesin vähibioloogia labori kursusel „Targeted nanosystems for imaging and therapy" Tartus (mai 2017).
- Osalesin JRC Suvekoolis alternatiivsetest meetoditest riskihindamises "The path from science to protection of human health and the environment" Ispras Itaalias (mai 2017).
- Osalesin TalTech IGIP kursusel "Väljendusoskus ja akadeemiline kirjutamine" Tallinnas (kevadsemester 2017)
- Osalesin ESTIV kursusel " Applied in vitro Toxicology" Belvaux-Luxembourgis (jaanuar 2017).
- Osalesin Karolinska Instituudi kursusel "Safety Assessment in Drug Discovery and Development" Stockholmis (september 2016).

- Osalesin COST MODENA kursusel " Assessing the dose of nanomaterials in toxicological studies: Advanced approaches utilising experimentation and modelling" Tallinnas (mai 2016).
- Osalesin Toksikoloogia õppekursusel "Principles of Toxicology" Zagrebis, Horvaatias (aprill 2016).

**Teenistuskäik:**

| | |
|---|---|
| 2016- | nooremteadur, KBFI, Keskkonnatoksikoloogia labor |
| 2010-2012 | molekulaarbioloog, HansaBioMed |
| 2008-2010 | laborispetsialist, Tallinna Diagnostikakeskus |
| 2007-2008 | teadur, Celecure AS |
| 2004-2007 | laborant, Tartu Ülikool, arstiteaduskond, immunoloogia õppetool |

**Tunnustused:**

2018　ESFUSA (Eesti Üliõpilaste Toetusfond USAs) George ja Selma Madisoni nimelise stipendiumi laureaat

2018　DoRa Pluss 1.1 doktorantide õpirände toetus EUROTOX2018 konverentsil osalemiseks

2017　ESFUSA Eesti Üliõpilaste Toetusfond USAs Ene Silla nimelise stipendiumi laureaat

2017　DoRa Pluss 1.1 doktorantide õpirände toetus EUROTOX2017 konverentsil osalemiseks

2017　European Consensus Platform for Alternatives (ecopa) reisitoetus ecopa ja SSCT seminaril osalemiseks

2005　auhind posterettekandele EFIS John Humphrey konverentsil „Kaasasündinud ja adaptiivne immuunvastus patogeenidele" 5.-8. oktoobril 2005, Vilnius.